



University Library

Author/Filing Title G O L Y S H E V A

Class Mark T

Please note that fines are charged on ALL
overdue items.

--	--	--

0402948734



Hand-held electro-pneumatic percussion machine with reduced vibration emission


by Evgenia Golysheva

A Doctoral Thesis

Submitted in partial fulfilment of the requirements for the award of Doctor
of Philosophy of Loughborough University

June 2003

© by E. V. Golysheva 2003

 Loughborough University Pitt-Rivers Library
Date <i>July 04</i>
Class
Acc No. <i>040294873</i>

Abstract

Millions of hand-held percussion machines are used daily throughout industry. Every year, thousands of operators of these machines suffer from a variety of disorders caused by exposure to harmful vibration. The government is faced annually with compensation claims running into hundreds of thousands of pounds, but more importantly, the quality of life of these workers is of particular concern. The design of low-vibration hand-held percussion machine is a challenging and topical engineering problem that is addressed in the current study.

One of the main sources of hazardous vibration of electro-pneumatic percussion machine is an impulsive pressure force developed within an air cushion and applied directly to the machine casing. The present study showed that an additional flexible element added to the driving piston of the electro-pneumatic hammer improves excitation performance, leading to an extension of acceleration time and a reduction in the intensity of impulses of pneumatic impacts thereby relieving load on the operator.

Furthermore, the passive system of vibration attenuation, which combines principles of vibration isolation and dynamic absorption was developed in the present study. Such system can be effectively used in hand-held percussion machines. The vibration isolator between the handle and the casing of the machine reduces the high frequency components of acceleration perceived by an operator, whereas the tuned dynamic absorber attached to the handle allows suppression of the dominating harmonics of machine acceleration that are not affected by vibration isolators. Such a vibration attenuation system permits use of relatively stiff isolators and significantly reduces hand-transmitted vibration perceived by an operator without essential increase in weight of the tool. Results of numerical simulations have been verified by experiment.

Acknowledgements

I would like to express my deep gratitude to Professor Vladimir Babitsky and Dr Alexander Vepruk for their supervision, support and guidance during my studies.

My postgraduate studies would not have been possible without the generous financial support from the Department of Mechanical and Manufacturing Engineering of Loughborough University and through an Overseas research Student Award. I would also like to express my sincerest gratitude to Michail Zaharovich Kolovsky and all academic staff of the Department of Theory of Mechanisms and Machines of Saint-Petersburg State Technical University for their friendship, interest and encouragement.

A number of people have helped me during my studies. In particular, I would like to acknowledge Dr Ilia Sokolov for his constructive criticism, Brian Mace and Alan Wilkinson for their technical support and for their help and patience with my machining skills.

Last, but by no means least, I would like to thank my parents, Danish and my friends for simply being there.

Table of Contents

Abstract.....	ii
Acknowledgements.....	iii
Chapter 1 Introduction.....	1
1.1 General introduction.....	1
1.2 Objectives of the study.....	4
1.3 Outline of the thesis.....	4
Chapter 2 Hand-transmitted vibration.....	7
2.1 Medical aspects.....	7
2.2 Measurements and standards of hand-transmitted vibration.....	10
2.2.1 Vibration axes.....	10
2.2.2 Vibration type, magnitude, frequency and duration.....	10
2.2.3 The influence of individual factors on the effect of human exposure to hand-transmitted vibration.....	16
2.2.4 Hand-transmitted vibration standards.....	17
2.3 Conclusions and discussions.....	20
Chapter 3 Models of the dynamic response of hand-arm system.....	22
3.1 One-and two-degree-of-freedom models.....	24
3.2 Three-and more degree-of-freedom models.....	27
3.3 Models with distributed parameters.....	31
3.4 Development of dynamic model of hand-arm system.....	34
3.5 Conclusions and discussions.....	41

Chapter 4 Dynamics of hand-held percussion machine.....	43
4.1 Major sources of vibration.....	45
4.2 Development of the dynamic model of an electro-pneumatic hammer.....	49
4.3 Numerical simulations.....	56
4.3.1 Block diagrams.....	57
4.3.2 Model parameters.....	61
4.3.3 Frequency analysis.....	63
4.3.4 Results of numerical simulations.....	66
4.4 Conclusions and discussions.....	77
Chapter 5 Methods of reducing vibration of hand-held percussion machines.....	80
5.1 Reduction of the intensity of sources of vibration.....	80
5.1.1 Optimal excitation.....	81
5.1.2 Optimal striker mass and impact velocity.....	82
5.1.3 Specific distribution of the counter-force.....	83
5.1.4 Additional inertial elements (dynamic balancing).....	85
5.1.5 Other methods.....	86
5.2 Vibration isolation.....	88
5.2.1 Passive methods of vibration isolation.....	94
5.2.2 Active methods of vibration isolation.....	100
5.2.3 Mechanisation and remote control.....	101
5.3 Dynamic absorption.....	102
5.4 Other methods.....	109
5.5 Conclusions and discussions.....	109
Chapter 6 Dynamic correction of excitation of the hand-held percussion machine.....	111
6.1 Optimal striker motion.....	113

6.2 Dynamic model of electro-pneumatic hammer with modified source of excitation.....	118
6.3 Numerical simulations.....	122
6.4 Conclusions and discussions.....	128
Chapter 7 Design of vibration attenuation system for a hand-held percussion machine.....	130
7.1 Principle of vibration attenuation system.....	130
7.2 Dynamic modelling and numerical simulations of electro-pneumatic hammer with vibration attenuation system.....	131
7.2.1 Vibration isolation.....	133
7.2.2 Vibration isolation in combination with dynamic absorber.....	142
7.3 Experimental verification.....	153
7.3.1 Mechanical set-up.....	153
7.3.2 Synthesis of the excitation signal.....	157
7.3.3 Experimental results.....	163
7.4 Frequency response of vibration attenuation system.....	171
7.5 Conclusions and discussions.....	174
Chapter 8 Concluding remarks.....	177
8.1 Present contribution.....	180
8.2 Recommendations for future work.....	180
References	171
Appendix A Search routine for optimal parameters of dynamic model.....	178
Appendix B Frequency calculations.....	185
Appendix C Parameters of dynamic model of electro-pneumatic hammer with modified source of excitation.....	186
Appendix D Analog output.....	188

Chapter 1

Introduction

1.1 General introduction

Hand-held percussion power tools (road breakers, hammer drills, chisels etc.) are very popular in various areas of industry, particularly in the construction and manufacturing sectors. Pneumatic breakers are used for demolishing concrete structures and rock shattering; hammer drills are employed in construction and mining; at large steel works, defects in steel casing are removed using pneumatic chisels and chipping hammers. The operating principle of such machines is based on periodic impacts of high intensity, which enables effective breaking or trimming of diverse materials. Millions of hand-held power tools of various sizes, with different types of drives and directions of impact are produced every year. Such popularity is accounted for by high productivity, adaptability for various types of work, simple design and ease of manufacturing of this type of machinery. In many areas, hand-held portable power tools are indispensable, especially in operations where stationary equipment cannot be used.

Hand-held percussion machines are widely used due to their efficiency as impact vibration devices. However impact vibration arising from their use has a serious

negative effect on the health of the operator of equipment. The specific feature of this type of machinery is the constant contact with an operator who carries, guides and, most importantly, has to press the tool against treated material during operation (see Figure 1.1). Hence, the operator directly perceives vibration emitted by the tool.



Figure 1.1. Hand-held power tools.

Operators of hand-held vibrating power tools have long complained of tingling and numbness in their hand or of fingers blanching. These cases of “white fingers” or “dead fingers” were first reported in the literature between 1911 and 1920. The spasm of the arteries in the fingers was attributed to the vibration of the rotary-percussive air driven drills used by stonecutters and rock miners. With increasing technological development, the use of vibrating hand-held tools expanded and epidemiological reports by associations whose members were exposed to

hand-transmitted vibration (for example, quarrying, mining, foundries, ship and aircraft manufacture) appeared with increasing frequency in the medical literature.

Modern medical studies have proved that regular exposure to excessive vibration produces serious irreversible diseases of fingers and hands called Hand-Arm Vibration Syndrome (HAVS). HAVS is a general term embracing various kinds of damage including vascular, neurological, muscular and other possible kinds of damage.

With constantly increasing number of sufferers from HAVS, the problem of vibration perceived by operators of hand-held percussion machines is a serious, challenging, inter-disciplinary problem. The medical approach to the problem is to investigate the mechanisms of hand-transmitted vibration, to diagnose of the vibration effect on the operator and to develop health surveillance programmes. Administrative measures are necessary in order to carry out preventative programmes, which include the training of staff and circulating of information regarding the nature of risk and signs of injury. The engineering approach is to deal with vibration control through replacing hazardous processes, improving the design of the tools and attenuating the harmful vibration perceived by operators of hand-held power tools.

Needless to say, the most effective way to prevent vibration reaching the operator's hands is to avoid using processes which require operators to hold vibrating surfaces. For example, using an adhesive or welded joint in a fabricated product rather than riveted joints can help to avoid the use of pneumatic hammers; fragmentation of large blocks by employing hydraulic expanding devices inserted into predrilled holes can reduce the use of road drills; mechanisation or automation of the processes can significantly reduce exposure duration of the operator to harmful vibrations.

However, not every process can be replaced or avoided. Despite numerous studies and patent applications in this area, every year thousands of operators of hand-held power tools suffer from HAVS and the government is faced with compensation claims running into hundreds of thousands of pounds. Manufacturers are reluctant to implement new designs unless they offer significant benefits over existing design and manufacturing processes. At the same time, most of the current engineering solutions are not universal or offer only partial reduction of hand-transmitted vibration. Hence, the problem of dynamic analysis and the design of low-vibration percussion power

tools remains a challenging and topical engineering problem. This is the topic of the current study.

There is a large variety of this type of machinery, which can be classified according to type of drive (hydraulic, pneumatic or electric) or direction of impacts (axial or rotary). The electro-pneumatic hammer which is one of the most representative piston-operated vibrating tools and has been widely used as a concrete breaker, hammer-drill and impact ripper in various areas of industry and construction will be analysed in the present study.

1.2 Objectives of the study

The objectives of the research are:

1. To develop a comprehensive dynamic model of a hand-held electro-pneumatic percussion machine which would enable better understanding of the dynamic processes, sources of vibration and their individual contribution to the vibration perceived by the operator, and provide a basis for future optimisation.
2. To investigate mechanisms of interaction between the operator and the tool with the aim of establishing the influence of the operator on the tool's performance and developing a vibration protection system that is independent of the operator.
3. To develop a new design concept for vibration protection of the operator of a hand-held percussion machine by means of rationally matching the characteristics of the source of excitation and structure of the vibration protection system that is independent of the operator.

1.3 Outline of the thesis

The rest of the thesis is organised into seven chapters.

Chapter 2 is concerned with the medical aspects, measurements and standards of hand-transmitted vibrations. The chapter contains a brief description of diseases associated with hand-transmitted vibrations, current data on the HAVS as an

occupational hazard and main factors influencing cause-effect relationship for hand-transmitted vibration. The main principles of measurements and standardisation of hand-transmitted vibration are also described.

Chapter 3 is devoted to the dynamic modelling of an operator's hand and arm. It contains a detailed literature review on existing models of the dynamic response of a hand-arm system and describes the methodology behind the experiment that was carried out in the present study in order to develop a dynamic model of hand and arm that was subsequently used for further investigations of operator-machine interactions.

The dynamics of a hand-held percussion machine is studied in Chapter 4 using an electro-pneumatic hammer as the basis. Development of the dynamic model of an electro-pneumatic hammer and numerical simulations of this model are presented. Results of numerical simulations confirm general assumptions about the nature of the main sources of vibration and provide information on their individual contribution to the vibration perceived by the operator of an electro-pneumatic hammer.

Chapter 5 presents a literature review and analysis of methods of reducing harmful vibration of hand-held percussion machine. The chapter consists of three parts that discuss the reduction of the intensity of sources of vibration, vibration isolation and dynamic absorption. In conclusion, the specific criteria for design of a percussion machine with reduced hand-transmitted vibration are formulated.

Optimisation of the excitation of an electro-pneumatic hammer with the aim of improving the performance of the tool and reduction of vibration perceived by the operator is presented in Chapter 6. The chapter contains a theoretical analysis of a quasi-optimal striker motion and numerical modelling of an electro-pneumatic hammer with a modified source of excitation.

Chapter 7 is devoted to the development of a new vibration attenuation system which combines principles of vibration isolation and dynamic absorption. The chapter contains dynamic modelling and numerical simulations of an electro-pneumatic hammer with such a vibration attenuation system. Results of

numerical simulations are verified by experiment, details of which are to be found in this chapter.

Chapter 8 summarises the outcomes of the present work, draws conclusions and recommends areas for future work.

Chapter 2

Hand-transmitted vibration

Percussion hand-held power tools typically rely on systematic impacts for demolition or treatment of hard materials. Millions of portable chipping tools, riveting and other types of hammers, concrete breakers, impact wrenches and hammer-drills are widely used in various fields of industry, construction and transport. However, a wide range of such machines presents vibration magnitudes for exposure durations, which are sufficient to produce observable injurious effects. While some effects can only occur in the fingers or hand, the vibration is transmitted further into the body, and the effects it produces there may be more harmful. That is why the term *hand-transmitted vibration* is used for vibration entering the body through the hand.

2.1 Medical aspects

Hand-held percussion machines are convenient in service, highly efficient and adaptable for various types of work. At the same time, a specific feature of this kind of machinery is a high level of produced vibration and constant direct interaction between the operator and the machine.

Exposure of the hands and fingers to vibration can result in a complex combination of signs and symptoms of physiological disorder. Mild disorders include skin redness and swelling on the fingers. These effects are usually temporary in nature and pose no serious medical problems. However, regular exposure to excessive vibration produces serious irreversible diseases of fingers and hands called hand-arm vibration syndrome (HAVS).

It has been suggested that these disorders caused by exposure to hand-transmitted vibration could be grouped into the following types [1]:

- Vascular disorder was first discovered in 1918 and casually linked to hand-arm vibration exposure. It was originally called *Vibration White Finger* (VWF) or *Raynauld's syndrome* (after Maurice Raynauld, a French physician who first described it in 1862). VWF is triggered by cold temperature and appears as impaired blood circulation and the tingling, numbness and blanching of affected fingers and parts of the hand. Some persons exposed to prolonged periods of vibration develop cyanosis and gangrene.
- Bone and joint disorders occur as pain and stiffness in the hands and joints of the wrist, elbow and shoulders.
- Peripheral neurological and muscular disorders include sensory and hearing losses, *Carpal tunnel syndrome* (a median nerve compression disorder), reduced grip strength and dexterity.
- Other disorders (e.g. of the whole-body and central nervous system). A generalised syndrome of "vibration disease" includes symptoms such as fatigue, vertigo and headaches, the causes of which are difficult to establish. There is also a suggestion that vibration-exposed workers who develop vascular symptoms of HAVS may develop noise-induced hearing loss.

The effects of hand-transmitted vibration are cumulative and as time passes, the attacks may involve considerable pain and loss of manual dexterity, resulting in clumsiness and reduced grip strength. In severe cases, blood circulation may be permanently impaired and fingers may take on a blue-black appearance. After the onset of vascular and neurological symptoms, the longer an individual is exposed to vibration, the worse the symptoms become. The degree to which symptoms regress on removal from exposure to vibration is not known with any certainty. The present

limited evidence suggests that the neurological symptoms do not improve, but the vascular symptoms may do so after some years have elapsed. This is thought to be the case if the individual is below 50 years of age and the vascular symptoms have not progressed to the severe stage.

According to Health and Safety Statistics [2] the number of new cases of VWF assessed to disablement benefit in Great Britain was 3212 in 1999/2000 and has remained fairly constant over the last five years with an average of some 3140 cases annually. Of the cases assessed in 1999 and 2000, 85% of workers had been employed in coal mining, 3% in ship building, repair or breaking, 5% in other manufacturing industries and 4% in construction. A survey in 1997/98 gave a national prevalence estimate of 301 000 sufferers from VWF and these numbers do not include sufferers from carpal tunnel syndrome and other diseases caused by hand-transmitted vibration.

VWF and vibration-related carpal tunnel syndrome are both prescribed diseases under the Department for Work and Pensions (DWP) Industrial Injuries benefit Scheme. In recent years there have been several high-profile compensation awards for VWF. In one case, a recent High Court judgment will lead to compensation awards to over 140,000 retired coal miners and their families at a total cost of up to £3 billion [3]. To estimate the costs of VWF to the economy, values need to be placed on the following: the main costs will fall on individuals through loss of income and increased pain, grief and suffering, but there will also be costs to employers and to society in general. Wider costs to society include extra administration, medical costs and loss of future output. Estimated annual cost of HAV illness is of £447 million, but more importantly, the quality of life of the operators of hand-held power tools is of particular concern. Although research is continuing, there is little effective treatment for the vascular symptoms of HAVS. There is no treatment for its neurological component.

HAVS has gained increasing attention in the literature and is now regarded as one of the most important occupational problems [1-15]. The mechanisms which cause HAVS are very complex. HAVS can be affected by many factors related to work conditions, physical characteristics of vibration and biological susceptibility. The risk assessment of hand-transmitted vibration as well as development of low-vibration hand-held power tools should take all these factors into account, even though their individual importance in the etiology of vibration syndrome is not yet clearly known.

2.2 Measurements and standards of hand-transmitted vibration

Exposures to hand-transmitted vibration are complex and cannot be simply quantified, because it is a combination of different factors such as axes, frequency and type of vibration, method of calculating vibration magnitude, exposure duration, operator's posture and etc. There is extensive clinical literature on HAVS. Although it is apparent that these diseases are associated with vibration, which is transmitted through the hand, there has been no unanimity as to the mechanisms causing it. This uncertainty together with a wide variety of hand-held power tools and operating processes has raised a need for uniform evaluation of risk of hand-transmitted vibration exposure. Therefore, it is necessary to develop and follow consistent standards for the measurement and the assessment of human exposure to hand-transmitted vibration.

2.2.1 Vibration axes

The vibration along one direction of a hand-held machine may differ from that in an other direction. The dynamic response of the hand-arm system also varies with different directions of motion. Therefore, there is need for universally defined axes along which vibration should be measured. The possible co-ordinate systems for the hand, according to British Standard [16, 17], are shown in Figure 2.1.

Here, the axes of the basicentric coordinate system are related to the specific direction of the tool or workpiece, while axes of biodynamic system are related to the hand. In practice, the axes are often decided for each tool or type of operation and there is no universal method. For example, the x -axis may be defined with respect to the tool features, the y -axis may be along the axis of the handle and the z -axis may be perpendicular to the above two axes. However, the choice of the co-ordinate system is very important in measurements, evaluation and standardisation of vibration produced by hand-held power tools, so if standard axes are not used, an alternative orthogonal system should be reported.

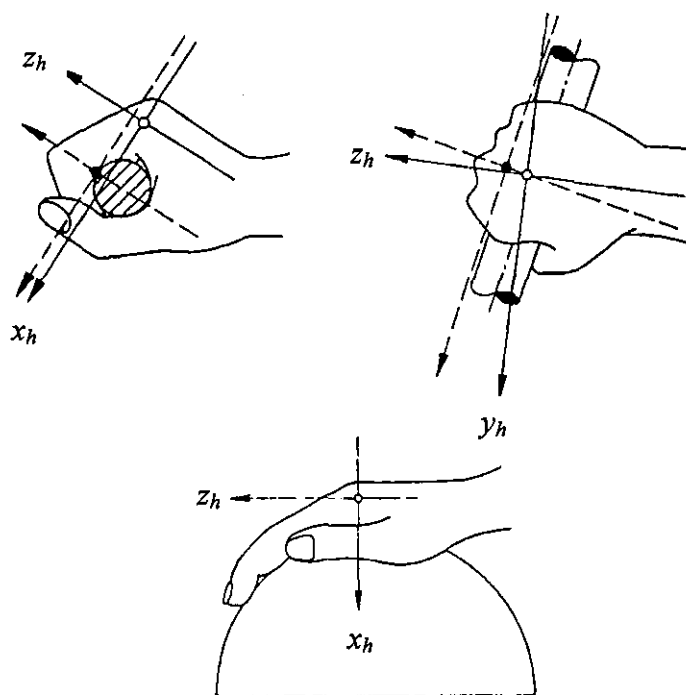


Figure 2.1. Co-ordinate system for the hand (reproduced from [16]);

— - biodynamic coordinate system, ---- basicentric coordinate system

With the axis not defined in an universal manner for all tools, it is difficult to decide on a universal method of evaluating vibration, which differs between the axes. ISO 5349 [18] required that vibration be assessed in the dominant axis only. The currently proposed revision of ISO 5349 [16, 17] specifies that the root-mean-square (r.m.s.) of the weighted values in the three axes should be the basis of the assessment. However, such vibration evaluation might underestimate the harmful effect of vibration produced by percussion machines, which have dominant components in one axis, and overestimate severity of tools powered by internal combustion engines, which often have significant components in all axes [19, 20].

2.2.2 Vibration type, magnitude, frequency and duration

Exposure to hand-transmitted vibration is quantified in terms of the acceleration of the surface in contact with the hand. The acceleration of the surface is normally expressed in units of meters per second squared (m/s^2) or acceleration level (dB). The acceleration level is defined as

$$L_h = 20 \lg \left(\frac{a}{a_0} \right),$$

where a is the r.m.s. acceleration, m/s^2 ; a_0 is the reference acceleration of 10^{-6} m/s^2 . If the single value is required root-mean-square magnitude is usually quoted.

According to the current standards, the human perception of vibration differs depending on frequency of vibration and, therefore, frequency weighting should be employed when vibration transmitted to the operator is reported. Here, frequency weighting is used to modify a signal spectrum according to required dependence on vibration frequency. In human response to vibration, various frequency weightings have been defined in order to reflect known or hypothesized relationships between vibration frequency and the various human responses.

Frequency weighting of hand-transmitted vibration based on the assumption that low frequency vibration, from 5 to 20 Hz, is thought to be potentially more damaging (because vibration is transmitted to the arm) than higher frequency vibration. Vibration at frequencies below 2 Hz and above 1500 Hz is not thought to cause damage. To allow for this frequency dependence, a frequency weighting is applied to measurements of vibration magnitude. The frequency weighting function is shown in Figure 2.2

At the same time, some researchers have suggested that the standardised weighting curve is unsuitable for the assessment of VWF and have proposed that it should not be used for assessing vibration emitted by percussive tools. It was shown [12, 14, 15, 22] that because of the shape of the frequency-weighting curve allowing very high magnitudes at high frequencies, the rank order of importance of tools is significantly changed. When choosing between tools with different vibration spectra, but the same frequency-weighted vibration magnitudes, acceleration will not have the same unweighted magnitude and may not have the same potential for

causing injury. Therefore, unweighted acceleration might be preferable to assess vibration exposure and health risk [21, 23].

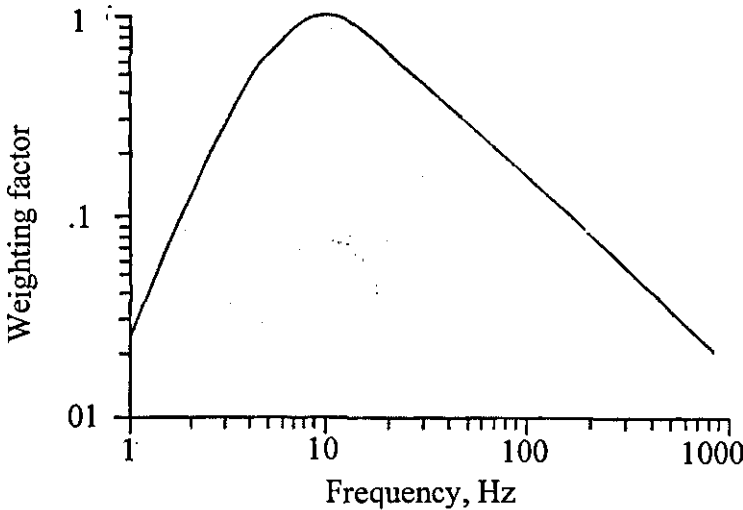


Figure 2.2. Frequency weighting function (reproduced from [6]).

The impulsiveness of acceleration, perceived by an operator of hand-held percussion machine, is another important factor to consider in the design and the risk assessment of percussive machines in use. The measurement of the r.m.s. acceleration of vibration as well as calculation of frequency-weighted magnitude of acceleration do not take into consideration the short and high peak values of the vibratory signal. According to several authors, shock-type vibration might have an underestimated influence on the human and, therefore, produces a higher prevalence of vascular disorders than non-impulsive vibration [24-29]. It was suggested that the impulsiveness of vibration may create shock waves in tissues, and these waves may be transmitted at a higher velocity and to larger body areas than nonimpulsive vibration. Shock-type vibration has also been associated with effects on the locomotor apparatus of the hand-arm system, especially located at the wrist and elbow. A strong association was found between the development of finger blanching and use of impulsive tools (jack hammers, electric hammers, stopper drills and etc.). On the contrary, studies have also been presented where no difference was found between shock-type and non-impulsive vibration [30].

Although there is no final conclusion on how the impulse character of vibration perceived by an operator of hand-held percussion machines affect the risk of

developing HAVS, the mechanism of measurement and evaluation of impulsiveness of vibration is necessary. Assessment of impulsiveness can be based on the fact that if impulses are short, the r.m.s. level remains low in comparison with the peak level. Hence the impulsiveness of a signal can be estimated as the difference between the peak amplitude and r.m.s. of the signal.

Neither peak, not average measures reflect the importance of the duration of the vibration motion: the peak value is determined by the magnitude at one instant while the r.m.s. magnitude can either increase or decrease with increasing duration. In practice, vibration characteristics vary greatly from moment to moment, so the period over which the r.m.s. magnitude should be determined is not always apparent and the r.m.s. value can sometimes be an inappropriate measure. For example, cumulative measure – *energy-equivalent* magnitudes of hand-transmitted vibration seems to be more reliable. An inverse relationship between the exposure duration and the square of the frequency-weighted acceleration is convenient for instrument manufactures and familiar to engineers as an “energy” or “power” relationship.

Further, the daily exposure usually expressed in terms of the 8h energy equivalent frequency-weighted root-mean-square acceleration, is $a_{hw(eq,8h)}$. If the total daily exposure to vibration is other than 8 h, the 8 h energy equivalent acceleration is determined by integration of the square of the frequency-weighted acceleration over the whole of the daily exposure:

$$a_{hw(eq,8h)} = \left\{ \frac{1}{T_{(8)}} \int_{t=0}^{t=T} [a_{hw}(t)]^2 dt \right\}^{1/2}, \quad (2.1)$$

where $T_{(8)}$ is 28 800s (i.e. 8h); T is the total duration of working day in hours; $a_{hw}(t)$ is the instantaneous value of frequency-weighted acceleration in m/s^2 .

Hence, daily exposure is used as a base for the assessment of vibration exposure, in order to facilitate comparisons between different durations of exposure. This concept has not been justified by epidemiological or experimental data but might be employed as being so far the only practical method commonly available.

So far, magnitude of acceleration perceived by the operator was considered as one of the main factors responsible for HAVS. However, there have been several studies on alternative methods of measuring the influence of shock-type vibration on humans. The human hand and arm are elastic systems that can store potential and

kinetic energy. Potential energy is stored as a result of the relative compression or extension of tissues. Kinetic energy results from the motion of tissues in the hand and arm. In an ideal system (i.e. without damping), the vibration results in the transfer of energy between the hand-arm system and the tool and the time average transfer is zero. However, the hand-arm is a highly damped system. Hence, part of the energy is absorbed. This part can be determined as follows:

$$P = \text{Re} \int (\nu(\omega) \cdot F(\omega)) d\omega, \quad (2.2)$$

where Re is the real part of the complex integral, ν the complex velocity vector and F is the complex conjugated force vector.

Assuming that a higher quantity of absorbed energy per unit time represents an increased risk of vibration injuries or reduction in comfort [1, 28, 29, 31], the amount of energy absorbed in the human hand and arm can be used for the risk assessment of hand-transmitted vibration.

L. Burstrom *et al* [31], for example, measured the mechanical energy absorption in the hand-arm system over the frequency range of 4 to 1000 Hz. Using the results of this investigation for all three vibration directions, the mean value of mechanical impedance was calculated and compared with ISO 5349 [18] vibration acceleration limit curve. Authors conclude that international standard underestimates the risk of the development of vibration injuries, especially for exposure in z direction below 60 Hz and above 200 Hz as well as for frequencies above 600 Hz in x direction. On the contrary for frequencies below 100 Hz and 16 Hz the standard overestimates the risk for vibration exposure in the x and y direction respectively. Nevertheless, in the absence of evidence for the benefits of using alternative methods, r.m.s. averaging is commonly used.

The extent of damage caused to the hand and arm also depends on the frequency of the energy being transmitted from the vibrating surface. There is strong evidence that vascular disorders of the fingers occur most often with tools having their dominant frequencies of vibration in the approximate range 25-250 Hz. However these findings may arise either because they are the most common frequencies on vibrating tools or because they are the most damaging frequencies [1]. It is commonly (although not universally) assumed that the frequency range of significance is from 8 Hz to about 1000 Hz.

2.2.3 The influence of individual factors on the effects of human exposure to hand-transmitted vibration

The vibration level and frequency of the vibration have a strong influence on the magnitude of the quantity of energy absorbed by an operator and consequently vibration effect [28]. The reason for this is probably changes in the dynamic mass of the hand-arm system. When the amplitude of vibration increases, a major part of the hand-arm system is mechanically activated. The energy-consuming part of the system therefore increases and leads to the possibility of more energy dissipation in the hand and arm.

The grip and feed force also increases when the vibration level increases. One possible explanation could be contraction of the muscles when the hand-arm system is exposed to vibration, so-called tonic vibration reflex (TVR). Even smooth vibration of the modern chain saw is capable of causing this reflex. An uncontrolled increase in muscle tone may interfere with natural protective reflexes, and therefore increase risk of having an accident. An increase in muscle tone also increases the transmission of vibration in the hand-arm system. The reason for this phenomenon could be that higher tension allows vibrations to put a larger part of hand-arm system in motion which causes the apparent mass of hand-arm system to increase, leading to increased absorption [31].

The direction of the vibration transmitted to the hand, area of contact with vibration, operator posture (angles of wrist, elbow and shoulder joints), subject variability and other mechanical factors influence the “dose” of vibration received by an individual. The hazardous effects of occupational exposure depends also on several factors related to work conditions, e.g., physical characteristics of vibration, how the tool is handled and differences in work involved, types and conditions of vibrating machinery. To establish the injurious potential of a vibration exposure it may be necessary to consider the temperature, tool weight and other non-vibration conditions. The risk assessment of hand-transmitted vibration should take all these observations into account, even though their individual importance in the etiology of vibration syndrome is not clearly understood.

2.2.4 Hand-transmitted vibration standards

The first approach to prevent HAVS is to control vibration exposure. However, knowledge of the dose response relationship of vibration exposure is incomplete and cannot be relied on to prevent symptoms in all workers. At the same time, the mechanism of hand-transmitted vibration is very complex and depends on so many factors that it is impossible to define risk of vibration exposure by a single figure. The procedures defined in the current standards imply how injuries depend on vibration frequency, direction and duration, but they are greatly influenced by practical convenience and desire for uniformity between countries. Reliable scientific evidence of the relative injury potential of vibration of different frequencies, directions and duration is not available.

In order to gain some guidance on conditions, which may be hazardous for the operator, an “action level” can be used [32]. Exposures, which are higher than the action level, are not necessarily prohibited. But if vibration magnitude exceeds this level, source of vibration must be investigated and caution should be exercised in whether such exposures cause health problems.

Figure 2.3 shows the r.m.s. acceleration, peak velocities and peak to peak amplitudes of displacements corresponding to the action levels for periods of 0.5, 2 and 8h.

These action levels were obtained in accordance with the old standard BS 6842 [32] (now withdrawn) where the vibration was measured in three directions, but the exposure was calculated from the magnitude of vibration in the *dominant axis* only. The Physical Agents (Vibration) Directive defines an exposure action value (EAV), $a_{hw(eq,8h)} = 2.5 \text{ m/s}^2$ and an exposure limit value (ELV), $a_{hw(eq,8h)} = 5 \text{ m/s}^2$. However, these quantities are based on the *vibration total value*, a vibration magnitude obtained from measurements in three directions, using the method defined in the new standard BS EN ISO 5349 [16, 17].

The *vibration total value* is greater than the *dominant axis* magnitude by a factor of between 1.0 and 1.7 (depending on the tool type), but has been found to be about 1.4 on average. Thus, the current action level $a_{hw(eq,8h)} = 2.8 \text{ m/s}^2$ (given in the current HSE guidance on hand-arm vibration [6] and obtained in accordance with the old standard BS 6842) is approximately 4 m/s^2 daily exposure expressed as a

vibration total value. This means that the current action level lies between the proposed exposure action and limit values.

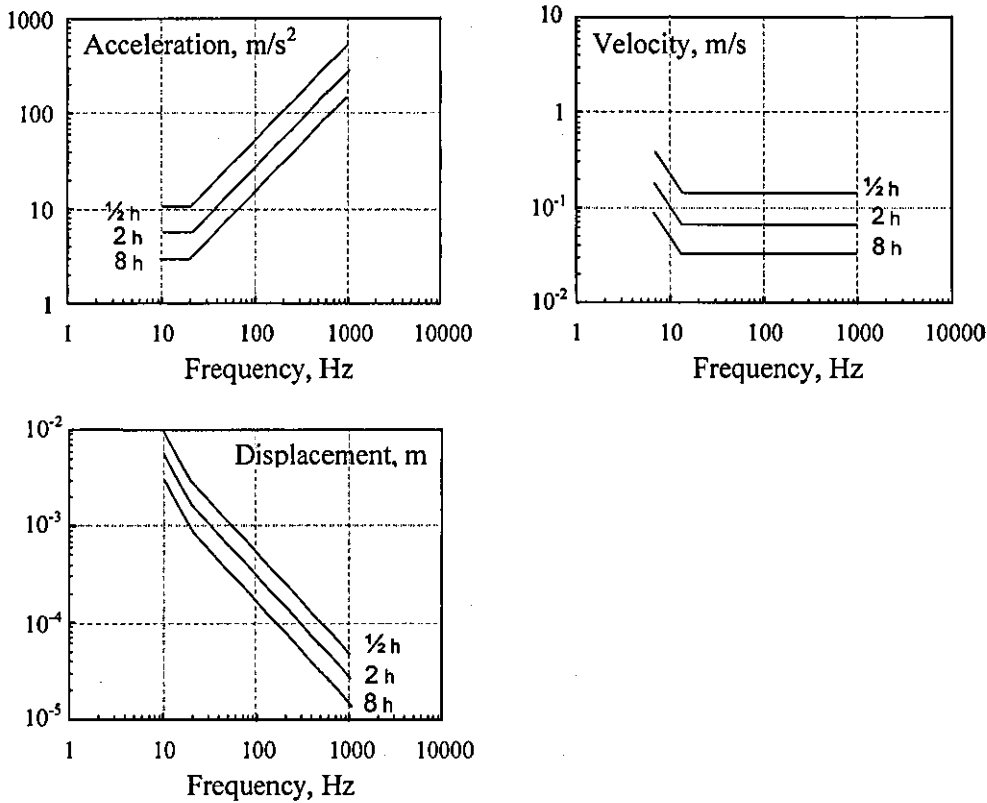


Figure 2.3. Root-mean-square accelerations, peak velocities and peak to peak displacements of sinusoidal vibration corresponding to 0.5, 2 and 8h action levels derived from BS 6842 (redrawn from [1])

If the vibration magnitude is sufficiently great, the probability of developing finger blanching increases with increased years of vibration exposure. There is some evidence that the cumulative exposure before the first onset of finger blanching in inversely proportional to the magnitude of the frequency weighted acceleration. Vibration acceleration magnitudes which may be expected to produce finger blanching depending on time of work presented in Table 2.1.

Such a way of assessment of vibration exposure allows fairly high magnitudes of vibration at short durations, thereby neglecting the probable harmful effect of short impulses with high magnitude. There is also currently no agreed way of allowing for intermittent exposures, either variable tool use over a week, over a month or over

years. This means that severe short-term exposures might be rated lower by averaging the exposure over a year.

Table 2.1. Frequency-weighted vibration acceleration magnitudes (r.m.s. m/s^2) which may be expected to produce finger blanching in 10% of persons exposed [32].

Daily exposure	Life-time exposure					
	6 month	1 year	2 years	4years	8years	16 years
8 hours	44.8	22.4	11.2	5.6	2.8	1.4
4 hours	64.0	32	16	8.0	4.0	2.0
2 hours	89.6	44.8	22.4	11.2	5.6	2.8
1 hours	128.0	64	32	16.0	8.0	4.0
30 min	179.2	89.6	44.8	22.4	11.2	5.6
15 min	256.0	128	64	32.0	16.0	8.0

NOTE 1 *With short duration exposures the magnitudes are high and vascular disorders may not be the first adverse symptom to develop.*

NOTE 2 *The numbers in the table are calculated and the figures behind the decimal points do not imply an accuracy which can be obtained in actual measurements*

NOTE 3 *Within the 10% of exposed persons who develop finger blanching, there may be a variation in the severity of symptoms.*

There are a number of various studies investigating the nature of hand-transmitted vibration, proposing new methods of assessing its hazardous effect and revising the current standards that are out of scope of present work. Unfortunately, in spite of a great number of studies in this area, the nature of hand-transmitted diseases is still poorly understood. This fact makes the development of the safety standards rather a difficult task. There are many factors which will limit the accuracy of modern standards for predicting the effects of hand-transmitted vibration, it would therefore be wise to use standards as a guidance, bearing in mind complexity of the hand-transmitted vibration and its effect on the operator.

2.3 Conclusions and discussions

Prolonged exposure to hand-transmitted vibration from hand-held percussion machines is associated with an increased occurrence of symptoms and signs of disorders in the vascular, neurological and other systems of the hand and arm. The complex of these disorders is usually referred to as HAVS.

The model illustrated in Figure 2.4 shows complex interactions between some of the many relevant HAVS variables [1]. Here *latency of disorder* is duration before symptoms develop; *prevalence* is occurrence of some sign or symptom in a group at some instance of time and, finally, *incidence of disorder* arises when low prevalence caused by persons entering the group and by persons leaving the group.

The available exposure and epidemiological data are insufficient to establish a clear exposure-response relationship for disorders caused by hand-transmitted vibration [19]. The results of various studies seem to indicate that the current ISO frequency-weighting method may be unsuitable for all types of vibration and for all kinds of vibration injury. The r.m.s. averaging also has potential risk of underestimating vibration emitted by percussive tools. This method of evaluating hazardous vibration does not include high acceleration peaks usually produced by this type of machinery. However, there is still no alternative method for evaluating exposure levels and assessing the HAVS hazards adapted by standard organisations.

With uncertain knowledge of human responses to vibration, the use of standards requires care. The current guidance is derived from limited quantitative data available from both practical experience and laboratory experimentation and based on limited information regarding current exposure conditions. Changes may be anticipated as research reveals the mechanisms of the various effects of vibration on human body. It is suggested that attention is required to avoid the misdirection that could arise from guidance based on consensus, which is not firmly supported by understanding [19].

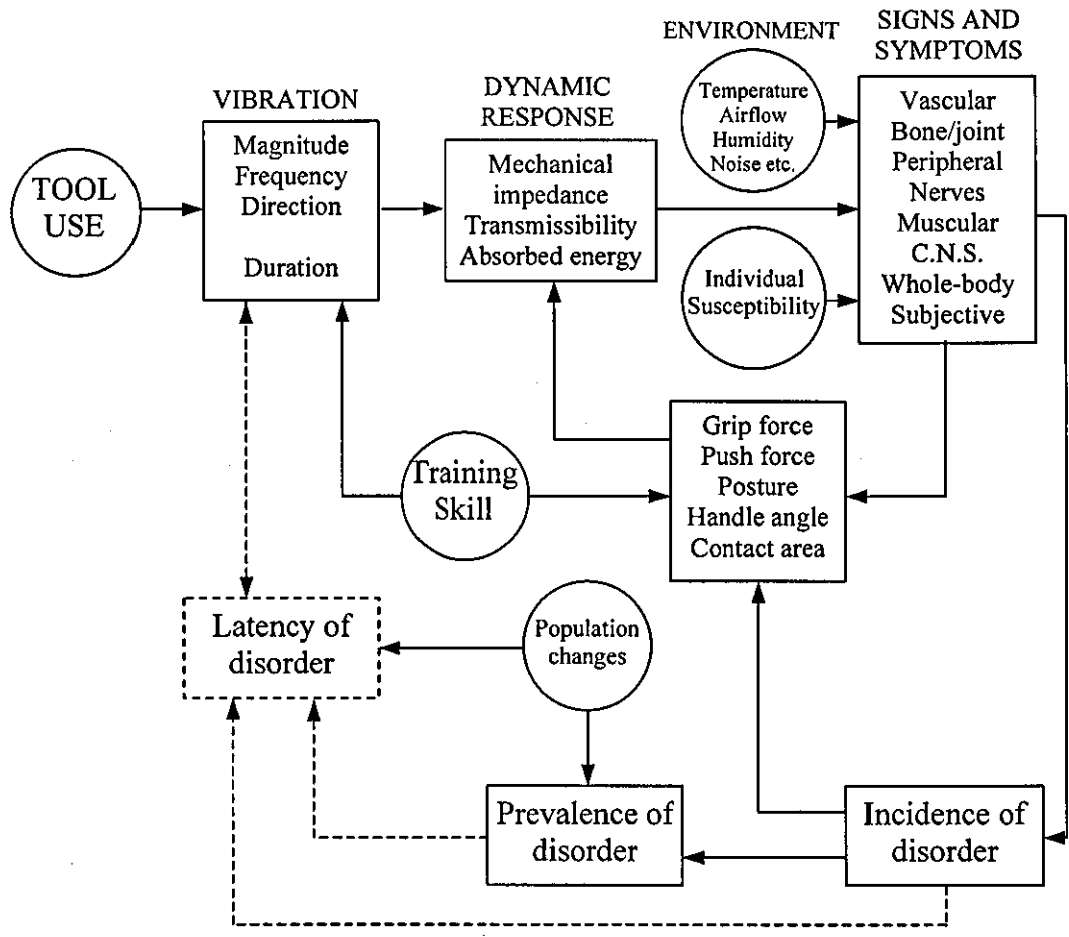


Figure 2.4. Conceptual illustration of factors influencing cause-effect relationships for hand-transmitted vibration (redrawn from [1]).

Because of the uncertainties surrounding dose-response of hand-transmitted vibration, one possible strategy for prevention of HAVS is not detailed prescriptive legislation but rise of awareness of employers and others of the risks and development of practical guidance and methods to reduce operator exposure to vibration.

Chapter 3

Models of the dynamic response of hand-arm system

The specific feature of the hand-held percussion power tools is the constant direct interaction between the operator and the tool. The operator, while holding the tool and pressing it against material being treated, significantly influences dynamic behaviour of the whole operator-tool system. It seems obvious that dynamic analysis of a hand-held percussion power tool should include a dynamic model of an operator-tool interaction.

A number of biodynamic models of hand-arm systems and their mechanical equivalents have been proposed to study the vibration amplitude and power flow in coupled hand, tool and work-piece system. The employment of such models offers potential for the development of a mechanical hand-arm simulator to enable efficient and consistent relative evaluations of different hand-held power tools during experimental studies and considerably reduces the risk of human subjects taking part in the experiment [33, 34]. On the other hand, such models could provide support for analysis and assessment of low-vibration hand-held power tools and protective devices through development of coupled hand-machine analysis models [35, 36].

Although dynamic models of hand and arm have been developed over the past 30 years there is little evidence of their application [33, 34]. The lack of applications

contributed to the complexity of the hand-arm system and, therefore, difficulties to create a model which will be in a good agreement with experimental data, but will not be overcomplicated.

In a simple classical vibration theory the vibrating mass is considered to be rigid and connected to a support by a spring and damper. In most biological systems the model is not so simple because the stiffness and damping are usually distributed throughout the body. The distributed system may be thought of as an infinite number of elements with springs and dampers all connected together, which will make mathematical description rather difficult. Approximations describing these systems in terms of a finite number of rigid bodies with external spring and dampers have been used successfully in dynamic modelling and are called *lumped parameters* systems. The main disadvantage of such a representation is that the stress state of each elementary body of the system is not known. However, these models are simpler than distributed parameters models and provide essentially all the information relating to the interaction of the system with its surrounding which makes the lumped parameters models convenient and widely used for biodynamic hand-arm models.

One approach for obtaining the response of the hand-arm system is to measure the *mechanical impedance* of the hand holding a handle mounted on a laboratory vibrator. Mechanical impedance magnitude is the ratio of the amplitude of the imposed driving force, to the amplitude of the resulting velocity when both are measured at the driving point:

$$Z(j\omega) = \frac{F(j\omega)}{v(j\omega)} \quad (3.1)$$

where $Z(j\omega)$ is the complex driving point mechanical impedance of a rigid body, ω is the frequency and v is the velocity. The impedance is commonly expressed in terms of the magnitude, $|Z(j\omega)|$ and phase, $\theta(j\omega)$ between the applied force and driving point velocity.

The real and imaginary components of driving point mechanical impedance are more than mathematical constructs, but they have important physical significances. The real part is proportional to the power actually dissipated by the system in the form of heat. As was mentioned previously, the significance of mechanical power dissipation in biological systems has not been finally determined (see Section 2.2.2).

The absorbed or dissipated power can therefore be calculated from the real part of the impedance times the driving point velocity squared.

The imaginary part is due to those components that do not dissipate power but simply transfer energy back and forth from the kinetic to the potential form. Kinetic energy is associated with body displacement or distortion, which produces a spring type restoring force. If displacement and distortion are too great, physical damage or modification of the system will occur.

The impedance is usually measured using sinusoidal excitation, but the concept can be extended to other types of excitations such as random or impulse excitations.

The human body is a very complex system, any attempt to exactly model it, or even part of it, would be an extremely difficult task. Therefore, it is necessary to examine the physical conditions that exist in the hand-tool interaction in order to determine what simplifications could be made in the modelling of the hand-arm system. However, there is still no sufficient data for agreement on which factors need to be included in the biodynamic model of a hand-arm system, how to evaluate experimental results or what is the best representation of such models. This causes an existing range of biodynamic models of human hand and arm from single-degree-of-freedom (SDOF) linear models to four-degree-of-freedom non-linear models. All of these models seem to be in good agreement with reported experimental data, however there is a lack of agreement between different models. The basic theories and experimental techniques that are currently employed for the development of biodynamic models of hand-arm system and several examples of such models are briefly considered further.

3.1 One- and two-degree-of-freedom models

C.W. Suggs [37] developed one of the first dynamic models of the human hand as overdamped SDOF linear system with natural frequency of about 77Hz and loss factor of 2.5 (mass of about 0.0454kg , a stiffness of approximately 10508N/m and a damping factor of about 108Ns/m), where natural frequency and loss factor were calculated as follows:

$$\Omega = \sqrt{\frac{k}{m}} \quad (3.2)$$

$$\zeta = \frac{c}{2m\Omega} \quad (3.3)$$

where m – mass, k – stiffness and c – damping ratio of the system.

The developed model is shown in Figure 3.1 and should be considered as a model of a hand-arm system for each direction of vibration axis independently.

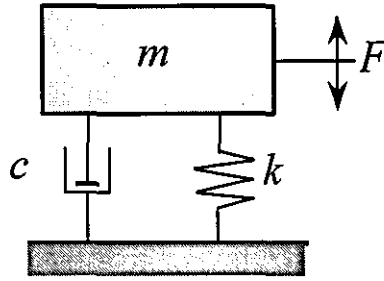


Figure 3.1. Rigid mass-spring damper system (adapted from [37]).

The experimental studies involved a steady state sinusoidal testing using a cadaver arm as well as live human subjects in a working position, for which driving point mechanical impedance techniques were used. The model has been validated based on this study for vibration in the range from 70 to 1670Hz and acceleration levels less than 10g peak to peak amplitude. This model does not take into account influence of a grip force (it was only suggested that tighter grip physically increases the effective stiffness of the tissue and elevates the force transmitted) and the mechanism of vibration transmitting into an upper arm. However, the model is simple and in good agreement with experimental data, therefore it can be used as basic model of operator-machine interaction.

D. D. Reynolds and W. Soedel [38] proposed three uncoupled SDOF mechanical models to characterise the biodynamic response of the human hand and arm under vibration in the 20-500Hz frequency range. Although the study suggested that two- and three-degree-of-freedom models are required to describe the biodynamic behaviour, a two-stage piecewise linear SDOF model with two sets of parameters applicable in two different frequency ranges was identified for each axis of vibration. Parameters of their model were: mass $m = 0.308\text{kg}$, natural frequency $\Omega = 25\text{Hz}$ and

loss factor $\zeta = 0.7$ for the excitation frequency range between 20 Hz and 73 Hz and $m = 0.0219\text{kg}$, $\Omega = 79\text{Hz}$ and $\zeta = 3.94$ for excitation frequency above 73Hz. Authors reported that within the limits of assuming a normal position for holding a vibrating tool, the position of the arm and the fact that the arm may be either relaxed or stiff have little influence on the vibrating characteristics of the hand-arm system. The tightness of grip and the firmness of handle pressure were found to have a significant influence upon the vibrating response of the hand-arm system.

Miwa *et al* [39] proposed an equivalent electric circuit, where correspondence of mass to capacitance was used. The mechanical analogy of the proposed circuit was obtained as a two-degree-of-freedom semi-definite system, as shown in Figure 3.2.

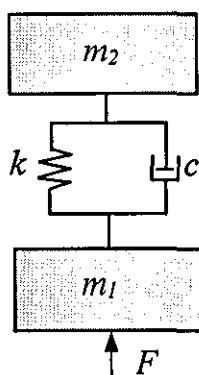


Figure 3.2. Dynamic model of the hand-arm system (adapted from [39]).

The mechanical impedance response was derived from the experiment in 10-1000Hz frequency range with constant the sinusoidal vibration acceleration level at 0.2g in two (y and z) vibration directions, while grip force was selected as 80N. Two feed force values were used: 50N and 80N. The results in y direction indicated that the peak was near 80Hz and a notch was near 250Hz. For z direction, the pattern of curve of mechanical impedance is similar to one in the y direction, but the peak and the notch are seen at about 35Hz and 120Hz respectively. Masses were calculated as 0.1kg and 0.8kg for z direction and 0.05kg and 0.3kg for y direction. Damping ratios were found to be 250Ns/m and 50Ns/m for z and y direction respectively.

3.2 Three- and more degree-of-freedom models

J. W. Mishoe *et al* [35], R. Gurram *et al* [40] and D. D. Reynold *et al* [41] have presented a number of linear three-degree-of-freedom models.

J. W. Mishoe and C. W. Suggs [35] proposed a linear dynamic model with structure presented in Figure 3.3. The number of tests involved a handgrip force of 13, 27 and 40N and was performed under vibration along the three axes in the 20-2000Hz frequency range. In the study, sinusoidal vibration with acceleration level of $6.93m/s^2$ was used as a standard and variations with respect to this level of input were investigated. Data for five subjects were collected.

On the basis of measured data, three-degree-of-freedom semi-definite mechanical equivalent models were proposed to characterise hand-arm system under x and y axes of vibration, where the axes of vibration were defined according to Figure 2.1.

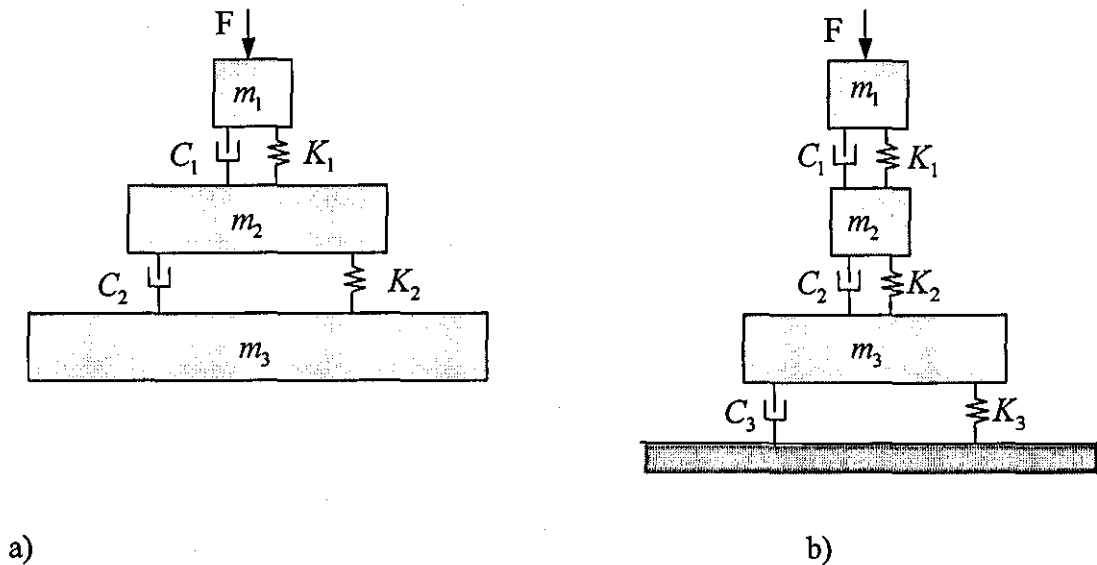


Figure 3.3. The dynamic model of the hand-arm system (reproduced from [35])

a) y and x vibration directions

b) z vibration directions.

A three-degree-of-freedom model with fixed support characterised the hand-arm system under z direction of vibration. The first body, m_1 , represented the mass of the tissue which was in contact with the handle. The value of this mass was very small and decreased as the handgrip force increased for all acceleration levels tested. The

second body, m_2 , in the model took a value of between 0.045kg and 0.09kg for all tests. This value is equivalent to between 10 and 20 percent of the apparent mass of the hand. The last body, m_3 , in the model can be assumed to be the remaining tissues of the hand, the wrist, and part of the forearm. The value of this mass tended to be unrelated to handgrip but it increased as acceleration level increased.

The authors concluded that the hand, in general, was a highly damped system with the damping increasing with increasing handgrip force and increasing acceleration level. As the frequency increased, the action of the body furthest from the input decreased as the spring and damper associated with it absorbed the vibration. At the same time, vibration transmitted up the arm decreased. This process continued and each of the elements became less active as the frequency increases with the lower elements being affected first. This finally resulted in a very small layer of tissue being excited at the upper frequency values of about 1000Hz and above. The absorbed power in this region, however, did not decrease, resulting in large amount of energy being dissipated in small volumes of tissue. Parameters of this model are represented in Table 3.1.

R. Gurram and S. Rakheja [40] proposed similar linear three-degree-of-freedom model with fixed support. The tests were conducted in 10-1000Hz frequency range for three orthogonal vibration axes and three different levels of grip forces (10, 25 and 50N). The used excitation levels (in case of sinusoidal excitation) were $10m/s^2$, $20m/s^2$ and $30m/s^2$ peak, and $0.2m/s^2$, $0.5m/s^2$ and $0.7m/s^2$ r.m.s. in the case of the stochastic excitation. The four individuals were asked to grip the vibrating handle with their dominant right hand in a specified standing posture and maintain nearly constant grip force throughout the experiment. The authors concluded that measured impedance data exhibited a high degree of inter-subject variations that may be attributed to the differences in weights and sizes of hands of the subjects. The effect of grip force and excitation frequencies on the driving point impedance was found to be significant. Grip force dependent restoring and dissipation constants were introduced. The impedance characteristics measured under sinusoidal and stochastic excitations differed. The parameters of this model are represented in Table 3.1.

The differences in parameters observed for these two similar models can be associated with dissimilar test conditions (vibration level, hand position, type of

excitation and etc.), variability among subjects that are participated in these tests and method of solution or parameter identification.

Table 3.1. Parameters for linear three degree of freedom biodynamic models of human hand and arm (adapted from [35, 40]).

Author(s)	Vibration axis	Grip force, N	Model parameters**
Mishoe and Suggs [35]*	x	27	$m_1=0.00081, m_2=0.041, m_3=0.943$ $K_1=1.804, K_2=119.4, C_1=110, C_2=54$
	y		$m_1=0.004, m_2=0.063, m_3=0.354$ $K_1=12.1, K_2=111.9, C_1=643, C_2=217$
	z		$m_1=0.017, m_2=0.023, m_3=0.49$ $K_1=1.58, K_2=112.4, K_3=69.7,$ $C_1=159, C_2=102, C_3=102$
Gurram et al [40]	x	25	$m_1=0.0065, m_2=0.274, m_3=3.82$ $K_1=25.53, K_2=0.11, K_3=591.5,$ $C_1=81.1, C_2=35, C_3=8560$

NOTE: * Mishoe and Suggs excitation level- 6.93m/s^2 r.m.s. acceleration;

Gurram excitation- $10\text{-}30\text{m/s}^2$ peak in case of sine excitation and $0.2\text{-}0.7\text{ m/s}^2$ r.m.s. for random excitation;

** All the mass, stiffness and damping values are expressed in kg, kN/m and Ns/m respectively.

Five-degree-of-freedom linear lumped parameter model has also been proposed to characterise biodynamic response of the human hand and arm by T. Cherian et al [42]. The human hand-arm subject to z axis vibration is represented on Figure 3.4.

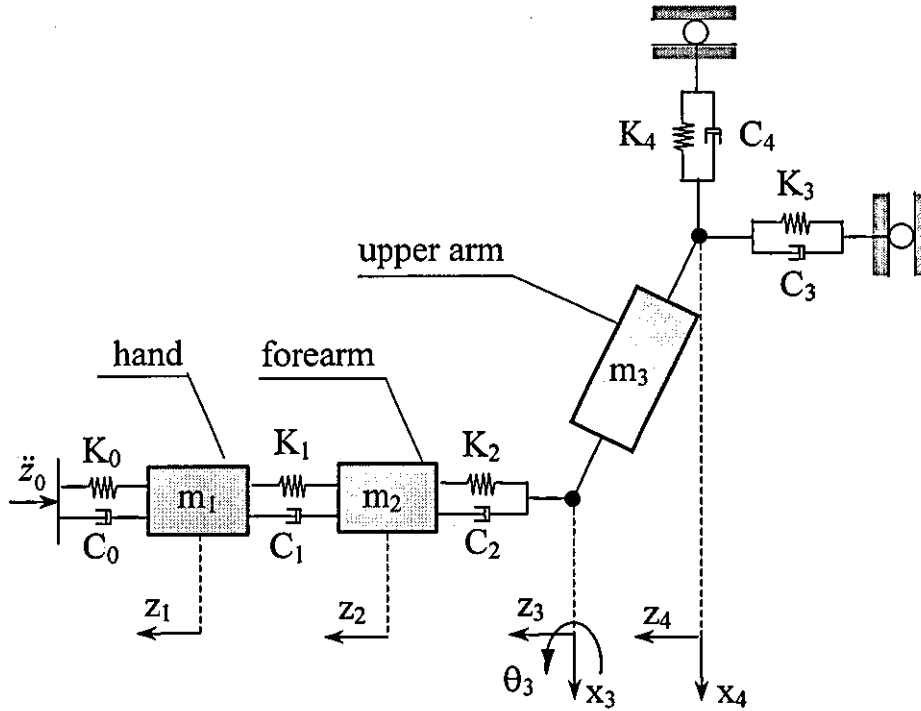


Figure 3.4. Schematics of the five degree of freedom bio-mechanical hand-arm vibration model (reproduced from [42]).

Assuming a given posture, the hand and forearm masses (m_1 and m_2) are constrained to move along the longitudinal coordinate. The m_3 , however, is assumed to undergo longitudinal, pitch and vertical motions due to translational and rotational elasticity of the shoulder and elbow joints. K_0 and C_0 represent the restoring and dissipative properties, respectively, due to visco-elasticity of the tissues of the palm and the hand-handle interface. The measurements were performed for constant sinusoidal acceleration excitations at 14 discrete frequencies in the 10-200Hz frequency range with constant grip force of 25N.

In this study authors did not use the method of mechanical impedance because they believed that models derived from using this method did not reflect bio-mechanical properties of the hand-arm system. Instead, the vibration transmitted to the hand, forearm and elbow was measured using miniature accelerometers mounted on a specially designed ring and bracelets. The primary resonance of the hand-arm system was identified in the 10-40Hz and 80-150Hz frequency ranges. The visco-elastic parameters of the analytical model and the response characteristics both revealed that less than 20% of impinged vibration was transmitted to the forearm and elbow above 100Hz. An amplification of hand-transmitted vibration, however, was

observed in the 10-100Hz excitation frequency range. The visco-elastic parameters of the analytical model and the response characteristics confirmed that the hand acts as a low-pass filter with most of the vibration energy localised to the hand itself at higher frequency excitation.

The similar four-degree-of-freedom system that included hand, its palmar tissues, forearm and upper arm was developed in [43]. The main distinction of these models was that unlike models obtained by employing mechanical impedance technique, these models were an attempt to describe “through-the-hand-arm” response function, i.e. transmission of vibration to specific segments of the hand and forearm.

3.3 Models with distributed-parameters

L. A. Wood *et al* [44] proposed distributed-parameter models of the entire hand-forearm-upper arm system. Dual beam model of the forearm is shown in Figure 3.5. Distributed mass (expressed as mass/unit length, ρ_1 and ρ_2 for radius and ulna bones respectively) and stiffness (expressed by the module, EI_1 and EI_2) parameters were obtained by representing each long bone of the forearm, the radius and ulna, as a homogeneous flexural member.

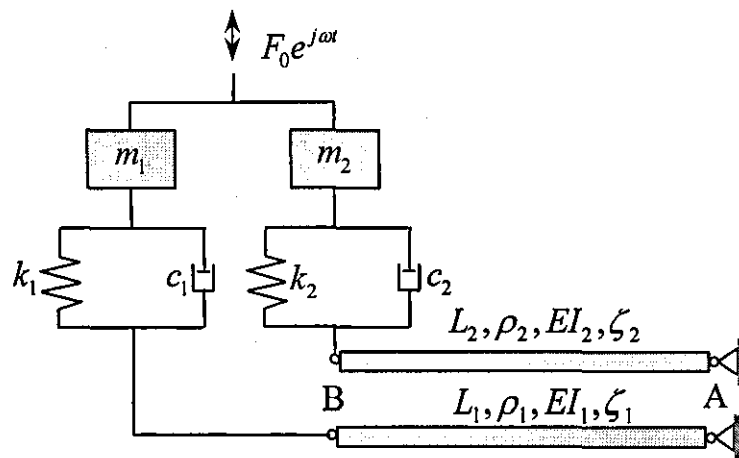


Figure 3.5. Dual beam model of the forearm (reproduced from [44]).

The viscous effect of soft tissues surrounding the bones was characterised by linear damping distributed along the bones (ζ_1 and ζ_2). The effective lengths of the beams (L_1 and L_2) were taken from the distance between the elbow joint and centre

of the gripped handle. The wrist was thus included as part of the two beams. The coupling between the driving point and the arm was represented by a discrete parameter system: a Kelvin viscoelastic model (parallel spring and damping elements) in series with lumped masses (m_1 and m_2), which represented the mass of tissue material of the hand.

Impedance data of the forearm was collected over a frequency range from 30 to 1000Hz under vibration in z direction (see Figure 2.1) and magnitude of 0.5g r.m.s. acceleration. Data for two subjects were collected. In order to isolate the upper arm from the forearm, the subject's elbow was supported on the molded elbow rest, while gripping a 25mm diameter handle mounted on a vibration exciter with a specific grip force. The proposed model was analysed to derive its impedance response under vibration along the z axis alone, using the transfer matrix approach. The distributed damping was incorporated in the model by considering complex beam stiffness. The impedance was obtained upon considering that the beams were hinged at the left end "B" and allowing the velocity at the right end "A" to vanish from the equation for mechanical impedance.

The model of the hand and forearm provided reasonable agreement with the measured data, unfortunately, the driving point mechanical impedance response of the total hand-arm model resulted in a poor fit.

Although the validity of each model in predicting the biodynamic response acquired in the particular study has been well established, there was considerable difference among the various models. As was mentioned already, experimental conditions and methods of obtaining analytical expressions for experimental curves are vary from one study to another. S. Rakheja *et al* [45] evaluated 12 reported mechanical equivalent models of the hand and arm system in an attempt to identify a suitable model that could be used for experimental and analytical representations of human hand and arm. The evaluation was performed using the following two criteria: (1) the driving point mechanical impedance of the human hand-arm system must lie within the ranges recommended by ISO-10068 [46] and (2) under a steady feed force the model must provide the range of deflections and vibration properties displayed by the human hand and arm. Authors concluded that three- and four-degree-of-freedom models, in general, showed acceptable driving point mechanical impedance characteristics while responses of the distributed parameter, single- and two-degree-of-freedom models lied outside the ISO-recommended limits.

At the same time, the majority of high order models invariably consisted of very light bodies and elastic elements with low stiffness and therefore excessive deflections occurred under application of steady feed force which made them inappropriate for using as mechanical hand-arm simulator. However, this criterion chosen by authors could be argued about, because under applied static load the human hand behaves rather like an active system with a feedback and strongly depends on the hand-arm posture.

According to the authors, high damping ratios that possessed by majority of these models may constrain their potential application. To conclude, the necessity of further studies using modern measurement methods was emphasised.

The present study is devoted to an analysis and development of a low-vibration hand-held percussion machine. Feed and grip force applied by an operator affect dynamics of hand-held machine and should therefore be included into the analysis. On the other hand, uncertainty about mechanisms of hand-transmitted vibration, a wide variety of existing bio-dynamic models of the hand and arm and inter-subject variability reported by a number of research suggest that effective system of vibration attenuation should be independent of parameters of an operator. Hence it would serve no purpose to include complicated dynamic model of the hand-arm system into the dynamic model of the hand-held percussion machine, because it would increase very rapidly the degree of difficulty of analysis of such a model while accuracy of results would still be doubtful. In order to reflect basic operator-machine interaction in a dynamic model of hand-held percussion machine, the simplest SDOF dynamic model would be ideal. The SDOF model developed in [37] could be used for current investigation, however, this model did not include information on grip and feed force, subject posture and etc. Therefore, for the purpose of present study an experimental study was carried out to obtain a dynamic model of the hand-arm system, which is suitable for further dynamic analysis of percussion hand-held machine.

3.4 Development of dynamic model of human hand-arm system

The technique used to determine the dynamic characteristics of the hand-arm system was based on measurements of vibration force, velocity and phase between these parameters, made as close as possible to the surface of the hand, i.e. method of driving point mechanical impedance (DPMI) was used. This was obtained by using rigid handle mounted on the electro-magnetic shaker through the force transducer. Driving point velocity and phase between driving force and velocity were measured at the same time. A diagram of the experimental rig is shown in Figure 3.6.

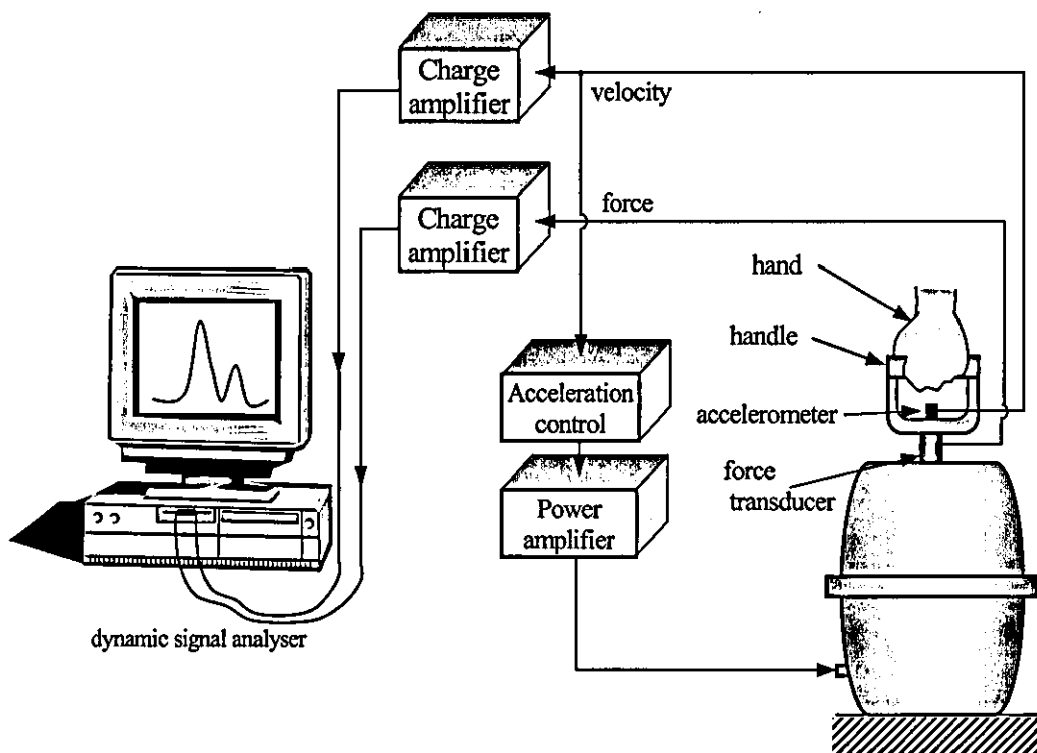


Figure 3.6. Diagram showing the experimental set-up

The handle was mounted on the electro-dynamic shaker (Ling Dynamic System, model V550) driven by digital vibration controller (LDS DVC 48) and power amplifier (LDS PA 500) as shown in Figure 3.7.

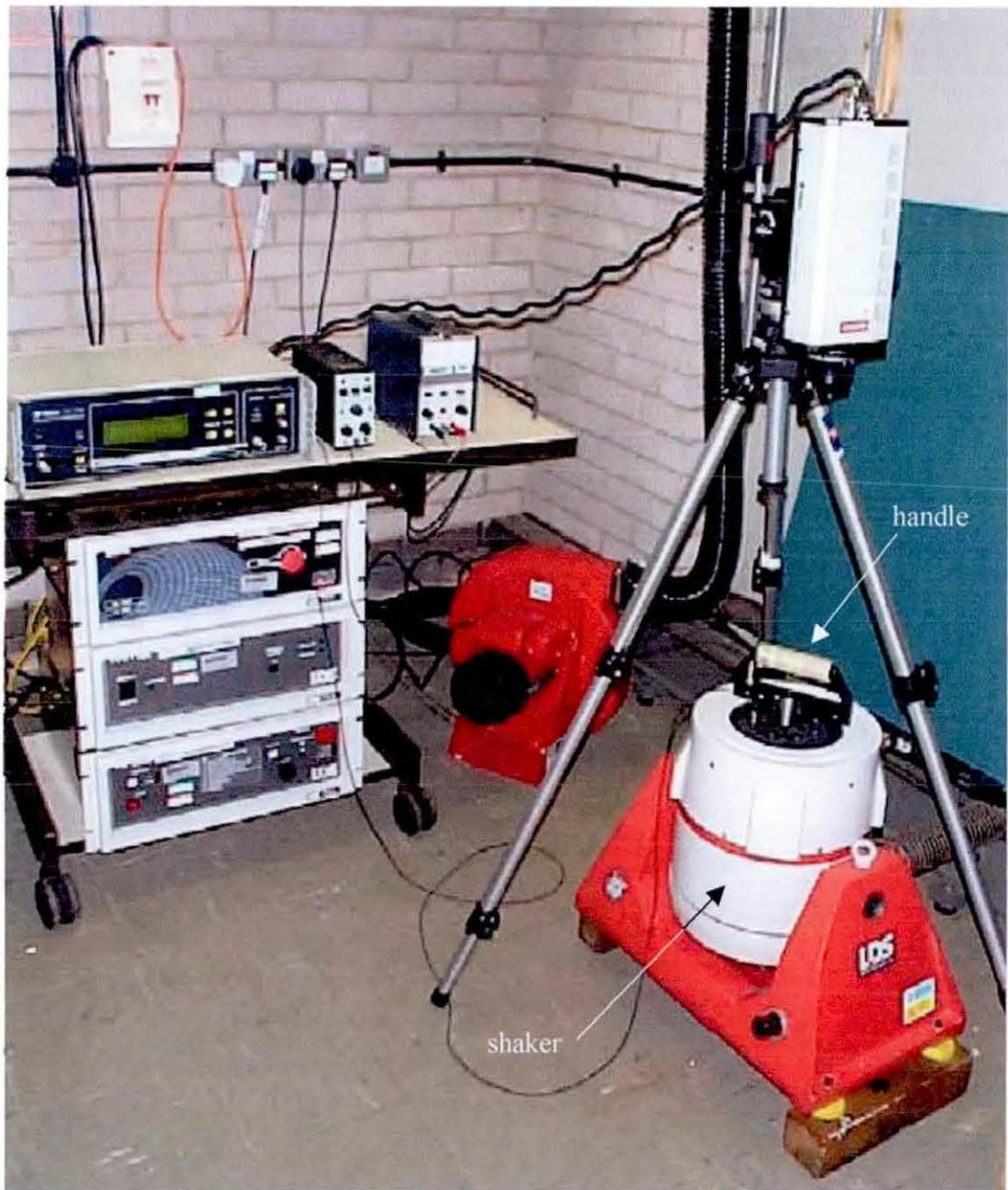


Figure 3.7. The experimental rig.

Sinusoidal vibration with acceleration amplitude $1.5g$ peak was applied to the handle at increasing frequencies from 10 to 500Hz. The sweep rate was 50s for each frequency decade. The output from the accelerometer was amplified and integrated to velocity by the charge amplifier (Brüel & Kjær, Type 2635) before it was sent to the dynamic signal analyser (Data Physics Corporation DP 104). The second accelerometer was attached to the shaker's mounting table and its signal was sent to the feed-back network facility on the vibration controller to maintain the acceleration

amplitude constant, independently of the frequency and the dynamic load. The output from the force transducer (Brüel & Kjær, Type 8200) placed between the shaker and the handle was amplified by the charge amplifier (Brüel & Kjær, Type 2635) and then sent to the dynamic signal analyser.

The handle was of a rigid stiff construction in order to avoid distortion due to resonance within the frequency range of interest. The first resonance for the unloaded handle, for the vibration direction, was at 1350Hz. No resonance was observed for other axes. The handle weight was of 200g and diameter of 38mm (see Figure 3.8).



Figure 3.8. The electromagnetic shaker with mounted handle.

The study was carried out on four healthy right-handed subjects with no previous professional exposure to vibration. Figure 3.9 shows the working hand-arm posture that was used to give a vibration exposure in z direction in accordance to BS EN ISO 5349 [16].

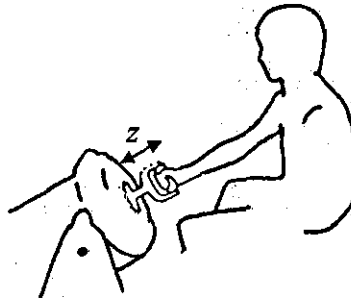


Figure 3.9. Hand-arm postures used in the experiment.

Grip tightness and hand pressure upon the tool handle influenced the vibration response of the hand-arm system, so subjects were advised to hold the handle with normal grip tightness. The posture of the subjects during the experiment was the same as in usual working process. The subjects were asked to ensure that no pull/push forces were affecting the handle.

In each experiment the measured dynamic force, driving point velocity and phase were transferred to the dynamic signal analyser, which calculated the DPMI.

The test was repeated three times for every subject, so the total number of tests was 12. In Figure 3.10 and Figure 3.11 the mean magnitude and phase of driving point mechanical impedance as well as standard deviation for all four subjects are shown. The magnitude of the “between-subject” standard deviation for the results was found to be relatively the same, about 25%, over the frequency range.

From Figure 3.10, mean curve of DPMI magnitude possesses several (even though not very distinctive) hollows, however character of the curve suggests that hand-arm system can be treated as overdamped SDOF system.

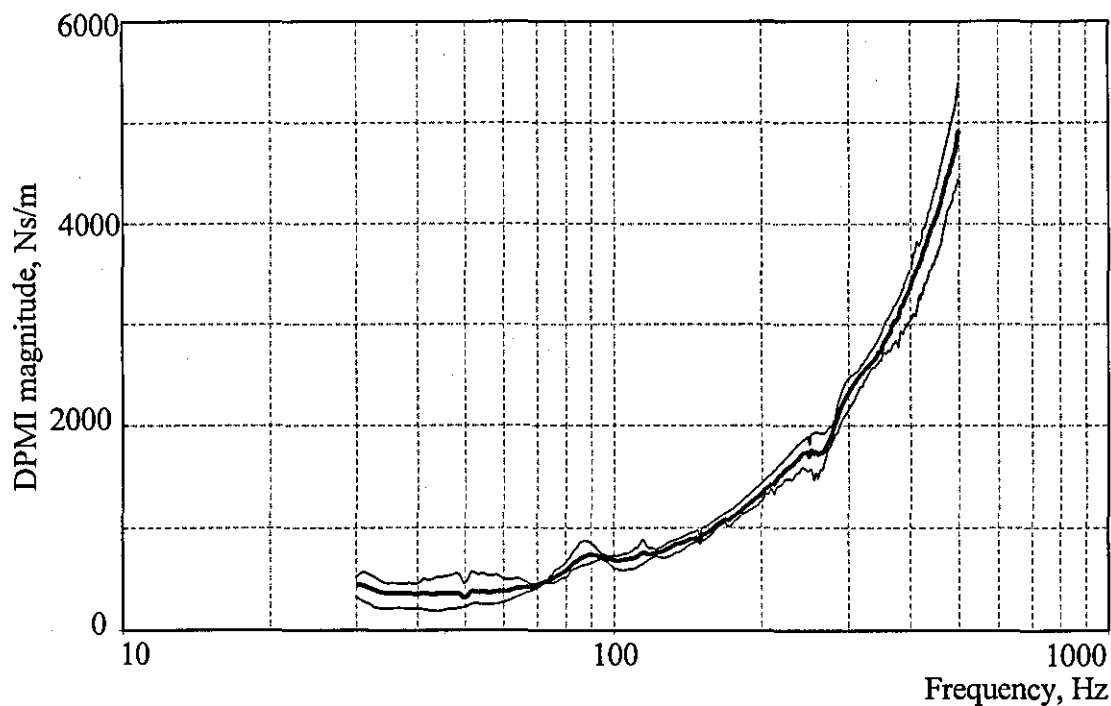


Figure 3.10. The mean value of DPMI magnitude for all subjects (thick line). The standard deviation about the mean values (thin lines).

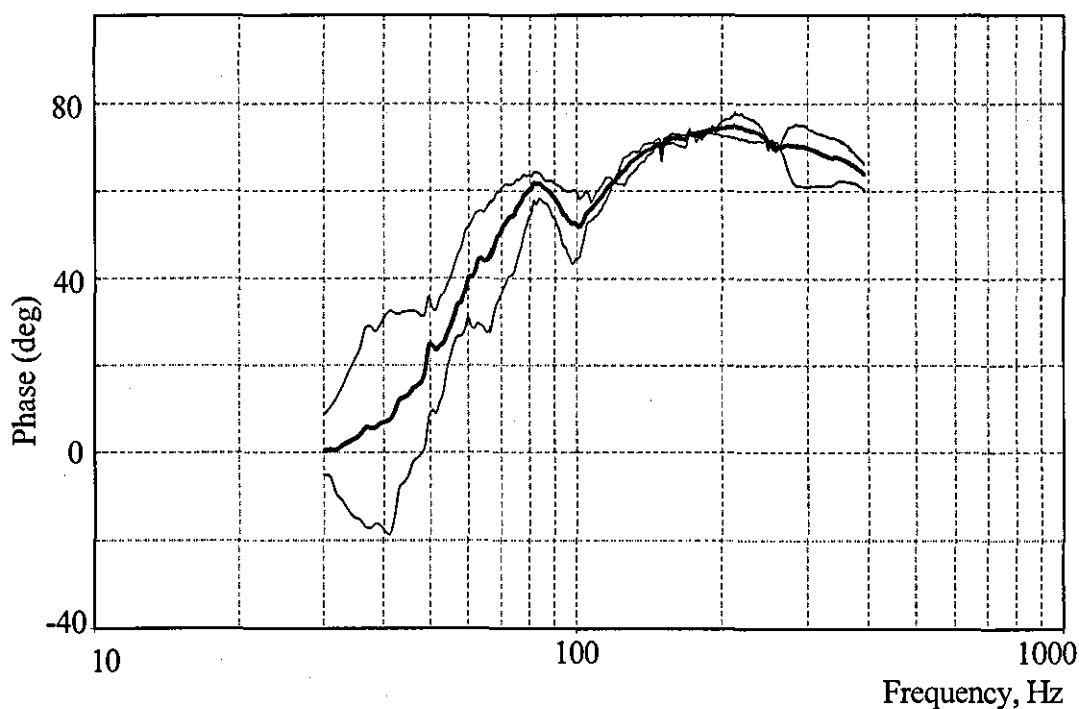


Figure 3.11. The mean value of DPMI phase for all subjects (thick line). The standard deviation about the mean values (thin lines).

If excitation force is applied to the body, for a SDOF system the equation of motion is:

$$m \frac{dv(t)}{dt} + cv(t) + k \int_0^t v(t) dt = F(t), \quad (3.4)$$

where m – mass of the system, $v(t)$ – velocity, $\frac{dv(t)}{dt}$ – acceleration, $\int_0^t v(t) dt$ – displacement, c – damping ratio, k – stiffness and $F(t)$ – driving force.

Taking the Laplace transform from the derived above equation of motion and using formal substitution $s = j\omega$ the following equation is obtained:

$$\left(mj\omega + c + \frac{k}{j\omega} \right) \cdot v(j\omega) = F(j\omega), \quad (3.5)$$

where $j = \sqrt{-1}$ and ω is angular frequency.

Then mechanical impedance, $\frac{F(j\omega)}{v(j\omega)}$, will take the form:

$$Z = c + j \left(m\omega - \frac{k}{\omega} \right). \quad (3.6)$$

where the magnitude and the phase of mechanical impedance are calculated as follows:

$$|Z| = \frac{\sqrt{(k - m\omega^2)^2 + (\omega c)^2}}{\omega}, \quad (3.7)$$

$$\theta = \arctan \left(\frac{m\omega^2 - k}{\omega c} \right). \quad (3.8)$$

The curve-fitting procedure based on the method of least squares was used for system identification. Standard MS Excel Solver procedure was applied to the mean value of DPMI magnitude for all four subjects. Direction of search was determined by the quasi-Newton algorithm, while the number of interim calculations was set to 300 and convergence 0.001.

The Figure 3.12 and Figure 3.13 show the curve-fitting result and the mean value of magnitude and phase of driving point mechanical impedance for all the four subjects.

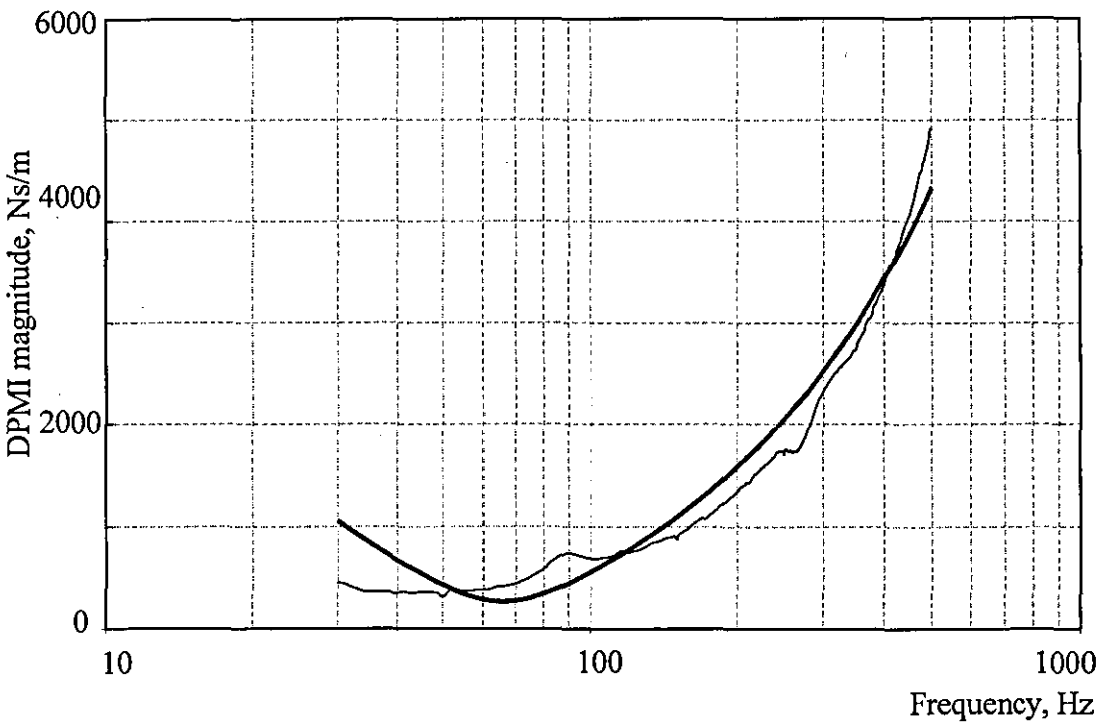


Figure 3.12. Magnitude of driving point mechanical impedance (DPMI).
Experimental-thin line and calculated-thick line.

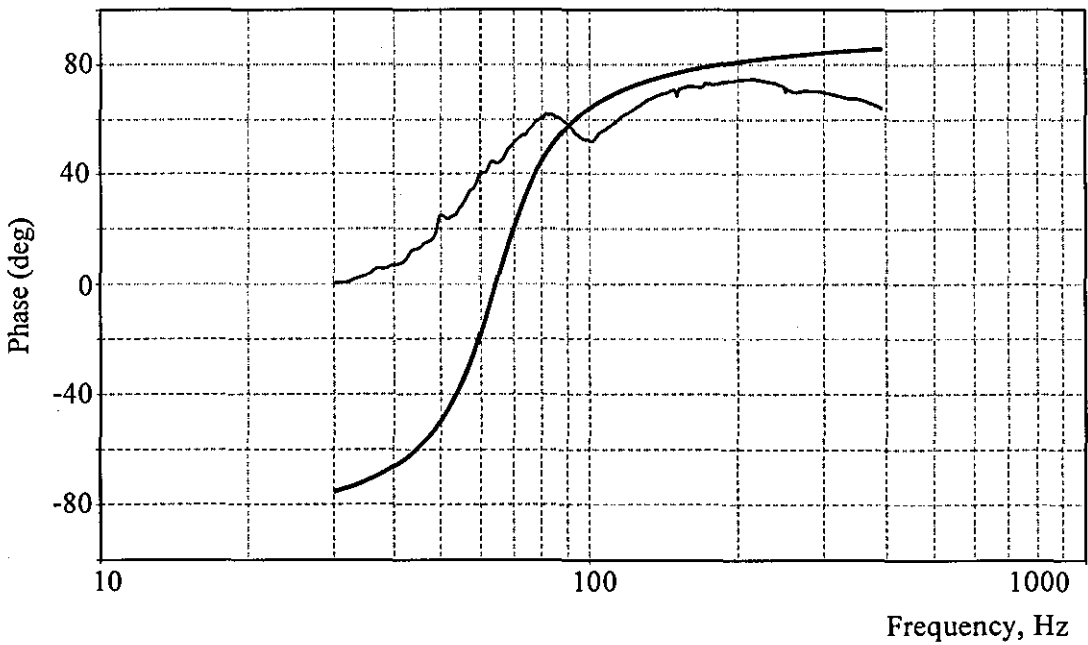


Figure 3.13. Phase of driving point mechanical impedance (DPMI).
Experimental-thin line and calculated-thick line.

While measured and theoretical curve for magnitude of DPMI are relatively close, the difference between measured and calculated phase is significant. Assuming that for the present study an approximation of Magnitude-Frequency characteristic is preferred over Phase-Frequency characteristic of DPMI, the current result of curve-fitting is taken as description for dynamic model of hand-arm system.

Finally, hand-arm system is represented as SDOF system with the following parameters:

Mass, $m = 1.4\text{kg}$; stiffness, $k = 243069\text{N/m}$; damping ratio, $c = 265.4\text{Ns/m}$.

The difference between the obtained dynamic model and SDOF model of hand-arm system reported by Suggs [37] is considerable. It can be explained by several factors: insufficient number of subjects and tests in both studies, the fact that grip force was controlled by subject sense only in the current experiment and was not measured in the study presented by Suggs, the lack of any information about feed force etc.

It should be noted, that taking into consideration all these factors together with wide variation between parameters of existing dynamic models of the hand-arm system (see Section 3.3), obtained values can be used only as a simple description of the operator-tool interaction in the dynamic model of the hand-held percussion machine. Proper allowance must be made for approximate character of such model and, therefore, sensitivity of the final results to the variations of hand-arm system parameters shall be checked.

3.5 Conclusions and discussions

Owing to the large scale of hazardous vibration effect on the operator of the hand-held percussion machine, it is essential to develop a suitable model of the hand-arm system. Such a model could form the basis for the development of a mechanical hand-arm simulator to enable consistent relative evaluations of different tools, and support the analysis and assessment of low-vibration power tools and protecting devices.

There is a number of reported dynamic models of the hand-arm system. Most of them are obtained by using a method of driving point mechanical impedance although there is a great difference between them due to different experimental techniques and results evaluation.

The dynamic model of hand-arm system developed in the present study is very simple and rather approximate. The number of subjects taking part in the experiment, the simple experiment methodology and approximation of results as SDOF system did not allow a universal reliable model to be obtained. The wide range of existing hand-arm models makes the choice of the model that is most suitable for investigation somewhat difficult, and to some extent stimulates the desire of conducting one's own experiment. However, the obtained results suite well the purpose of the reference model that could be used as part of the dynamic model of the hand-held percussion machine. Bearing in mind the difference in physical abilities of operators as well as great variety in parameters of existing hand-arm models, qualitative analysis of results obtained by means of this model must be evaluated.

Chapter 4

Dynamics of hand-held percussion machine

Percussion hand-held tools, which use periodic impacts for the demolishing of or treatment of materials, are widely used in different areas of industry. Pneumatic breakers are used for demolishing concrete structures and road surfaces; at a large steel works, defects in steel casting are removed using pneumatic chisels or chipping hammers etc.

The repeated impacts with very high impact forces in a zone of contact with work-piece make this type of machinery highly productive and irreplaceable in many areas of construction and industry. The design and manufacturing of hand-held percussive machines is relatively simple and inexpensive. Hand-held power tools are highly adaptable for different types of work and direction of impacts, they are easy to transfer and most efficient in cases when stationary machines cannot be used.

The schematic cross section of the electro-pneumatic hammer (see hammer-drill Hilti TE74 as an example) is shown in Figure 4.1.

The electric motor drives the exciting piston via a crank and connecting rod. The piston executing sinusoidal motion compresses the air in the pneumatic chamber, thereby setting striker motion. The striker hits the intermediate piston, which then hits the pick which in turn hits the surface being treated.

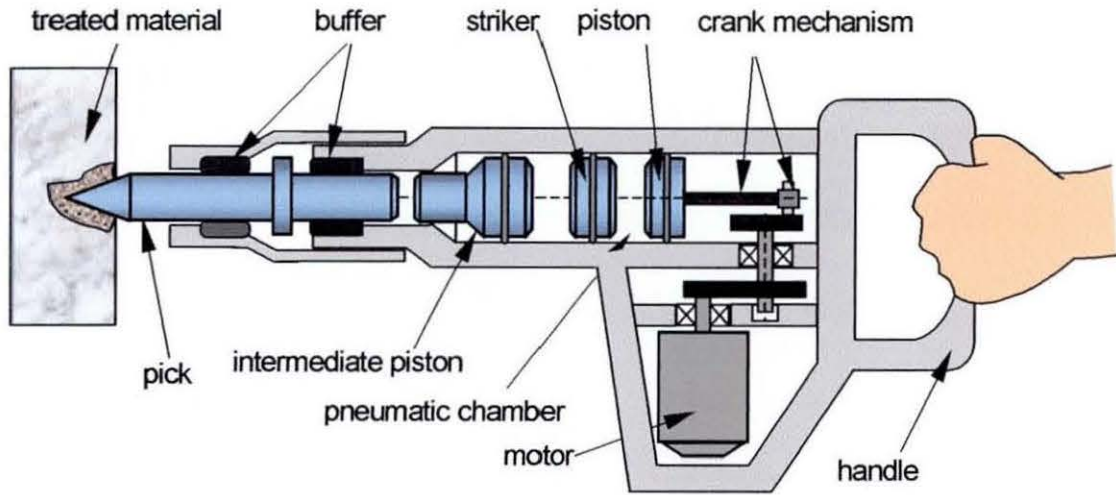


Figure 4.1. Cross-section of electro-pneumatic hammer.

The operator has to press the machine against the object of treatment with permanent force (this is called *feed force*). In order to prevent the pick from going too far into the mechanism while the operator presses the hammer against the surface, the pick has a special ledge, which also limits the pick's motion towards the hammer mechanism after rebound against surface of treatment. So, while rebounding, the ledge of the pick can hit the buffer mounted on the casing. The stiffness of this buffer is usually high in order to avoid large static deflection under applied feed force and to provide operation with minimum number of pick-surface impacts per period.

V.I. Babitsky [48] considered the electro-pneumatic hammer as a discrete pulse modulator which converts the permanent feed force into a series of impulses. In this case, the feed force can be treated as the main factor of transferring energy of constant feed into output series of periodic impacts.

Electro-pneumatic hammers as shown above are manufactured in a variety of sizes from small domestic to large industrial power hammers and can be used with various pick types, however, the main operating principle remains the same.

4.1 Major sources of vibration

The schematics of the electro-pneumatic hammer as it will be considered in present investigation is shown in Figure 4.2. The dynamic model includes the electric drive, the crank-slide excitation mechanism, the striker, the pick and the casing of an electro-pneumatic hammer. The design of an electro-pneumatic hammer has to provide the possibility of replacement of the pick in case it gets damaged or has to be changed as required by operation. Intermediate piston is used in order to avoid direct interaction between the striker and the pick and to make the process of the pick universal. In order to simplify dynamic analysis, intermediate piston (see Figure 4.1) was not included in present dynamic model because its motion was very similar to the pick motion and does not affect the main operation principles of an electro-pneumatic hammer in terms of its vibration activity.

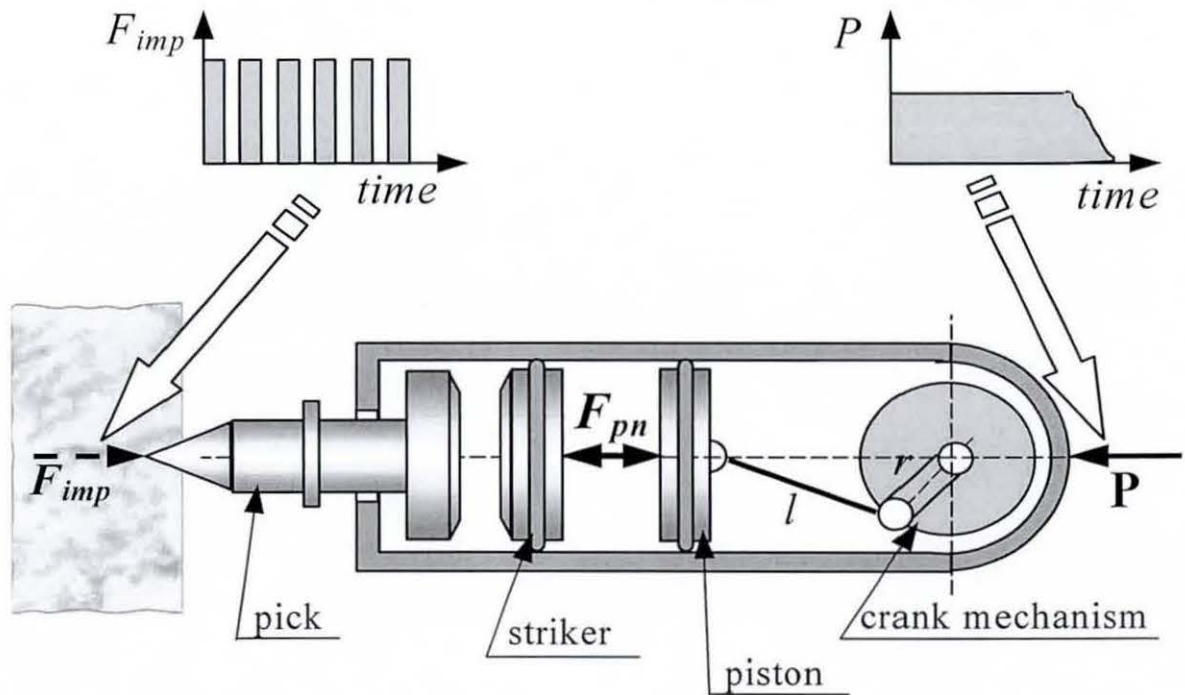


Figure 4.2. Schematics of an electro-pneumatic hammer.

We have considered repeatedly harmful vibration effect on an operator of hand-held percussion machine. Let us consider major sources of this vibration.

First, there is the motion of the striker towards the pick, caused by a pneumatic force between the driving piston and the striker. That force exerts a counter-force applied to the casing of the machine through the stiff crank-slide mechanism. A force, equivalent to the counter-force must be applied to the handle, otherwise the casing would start to move away from the work material. When the striker reverses to start a new stroke, a force on the casing applied by an operator presses it down against the work material. If it were possible to press the hammer against the material being treated with a force much greater than the counter force, the casing would not move. An operator, however, cannot produce such high static forces in the hand-arm system for long periods of time. So the casing may move and this difference between the constant feed force applied by the operator and the periodic force of impact against work material experienced by the operator as vibration. Schematically, this process is shown in Figure 4.2 where the constant feed force applied to the percussion machine as an input which results in a development of a series of high impact impulses produced by the machine at the output. So the difference between the constant feed force and output impact impulses is the main source of vibration that is due to its nature has been often been referred to as vibration due to pneumatic impacts (striker acceleration, counter-force).

The feed force, P , applied by the operator is the main factor in transferring energy of the excitation source into the medium being treated [47-50]. The feed force, which is considered to be the external force, equalises the internal forces that depend on the interaction of the machine as a whole with the object of treatment. This includes both the interaction of the striker with the pick or intermediate piston for processing and the positioning of the machine and the pick in appropriate position against the object of treatment. According to the principle of impulse and momentum, the feed force that is necessary for producing single-impact periodic motion is:

$$P_{ef} = M(1 + R)\dot{x}_-f \quad (4.1)$$

where P_{ef} – effort of feed from the operator;

M – mass of the striker;

R – coefficient of restitution of impact interaction between the striker and the pick;

\dot{x}_- – striker velocity just before impact against the pick;

f – frequency of impacts.

In practice, a series of secondary impacts against the material is produced by the pick after its rebound against the buffer mounted on the casing. This leads to an increase in necessary feed effort and imposes additional stress upon the operator. Therefore the expediency of the hand-held machine, from this point of view can be estimated by means of coefficient of feed effectiveness [48]:

$$\lambda = \frac{P_{ef}}{P}, \quad (4.2)$$

where P – actual feed effort applied by the operator.

Thus, the feed force of the operator is a more essential part of the whole operating process than it had been considered in previous investigations.

The output of the machine is defined as the energy of the striker before impact:

$$E_- = 0.5M\dot{x}_-^2 \quad (4.3)$$

Substitution of formula (4.1) into (4.3) yields the following relationship between the energy of impact and the feed force[48]:

$$E_- f^2 = \frac{1}{2(1+R)^2 M} P_{ef}^2, \quad (4.4)$$

Formula (4.4) shows a straight relationship between the feed force and the output, produced by the machine. From formula (4.4), an increase in the productivity, either from the rise of impact energy or frequency, can be achieved by the increasing P_{ef} . Usually, the manufacturer specifies the particular force for a particular machine without considering changes that occur in the operator response over the duration of work and possible differences between individuals' physical abilities. This disregard for feed force may affect final productivity of the machine. Hence, operator-machine interaction should be included in a dynamic analysis of hand-held percussion machine.

The second source of vibration is the force of impact between the pick and the buffer mounted on the casing. This impact arises when the pick rebounds against the treated material or the whole hammer has been pressed against object of treatment. It should be noted, that some designs (especially machines with pneumatic or hydraulic

type of drive) allow avoidance of these impacts as will be shown in Chapter 5. However, in the electro-pneumatic hammer under investigation this force is present and is of significant value as will be shown later.

It is obvious that there are some other sources of vibration in hand-held percussion machines. Unbalanced rotating parts as well as axis misalignment of reciprocating parts, poor finish and etc. might cause additional noise and vibration perceived by an operator. However, these are not principal but mainly manufacturing defects, which can be eliminated by careful design and engineering development and, therefore, will not be considered in the present study.

Jahn et al [34] developed a software program to simulate the motion of a percussion drilling machine and showed the main sources of vibration produced by such a machine. In this study, the dynamics of the hand-arm system was simulated by a three-degree-of-freedom lumped parameter model, which was valid in the frequency range from 10 to 500Hz. The simulating program included parameters such as length of the pneumatic chamber, driving piston diameter, the crank arm radius, the casing, the feed force, etc. Results of the simulations are presented in Figure 4.3.

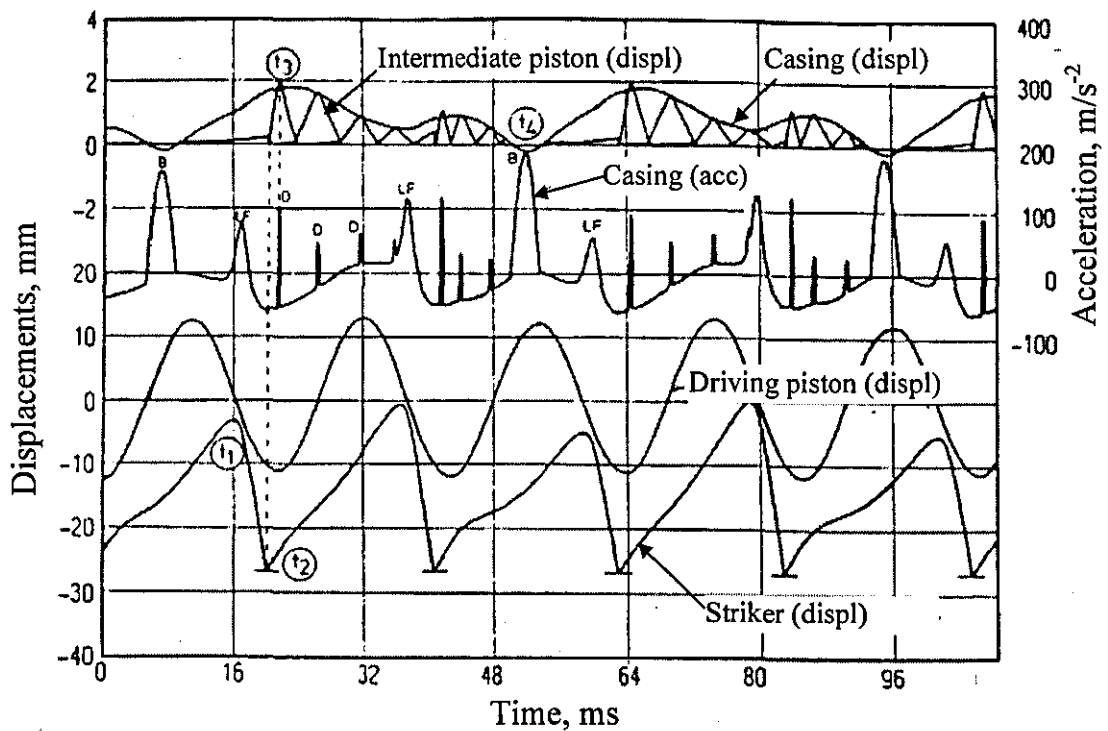


Figure 4.3. Displacement and acceleration of several hammer-drill elements (adapted from [34]).

The curve of the casing acceleration has distinctive acceleration peaks superimposed on a base curve similar to a sine wave. This curve results from a combination of the pneumatic impact between the piston and the striker (the peaks which are indicated by “LF”) and the collisions of the intermediate piston with the buffer, which lead to narrow but high peaks (indicated by “D”). The casing of the hammer-drill hits the collar of the intermediate piston during its motion towards the treated material (peaks “B”).

To summarise, the dilemma of distinguishing between “good” and “bad” vibration is particularly challenging in case of hand-held percussion machines, as the main operating principles of such machines are responsible for hazardous effect on the operator.

4.2 Development of the dynamic model of electro-pneumatic hammer

The objectives of the present study are to investigate the dynamics of a hand-held percussion machine and reduce harmful vibration produced by the machine and transmitted to the operator. Therefore detailed dynamic analysis that will include all main operating principles and all interactions between parts of the machine that are responsible for vibration is necessary.

Figure 4.4 shows the dynamic model that has been developed in the current study. The pneumatic impact in the pneumatic chamber between the striker and the driving piston, impact of the striker against the pick, impact between the pick and the buffer mounted on the casing, the crank-slide mechanism and the interaction between the pick and the object being treated have been included in the developed dynamic model as factors responsible for vibration. As was mentioned previously, the interaction between the operator and the machine is an important factor to consider in the dynamics of hand-held percussion machine. In order to include the coupling between the operator and the machine in present dynamic analysis, SDOF lumped parameter system has been introduced between the handle of the machine and rigid attachment on the right-hand side (see Figure 4.4). Hazardous vibration in the direction parallel to the stroke is believed to be the most significant, therefore, to

investigate the dynamic processes in the electro-pneumatic hammer, a one-axis lumped parameter model is suggested, while vibration in other directions is neglected.

The model reflects mutual interactions between all major components of the machine and also the “operator”-“machine” and “machine”-“treated material” interactions in the direction parallel to the stroke.

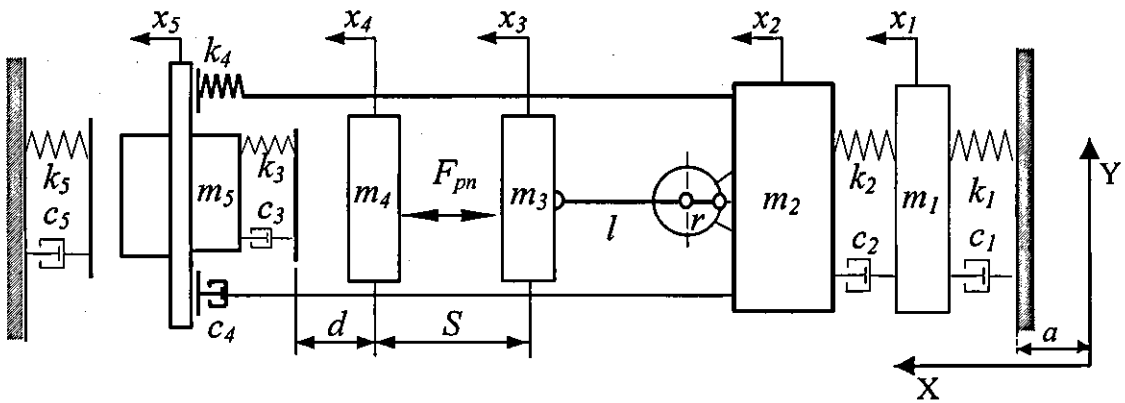


Figure 4.4. Dynamic model of the electro-pneumatic hammer.

The feed force, produced by an operator, is accounted for by changing parameter a , assuming that the attachment on the left-hand side is fixed (see Figure 4.4). Here a is the distance between origin of absolute co-ordinates $(0, 0)$ and the attachment of the system on the right-hand side. Parameters of SDOF model representing hand-arm system of an operator are following: $k_1 = 2.43 \times 10^{-5} \text{ N/m}$, $c_1 = 265 \text{ Ns/m}$, $m_1 = 1.4 \text{ kg}$. These values were obtained from the experiment which relied on the method of mechanical impedance and is described in Chapter 2.

Periodic impacts, produced by the hammer, cause the destruction of the treated material and the whole machine moves gradually in the direction of chiselling. This fact could confuse results of numerical simulations. It is, therefore, suggested that the treated material is restored before each new impact and the process of penetration into the material is not taken into consideration. It is assumed that the character of the demolishing process can be neglected in the current investigation of the electro-pneumatic hammer. Consequently, the object of treatment is represented as a linear spring damper combination and does not change its position during the operating process.

Finally, referring to Figure 4.4:

- $m_1 \dots m_5$ represent masses of the operator hand, the machine casing, the exciting piston, the striker and the pick, respectively;
- k_1, c_1 stiffness and damping ratio of coupling between the hammer and the hand-arm system;
- k_2, c_2 the parameters of the vibration isolation system between the hand-arm system and the handle of the percussion machine (usually the rubber cushion covering the handle);
- k_3, c_3 the mechanical characteristics of contact between the striker and the pick;
- k_4, c_4 the parameters of the buffer mounted on the casing;
- k_5, c_5 the parameters of the linear spring-damper combination reflecting the mechanical characteristics of the treated material;
- F_{pn} the pneumatic force between the driving piston and the striker;
- r, l the radius of the crank and the length of connecting rod correspondingly;
- S the length of the pneumatic chamber between the driving piston and the striker when the pressure in the chamber is atmospheric;
- d the stroke length (when all elastic elements are not deformed, the driving piston is in extreme right position from the pick and position of the striker is determined by the atmospheric pressure in the pneumatic chamber).

Equations of motion of each body take general form:

$$m_i \ddot{x}_i = \sum_i F_i^{imp} + \sum_i F_i^{el} + \sum_i F_i \quad i=1 \dots 5 \quad (4.5)$$

where m_i and \ddot{x}_i - mass and absolute acceleration of a body with an index i in accordance with Figure 4.4.

$\sum F_i^{imp}$ - sum of impact forces applied to the body,

$\sum F_i^{el}$ - sum of elasticity forces applied to the body,

$\sum F_i$ - forces that cannot be described by general formula for force of elasticity or impact (pneumatic force, driving force).

The model of visco-elastic impact, which relies on the Kelvin-Voigt model, is used as the basis for a description of collisions between parts of the machine. The limiter is modelled as a parallel spring and dashpot combination and the impact force is calculated using the following formula [52]:

$$F_j^{imp}(z_j, \dot{z}_j) = \begin{cases} c_j \dot{z}_j + k_j(z_j - \Delta_{0j}) & \text{if } z_j - \Delta_{0j} > 0 \text{ and } F_j^{imp}(z_j, \dot{z}_j) > 0 \\ 0 & \text{if } z_j - \Delta_{0j} > 0 \text{ and } F_j^{imp}(z_j, \dot{z}_j) \leq 0, \\ 0 & \text{if } z_j - \Delta_{0j} < 0 \end{cases} \quad (4.6)$$

where z_j is the relative displacement of the colliding bodies; Δ_{0j} is the initial gap between the colliding bodies; k_j is the stiffness at impact and c_j is the damping ratio at impact.

Equations of motion for all bodies are written in an absolute co-ordinate systems where initial positions of the bodies counted from their equilibrium position under applied feed force.

The motion of the body m_1 , which represents coupling between the operator and the tool, is governed by the single second-order differential equation, where the resilient force that is exerted by the hand is on the left hand-side and the force developed by the coupling between the operator and the machine is on the right hand-side:

$$m_1 \ddot{x}_1 + c_1 \dot{x}_1 + k_1(x_1 + \Delta_{st1}) = c_2(\dot{x}_2 - \dot{x}_1) + k_2(x_2 - x_1 - \Delta_{st2}) \quad (4.7)$$

where x_1 and x_2 represent absolute co-ordinates of the operator hand and casing of the machine, respectively; Δ_{st1} , Δ_{st2} are the static deformations of corresponding springs under applied feed force.

Equation of casing motion takes form:

$$m \ddot{x}_2 + c_2(\dot{x}_2 - \dot{x}_1) + k_2(x_2 - x_1 - \Delta_{st2}) = F_r + F_4^{imp} \quad (4.8)$$

where F_r - reaction force produced by the crank-slide mechanism and applied to the casing of the machine; F_4^{imp} - force of impact between the pick and the buffer mounted on the casing.

The diagram of forces applied to the “crank mechanism - electric drive” system is shown in Figure 4.5. The high-speed alternating current commutator motor and high gear ratio reducer, which are currently used in the electro-pneumatic hammers have been taken as a model in the current study. This allows employing the uniform rotation of the crank with angular velocity \dot{q} .

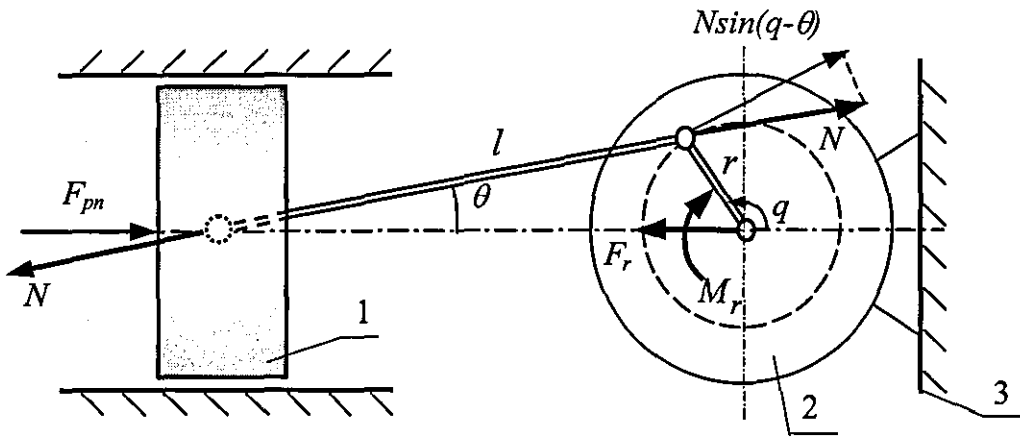


Figure 4.5. Schematics of forces between the crank-slide mechanism and the electric drive. 1 – driving piston, 2-electric motor, 3 – casing of the machine.

The piston is moving along a horizontal line and its position is determined by the crank radius r and length of the connecting rod l . Equation for the displacement of the piston will take the following form (the extreme right position of the piston is coordinate reference):

$$x_3 = l \cos \theta - r \cos q, \quad (4.9)$$

where the first component on the right hand-side of the equation can be represented in the following form:

$$l \cos \theta = l \sqrt{1 - \sin^2 \theta}, \quad (4.10)$$

Referring to Figure 4.5:

$$\sin \theta = \frac{r}{l} \sin q, \quad (4.11)$$

Substituting two last formulae into equation (4.9):

$$l \cos \theta = l \sqrt{1 - \left(\frac{r}{l}\right)^2 \sin^2 q}, \quad (4.12)$$

Expanding this equation by binomial theorem and neglecting all powers r/l greater than the second [51] we find:

$$l \cos \theta \cong l \left[1 - \frac{1}{2} \left(\frac{r}{l}\right)^2 \sin^2 q \right], \quad (4.13)$$

Replacing $\sin^2 q$ by a function of the double angle $2q$, and substituting equation (4.13) into the equation (4.9) the following expression for the piston displacement is obtained:

$$x_3 = l - \frac{r^2}{4l} + r \left(\frac{r}{4l} \cos 2q - \cos q \right), \quad (4.14)$$

By differentiation this equation with respect to time, expressions for the velocity \dot{x}_3 and acceleration \ddot{x}_3 of the piston are obtained:

$$\dot{x}_3 = r\dot{q} \left(\sin q - \frac{r}{2l} \sin 2q \right), \quad (4.15)$$

$$\ddot{x}_3 = r\dot{q}^2 \left(\cos q - \frac{r}{l} \cos 2q \right). \quad (4.16)$$

From Figure 4.5, F_r is reaction force due to the rigid coupling between the stator and the casing of the machine and M_r is torque of resistance force applied to the crank-slide mechanism and transferred to the rotor of the motor. In this case only vibration in the direction parallel to the stroke is considered.

$$\begin{aligned} F_r &= N \cos \theta, \\ M_r &= N \sin(q - \theta)r, \end{aligned} \quad (4.17)$$

where $N \cos \theta = m_3 \ddot{x}_3 + F_{pm}$ is the force applied by the crank-slide mechanism to the driving piston, θ is the angle between the connecting rod and horizontal axis and r is the crank radius.

In this analysis, the only force applied horizontally on the crankshaft bearings is taken into consideration. The vertical component of the reaction force which is equal

$N \cos(q - \theta)$ is neglected, because the casing motion is considered only in axial direction; vertical component of force N applied to the piston from the motor is assumed to be compensated by the piston guides.

Assuming that the mass of air between the driving piston and the striker remains constant at all times, the conditions in the pneumatic chamber might be considered approximately to be close to isothermal and the pressure in the chamber between the driving piston and the striker is atmospheric. Hence the force developed by the air cushion is defined as:

$$F_{pn} = pA[S/(S + x_3 - x_4) - 1] \quad (4.18)$$

where p is the atmospheric pressure; A is the cross-section area of the driving piston; x_3, x_4 are the absolute co-ordinates of the striker and exciting piston. Calculations show that the above simplification of the thermodynamical process does not essentially influence the dynamic behaviour of the model [49].

The force of the impact between the pick and the buffer:

$$F_4^{imp} = \begin{cases} c_4(\dot{x}_5 - \dot{x}_2) + k_4(x_5 - x_2 - \Delta_{st4}) & \text{if } x_5 - x_2 - \Delta_{st4} < 0 \text{ and } F_4^{imp} < 0 \\ 0 & \text{if } x_5 - x_2 - \Delta_{st4} < 0 \text{ and } F_4^{imp} \geq 0, \\ 0 & \text{if } x_5 - x_2 - \Delta_{st4} > 0 \end{cases} \quad (4.19)$$

where x_5, x_2 are the absolute co-ordinates of the pick and the casing; Δ_{st4} -static compression of the buffer under applied feed force.

In a similar manner, equation of motion for the striker will take form:

$$m_4 \ddot{x}_4 + F_3^{imp} = F_{pn}, \quad (4.20)$$

where m_4 and \ddot{x}_4 are the mass and the absolute acceleration of the striker; F_{pn} is the pneumatic force between the driving piston and the striker; and, finally, the force of impact between the striker and the pick, F_3^{imp} is:

$$F_3^{imp} = \begin{cases} c_3(\dot{x}_4 - \dot{x}_5) + k_3(x_4 - x_5 - d) & \text{if } x_4 - x_5 > d \text{ and } F_3^{imp} > 0 \\ 0 & \text{if } x_4 - x_5 > d \text{ and } F_3^{imp} \leq 0 \\ 0 & \text{if } x_4 - x_5 < d \end{cases} \quad (4.21)$$

where x_4, x_5 represent the absolute displacements of the striker and the pick respectively; d is the stroke length.

Finally, equation of motion for the pick:

$$m_5\ddot{x}_5 + F_5^{imp} + F_4^{imp} = F_3^{imp}, \quad (4.22)$$

where impact forces F_3^{imp} and F_4^{imp} are calculated according to the formula (4.21) and (4.19). According to the formula (4.6), expression for the impact between the pick and the object of treatment can be written as follows:

$$F_5^{imp} = \begin{cases} c_5\dot{x}_5 + k_5(x_5 + \Delta_{st5}) & \text{if } x_5 + \Delta_{st5} > 0 \text{ and } F_5^{imp} > 0 \\ 0 & \text{if } x_5 + \Delta_{st5} > 0 \text{ and } F_5^{imp} \leq 0 \\ 0 & \text{if } x_5 + \Delta_{st5} < 0 \end{cases} \quad (4.23)$$

where Δ_{st5} -static compression of the treated material under applied feed force.

The above set of equations (4.5)-(4.23) for the proposed model allows investigation of the operator-machine interaction and the main sources of vibration as it includes all major parts of the machine and their mutual interactions.

Nonlinearity and complexity of the model make analytical solutions rather difficult and unpractical [53], for this reason, the model has been investigated numerically using Simulink (part of the Matlab software suite).

4.3 Numerical simulations

Simulink contains a graphical interface and several block libraries, it allows a system to be built out of standard or customised blocks, deals with discontinuities and non-linear elements and, hence, appears to be more convenient than programming in standard language. The Simulink software enables all the dynamic characteristics of the model to be obtained and includes variation of the parameters

which are essential for the design of electro-pneumatic hammer, such as size of pneumatic chamber, crank arm radius, masses of different parts, feed force, etc.

4.3.1 Block diagrams

A block diagram of the electro-pneumatic hammer is shown in Figure 4.6 where each block represents a subsystem (usually body motion or force) built using Simulink blocks according to Eqs. (4.14)-(4.23).

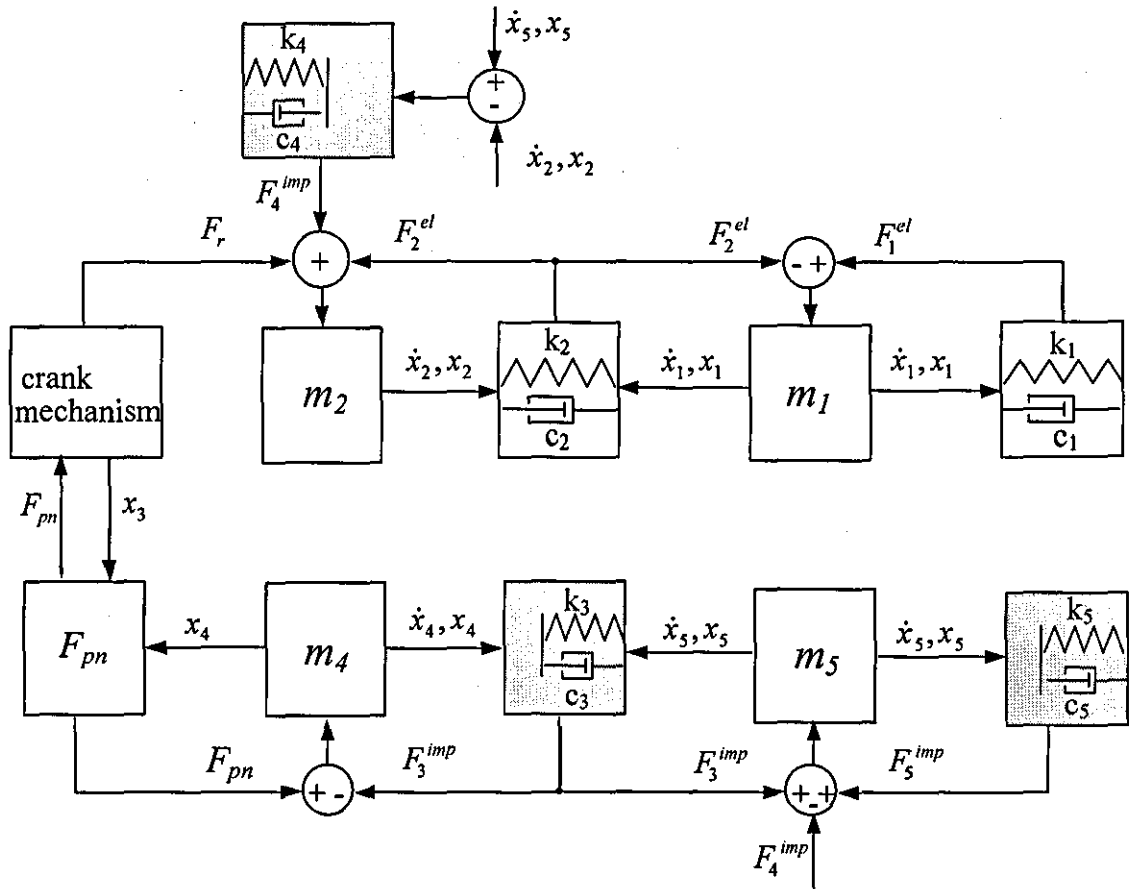


Figure 4.6. Simulink block diagram of the electro-pneumatic hammer.

In Figure 4.6 blocks marked " m_1 "..." m_5 " represent subsystems calculating acceleration, velocity and displacement of corresponded bodies; in a similar manner, subsystem marked "crank mechanism" built according to Eqs. (4.14)-(4.16) and calculates driving piston displacement and reaction force applied to the casing from crank mechanism; block marked " F_{pn} " is a simple calculation of pneumatic force

according to Eq. (4.18); the grey blocks with spring-dashpot combination are responsible for calculation of impact forces and, finally, the white blocks with spring dashpot combination represent elasticity forces.

Figure 4.7 shows the Simulink block diagram of the subsystem “crank mechanism”. Crank rotation was assumed to be uniform, so far left block specifies angular rotation speed as 282.74 rad/s .

In order to obtain the angle of crank rotation, this constant signal is sent through the *continuous-time integration block*. This block can reset its state to the specified initial condition based on an external signal. A *Hit crossing* block is used to detect the crossing point which is set to be 2π , so every time an angle of crank rotation equals 2π , this block resets the initial condition of the *continuous-time integration block* to 0. After a series of simple algebraic operations where blocks marked *sin* or *cos* perform simple trigonometric functions, the block *Product* multiplies inputs, block *Sum* outputs the sum of inputs and block *Gain* multiplies block input by a specified value, finally, driving piston displacement and reaction force was applied to the machine casing is obtained.

Uniform rotation of the crank with angular velocity \dot{q} was employed in the present study, so the torque of resistance force applied to the mechanism and transferred to the rotor of the motor, M_r , was not calculated.

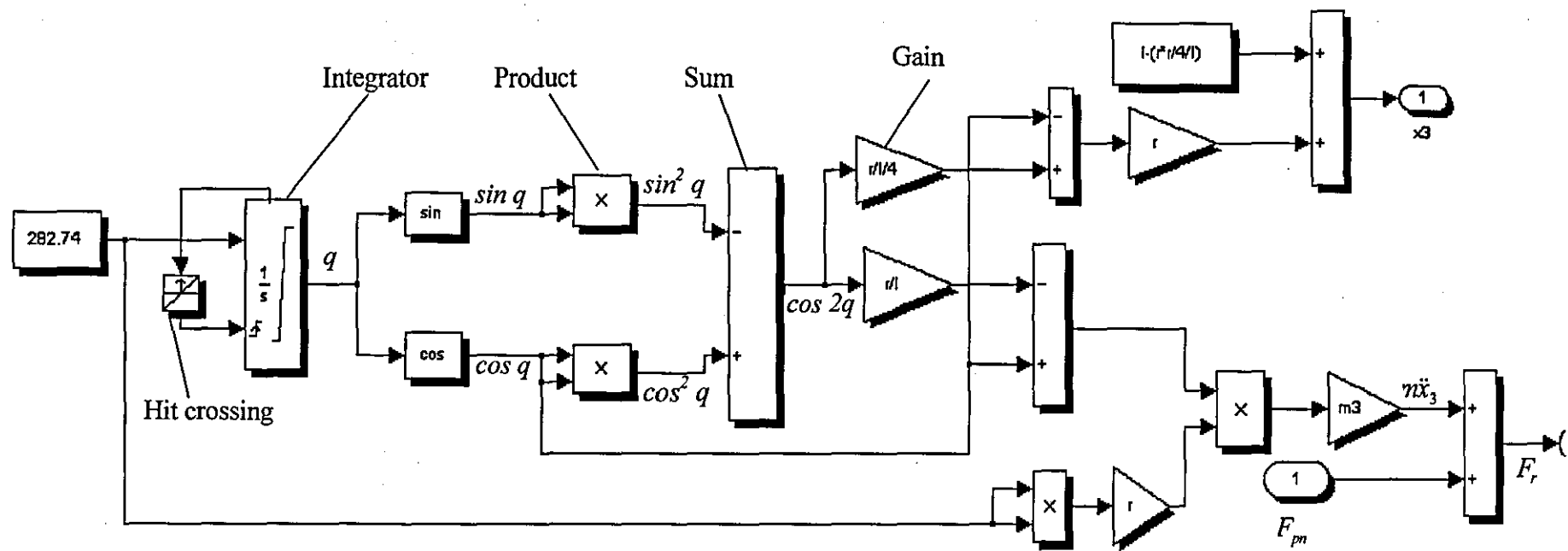


Figure 4.7. Simulink block diagram of the crank-slide mechanism.

Figure 4.8 shows a Simulink block diagram for the impact force between the pick and the striker (F_3^{imp}), the mass of the striker (m_4), and the force of the pneumatic impact (F_{pn}).

The sum of the signals of " F_{pn} " and " F_3^{imp} " (left upper corner in Figure 4.8) is passed through *Gain* block " $1/m_4$ " producing the striker acceleration. This signal passes through two *Integrator* blocks marked " $1/s$ " to give velocity and displacement of the striker. Relative displacements between the striker and the driving piston pass through block *Sum* (upper right-hand corner) and then through the *Function* block that applies a specified expression to the input referred to as u , and calculates pneumatic force between the striker and the driving piston in accordance with Eq. (4.18). Relative displacement between the striker and the pick (after block *Sum*) is sent to the *Dead Zone* block. The block outputs zero for inputs within the dead zone which is set accordingly to impact conditions. In this particular case the start of a dead zone is " $-\infty$ " and end of a dead zone is $(d - \Delta_{st4})$, where d – is the stroke length, i.e. the distance that the striker travels from its equilibrium position before it hits the pick in its equilibrium position, Δ_{st4} is static deformation of the buffer mounted on the casing under applied feed force.

The block *Sign* gives output " -1 " for negative input and " $+1$ " for positive input value. The *Relational operator* block marked " $=$ " performs a relational operation on its two inputs and produces an output equal to " 1 " if the first input is equal to the second input, otherwise the output is " 0 ". These blocks have been used in order to specify the moment when two collided bodies were not in contact any more after impact.

So the impact interaction begins when the impacting body crosses the "impact level" in positive direction. The impact is completed when the value of the limiter response crosses its zero level in the "negative" direction. The condition of equality between signs of impact force and displacement is necessary in order to avoid effect of "adhesion" between bodies in contact. The *Gain* blocks marked " k_3 " and " c_3 " represent the parameters of the impact interaction between the striker and the pick.

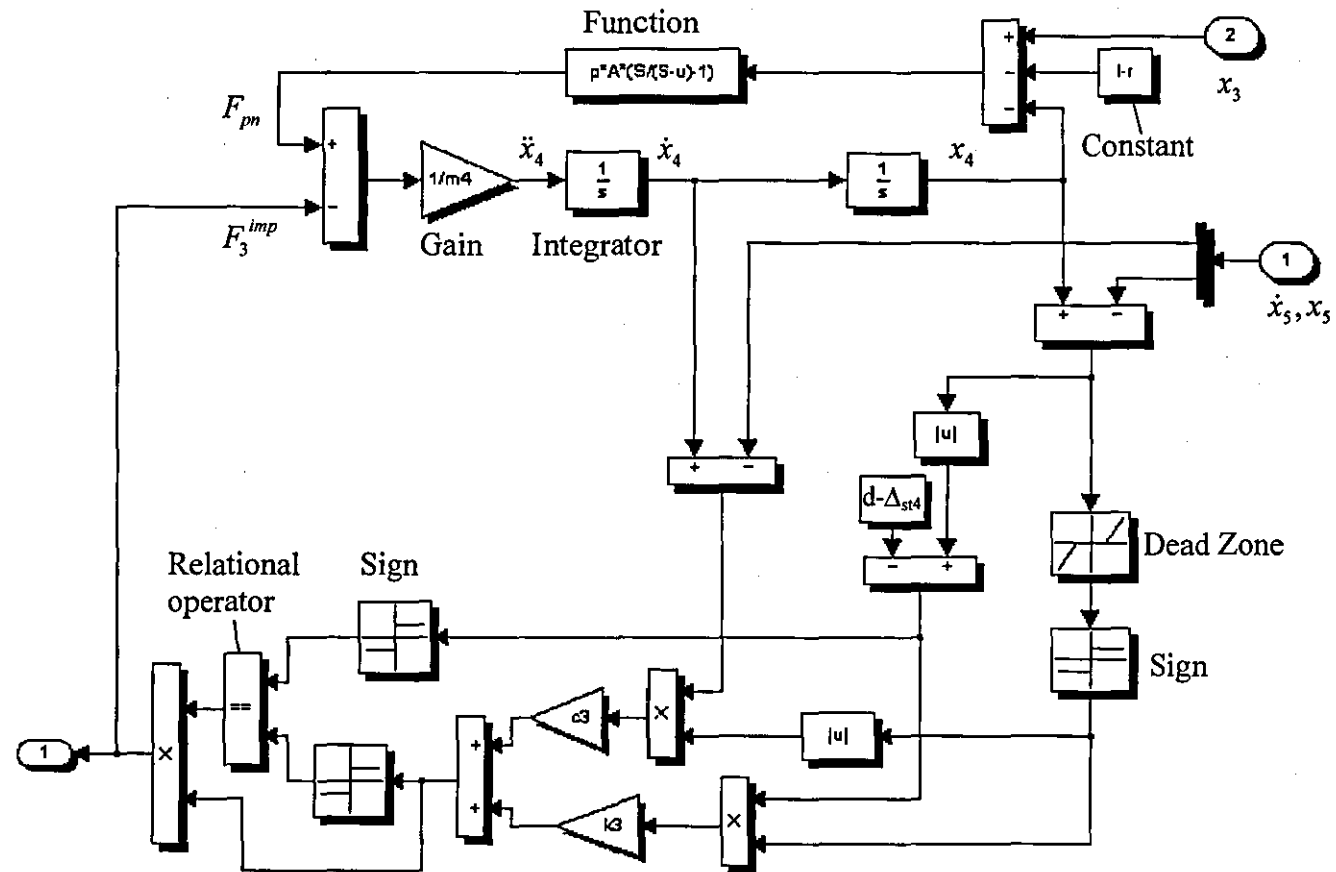


Figure 4.8. Simulink block diagram of the striker motion, impact force between the striker and the pick and the pneumatic force.

Figure 4.9 shows a Simulink block diagram for the bodies m_2 and m_5 , and the forces of impact between the pick and the treated material and the pick and the casing.

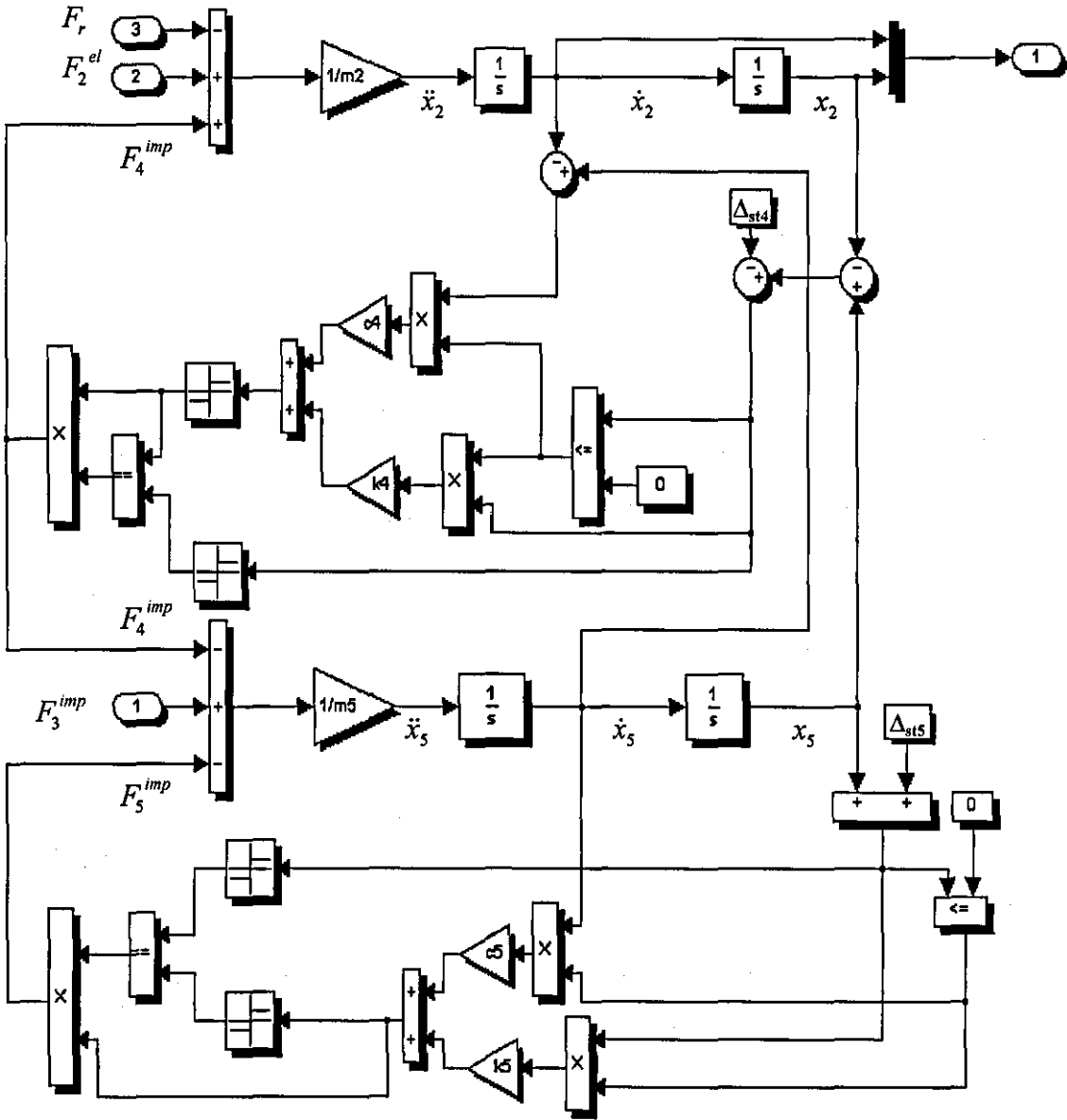


Figure 4.9. Simulink block diagram for subsystems m_2, m_5, F_4^{imp} and F_5^{imp} .

The principle of this diagram is very similar to the previous one. After summation of elastic force developed between the casing and the hand-arm system, reaction force from the crank-slide mechanism and impact force between the pick and the buffer, signal passes through two *Integrator* blocks giving as a result casing velocity

and displacement. “Pick-Casing” impact force is obtained in accordance to Eq. (4.19) in a manner similar to previously described for F_3^{imp} . As before, Δ_{st4} and Δ_{st5} are static deformations of springs k_4 and k_5 under applied feed force, respectively.

Figure 4.10 shows a block representing the subsystem “ m_1 ”. This subsystem is made according to equation (4.7) and includes blocks calculating two elastic forces which represent a hand-arm system and coupling between the handle of the machine and the hand.

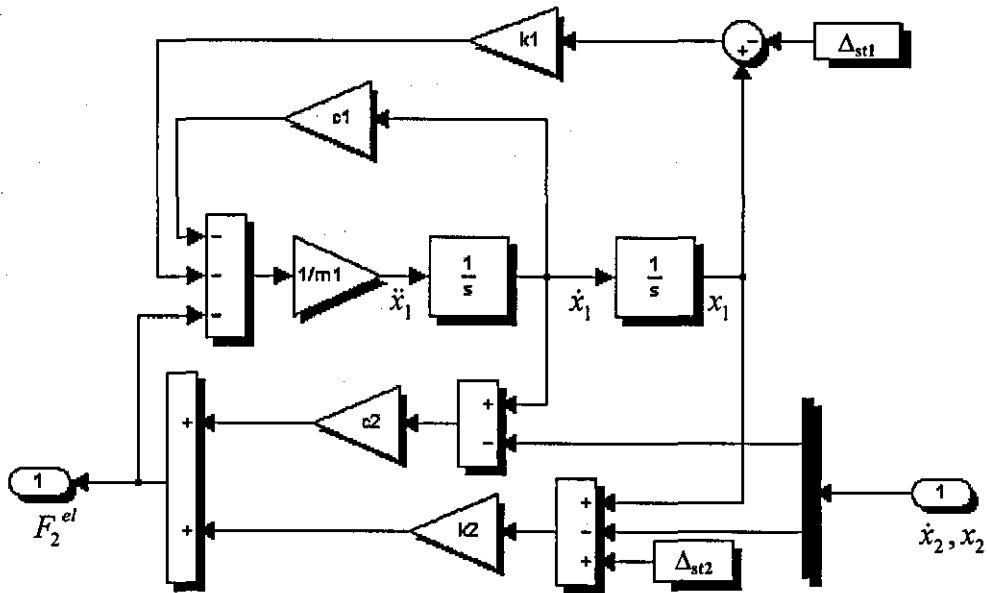


Figure 4.10. Simulink block diagram of the “ m_1 ”

Simulation of models involves the numerical integration of sets of ordinary differential equations (ODEs). Simulink provides a number of solvers for simulation of such equations. The model under consideration has continuous states, so variable-step solver *ode45* was chosen. *Ode45* is based on an explicit Runge-Kutta (4,5) formula, the Dormand-Prince pair. Variable-step solvers can modify their step sizes during simulation. They provide error control and zero crossing detection. The maximum step size was set as $\frac{1}{4}$ of the period of the process (0.005s) and the initial

step size as 0.0001s. The solver uses standard local error control techniques to monitor the error at each time step. During each time step, the solvers computed the state values at the end of the step and also determined the local error, and estimated error of these state values. They then compared the local error to the acceptable error, which was a function of the relative tolerance (was set as 10^{-3}) and absolute tolerance (10^{-4}). If the error had been greater than the acceptable error for any state, the solver would have reduced the step size and tried again. After the simulation had been run, the results were sent to a Matlab workspace for further processing or stored in a file.

4.3.2 Model parameters

Some of the parameters of a dynamic model such as mass of the pick, mass of the machine casing, mass of the piston, the crank radius, length of the connecting rod, effective area of the piston, frequency of impact of the pick against the surface of treatment for the model were taken from typical parameters of a heavy electro-pneumatic hammer-drill Hilti TE74. Approximate stiffness of the treated material, $k_s = 3 \times 10^7 \text{ N/m}$, and loss factor of the treated material, $\zeta_s = c_s / 2\sqrt{k_s m_s} = 0.7$, were obtained using typical characteristics for concrete loading and formula (7) in reference [48].

Energy and frequency of impacts are the main characteristics of this type of machinery. Energy of impacts is usually within 1-100J range [50]. For the electro-pneumatic hammer under investigation the value chosen was 1.5 J with acceptable deviation value for pick velocity just before the impact of 20%.

The size of the pneumatic chamber, the stroke length, parameters of the buffer between the pick and the casing, optimal feed force of the operator, masses and the rest of the parameters used in the dynamic model of the machine had to be chosen in such a manner that the machine was working with a prescribed frequency and the energy of impacts and vibration applied to the operator was minimal. Finding such parameters is a problem of multi-parametric optimisation. The number of variables of optimisation and lack of any prior knowledge of the internal interaction of the system (the r.m.s. of hand acceleration as a function of parameters of the machine) restrict the choice of the potential optimisation methods. Ideally, a simple search by employing regular multi-dimensional mesh would guarantee that the entire region of

search is covered. However, in the case of several of the parameters, this approach was not satisfactory, because in this case the number of necessary simulations sometimes exceeded the limit of the computer memory.

Under these circumstances, the random search technique (Monte-Carlo optimisation) is simple and well suited for the purpose of finding parameters for the reference model of electro-pneumatic hammer [54, 55]. It is not necessary to determine partial derivatives or make moves in particular directions within the search region while using random search so, the objective function does not need to be continuous or unimodal. Hence, random search method can be employed for optimising an objective function that has several local optima.

In order to illustrate the method, a simple example can be considered [56]. Suppose the area of figure S needs to be calculated (see Figure 4.11). N random numbers are chosen in such a way that all of them lay within the unit square. The number of points that lie within the “ S ” are marked N' . From simple geometrical considerations, the area of figure S can be found as ratio N'/N . It can be easily concluded that the number of these random points determines the accuracy of our calculations.

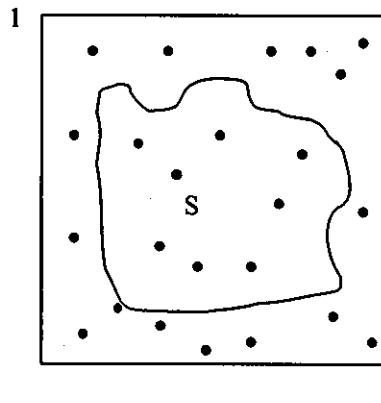


Figure 4.11. Figure S .

In order to increase the accuracy of the search without dramatically increasing the number of the simulations, the adaptive random search was chosen. For each parameter a minimum and maximum possible value was set, then, by using a random number generator in MATLAB, N number of simulations were made while values of the parameters were changed randomly and independently in this fixed region.

MATLAB 6 uses a new random number generator that can produce a uniformly distributed all floating-point numbers in the closed interval $[2^{-53}, 1-2^{-53}]$. Theoretically, it can generate over 21492 values before repeating itself.

After N simulations, the “best” set of values for the parameters was obtained. This set of search points corresponded to the operating frequency 45 Hz, energy of pick impacts against the treated material 1.5 J and minimum r.m.s. of acceleration perceived by the operator. These characteristics of optimal regimes had to be stable to the changes in the feed force and parameters of the operator. The “best” search point became the centre for the next search region, the size of which was approximately two thirds of the size of the previous one. The number of simulations, N , was set equal to 5000 for the first step of optimisation and thereby reduced by $\frac{1}{4}$ for each subsequent step. The program run until the optimum value of the r.m.s. acceleration perceived by the operator differed from the value obtained during the previous step of search by less than 5%. In case of a function with several possible local optimums, this method cannot guarantee that the absolute optimum solution is found, however with a sufficient number of simulations the result suits the purpose of obtaining the suitable reference model of an electro-pneumatic hammer.

The Matlab program that has been developed to perform the search of optimum parameters is in Appendix A.

Thus, the model of the electro-pneumatic hammer without vibration isolation was developed. The acceleration perceived by the operator of such a hammer was minimal for a predesigned pick velocity and frequency of impacts. This model will be used as a basis for dynamic analysis of the electro-pneumatic hammer and further development of vibration attenuation system.

4.3.3 Frequency analysis

There are several blocks for spectrum and frequency analysis within the Simulink software. They record the signal being analysed with the chosen sampling rate and then a standard mathematical procedure is performed. The spectrum of the casing's acceleration contains an infinite number of high frequency harmonics. Although their amplitudes decrease as the frequency increases, the standard frequency analysis blocks should be used with care due to aliasing problems. The sampling rate used in

simulations can be increased in order to alleviate these problems, however this will significantly increase the required simulation time. On the other hand, the driving frequency of the electro-pneumatic hammer is constant and predetermined. Hence, spectrum of casing acceleration contains harmonics that are multiple to the driving frequency. So customised blocks can be easily designed for frequency analysis.

The following algorithm of segment analysis was developed for calculation of the impact frequency of the pick against the treated object. After the simulation had been run, the maximum value of the pick velocity was recorded and a level of 80% of maximum value (due to 20% acceptable deviation of pick's velocity just before impact) was set. The next step was calculating how many times the curve of time history of the pick's velocity crosses this level while rising. Thus, the frequency of the process was a number of these crossings divided by the time of simulation. The m-file containing this algorithm is presented in Appendix B.

A special block was developed in order to perform spectral analysis of the system. The predetermined operating frequency of the studied electro-pneumatic hammer is 45Hz, consequently the simple Fourier series can be used in order to calculate harmonics amplitudes.

Fourier series arise from the practical task of representing a given periodic function $f(t)$ with any period $p = 2L$ in terms of cosine and sine functions [57]:

$$f(t) = a_0 + \sum_{n=1}^{\infty} \left(a_n \cos \frac{n\pi}{L} t + b_n \sin \frac{n\pi}{L} t \right) \quad (4.24)$$

where coefficients are calculated according to the formulas:

$$a_0 = \frac{1}{2L} \int_{-L}^L f(t) dt \quad (4.25)$$

$$a_n = \frac{1}{L} \int_{-L}^L f(t) \cos \frac{n\pi}{L} t dt \quad (4.26)$$

$$b_n = \frac{1}{L} \int_{-L}^L f(t) \sin \frac{n\pi}{L} t dt \quad (4.27)$$

From equations (4.24) - (4.27), the amplitude of harmonic number n :

$$A_n = \sqrt{a_n^2 + b_n^2} \quad (4.28)$$

The subsystem that has been built according to these equations and used for spectrum analysis of the signal is shown in Figure 4.12.

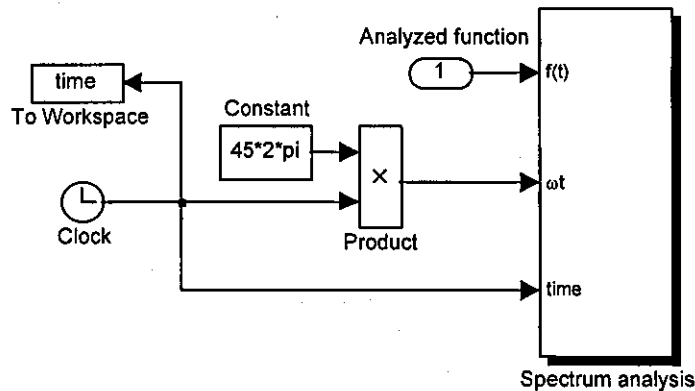


Figure 4.12. The Simulink block diagram for spectrum analysis of the signal.

The block marked “Clock” produced current simulation time as an output, then a signal was sent to the block marked “To workspace” where the signal was recorded to the Matlab workspace with prescribed name and sample time. The analysed signal was sent to the subsystem input, marked $f(t)$. The subsystem “Spectrum analysis” is represented in Figure 4.13. In order to make this block more universal, each harmonic is described by separate subsystem so that number of analysed harmonics could be easily changed. The block diagram of one such a subsystem is shown in Figure 4.14.

The blocks marked “sin” and “cos” simply performed the trigonometric operation. By integrating the result and then dividing it by the time of the simulation simple operation of definite integration $(\frac{1}{2L} \int_{-L}^L f(t) \dots dt, \text{ where } L - \text{ is period of the function})$ is accomplished. The result has to be multiplied by two according to equation (4.26).

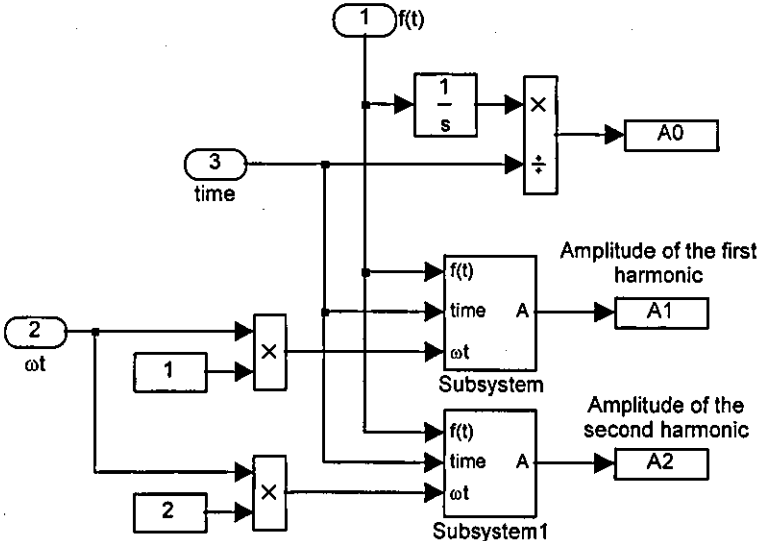


Figure 4.13. Subsystem “Spectrum analysis”

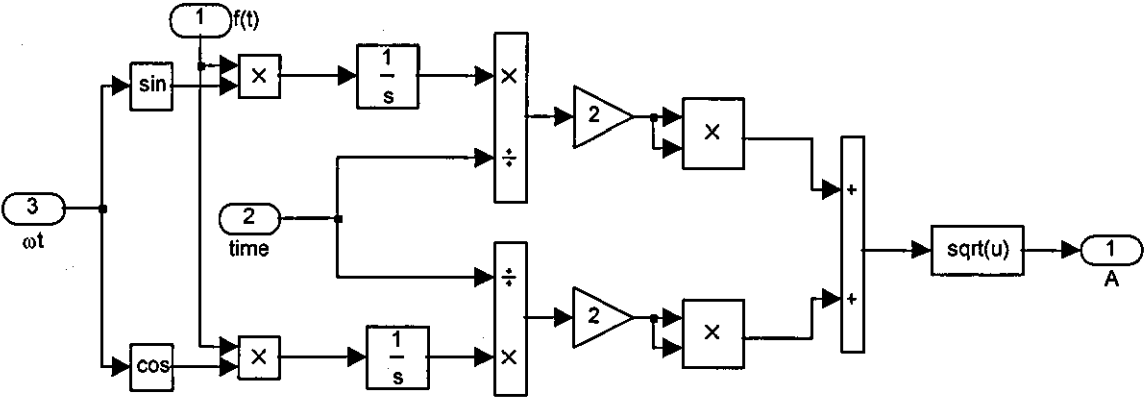


Figure 4.14. Block diagram of “Subsystem”.

4.3.4 Results of numerical simulations

As a result of optimisation, the model of the electro-pneumatic hammer without vibration isolation has been developed.

The model has following parameters: frequency of impact of the pick against the treated surface, $f = 45\text{Hz}$; energy of pick impacts, $E = 1.5\text{J}$; mass of the operator hand, $m_1 = 1.4\text{kg}$; mass of the machine casing, $m_2 = 8\text{kg}$; mass of the piston, $m_3 = 0.13\text{kg}$; mass of the striker, $m_4 = 0.2\text{kg}$; mass of the pick, $m_5 = 0.35\text{kg}$;

crank radius, $r = 0.02m$; length of the connecting rod, $l = 0.06m$; area of the piston, $A = 0.0015 \pi/4 m^2$; size of the compression chamber, $S = 0.043m$; stroke length, $d = 0.038m$; parameters of the operator hand, $k_1 = 243000N/m$ and $c_1 = 265Ns/m$; parameters of the coupling between the handle and the operator,

$$\Omega_2 = \sqrt{\frac{k_2}{m_2 + m_3}} = 1.5 \times 10^4 \text{ rad/s} \quad \text{and} \quad \zeta_2 = \frac{c_2}{2\Omega_2(m_2 + m_3)} = 0.2; \quad \text{parameters of the}$$

impact between the striker and the pick, $\Omega_3 = \sqrt{\frac{k_3(m_4 + m_5)}{m_4 m_5}} = 2.08 \times 10^4 \text{ rad/s}$ and

$$\zeta_3 = \frac{c_3(m_4 + m_5)}{2\Omega_3 m_4 m_5} = 0.5; \quad \text{parameters of the casing buffer,}$$

$$\Omega_4 = \sqrt{\frac{k_4(m_2 + m_5)}{m_2 m_5}} = 1215 \text{ rad/s} \quad \text{and} \quad \zeta_4 = \frac{c_4(m_2 + m_5)}{2\Omega_4 m_2 m_5} = 0.26; \quad \text{stiffness of the}$$

treated material, $k_5 = 3 \times 10^7 N/m$ and loss factor of the treated material, $\zeta_5 = 0.7$; feed force of the operator, $P = 150N$.

Figure 4.15 shows the displacements of the striker and the driving piston, the pneumatic force between the piston and the striker, the inertia force of the piston and the reaction force applied to the casing of the electro-pneumatic hammer due to the rigid coupling between the stator and the casing. The driving piston executing sinusoidal motion interacts with the striker through gas in the pneumatic chamber. The resulting pneumatic force produced is essentially the excitation force which is applied to the striker, which in turn hits the pick. At the same time, this force is applied to the casing of the machine, as can be seen from the time history of the reaction force, which contains well-pronounced sharp peaks resulting from pneumatic impact. In the case of there being no vibration isolation between the crank-slide mechanism and the operator, these peaks are directly perceived by the operator.

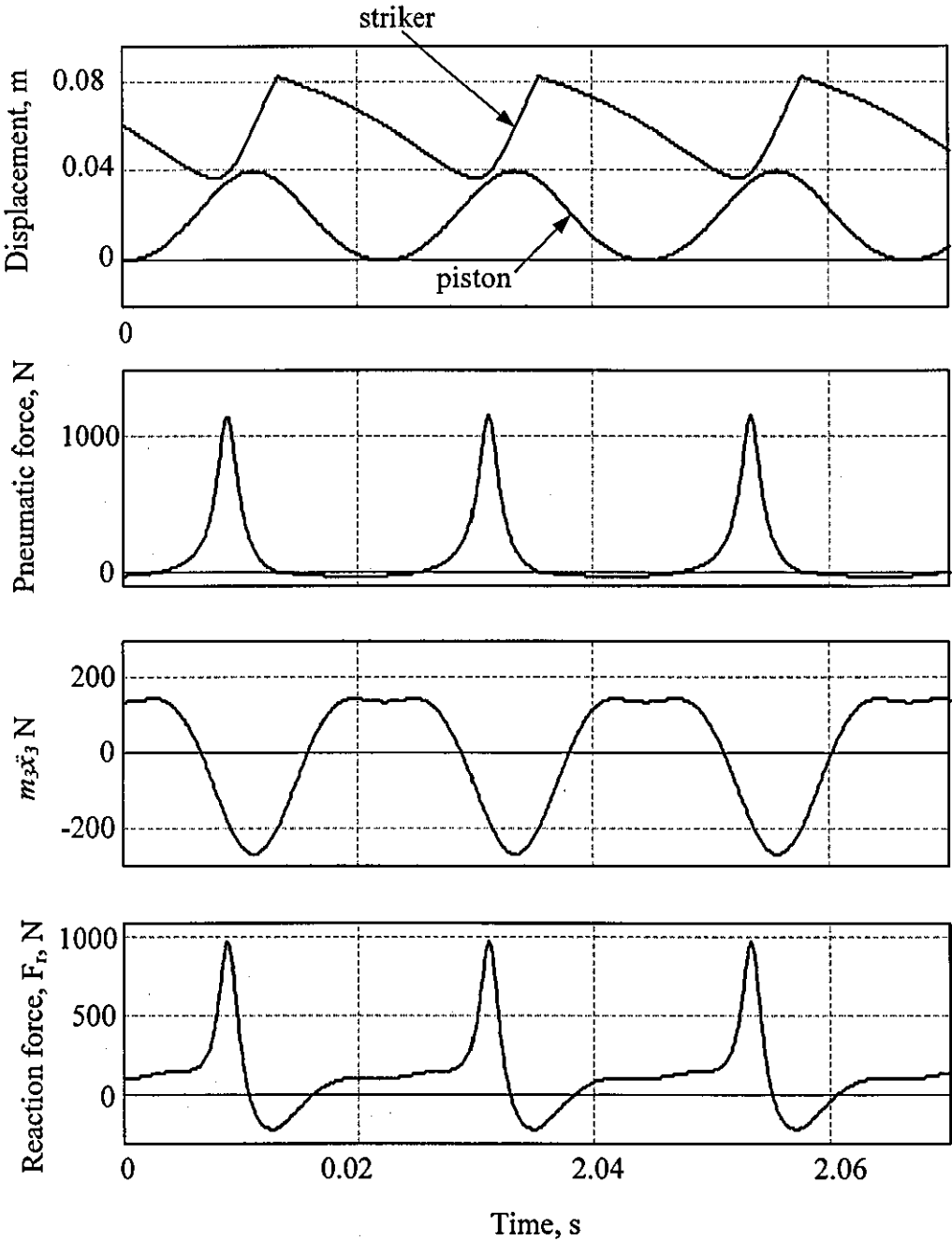


Figure 4.15. Time history of displacements of the striker and driving piston, pneumatic force, force of inertia of the piston and reaction force.

Figure 4.16 shows time histories of the displacements of the striker and the pick and forces as the result of their interaction. F_3^{imp} is the impact force between the striker and the pick (see Figure 4.4), F_5^{imp} is the force of the pick impact against the object of treatment. There are several smaller picks on the curve of F_5^{imp} after each main impact. Sharp peaks marked “B” are caused by the secondary impact of the

pick after rebound against the buffer, while other peaks marked “C” are caused by an operator pressing the hammer against the material being treated. These secondary peaks are the cause of additional unnecessary noise and vibration and should be avoided or at least minimised by a careful design of the tool.

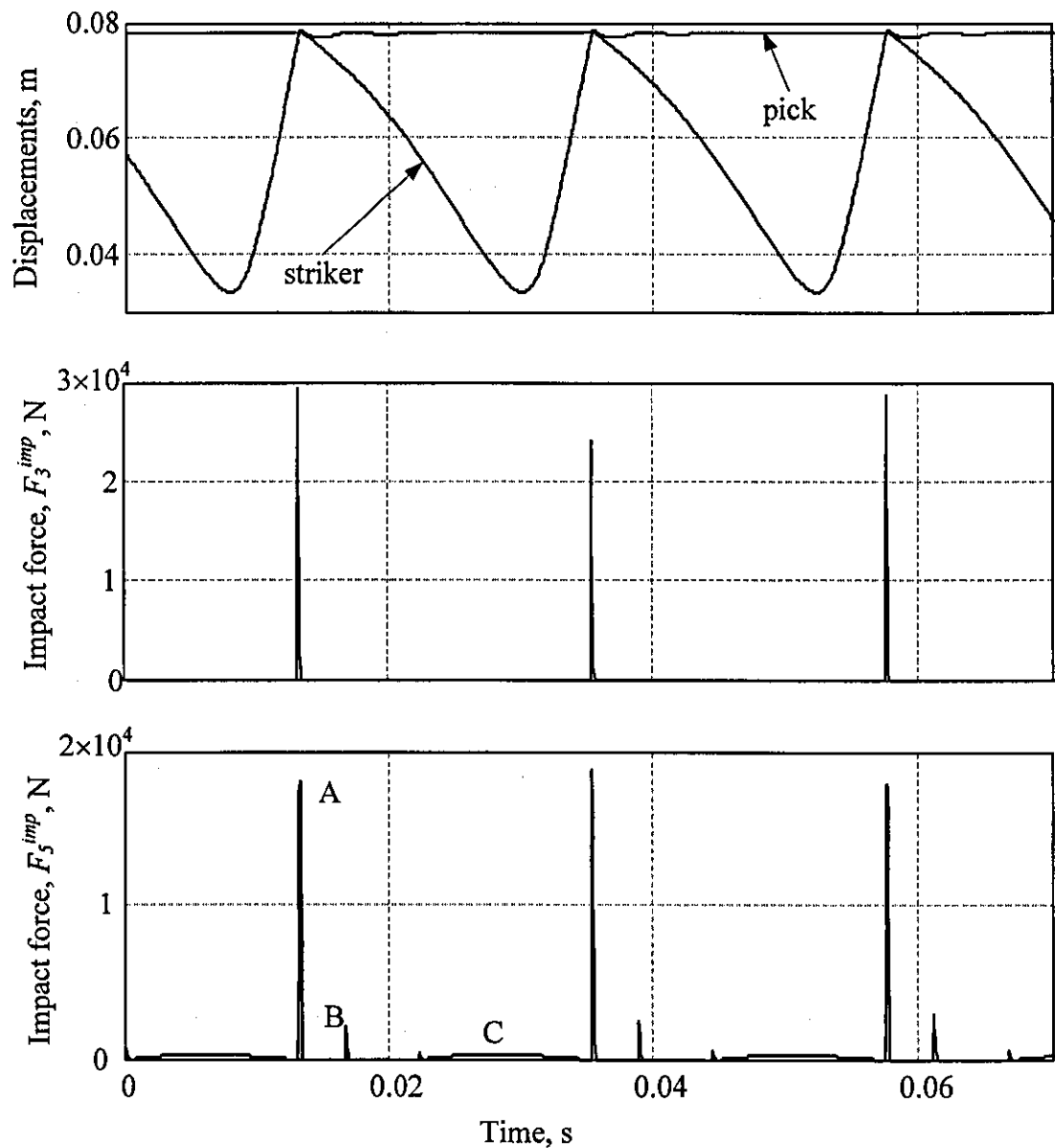


Figure 4.16. Time history of the displacements of the striker and the pick and some forces acting in electro-pneumatic hammer.

The operator constantly presses the tool against the treated material, so during pick recoil against the surface it inevitably hits the buffer mounted on the casing. Figure 4.17 shows the time history of the displacements of the pick and the casing and force of impact between the pick and the buffer (F_4^{imp}).

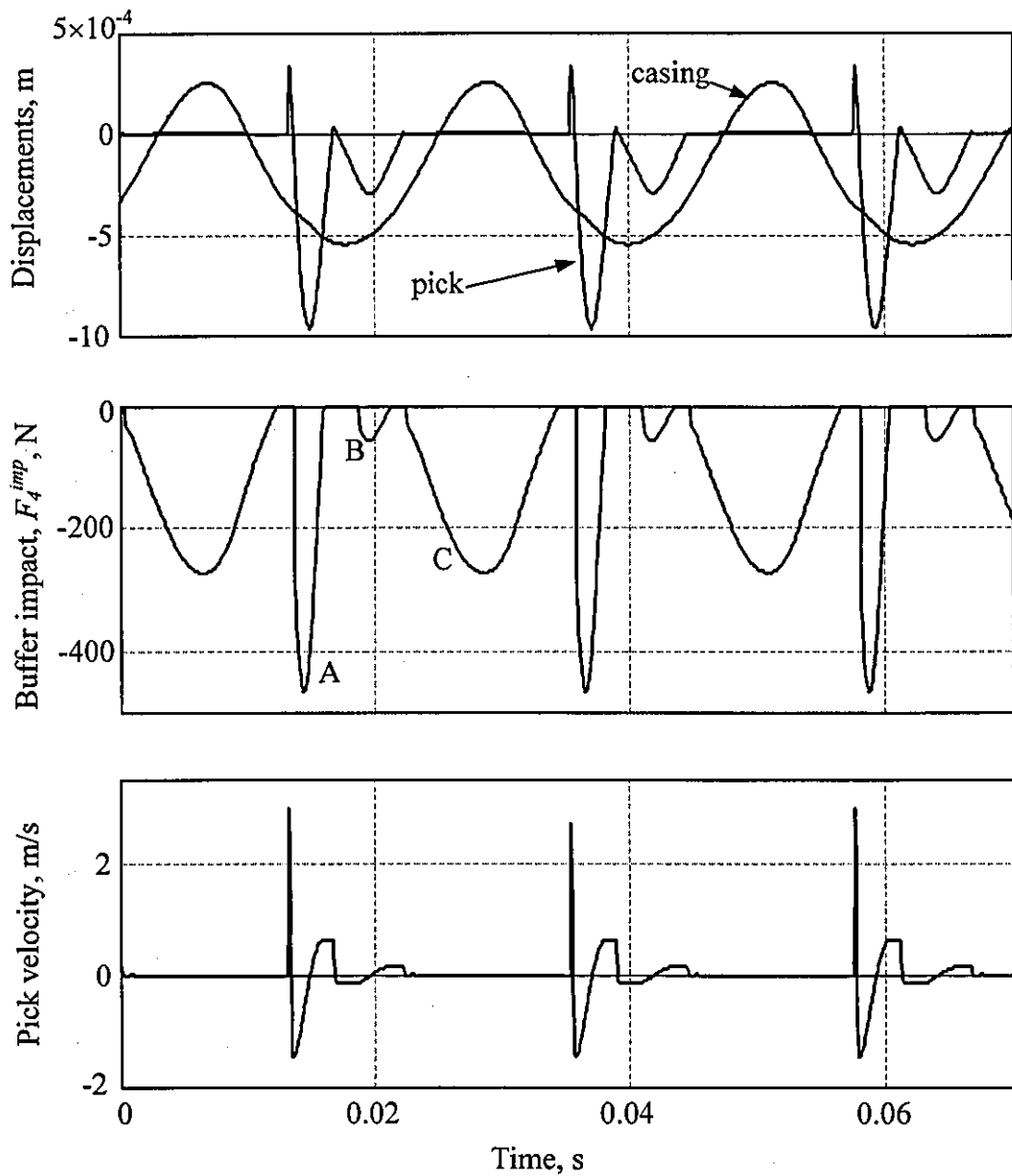


Figure 4.17. Time history of the displacements of the pick and the casing, force of impact between the pick and the buffer of the casing and velocity of the pick impact against object of treatment.

Similar to the time history of the force of impact against object of treatment there are several peaks on the curve showing F_4^{imp} . The peaks marked "A" are due to the main impact; smaller peaks marked "B" caused by rebounds of the pick against material being treated. Peaks marked "C" are the result of impact of the casing that is pressed against the pick after the pneumatic impact by the spring-dashpot

combination m_1 , k_1 and c_1 . Parameters m_1 , k_1 and c_1 represent characteristics of the operator of an electro-pneumatic hammer and these may vary from one operator to another. Simulations were carried out for different values of these parameters and the qualitative characteristics of the force of impact and the hand acceleration were found to remain unchanged. The time history of velocity of impact of the pick against the material being treated is also shown in Figure 4.17.

The time history of the hand acceleration is shown in Figure 4.18. This curve has distinctive peaks due to the pneumatic force (marked “a”), force of “pick-buffer” impact (marked “a”), force of secondary impact between the pick and the buffer (“b” and “d”).

The results of numerical simulations confirm the analysis of the main sources of vibration and allowed the estimate of their individual effect on acceleration perceived by the operator.

In characterisation of hand-transmitted vibration, it is common to measure and analyse acceleration in one octave and one-third octave bands to demonstrate compliance with regulatory requirements. Standards are often stated in terms of such spectra because they reflect the manner in which humans respond to annoying noise and vibration. However, as was shown earlier, such an averaging of hand-transmitted vibration may lead to underestimation of the hazardous impact on the operator. This method is suitable for standardisation rather than for analysis of a vibration isolation system, therefore, in the current investigation, r.m.s. and peak to peak amplitude of unweighted hand-transmitted acceleration are used as characteristics of vibration perceived by an operator. According to results of numerical simulations the r.m.s. value of acceleration perceived by an operator of the electro-pneumatic hammer in the current study is 29.5 m/s^2 , while peak to peak amplitude of hand-transmitted acceleration is 101 m/s^2 .

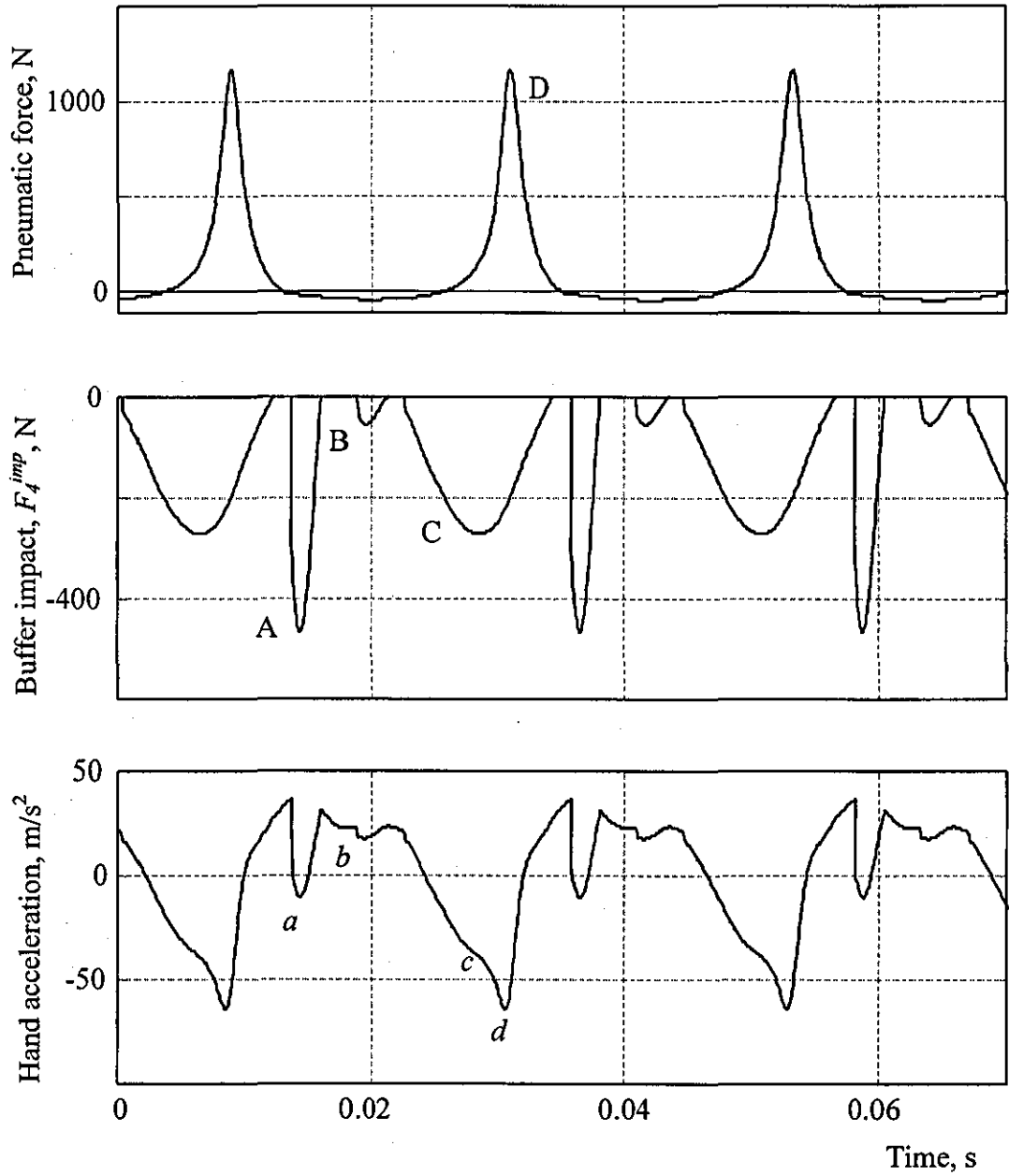


Figure 4.18. The time history of the hand acceleration.

A spectrum of hand acceleration based on the above simulation is shown in Figure 4.19. The harmonics amplitudes were obtained by using the Simulink model (see Figure 4.13) built in accordance with Eqs. (4.24)-(4.28).

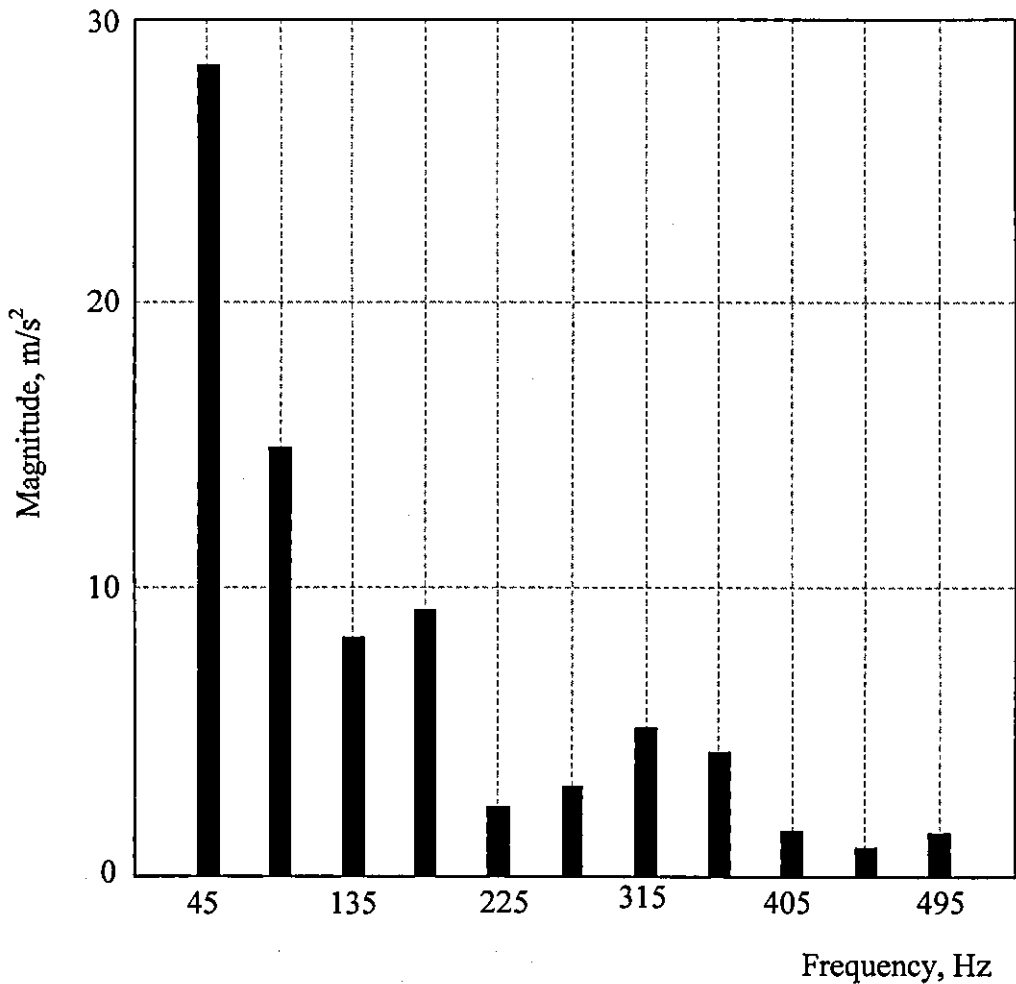


Figure 4.19. Spectrum of hand acceleration.

Only the first eleven harmonics were analysed, since higher harmonics are not of significant magnitude and can be easily attenuated by a simple vibration isolation system. The first four harmonics are of the highest magnitude and most hazardous for an operator.

The obtained spectrum can be compared to the frequency spectrum of the real machine. Figure 4.20 shows the experimental spectrum, which was measured using an accelerometer (Brüel & Kjær Type 4367) fitted to the main handle of the hammer-drill Hilti TE74 [58].

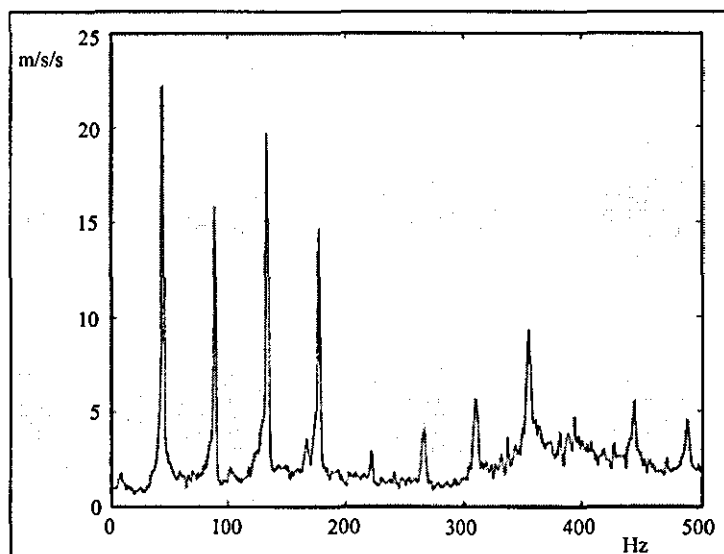


Figure 4.20. Frequency spectrum of hammer drill Hilti TE74 drilling into concrete (reproduced from [58]).

It can be seen that there is a particular difference between the spectrum obtained by the numerical modelling and the spectrum measured using the original hammer drill. This can be due to certain simplification in modelling, negligence of a drilling mode in the dynamic model of electro-pneumatic hammer. However, the amplitudes of the first four harmonics are of most significant value and of the same order for both spectra. There is an agreement between those spectra in a higher frequency range. So, the results of numerical modelling for the electro-pneumatic hammer are in good agreement with experimental data.

4.4 Conclusions and discussions

Percussive tools have been major sources of hand-arm vibration since their invention almost a century ago. Efforts to reduce the vibration of these useful tools began soon afterwards, and many patents have been issued over the years for vibration attenuation systems for percussive tools. However only few of them have been used in the standard product. The electro-pneumatic hammer of today is almost unchanged from the design of fifty years ago. The somewhat intuitive approach that

has been used in design of hand-held percussion machines so far proved to be very successful.

However, the problem of vibration protection for an operator of a hand-held percussion machine remains a serious engineering task. Although main sources of vibration of hand-held power tools are known (because in most cases they are determined by the operation principle), the dynamic modelling enables the estimate of their individual contribution to the overall vibration, to develop a systematic approach to the analysis and evaluation of vibration, to find the optimal design of the tool or develop a vibration attenuation system without lengthy costly trial and error experimental procedure. Dynamic modelling of hand-held percussion machine offers great opportunity for detailed investigation of their dynamics and development of new, low-vibration percussion tools.

The developed dynamic model of an electro-pneumatic hammer includes all major parts of the machine and their interactions responsible for hazardous vibration produced by the machine. The influence of feed force, excitation mechanism and hand-arm system are included in the dynamic model. Results of numerical simulations are in good agreement with experimental data in terms of nature, sources and level of vibration perceived by the operator. The model may be further improved by including vibration motion in other directions, incorporating the dynamic model of an AC commutator motor and taking into consideration the outlet orifice in the pneumatic camera.

The r.m.s. and peak amplitude of unweighted casing acceleration in the dynamic model of electro-pneumatic hammer was reported. However, all available standards operate with weighted acceleration magnitude. In order to compare developed dynamic model with existing guidelines on hand-transmitted exposure, weighted hammer acceleration was calculated from inverse Fourier transform of the multiplication of the Fourier transform of the acceleration time history with the frequency weighting. The r.m.s. of weighted acceleration perceived by the operator of electro-pneumatic hammer in the present study was 8.3m/s^2 .

Figure 4.21 shows a graph that enables rough estimation of vibration hazard produced by a hand-held percussion power tool [59]. The vertical axis of this graph is average (r.m.s.) vibration magnitude produced by the machine; the horizontal axis is length of daily exposure of an operator of such a machine.

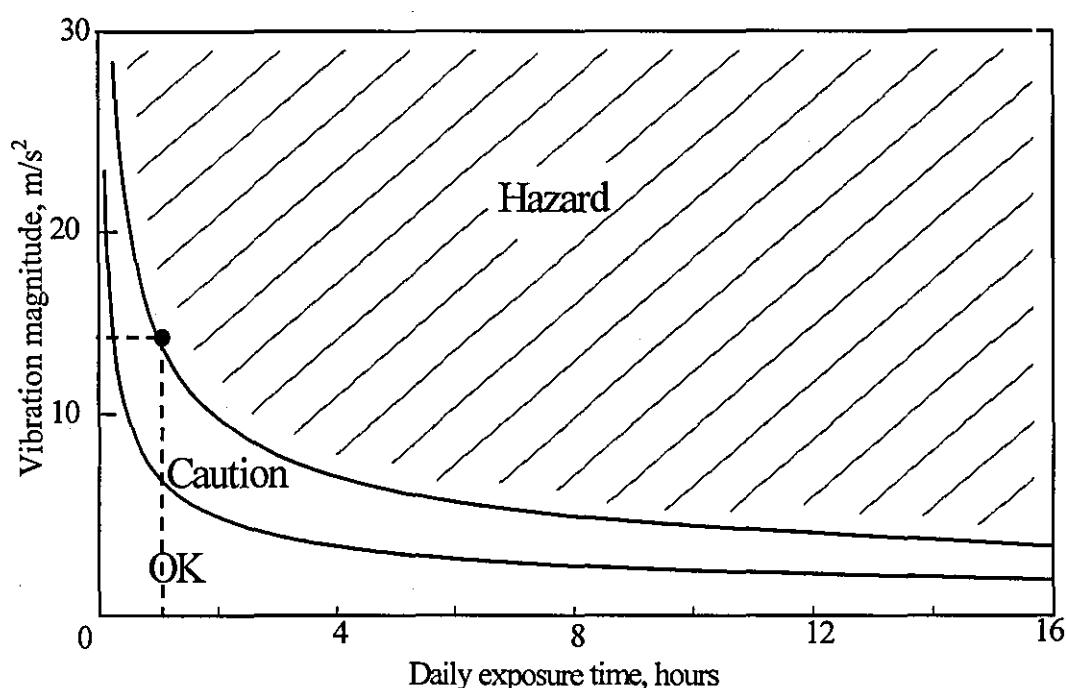


Figure 4.21. The relationship between vibration magnitude and duration for energy-equivalent exposures (adapted from [59]).

The caution limit (lower curve) is based on an 8-hour energy-equivalent daily exposure of 2.5 m/s^2 . The hazard limit (upper curve) is based on an 8-hour energy-equivalent daily exposure of 5 m/s^2 . The r.m.s. of weighted acceleration perceived by an operator in the developed model of electro-pneumatic hammer is 8.3 m/s^2 , but because vibration was calculated in dominant axis only, the obtained value of r.m.s. of casing acceleration should be multiplied by 1.7 before being compared with the guidance [16, 17]. The acceptable length of daily exposure for such an electro-pneumatic hammer is less than one hour (dashed line in Figure 4.21), which is hardly enough to complete any job. In reality, the vibration level of such an electro-pneumatic hammer is higher, because of certain simplifications assumed in the model vibration, which means that acceptable daily exposure is even smaller. In order to increase this value, vibration produced by this tool must be reduced.

Chapter 5

Methods of reducing vibration of hand-held percussion machines

The constant direct interaction between the operator and the hand-held percussion machine defines the necessity and the specific features of the vibration protection system for this type of machinery. The operator perceives any changes in the parameters of the machine, such as weight and vibratory motion of the machine and so there are a lot of limitations enforced on the design of vibration protection system.

There are a variety of different methods for protecting the operator from hand-transmitted vibration, though the comprehensive classification is difficult, we will mention some of them.

5.1 Reduction of the intensity of sources of vibration

The first method involves attenuation of the vibratory effects imposed by the machine upon the operator by reducing the intensity of the sources of harmful vibration through the proper design of the machine. The major sources of harmful vibration determined by principle of operation and dynamics of machine. The rest of vibration might be caused by improper design or manufacturing of the parts of the machine, operating conditions, etc. The latter are not fundamental and can be

eliminated during the design stage, therefore will not be considered in the present investigation.

In the case of the electro-pneumatic hammer an operating principle is responsible for the fundamental sources of vibration (pneumatic excitation force, force of “pick-buffer” impact), which were described in Chapter 4. Therefore these sources cannot be so easily eliminated. However, in some instances, the intensity of the generated vibration may be reduced considerably.

5.1.1 Optimal excitation

The following parameters of the hand-held percussion machine are essential characteristics of the performance of the machine:

- frequency of the steady-state motion with a single impact during one period,
- striker velocity just before impact against the pick (energy of striker impact).

In the present design of the electro-pneumatic hammer the crank-slide mechanism is used as an excitation mechanism. This mechanism is simple and reliable in executing sinusoidal motion of the driving piston. However, in case of excitation for electro-pneumatic hammer this motion is not the optimal one. The same parameters of “striker-pick” impact can be achieved via different waveforms of the exciting force.

In [48], a hand-held percussion machine is considered as a discrete pulse modulator, which transforms energy of a constant feed force into a series of periodic impact impulses. Theoretical optimal excitation (optimal dynamic conversion of energy between the driving piston and the striker) was obtained. This optimal excitation enables reduction in hazardous hand-transmitted vibration and relieves load on the drive. This can be achieved mainly by extending the excitation impulses (i.e. pneumatic impulses between the piston and the striker) thereafter reducing their magnitude without any changes in the performance of the machine.

Realisation of this principle in the electro-pneumatic hammer enables the reduction of vibration perceived by the operator and will be considered in detail in Chapter 6.

5.1.2 Optimal striker mass and impact velocity

The same value of striker impact energy, E , can be achieved under a given time of striker acceleration, t_a , for different values of the striker velocity just before impact \dot{x}_- and the striker mass M . These parameters can be chosen in such a manner that acceleration force applied to the striker is minimal, therefore the counter force applied to the casing is minimal as well.

Let us consider the simplest case as an example.

Expressions for velocity and displacement (stroke) of the striker just before impact can be written as follows:

$$\dot{x}_- = \frac{1}{M} \int_0^{t_a} F dt, \quad (5.1)$$

$$x = \frac{1}{M} \int_0^{t_a} \int_0^t F dt^2, \quad (5.2)$$

where F is the current value of acceleration force applied to the striker; M is the mass of the striker; t_a is time of the striker acceleration.

When $F = \text{const}$, the expressions (5.1)-(5.2) take form:

$$\dot{x}_- = Ft_a / M, \quad (5.3)$$

$$x = Ft_a^2 / 2M. \quad (5.4)$$

Impact energy can be written as

$$E = M\dot{x}_-^2 / 2 = F^2 t_a^2 / 2M = Fx. \quad (5.5)$$

Using equation (5.5), the expression for the acceleration force can be obtained as follows:

$$F = \frac{\sqrt{2E}}{t_a} \cdot \sqrt{M}. \quad (5.6)$$

Eq.(5.6) shows that under the given values of the impact energy and the acceleration time (impact frequency), the striker acceleration force that results as a load upon an operator can be decreased by a reduction of the striker mass [60]. Consequently, the striker velocity just before impact must be increased in order to keep the impact energy unchanged. However, there is a restriction for the impact velocity determined by the strength and fatigue for the material of colliding bodies.

5.1.3 Specific distribution of the counter-force

Specific distribution of the counter-force is applied usually for hand-held power tools with pneumatic or hydraulic type of drive. This method is based on a rational distribution of the counter-force between the casing and the striker.

A pneumatic hammer with vibration reduced by employing this approach is shown in Figure 5.1. The working principle is based on a differential striker with front area larger than the rear one and used in series of hand-held pneumatic hammers [61-63].

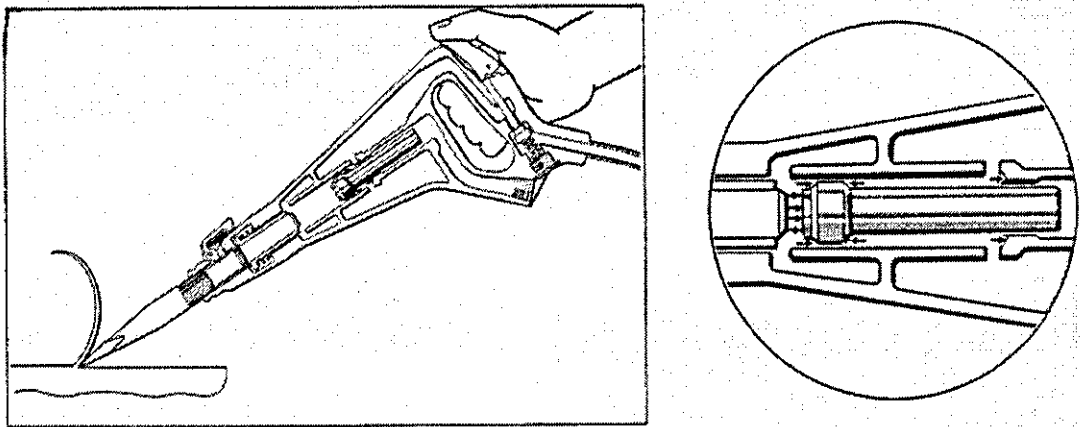


Figure 5.1. Pneumatic hammer with differential striker (reproduced from [63]).

Figure 5.2 shows a complete percussion cycle in a pneumatic chipping hammer with reduced vibration.

In Figure 5.2 (a) striker is in rear position and moving forward. Just before the striker hits the pick, air is blown into the closed front pneumatic chamber through the striker's air channel (see Figure 5.2 (b)). When the striker has hit the pick, it is forced backwards by the compressed air stored in the front chamber as it shown in

Figure 5.2 (c). The air is then exhausted, the striker changes direction and the cycle is repeated (see Figure 5.2 (d)). Air pressure in the rear pneumatic chamber between the casing and the striker is kept constant. This provides a constant force accelerating the striker. The alternating component of striker excitation force is provided by alternating pressure applied to the front area of the striker. The specific feature of this design is that alternating pressure in the front chamber does not produce a corresponding force applied to the casing, because the alternating counter-force is applied directly to the striking bit. As a result, only a constant counter-force created in the rear chamber is applied to the casing of the tool. The magnitude of this force is such that the operator can easily hold the hammer against the object of treatment.

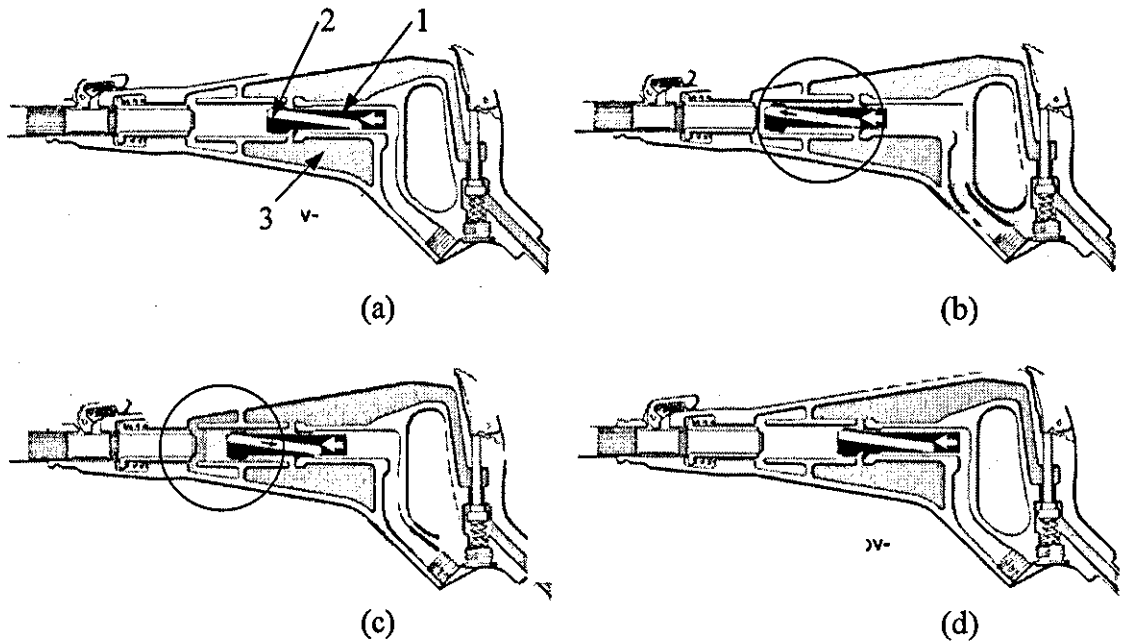


Figure 5.2. Pneumatic hammer with differential striker. 1-differential striker; 2-air channel in the striker; 3-grey area shows pneumatic chambers filled with air (reproduced from [63]).

The method seems to be very effective, however, thorough analysis reveals that there are limitations to its implementation. In order to eliminate vibration due to the pneumatic impact between the striker and the casing, the acceleration force applied to the striker (or, in other words, pneumatic force in the rear chamber) has to be smaller than the feed force applied by an operator. Therefore in the case being considered the maximum possible striker acceleration force is limited by the operator

physical abilities. As a result, the striker needs to be accelerated to the prescribed velocity just before impact, while acceleration time and constant acceleration force are limited by prescribed frequency of impacts and feed force applied by an operator. The latter limits the maximum achievable pick velocity just before impact and consequently energy of impacts, which is the main characteristic of the percussion machine. So the method described here is usually used for a light pneumatic hammer with relatively low impact energy.

5.1.4 Additional inertial elements (dynamic balancing)

Additional elements can be introduced for balancing the moving parts of the machine. The latter approach results in a decrease in low frequency vibration of the machine. The penalty, however, is an increase in the complexity of the design and also an increase in the weight and energy consumed by the machine. Figure 5.3 shows the operating principle of the SB-8 road breaker [64].

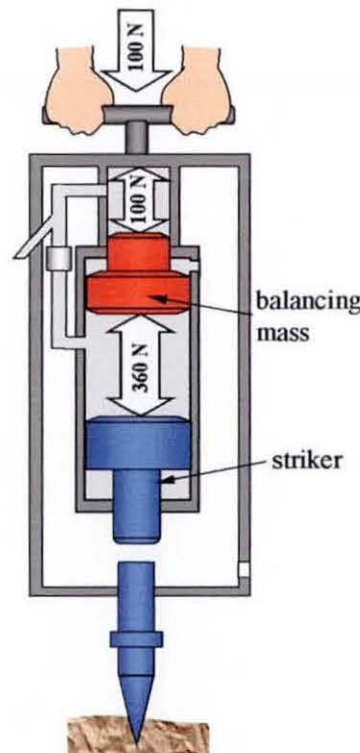


Figure 5.3. Schematics of operating principle of the SB-8 road breaker.

In this design, the alternating component of striker acceleration is cancelled by the motion of a balancing mass in the opposite direction. In this design, the operator perceives only constant pressure through the upper pneumatic chamber. This type of a system could be incorporated in a percussion machine and tuned to the operating frequency.

Alternatively, a second striker can be added which will act in turn with the first striker, thus, producing partial balancing. However, this usually leads to a cost-inefficient design [60].

In some cases, redesigning the machine can radically change the alternating force of excitation. In [66] imbalance of rotating parts was reduced by dynamic balancer driven by positive cam, although such solution was not always effective in reducing vibration of hand-held percussion machines because of the restricted size and weight of this type of machinery.

5.1.5 Other methods

The force of impact between the pick and the buffer mounted on the casing arises during pick motion towards work-piece and against it, applied directly to the casing and, therefore, causes vibration. Some designs allow this additional interaction to be avoided (especially pneumatic and hydraulic type of drive). For example, in the hammer presented in the current study, the parameters of machine were chosen in such way that the pick never hits the casing during its motion towards the work material but only during the pick's rebound against it (see Figure 4.17).

In the designs where such interactions are present, the buffer between the casing and the pick typically has high stiffness in order to maintain stability of the impact process. Reducing the stiffness of the buffer may lead to deterioration in the stability of the operating process and therefore, cannot be used for reducing vibration caused by these impacts.

Figure 5.4 shows a schematic sectional view of an interesting design of pneumatic hammer [67], which enables to reduce significantly the impact force between the pick and the casing. The percussion pneumatic power tool was designed as a handle-carrying frame 1, with elastic covered handles 2, that accommodates the casing 3

striking bit moving in the frame guides 4 and connected through a gas distribution system (not shown in Figure 5.4) to a compressed air source.

The obvious advantage of this design is the footplates 5 mounted on the frame that enable operator to step on it, therefore, to press the tool against the work material with bigger feed force using the weight of his body, and thus to reduce the physical effort required for pressing the tool against a treated surface. This also may solve the problem of the necessary constant acceleration force applied to the striker (see section 5.1.3.), because in this case, constant acceleration force that can be applied to the striker is equal to the weight of the operator, which is much higher than a feed force. In addition, there is a shock absorber 6 mounted between the striking bit and the frame, which applies constant pressure to the striking bit, therefore relieving load upon an operator.

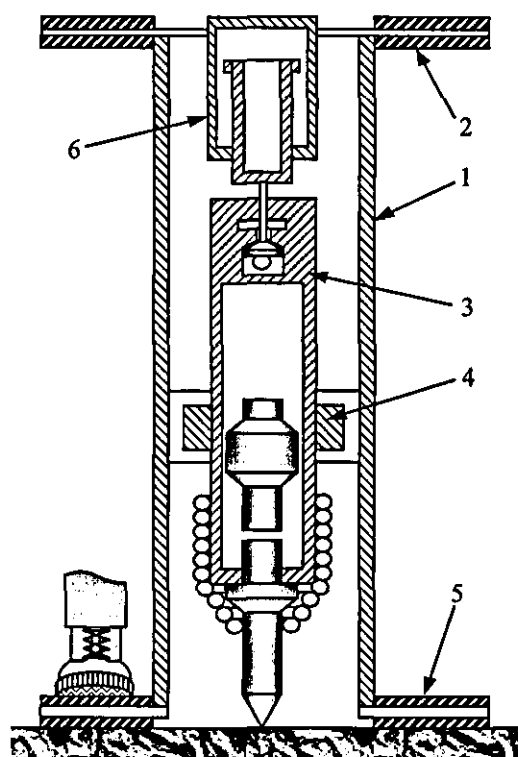


Figure 5.4. Schematic cross-sectional view of pneumatic hammer
(adapted from [67]).

The actual feed force applied by the operator can be reduced by employing tension chains (sometimes called balancers) and manipulators in order to support vibrating tools such as heavy drills, nut runners and pneumatic chisels. Changes in the texture and material of a grip surface may allow the operator to use a lighter grip to hold and control the tool. However, this method is unlikely to lead to any significant reduction in muscle tension of the operator.

Using lighter tools in order to reduce the vibration perceived by an operator seems to be another logical solution. However, in order to reduce the vibration level of a 10-kg tool by 10dB, the weight of the tool must be reduced to 300g [69]. In addition, the vibration emitted by a tool is proportional to the power of the tool but inversely proportional to the weight. Hence, if weight of the tool is decreased without changes of power, the intensity of the vibration of the tool increases. This suggests that an increase in weight of the tool would reduce the vibration level. However, this solution seems unrealistic because, in addition to vibration disorders, workers often suffer from symptoms caused by the handling of heavy tools, e.g., strained muscles and joints.

Additional damping can reduce vibration of hand-held power tools. For example, damping techniques applied to the percussive rivet tool were investigated in [68]. The result showed that additional damping between the pick and the casing could reduce vibration produced by the tool. However, results were different for frequency-weighted and unweighted acceleration produced by the tool and so some further investigations might be necessary.

5.2 Vibration isolation

The second and the most widespread method of vibration protection is vibration isolation [71-73]. A vibration isolator in its most elementary form may be considered as a resilient member placed between source of vibration and protected system (vibrating mass) in order to reduce an undesirable vibratory effect on the system. The concept of vibration isolation can be illustrated on a SDOF system as shown in Figure 5.5

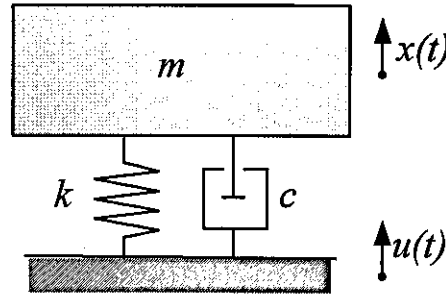


Figure 5.5. SDOF model of vibration isolation

This system consists of a rigid body representing a protected system connected to a foundation by an isolator having resilience and energy-dissipating means. In this case the equation of motion is written as follows:

$$\ddot{x} + 2\zeta\Omega(\dot{x} - \dot{u}) + \Omega^2(x - u) = 0 \quad (5.7)$$

where $(\dot{x} - \dot{u})$ and $(x - u)$ denote the relative velocity and relative displacement of the spring and damper, respectively.

If $u(t) = U \sin \omega t$, equation (5.7) becomes

$$\ddot{x} + 2\zeta\Omega\dot{x} + \Omega^2 x = 2\zeta\Omega\dot{u} + \Omega^2 u = 2\zeta\Omega\omega U \cos \omega t + \Omega^2 U \sin \omega t = A \sin(\omega t - \alpha) \quad (5.8)$$

where $A = U \sqrt{\Omega^4 + (2\zeta\omega\Omega)^2}$ and $\tan \alpha = -\frac{2\zeta\omega}{\Omega}$.

This shows that giving excitation to the base is equivalent to applying a harmonic force of magnitude A to the body. In this case the steady state response of the body, $x(t)$ can be expressed as

$$x(t) = \frac{U \sqrt{\Omega^4 + (2\zeta\omega\Omega)^2}}{\sqrt{(\Omega^2 - \omega^2)^2 + (2\zeta\Omega\omega)^2}} \sin(\omega t - \alpha - \varphi_1), \quad (5.9)$$

where

$$\varphi_1 = \arctan \frac{2\zeta\Omega\omega}{\Omega^2 - \omega^2} + \frac{1}{2} \left(\operatorname{sgn} \left(\frac{\omega}{\Omega} - 1 \right) + 1 \right) \pi, \quad (5.10)$$

where $\Omega = \sqrt{\frac{k}{m}}$ is the natural frequency and $\zeta = \frac{c}{2m\Omega}$ is the loss factor of the system.

The ratio of the amplitude of the response $x(t)$ to that of the base motion $u(t)$, is called the displacement transmissibility, T_d .

$$T_d = \sqrt{\frac{1 + (2\zeta r)^2}{(1 - r^2)^2 + (2\zeta r)^2}}, \quad (5.11)$$

where r is the frequency ratio ω / Ω .

Equation (5.11) is also shows the ratio of the maximum steady state accelerations of the mass and the source of vibration. Vibration attenuation is taking place when $T_d < 1$. From Eq. (5.11) the necessary frequency ratio can be found:

$$r > \sqrt{2} \quad (5.12)$$

The variations of T_d given by equations (5.11) are shown in Figure 5.6 for different values of the loss factor and the frequency ratio.

For hand-held machines, the source of vibration and protected system have commensurable masses, hence, these conditions for vibration attenuation are not quite adequate, although give a good general idea of vibration isolation principles. The main rule remains the same: performance of vibration isolation system improves when ratio between excitation frequency and natural frequency of the isolator increases and loss factor decreases.

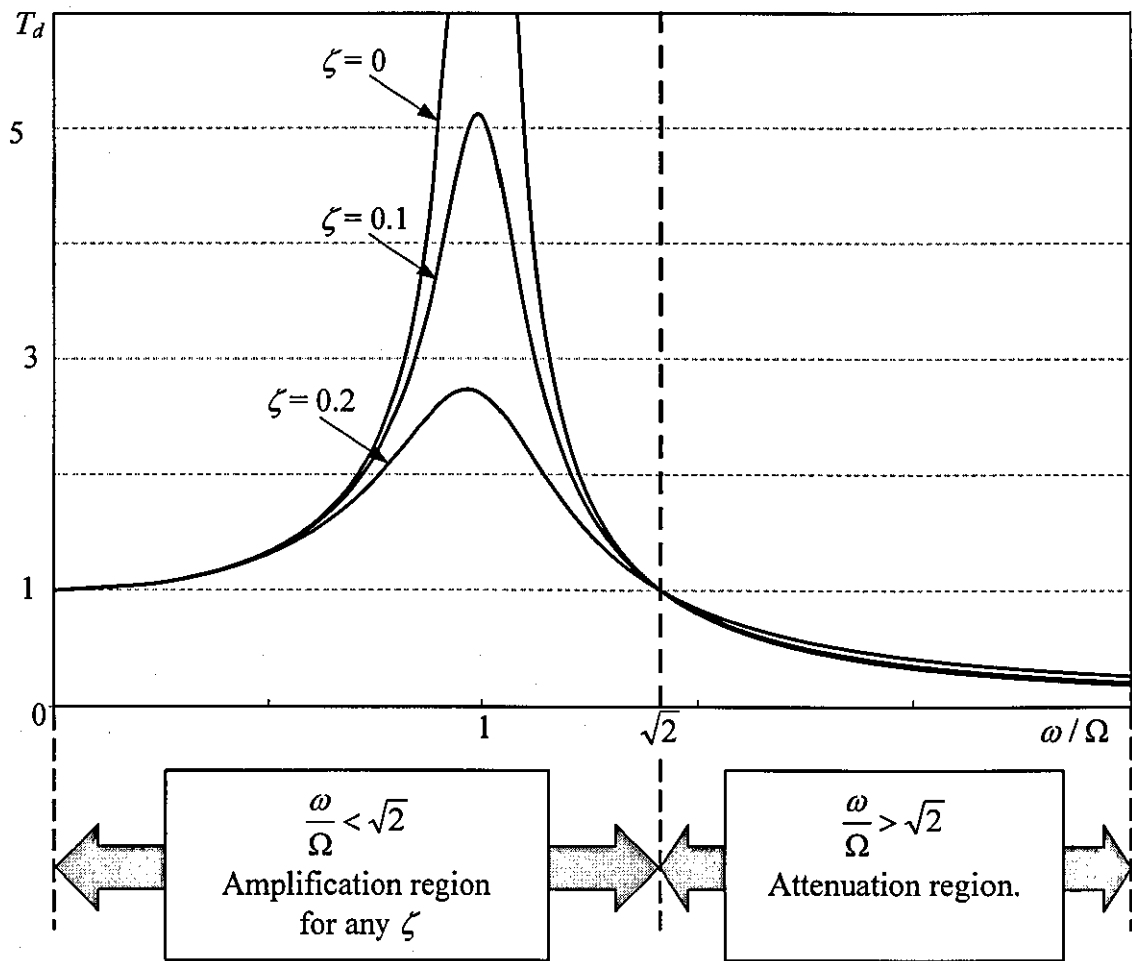


Figure 5.6. Amplitude versus frequency characteristic of transmissibility for SDOF system.

Two-degree-of-freedom models are closer to description of vibration isolation for hand-held power tools. Such a system is shown in Figure 5.7, where the structure of source of vibration to which the isolator is connected moves with the protected system.

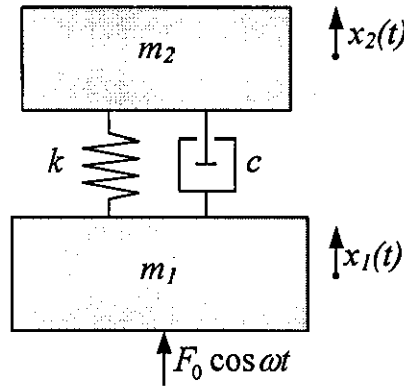


Figure 5.7. Two-degree-of-freedom model of vibration isolation

Equation of motion for such system will take form:

$$m_1 \ddot{x}_1 + c(\dot{x}_1 - \dot{x}_2) + k(x_1 - x_2) = F_0 \cos \omega t \quad (5.13)$$

$$m_2 \ddot{x}_2 - c(\dot{x}_1 - \dot{x}_2) - k(x_1 - x_2) = 0 \quad (5.14)$$

By solving Eqs. (5.13) and (5.14) we obtain expression for efficiency factor of vibration isolation:

$$\eta = \sqrt{\frac{(1-r^2)^2 + 4\zeta^2 r^2}{1 + 4\zeta^2 r^2}} \quad (5.15)$$

where efficiency factor, η is the displacement ratio of protected object without and with vibration isolation; $r = \frac{\omega}{\Omega}$ is the frequency ratio; $\zeta = \frac{c}{2m\Omega}$ is the loss factor;

$$m = \frac{m_1 m_2}{(m_1 + m_2)} \quad (5.16)$$

is effective mass of the system.

The efficiency of vibration isolation for such a system increases with increasing the frequency ratio r , in quite the same manner as vibration attenuation in SDOF system. So the natural frequency of the appropriate vibration isolator must be lower than the fundamental excitation frequency in order to achieve effective vibration isolation.

Low stiffness of the vibration isolator or a large mass of the system being isolated can provide the low natural frequency of the vibration isolator. However, low stiffness leads to a high static deflection under nominal feed force, which is

undesirable for hand-held machines. At the same time, an increase in the mass of hand-held machine is unacceptable because this will result in an increase of the load on the operator. The only option for optimisation parameters of vibration isolator is increasing of effective mass of the tool. It is clear, that maximum effective mass can be achieved when $m_1 = m_2$ in Eq. (5.16) i.e. total mass of the machine equally divided between source of vibration and protected object.

When the operator is taken into consideration, the whole picture of vibration isolation for hand-percussion machines becomes even more complicated [74-76]. The hand-arm system itself is a very complex, active biological system and there have been many attempts to measure its dynamical characteristics (see Chapter 3). It is very difficult to build a general model of such a system and therefore develop a universal approach for optimal vibration isolation. Dynamics of the machine-isolation-operator system may be affected by force, tactile, vision and auditory feedbacks between an operator and machine. Apparently, the influence of these factors even increases with decreasing of operating frequency [60].

Synthesis of the optimal isolation system of hand-transmitted vibration is a challenging task. There are principal factors that influence the problem of vibration isolation of the hand-arm system. The hand-transmitted vibration can have a very diverse character. This character varies greatly depending on the kind of hand-held machine used, the shape, mass and material of the object being treated, the type and conditions of the work as well as operator technique. The power spectral densities of hand-held percussion machine have irregular shape and are difficult to approximate by rational functions.

However, general criteria for vibration protection of the operator can be formulated simply from a common sense. From the operator perspective, the static stiffness of the flexible component should be high enough to ensure small static deflection of the machine as well as a wide range of acceptable feed force that would not affect operating process. At the same time, in order to achieve vibration attenuation, dynamic stiffness of the isolator must be low. Consequently, an effective vibration protection system for the hand-held power tool is characterised by a high static stiffness as compared with dynamic stiffness.

An important factor that may affect performance of vibration isolation system is a feed force applied by an operator. Usually, the manufacturer specifies the feed force for every particular machine. In practice, however, the operator cannot maintain the

same force over the whole work duration. Also, physical abilities of an operator differ from one person to another. Apart from affecting productivity of the machine as was shown earlier, this fact has to be taken into consideration when a vibration isolation system is designed.

Lets consider a simple example. A riveting hammer requires a static feed force of 150 N. The impact frequency of the tool is 30 Hz. The handle and hand corresponds to a mass of 0.5 kg. With a spring providing a natural frequency equal to half the frequency of the excitation force, the static deflection will be 30 mm. A riveting hammer with such a large static deflection is experienced to be difficult to control. It is obviously possible to pre-load a spring so that a moderate deflection is obtained at nominal static load, however this implies that the attenuation is ineffective for feed forces that are smaller than the nominal feed force. So, ideally, a vibration protection system shall be independent on changes of feed force.

The operator is constantly holding the tool during operation, therefore, he/she directly perceives any modification of size, weight etc. Hence, a vibration protection system, which eliminates vibration hazard should be designed in such way, that no additional hazard for an operator is added.

Justification of the cost of a vibration protection system is also necessary, because low manufacturing cost of hand-held power tools is an important factor that contributes to their wide application.

5.2.1 Passive methods of vibration isolation

Vibration isolation in the hand-held percussion machine is primarily attained using two approaches: isolation of the tool handle from the vibrating source and isolation of the hand from the vibrating handle (this is achieved by using gloves, energy flow dividers, operator substitution by a guided machine or a robot, remote control, etc).

The use of gloves in order to reduce vibration transmission is the simplest method for decreasing risk of injury. There are several types of gloves commercially available. It is not clear however, whether these gloves do result in a reduction of vibration exposure or not. Measurements have shown that in most cases, gloves have no effect on the vibration load with respect to low-frequency exposure. At higher

frequencies, their isolation properties are greater, although to a limited extent. At the same time, these measurements were based on frequency-weighted magnitudes of acceleration which might cause underestimation of gloves effect [19]. Sometimes operators are supplied with standard lattice-coated knitted gloves that are chosen specifically to keep their hands warm [65]. Although this solution does not affect the actual measured vibration exposure, hand and body temperature do affect peripheral circulation and are believed to have an effect on the development of vibration white finger.

A concept of a flow-divider, comprising two rigid links coupled through a parallel combination of energy restoring and dissipative elements, is proposed to attenuate hand-transmitted vibration in [42]. The flow divider, when attached between the hand and the elbow joint, permits the flow of portion of vibrating energy through the links. While the energy directed through the divider links is partially dissipated within the isolator, a part of the vibration energy is injected into the elbow joint. The vibration levels at the elbow joint may thus be expected to increase. Although an increase in vibration transmitted to the elbow joint is not desirable, a compromise in exchange of vibration energy between the hand and the other parts of the arm may be achieved by tuning the flow divider parameters.

The simplest and most common way to isolate the hand from the vibrating handle is an elastic cover on the handle. It is cost-effective, because there is no need to modify machine itself, that is why all hand-held machines have isolated handles. It is evident, however, that such resilient element attenuates vibration in high frequency range only.

In a similar manner, a flexible element can be introduced between the handle and the source of vibration. For example, elastic coupling between the crankshaft incorporated in the cylinder body and the motor section was used in order to reduce the reaction force of the connecting rod via the piston, resulting from rapid air compression between the piston and the striker in [66].

In [39], a mechanical low pass filter between the hand-arm and vibrating machine was designed. Figure 5.8 shows such element, which allows achieving vibration isolation in three vibration directions.

The idea is interesting, but did not find commercial application for several reasons. Measurements of vibration produced by hand-held percussion machines

show that for most of these machines, vibration in the direction parallel to the stroke is of most significance. In this case, introduction of such a complex system with significant additional weight does not seem to be justifiable. In addition, the problem of obtaining high static stiffness in comparison with dynamic one remains the same.

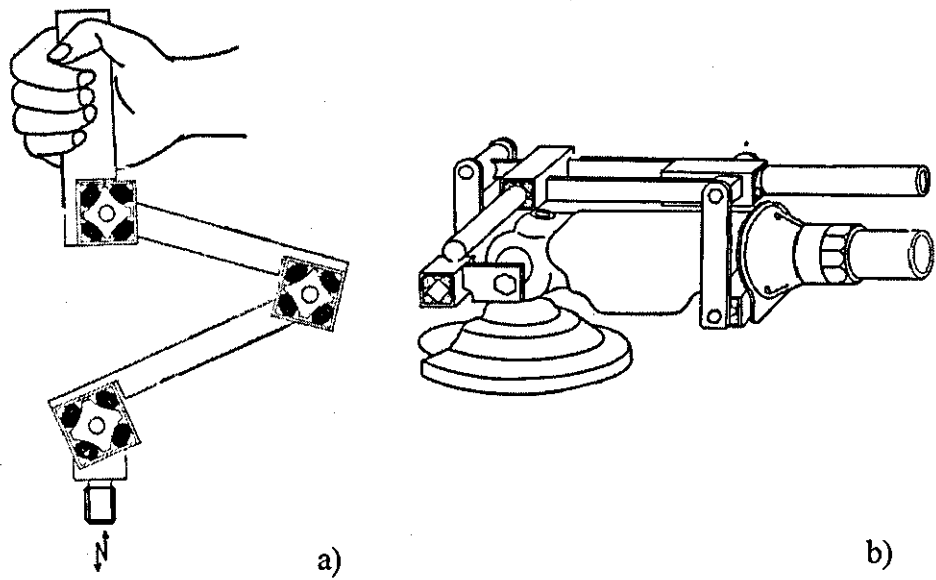


Figure 5.8. (a) An element of vibration isolator in which three pieces of Nighthart system were used; (b) the grinder with vibration isolator (reproduced from [39]).

There are some resilient elements that can offer a solution to this problem. These elements have less stiffness when static deformation is increased. When feed force reaches the nominal (optimal for particular type of the tool) value, the stiffness of such an element becomes zero and attains ideal vibration isolation. These elements have been referred to as zero-stiffness elements [60]. Figure 5.9 shows one of these systems.

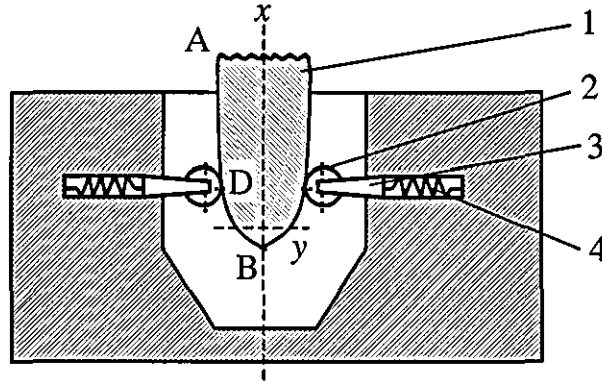


Figure 5.9. Zero-stiffness vibration isolation element (redrawn from [60]).

Wedge 1 is moving down under feed force applied by an operator and compressing linear springs 4 through the roller 2 and the slide blocks 3. Horizontal component, F_h , of spring force calculated as follows:

$$F_h = k_h y, \quad (5.17)$$

where k_h - stiffness of the spring 4, y - spring deformation under applied feed force.

Further, the vertical component that is applied to the wedge through the rollers, i.e. effort applied by the operator (friction force is neglected):

$$F_v = 2F_h \tan \alpha = 2k_h y dy / dx, \quad (5.18)$$

where α - the angle of the curve AB at the point D (see Figure 5.9). Thus, stiffness of the whole element in vertical direction:

$$k_v = \frac{dF_v}{dx} = 2k_h \left[y \frac{d^2 y}{dx^2} + \left(\frac{dy}{dx} \right)^2 \right]. \quad (5.19)$$

As the wedge profile is chosen in such a manner that the reactive force of the rollers is an increasing function and vertical stiffness is decreasing function, the vertical stiffness becomes zero when F_v has reached a particular value.

The disadvantage of this system is that the ideal vibration isolation can be achieved only for particular feed force determined by the wedge profile. As a consequence, such a vibration isolation system cannot be adapted to the intrasubject

and intersubject operator's parameters variability. Connecting such elements in sequence can increase the effective feed force range. Such a system will have a stepwise force-displacement characteristic, but for slope parts of this characteristic, risk of sufficient increase of the element stiffness in vertical direction exists. Another point of concern is the fact that with "zero-stiffness" between the operator and the machine the operator cannot "feel" the machine and therefore cannot control it.

Another possible "zero-stiffness" element is shown in Figure 5.10. This element is a radially compressed thin-walled rubber tube placed between the casing and the handle [60]. When the feed force P initially increases from $P=0$, the load-deflection characteristic is shown as line 1 in Figure 5.11, where $\varepsilon = \Delta/R$ is a relative compression. So initially, the stiffness of such an element is quite high (see Figure 5.10 (a)). The second stable configuration (the buckled tube) is shown in Figure 5.10 (c) and the corresponding load-deflection characteristic is shown as line 2 in Figure 5.11. The transition between the two stable configurations starts when the feed force P exceeds predesigned value and is shown in Figure 5.10 (b). The load deflection characteristic is presented as line 3 in Figure 5.11, where this configuration is characterised by negative stiffness. The size and character (negative stiffness, low positive stiffness or quasi-zero stiffness) of line 3 can be modified by changing parameters of the tube. Many other shapes of rubber flexible elements possessing quasi-zero stiffness can be designed [70].

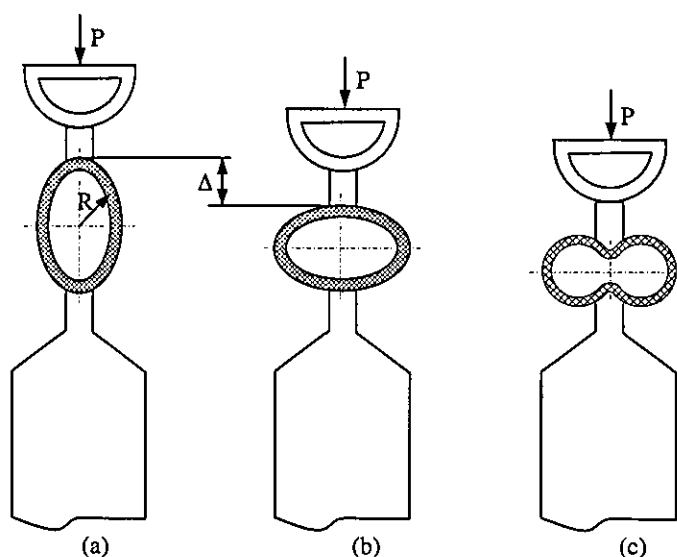


Figure 5.10. Oval tube vibration isolation element (reproduced from [60]).

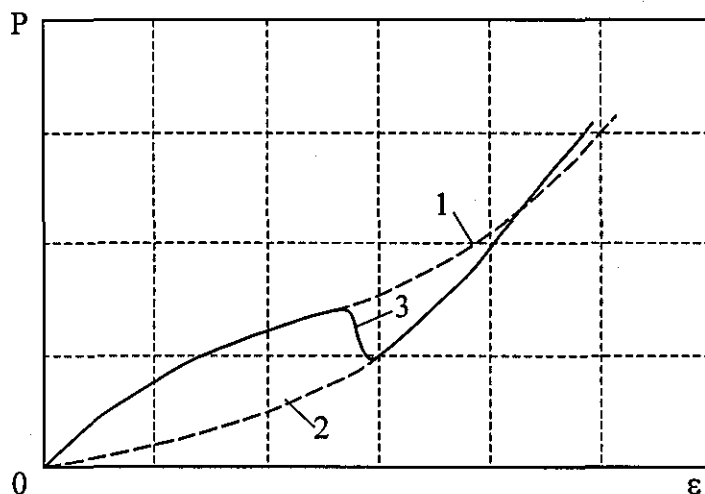


Figure 5.11. Load-deflection characteristics.

So far, only mechanical springs have been considered in the present review. There is another class of springs, which employs a compressible gas as a resilient element [71, 77, 78] and which are referred to as pneumatic springs. The simplest pneumatic spring is a gas chamber and a piston. Thus the force generated by any pneumatic spring depends on the pressure in the chamber and the effective area. Pneumatic springs do not require a large static deflection because the energy storage capacity of the air is better than that of rubber or metal. Although it is not worthwhile to introduce another passive pneumatic spring in the machine where the pneumatic chamber is already present, different combinations of chamber and piston enable variable characteristics of the resilient element for vibration isolation of other types of hand-held machines to be obtained. But, nonlinearity of their characteristics due to the air properties and sensitivity to changes in temperature limits their application.

Vibration isolation methods that have been considered thus far are passive methods of vibration isolation, where protection against vibration is achieved without expending additional energy from an energy source. These methods are well studied and relatively simple. At the same time, in passive elements of vibration isolation it is difficult to realise high static stiffness compared with dynamic stiffness. In certain applications, an active or semi-active vibration protection system may prove to be more successful, as they can be specifically designed in order to meet these criteria. Although active vibration control systems can generally provide performance beyond

that possible using passive systems, this increase in performance is purchased at the price of increased cost and complexity.

5.2.2 Active methods of vibration isolation

An active pneumatic spring for vibration isolation of hand-held pneumatic riveter was designed in [79]. The pneumatic spring is shown in Figure 5.12 and was designed as a flow chamber with a changing volume and pressure, which is controlled by the relative displacement of the rigid piston. Flow out takes place through the oblong orifice with a changing area $A_2(x)$, into a second tank with a constant discharge pressure P_2 . The piston motion causes a change in the chamber volume and the dimensions of the working part of the discharge orifice. As the active area $A_2(x)$ considerably influences the chamber pressure P through changing the mass rates of flow in and out, the periodic motion of the piston induces periodic changes in the chamber pressure of amplitude ΔP around a certain value P_0 . From knowledge of how ΔP and P_0 depend on the parameters of the system, the authors determined the static and dynamic stiffness of the pneumatic spring.

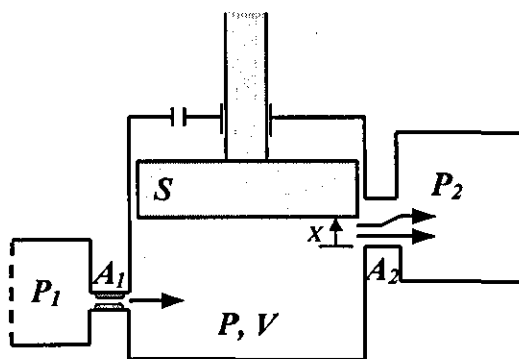


Figure 5.12. A schematic diagram of the active pneumatic spring (reproduced from [79]).

The principle of this spring is similar to the idea of the pneumatic hammer with differential striker (see Section 5.1.3). The pressure in the pneumatic chamber P between the striking bit and the casing maintained constant and if this pressure is equal to the feed force, the operator does not perceive alternating load due to

vibration of the striking bit. The advantage of the active pneumatic spring is that such spring is to some extent adaptable to the feed force applied by the operator. However, striker acceleration force is limited by the operator's physical abilities as in case of pneumatic hammer with differential striker.

The stiffness ratio between the dynamic and static stiffness of such active pneumatic spring is a decreasing function of the dimensionless frequency, the width of the discharge orifice and the overall pressure ratio. Authors pointed out that the minimal value of this ratio occurs when the area of the discharge orifice is almost twice as great as the area of the inlet orifice. Optimal parameters of the spring can be chosen in such a manner that the static stiffness is almost 20 times higher than the dynamic one. Such spring was implemented into the pneumatic riveter, as a result, the r.m.s. value of the handle acceleration was reduced by a factor of 4, while the relative displacement of the handle was limited to 2mm.

5.2.3 Mechanisation and remote control of the hand-held tools

There is another possibility of eliminating the hazard caused by vibration impact processes by substituting it with other non-hazardous processes. Mechanisation and remote control or automation can greatly reduce operator exposure to vibration. Robots are being used increasingly in manufacturing; various industrial organisations have developed robot or highly automated grinders and burning machines for the removal of casting feeder heads and other fettling operations.

For example, it is possible to reduce the vibration exposure of an operator by using a larger breaker attachment mounted on the arm of an excavator [65]. A utilities contractor for digging telecommunications trenches successfully used this method. The breaker was powered using the excavator hydraulic and was activated by a foot pedal. A pair of levers, passing very little vibration to the operator's hands, controlled the arm position. This method reduces the duration of vibration exposure to the operator, but the problem of vibration transmitted from the breaker to the excavator is topical.

5.3 Dynamic absorption

The third fundamental method of vibration attenuation is dynamic absorption of vibration. Since its invention almost a century ago, the dynamic absorption has been used widely for reducing vibrations of machinery, bridges, buildings, ships and many other mechanical systems.

The principle of dynamic absorption is very simple. If primary system is excited by a force or displacement that has a constant frequency, then it is possible to modify the vibration pattern and to reduce its amplitude significantly by using of an auxiliary body on a spring attached to the primary system. This additional auxiliary body is referred to as a dynamic absorber. Lets consider the principle of dynamic absorption on a simple SDOF primary system shown in Figure 5.13 [72]. Here m_1 is the mass of the primary system, m_2 is the mass of the auxiliary body attached to it.

The equations of motion for the bodies m_1 and m_2 are:

$$m_1 \ddot{x}_1 + k_1 x_1 + k_2 (x_1 - x_2) + c_2 (\dot{x}_1 - \dot{x}_2) = F_0 \sin \omega t \quad (5.20)$$

$$m_2 \ddot{x}_2 + k_2 (x_2 - x_1) + c_2 (\dot{x}_2 - \dot{x}_1) = 0. \quad (5.21)$$

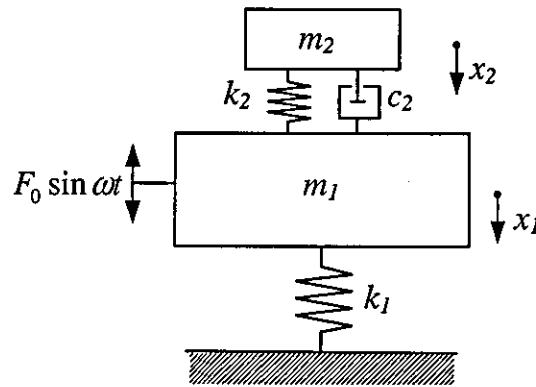


Figure 5.13. Damped dynamic vibration absorber

By assuming solution to be

$$x_j(t) = X_j \sin \omega t, \quad j=1, 2 \quad (5.22)$$

the steady-state solution of Eqs. (5.20) and (5.21) can be obtained:

$$X_1 = \frac{F_0(k_2 - m_2\omega^2 + ic_2\omega)}{[(k_1 - m_1\omega^2)(k_2 - m_2\omega^2) - m_2k_2\omega^2] + i\omega c_2(k_1 - m_1\omega^2 - m_2\omega^2)} \quad (5.23)$$

$$X_2 = \frac{X_1(k_2 + i\omega c_2)}{(k_2 - m_2\omega^2 + i\omega c_2)} \quad (5.24)$$

By defining:

mass ratio, $\mu = m_2 / m_1$; static deflection of the system, $\delta_{st} = F_0 / k_1$;

natural frequency of the absorber, $\Omega_a = \sqrt{\frac{k_2}{m_2}}$;

natural frequency of the main mass, $\Omega_1 = \sqrt{\frac{k_1}{m_1}}$;

ratio of natural frequencies, $f = \frac{\Omega_a}{\Omega_1}$; forced frequency ratio $g = \frac{\omega}{\Omega_1}$;

critical damping constant $c_c = 2m_2\Omega_2$, loss factor $\zeta = \frac{c_2}{c_c}$

the magnitudes, X_1 and X_2 , can be expressed as follows:

$$\frac{X_1}{\delta_{st}} = \left[\frac{(2\zeta g)^2 + (g^2 - f^2)^2}{(2\zeta g)^2 (g^2 - 1 + \mu g^2)^2 + (\mu f^2 g^2 - (g^2 - 1)(g^2 - f^2))^2} \right]^{1/2} \quad (5.25)$$

$$\frac{X_2}{\delta_{st}} = \left[\frac{(2\zeta g)^2 + f^4}{(2\zeta g)^2 (g^2 - 1 + \mu g^2)^2 + (\mu f^2 g^2 - (g^2 - 1)(g^2 - f^2))^2} \right]^{1/2} \quad (5.26)$$

The variation of the vibration amplitude $\left(\frac{X_1}{\delta_{st}} \right)$ of the composed system as a function of the forced frequency ratio g is shown in Figure 5.14. Here, $f = 1$, $\mu = 1/5$ and ζ varies.

As can be seen from Figure 5.14, the dynamic absorber alters the frequency response of the primary system by introducing the additional degree-of-freedom into it. When damping is zero ($c_2 = \zeta = 0$) and the absorber is tuned to the natural frequency of initial system ($\Omega_a = \Omega_1$), the force exerted by the auxiliary spring is opposite to the impressed force and neutralises it, thus reducing X_1 to zero. For effective performance of dynamic absorber that suppresses vibration on excitation

frequency, precise tuning to the excitation frequency and low loss factor of dynamic absorber are the main design criteria. If the tuning is incorrect, the attachment of dynamic absorber may bring the composite system into resonance with the excitation force.

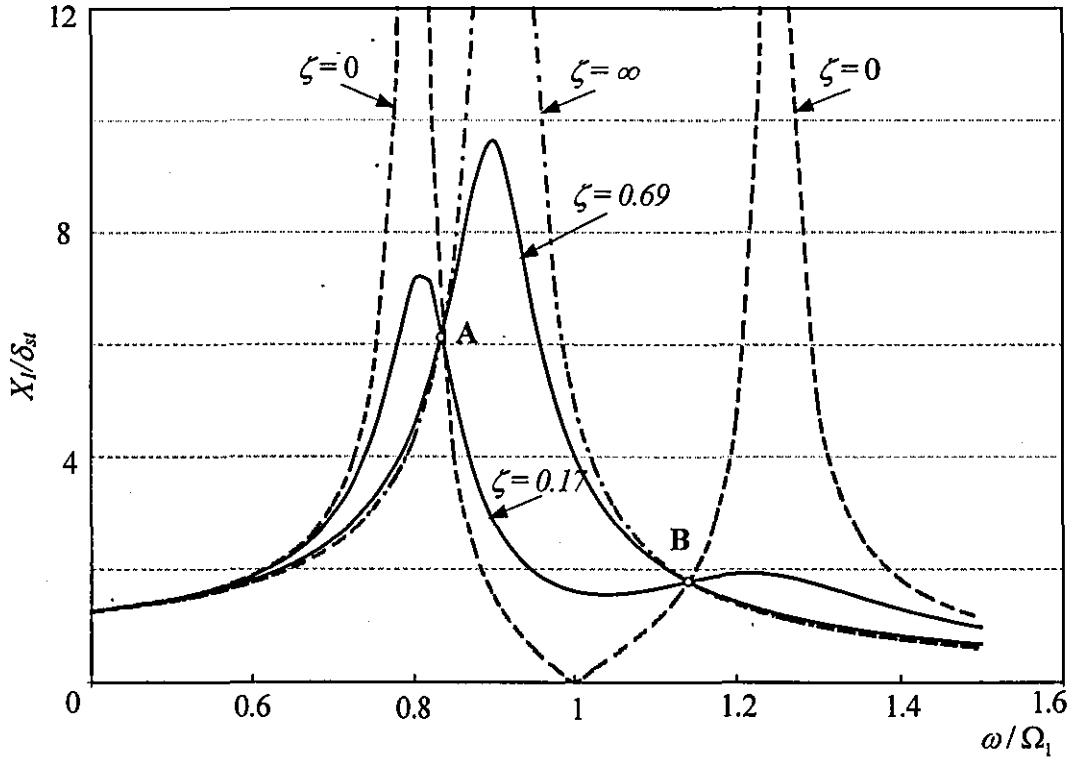


Figure 5.14. Amplitude versus frequency response of SDOF system with damped dynamic vibration absorber

When frequency of the excitation applied to the primary system is varying, the effective frequency range of dynamic absorber can be increased by rational use of its damping characteristics. In this case, the dynamic absorber is designed to add damping to and change the resonant characteristics of a primary system in order to maximally dissipate vibration energy over a range of frequencies. So, the design principles for this type of dynamic absorber will be different.

A classical design method for broadband applications, known as the equal-peak method is studied in [80-82]. It can be seen from Figure 5.14 that all curves intersect at points A and B regardless of their value of damping. Consequently, optimal parameters of damped dynamic absorber should be chosen in such a way that ordinates of the points A and B are equal and correspond to the maximum of amplitude-frequency response of the compound system, because this common value

will be exceeded if the absorber is tuned differently. By following this method, the optimal parameters of dynamic absorber can be found.

The points A and B can be located by substituting the extreme cases of $\zeta = 0$ and $\zeta = \infty$ into Eq. (5.25). This yields:

$$g^4 - 2g^2 \left(\frac{1 + f^2 + \mu f^2}{2 + \mu} \right) + \frac{2f^2}{2 + \mu} = 0 \quad (5.27)$$

The two roots of Eq. (5.27) indicate the values of the frequency ratio, $g_A = \frac{\omega_A}{\omega}$ and $g_B = \frac{\omega_B}{\omega}$ corresponding to the points A and B. The ordinates of A and B can be found by substituting the values of g_A and g_B into Eq. (5.25). The most efficient vibration absorber is the one for which the ordinates of the points A and B are equal. This condition requires that

$$g_A^2 + g_B^2 = \frac{2}{1 + \mu} \quad (5.28)$$

In an equation Eq. (5.27) having unity for the coefficient of its highest power, the sum of the roots is equal to the coefficient of the second term with its sign changed (Vieta principle):

$$g_A^2 + g_B^2 = 2 \frac{1 + f^2(1 + \mu)}{2 + \mu} \quad (5.29)$$

By equating the right parts of Eqs. (5.28) and (5.29), the optimal condition for tuning of the damped dynamic absorber is the following:

$$f_{opt} = \frac{1}{1 + \mu} \quad (5.30)$$

The optimal value of the loss factor ζ can be found by making the response curve $\frac{X_1}{\delta_{st}}$ as flat as possible at peaks A and B. By setting the slope equal to zero at points A and B, and finding a convenient average value of ζ^2 for the points A and B, we obtain:

$$\zeta_{opt}^2 = \frac{3\mu}{8(1 + \mu)^3} \quad (5.31)$$

According to Eq. (5.30), the tuning frequency of damped dynamic absorber is always less than the primary system resonance. Figure 5.15 is a case of such tuning for $\mu = 0.25$.

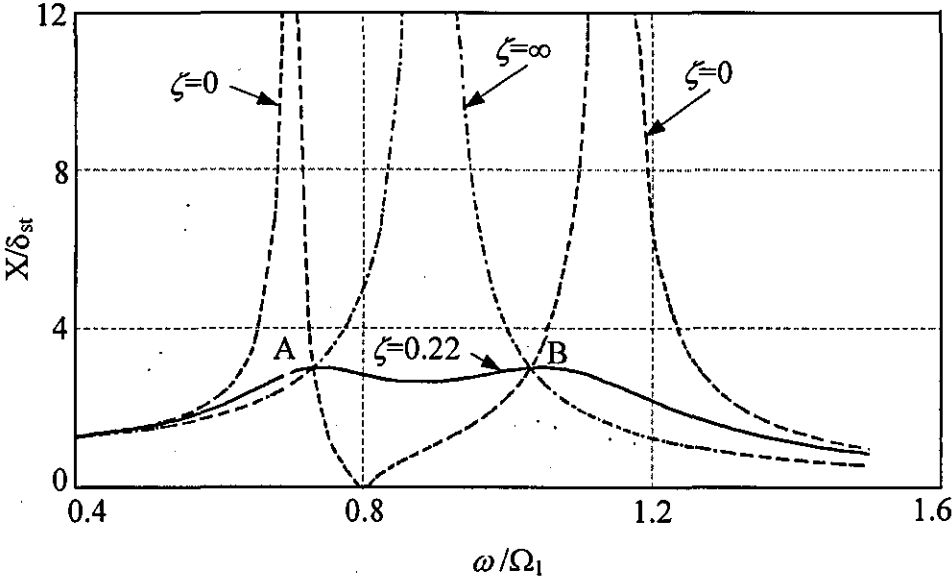


Figure 5.15. Amplitude versus frequency response of SDOF system with optimally tuned damped dynamic absorber.

In a manner, similar to the dynamic absorber with low damping, the performance of damped dynamic absorber improves as the mass of the dynamic absorber increases.

Besides the equal-peak method, there have been many studies of other optimal designs of damped dynamic absorbers [83], however, the equal-peak method is a most commonly used.

The simplest design of dynamic absorber is a spring-mass oscillator. While this simple design remains a favourable choice, there have been many design variations of dynamic absorbers [83] namely, pendulum-type absorber, rotary dynamic absorber (which is similar to pendulum type except that the restoring force is provided by centrifugal force rather than the gravity), ring type dynamic absorber with a distributed support spring, ball absorber, magnetic dynamic absorber and many others. There are also studies of multi-degree-of-freedom dynamic absorbers, where by allowing the reaction mass to have more than one degree-of-freedom, it is

possible to develop a single-mass dynamic absorber that can reduce vibration at several frequencies and thereby achieve weight savings. Finally, it is the nature of vibration and forces acting in the primary system that determines the final choice of the type of dynamic absorber.

The point of attachment of dynamic absorber is important factor for effective vibration attenuation. A dynamic absorber attached to the system at the same point where excitation is applied neutralises vibration effect on the system. A dynamic absorber attached to any other point gives only local effect of vibration attenuation in the area of attachment. Consequently, when vibration load is distributed over the system, the effect of the dynamic absorber is local.

In general, only one mass is used in a dynamic absorber. However, it is possible to provide a dynamic absorption that is effective for a wider frequency range by attaching additional absorbers tuned to several different frequencies. In this case, detuning of every individual absorber plays a very important role. If natural frequencies of some of the absorbers higher and others lower than excitation frequency, their actions are mutually cancelled. This neutralises effect of dynamic absorption. Hence, when several dynamic absorbers are used, their detuning have to be of the same sign [84].

It is possible to extend the frequency range over which the dynamic absorber is effective by using a nonlinear spring or impact interaction. The non-linear dynamic absorber was first considered by Roberson [85] who studied a dynamic vibration absorber with a linear and cubic spring in parallel, and showed that such a non-linear dynamic absorber had a wider suppression band than the linear vibration absorber. Since then, the need to design absorbers which are efficient over broad bands of excitation frequencies has led to studies on absorbers with non-linear [86-88] or piecewise linear [89, 90] characteristics. An impact vibration absorber has the advantage of not exhibiting the amplitude peaks that are generated by a linear vibration absorber on both sides of the resonance frequency. However, it has a smaller suppression band than that of a linear dynamic absorber. If a form of excitation is known, nonlinearity of the absorber spring can be chosen in such a manner that effective frequency range of dynamic absorber is widen [84]. However, due to the complexity of the analysis of a nonlinear system, analytical study of optimal parameters of dynamic absorber is difficult, so it is necessary to use a trial-and-error procedure, which might prove to be difficult. Another general point of

concern with non-linear dynamic absorbers is that they may lead to instabilities of the combined system with unwanted consequences.

It is obvious, that passive dynamic absorbers are effective only when the tuning and damping are appropriate for particular operating and environmental conditions. Because these conditions often change with time, passive dynamic absorbers may become detuned and lose their effectiveness. In some cases detuned dynamic absorbers may even increase in the undesired vibration of the primary system. So researchers are working towards developing dynamic absorbers with controllable or adjustable parameters such that their behaviour can be tuned automatically [83]. However, such absorbers are vulnerable because of instability, which may be induced by the nature of the active control element. This is a serious concern that prevents the active dynamic absorbers from common usage in most industrial applications.

The operating frequency of a typical hand-held percussion machine, supported by a drive mechanism with stiff characteristic, is constant. Hence, it is possible to effectively reduce the vibration by employing a dynamic absorber tuned to the driving frequency. However, there are some disadvantages associated with this method.

Firstly, as a rule of thumb, the mass ratio between the mass of the dynamic absorber and the mass of the primary system is usually taken to be between 0.05 and 0.25 [91]. The dynamic absorber with high mass is unacceptable, because a significant increase in mass of the machine will lead to an additional load imposed upon the operator. Using absorber with smaller mass will lead to large absolute displacement of the dynamic absorber, which makes it impossible to use for hand-held machines.

Secondly, only one frequency component can be suppressed when a passive tuned dynamic absorber is used. Therefore, this method cannot be used for vibration attenuation of hand-held percussion machines where significant high-frequency component are present.

5.4 Other methods

There are some other methods of reducing vibration of hand-held percussion machines. For example, minimisation of the forces that are necessary in order to control the tool will reduce muscle tension of an operator and according to some research (see Chapter 2) hazardous vibration effect. At the same time, as was shown earlier, the main operating principle of hand-held percussion machines requires the operator to apply feed force sufficient to hold the machine against the treated material. Impact energy of the machine also depends on the value of the feed force. So evaluation of this method requires introduction of some additional means to support the machine and is unlikely to be solved by simple redesign.

The simplest approach taken aboard by most manufactories and employers is to reduce the length of vibration exposure, for example, through job rotation or sharpness of pick. In this case, the reasonable compromise between length of exposure and possible increase in vibration level is doubtful and dictated by the convenience of the situation.

5.5 Conclusions and discussions

The operating principle of hand-held power tools requires constant interaction between the operator and the tool. This fact determines necessity and main specific criteria for the design of a low-vibration percussion machine:

- operator perceives any modification of machine, so engineer needs to ensure that when eliminating one hazard, no additional hazard is created (additional mass will increase load on the operator, etc);
- operator needs to control the machine, so static stiffness of the element between operator hand and percussion machine needs to be relatively high (this will also ensure operational safety);
- hand-held percussion machines are widely used due to their relatively simple design, performance reliability and inexpensive manufacturing costs, so new low-vibration hand-held percussion machines will not find wide application unless they meet these criteria.

As was shown, there is a large variety of different methods for reducing vibration perceived by an operator of a hand-held percussion machine. Passive methods of vibration protection have the unquestionable advantage of simplicity and robustness, provided that they are effective. However, methods of reducing intensity of sources of vibration usually require redesign of the machine; simple vibration isolation cannot provide high static stiffness as compared with a dynamic one; dynamic absorption means significant increase of weight of the tool and effective for suppression particular frequency only. Active methods of vibration protection are usually more effective, but limited in use due to their cost and complexity. So, combination of different passive methods of vibration attenuation might offer a solution to the problem of vibration protection of an operator of a hand-held percussion machine.

Chapter 6

Dynamic correction of excitation of the hand-held percussion machine

Optimal excitation in electro-pneumatic hammer as a method for improving performance of the tool as well as reducing vibration perceived by an operator has already been mentioned earlier (see Section 5.1.1).

In the current design of electro-pneumatic hammers, excitation is provided by an electrical motor and crankshaft mechanism. Under these circumstances, the sinusoidal motion of the driving piston is determined by the parameters of crankshaft mechanism and cannot be changed or adjusted.

Figure 6.1 shows time histories of the striker and the driving piston displacements, pneumatic force as a result of their interaction and time history of the handle acceleration obtained by numerical simulations. The operating cycle is such, that after the piston hits the striker through an air cushion (see area marked A in Figure 6.1) it continues motion in the same direction. After the striker hits the pick and rebounds (see point B in Figure 6.1), the driving piston just starts its motion backward and somewhat resists the backward motion of the striker.

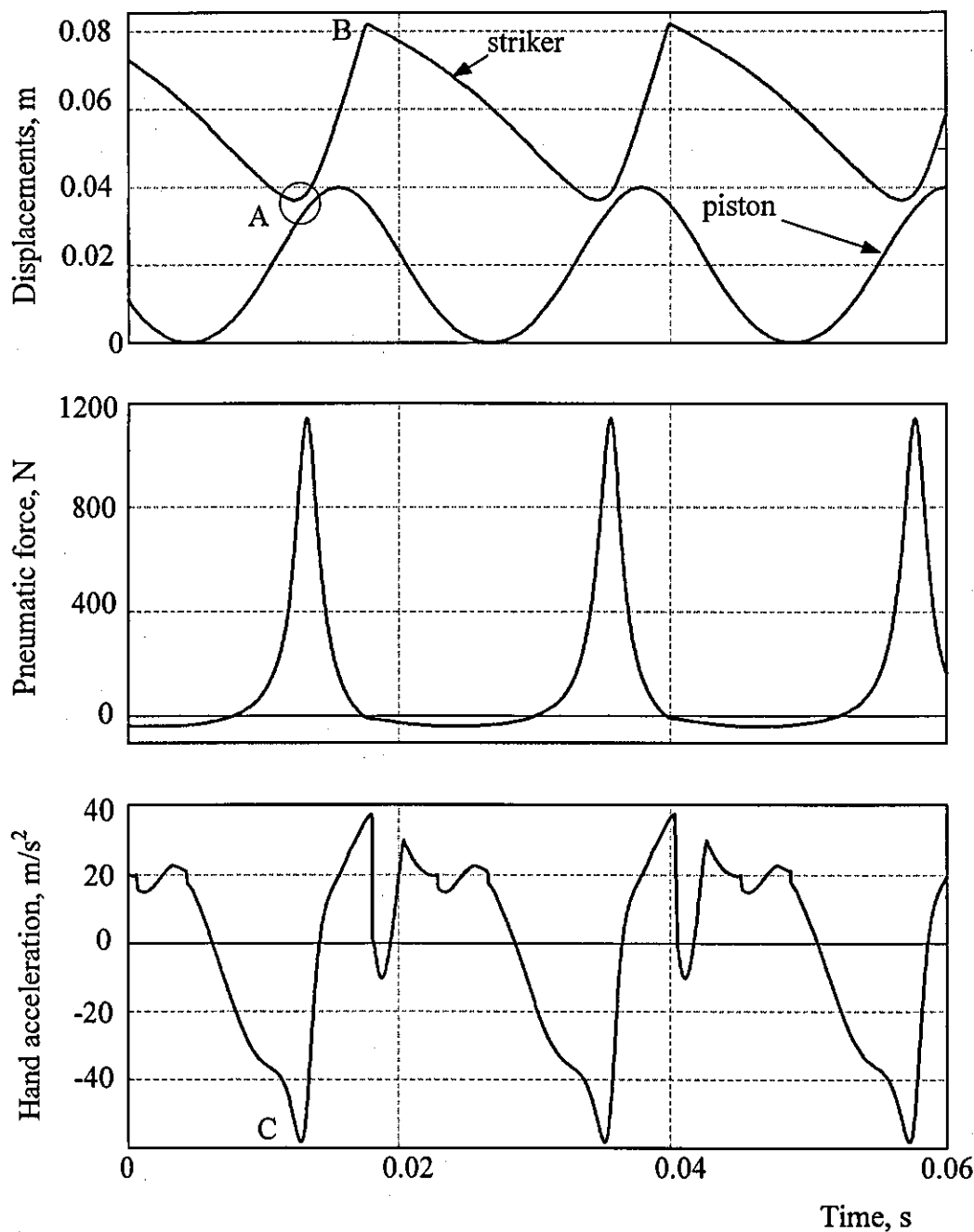


Figure 6.1. Time history of displacements of the moving parts of the excitation mechanism, force of pneumatic impact and handle acceleration.

Consequently, the striker does not have sufficient acceleration distance and the necessary impact velocity is obtained by increasing the force of pneumatic impact between the driving piston and the striker rather than by optimising their interaction.

The following equation for the reaction force applied to the machine casing through rigid driving mechanism was obtained in Chapter 4:

$$F_r = (m_3 \ddot{x}_3 + F_{pn}) \cos \theta \quad (5.32)$$

In the absence of vibration isolation between the casing and the hand-arm system this force is directly transferred into vibration perceived by an operator. Numerical simulations prove results of this analysis. The time history of the handle acceleration, which is perceived by the operator has very distinctive peaks (marked C) due to the air compression within the pneumatic chamber.

Thus, dynamic analysis of the percussion machine shows that the periodic excitation force acting on the striker has a simultaneous opposite action on the casing of the machine and through it on the operator. Therefore, performance of the percussion machine may be improved by optimising the force of excitation.

6.1 Optimal striker motion

In order to improve the current mechanism of interaction between the striker and the pick, it is necessary to find the optimal dynamic conversion of energy in a hand-held percussion machine.

Babitsky [48] performed detailed analysis of the excitation in a percussion machine as a problem of optimal control. The dynamic model of the striker is shown in Figure 6.2. where M_1 is the mass of the striker and $\tilde{u}(t)$ is the unknown periodic excitation force applied to the striker. In the case of the electro-pneumatic hammer, this force is due to pressure variation in pneumatic chamber between the driving piston and the striker.

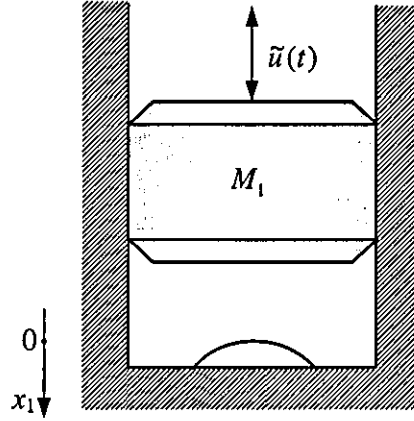


Figure 6.2. Dynamic model of striker (adapted from [48]).

The differential equation of motion of the striker is written as follows:

$$\ddot{x}_1 = u(t) \quad (5.33)$$

where x_1 is the coordinate of the striker measured from the point of its impact, when $x_1 = 0$, $u(t) = \tilde{u}(t) / M_1$.

The required periodic conditions are set in order to achieve the periodic motion of the striker with the prescribed energy E_- or velocity \dot{x}_{1-} of the striker just before impact and frequency f , as follows:

$$\begin{aligned} t = 0 \quad x_1 = 0 \quad \dot{x}_1 &= \dot{x}_{1+} \\ t = T \quad x_1 = 0 \quad \dot{x}_1 &= \dot{x}_{1-} \end{aligned} \quad (5.34)$$

where $T = 1/f$ is the period of the motion, $\dot{x}_{1+} = -R\dot{x}_{1-}$ and R is the restitution ratio of the striker.

Then Eq. (5.33) is rewritten in Gauchy form:

$$\begin{aligned} \dot{x}_1(t) &= \dot{x}_{1+} + \int_0^t u(\tau) d\tau \\ x_1(t) &= x_1(0) + t\dot{x}_{1+} + \int_0^t (t - \tau)u(\tau) d\tau \end{aligned} \quad (5.35)$$

Application of periodic conditions yields the following result:

$$\begin{aligned}
 (1+R)\dot{x}_{1-} &= \int_0^T u(\tau) d\tau \\
 RT\ddot{x}_{1-} &= \int_0^T (T-\tau)u(\tau) d\tau
 \end{aligned}
 \tag{5.36}$$

The left hand-side parts of Eqs. (5.36) are prescribed numbers. The right hand-side parts represent the scalar products of the unknown function $u(t)$ with known linear independent basic functions $h_i(t)$ ($i=1, 2$) where $h_1(t)=1, h_2(t)=T-t$ and all functions are defined in segment $t \in [0, T]$. The problem of finding the unknown function $u(t)$ under such conditions is known in mathematics as the moment problem [48].

As was mentioned previously (see Section 4.1), the acceleration force applied to the striker has a simultaneous opposite effect on the casing of the machine and through it perceived by an operator. In order to reduce the effect of this force on the operator, the peak value of the excitation force has to be limited. V.I. Babitsky [48] used $|u(t)|$ which represents a characteristic that influences vibration of the casing of the machine. As a result, the optimal solution of the moment problem for periodic excitation with prescribed period T was minimised as follows:

$$\min_U \max_{t \in [0, T]} |u(t)|
 \tag{5.37}$$

Thus, the optimal excitation that is necessary to realise a steady-state vibration-impact process with a single impact during the period and reduced load upon the operator is obtained. In practice, it is difficult to realise an optimal excitation, therefore, the quasi-optimal excitation, $u(t)$, with condensed acceleration impulse is introduced as follows:

$$u(t) = \begin{cases} -U & \text{if } t \in [0, t_1) \\ +nU & \text{if } t \in [t_1, T) \end{cases}
 \tag{6.1}$$

where

$$U = \frac{(1+R) \cdot \dot{x}_{1-} \cdot f}{n - \frac{1+n}{1+R} \left[1 - \sqrt{1 - \frac{n(1-R^2)}{1+n}} \right]},
 \tag{6.2}$$

$$\frac{t_1}{T} = \frac{1}{1+R} \left[1 - \sqrt{1 - \frac{n(1-R^2)}{1+n}} \right], \quad (6.3)$$

where R is the restitution ratio; \dot{x}_{1-} is the velocity of the striker just before the impact against the pick; f is the frequency of impacts; n is the approximating coefficient reflecting the permissible ratio of excitation during acceleration of the striker towards the pick and during rebound ($n=1$ corresponds to the optimal excitation), $T = \frac{1}{f}$ is the period of the impacts.

The tendency to reduce the initial negative acceleration and to condense the positive acceleration impulse was observed as a sequence of quasi-optimal approximations. The excitation force acts in the positive direction only when the approximating coefficient takes value $n = 100$. Further possible estimations of these condensed positive impulses were carried out. The different possible excitations of the striker with the introduction of permissible duration of the positive impulse, Δ , were obtained. In this case:

$$u(t) = \begin{cases} 0, & \text{if } t \in [0, t_1) \\ U, & \text{if } t \in [t_1, t_1 + \Delta) \\ 0, & \text{if } t \in [t_1 + \Delta, T) \end{cases} \quad (6.4)$$

where U , t_1 are unknown values and $(t_1 + \Delta)/T \leq 1$. The formulas for variables t_1 and U are as follows [48]:

$$\frac{t_1}{T} = 1 - \frac{1}{2} \left(\frac{\Delta}{T} \right) - \frac{R}{1+R}, \quad (6.5)$$

$$U = \frac{(1+R) \cdot \dot{x}_{1-} \cdot f}{\Delta / T}, \quad (6.6)$$

Figure 6.3 shows the possible quasi-optimal excitations drawn in accordance with the expressions (6.1) - (6.6) for the dynamic system under consideration.

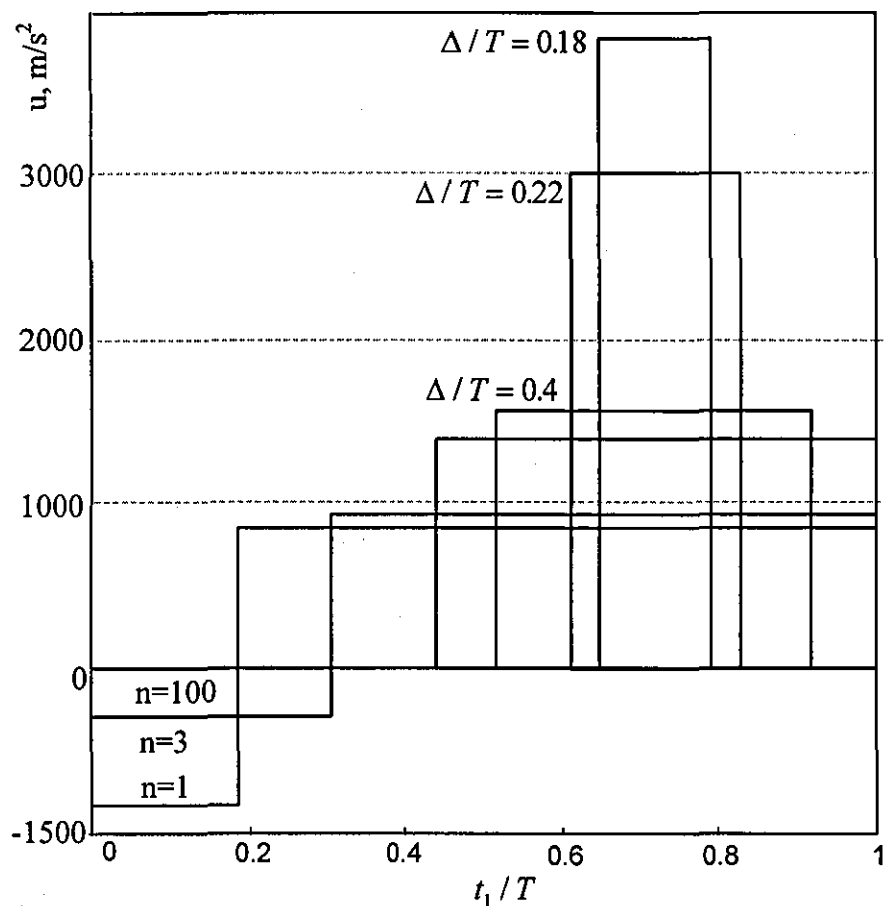


Figure 6.3. Quasi-optimal excitations with reduced rebound of striker
(adapted from [48]).

The highest value of the excitation force (acceleration impulse) corresponds to the shortest value of the interval Δ . The worst case, when $\Delta/T=0.1$, corresponds approximately to the excitation of modern hammers. As can be seen, the force of the pneumatic impact obtained by numerical simulations (see Figure 6.1) is consistent with Figure 6.3 as short interactions between the driving piston and the striker results in high and narrow pneumatic impulses.

This analysis of the quasi-optimal excitations suggests that extending the duration of the positive impulses of the excitation force (striker acceleration) may decrease unfavourable vibration and also relieve load on the drive without affecting the entire performance of the machine.

The crank-slide mechanism is a widely used, is a simple and reliable system to convert rotation into reciprocating motion. However, in this case motion of the

driving piston is set and cannot be altered in order to obtain optimal excitation. The sluggishness of the crank-slide mechanism and the electric motor do not allow permanent control of the striker motion. Alternative link mechanisms designed to perform quasi-optimal striker motion prove to be complicate and cumbersome.

As a possible solution, the additional flexible element attached to the driving piston is suggested in this study to modify the existing excitation mechanism. Such an element can reduce the magnitude of pneumatic impulses by simply extending their duration.

6.2 Dynamic model of electro-pneumatic hammer with modified source of excitation

The source of excitation was modified by an additional passive flexible element attached to the driving piston. When the natural frequency of the additional dynamic system is higher than the operating frequency, this element works in a spring-control mode and allows extension of the positive impulses of the pneumatic impact.

Figure 6.4 shows the dynamic model of the electro-pneumatic hammer with a modified source of excitation. In order to evaluate the results of such modification, the additional flexible element attached to the driving piston is introduced into the existing dynamic model of electro-pneumatic hammer (see Section 4.2). The flexible element is represented as a body, m_e , attached to the driving piston by a linear spring and dashpot combination (c_e, k_e) .

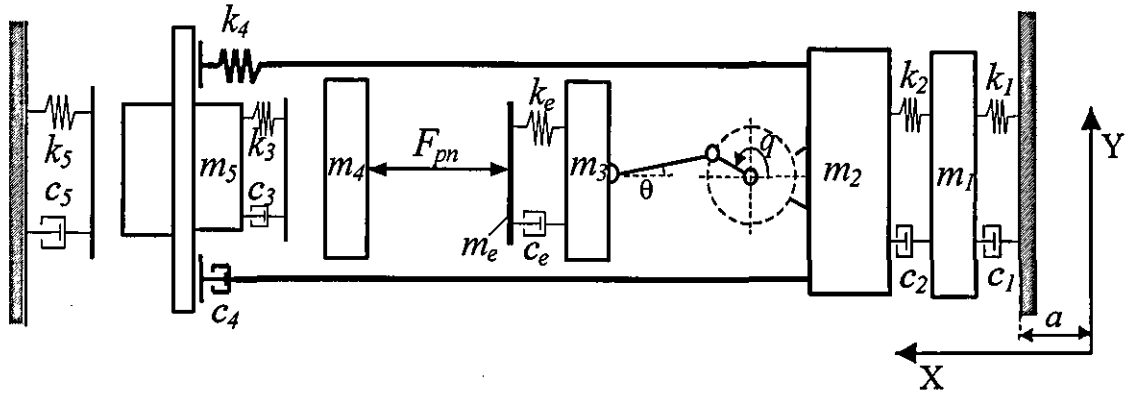


Figure 6.4. A dynamic model of the electro-pneumatic hammer with additional flexible element.

Equation of motion for additional element is written as follows:

$$m_e \ddot{x}_e + c_e (\dot{x}_e - \dot{x}_3) + k_e (x_e - x_3) = -F_{pn} \quad (6.7)$$

where \dot{x}_e, \dot{x}_3 and x_e, x_3 are absolute velocity and displacement of the flexible element and the driving piston, respectively. The pneumatic force developed between the additional element and the striker is:

$$F_{pn} = pA[S / (S + x_4 - x_e) - 1] \quad (6.8)$$

where S – is the distance between the additional element and the striker which results in the atmospheric pressure in a pneumatic chamber (driving piston is in extreme right position and flexible element is not deformed).

The equation for resultant force applied to the rotor of AC universal motor takes the following form:

$$N = m_3 \ddot{x}_3 + c(\dot{x}_3 - \dot{x}_e) + k(x_3 - x_e) \quad (6.9)$$

The numerical model was built in accordance with Eqs. (4.5)-(4.23) using Simulink. Figure 6.5 shows block diagram of electro-pneumatic hammer with modified source of excitation where each block represents a subsystem (usually body motion or force) which is built according to equations (4.14) - (4.23).

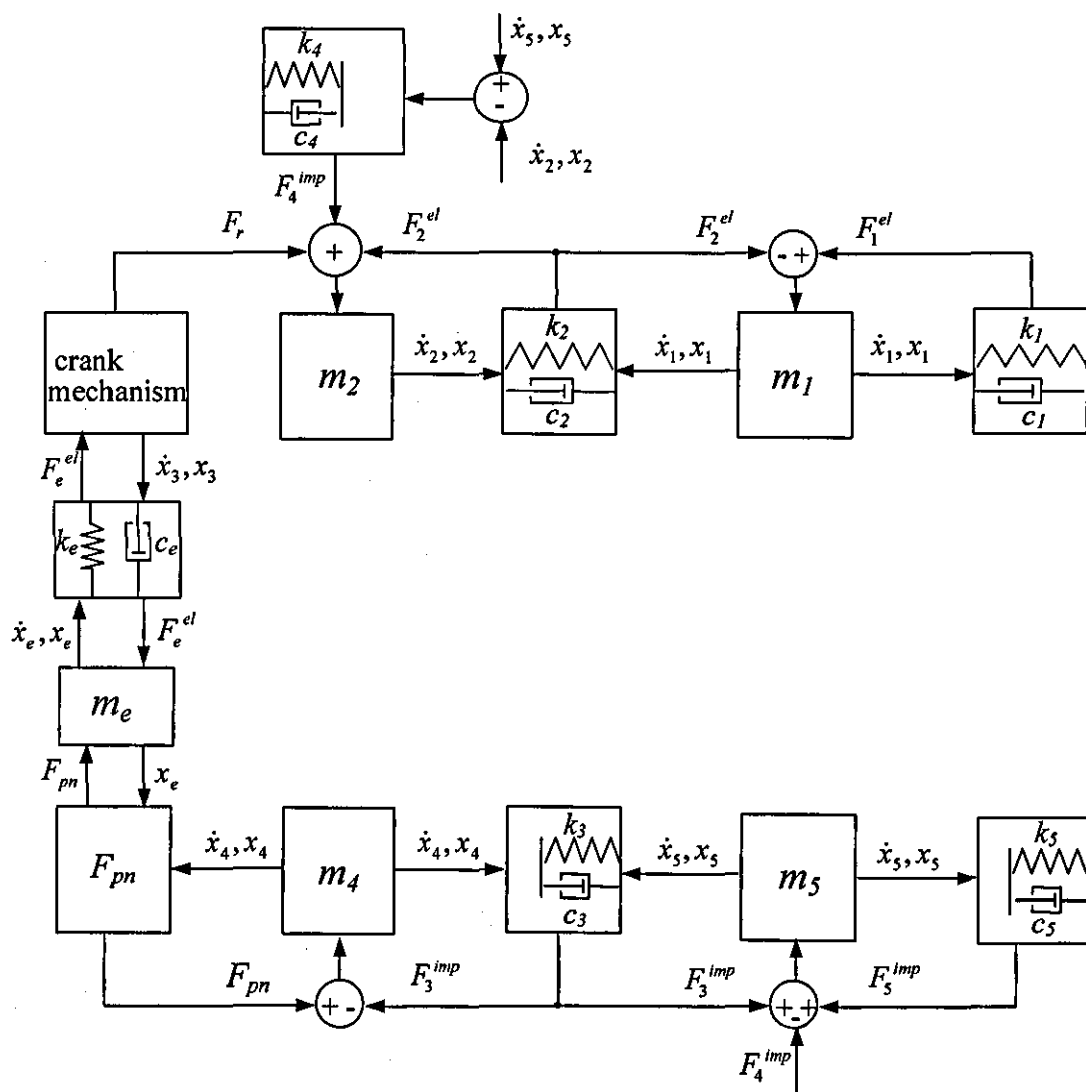


Figure 6.5. Simulink block diagram of the electro-pneumatic hammer.

This block diagram is very similar to the block diagram that was built for the original electro-pneumatic hammer, apart from the new blocks representing flexible element. Subsystem that represents additional element attached to the driving piston is shown in Figure 6.6.

6.3 Results of numerical simulations

Figure 6.7 shows displacements of the driving parts, force of pneumatic impact and handle acceleration for an electro-pneumatic hammer with modified source of excitation (dashed line shows the same characteristics for the original model). As can be seen, the passive flexible element permits changes of the excitation force so that it is closer to the optimal one. The value of positive impulse that corresponds to the force developed in the pneumatic chamber between the striker and the driving piston is reduced due to an increase in its time duration. In comparison with previous characteristics (see Figure 6.1), magnitudes of pneumatic impulses are reduced by a factor of 2.5, whereas the frequency of the process and pre-impact velocity of the pick remained unchanged.

The time history of the handle acceleration is also shown in Figure 6.7. The r.m.s. of the hand acceleration for the new system with a flexible element was reduced by a factor of 1.8 (see Figure 6.1).

One might argue that this reduction of r.m.s., which is not very significant does not justify current modification of excitation source. However, a more significant effect of additional flexibility in excitation mechanism is the reduction in peak amplitude of the hand acceleration.

The impulsiveness of the acceleration perceived by the operator is an important factor to consider in the design of vibratory machines, as well as in assessment of human exposure to vibration. High-frequency components may be more hazardous in the aetiology of the vibration syndrome than has been thought previously, for example short impulses with high magnitude can have a most destructive effect on the human joints (see Section 2.2.2.). Decreasing the risk of injury depends essentially on the degree of impulsiveness of the acceleration perceived by the operator of hand-held machines. In some cases protection from injury can be achieved more effectively by a reduction of the peak amplitudes of hand acceleration rather than by a reduction of the value of its r.m.s. Modification of the source of excitation enables the reduction of peak amplitude by a factor of 2.5.

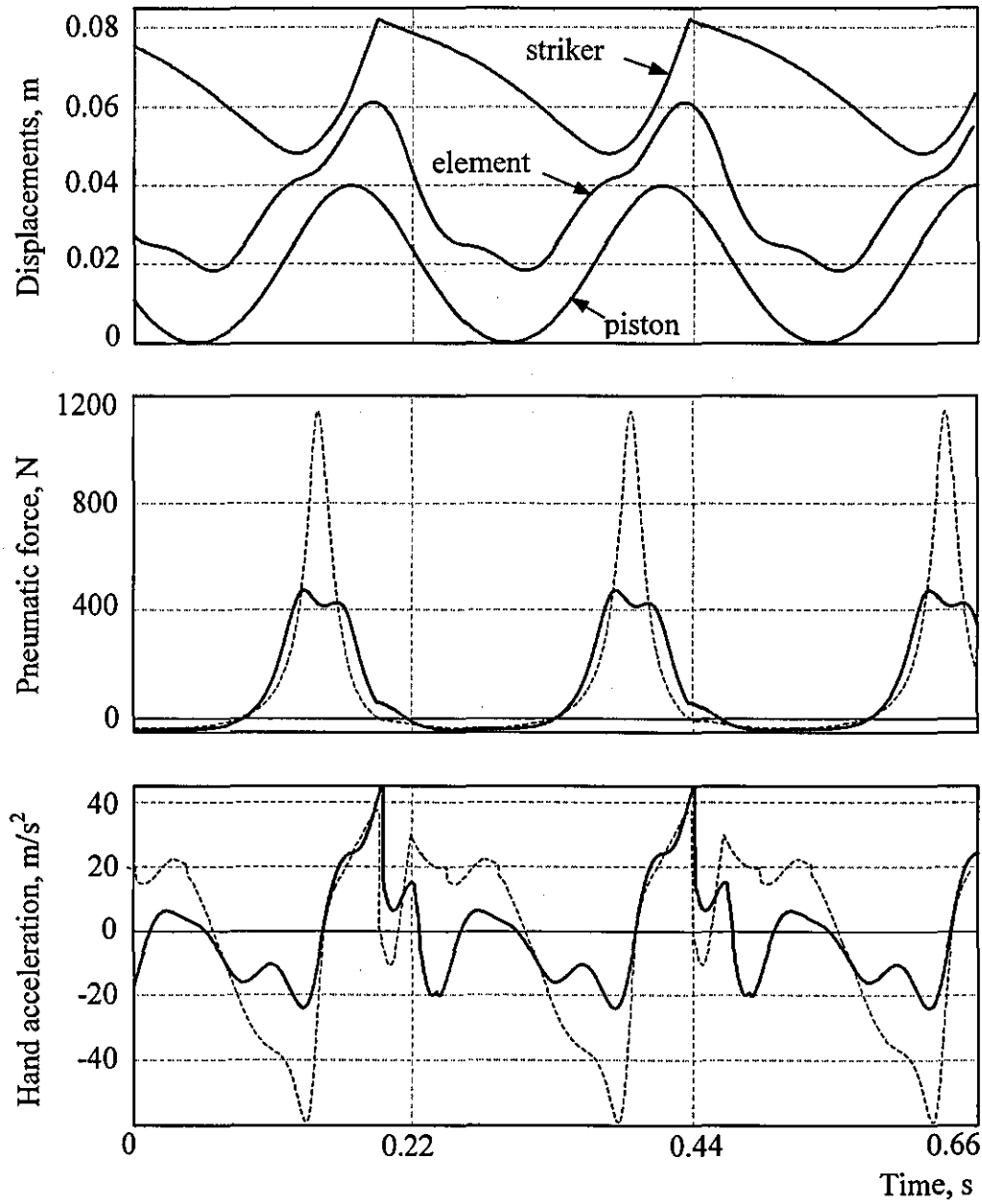


Figure 6.7. Time history of displacements of the moving parts of the excitation mechanism, force of pneumatic impact and handle acceleration for the electro-pneumatic hammer with modified source of excitation (solid line) and for the original hammer (dashed line).

Figure 6.8 shows the spectra of the handle acceleration for the original and modified hammer. The amplitudes of the first and the fourth harmonics were significantly reduced by a factor of 2.2 and 4 respectively, while changes in higher

frequency range were insignificant. There is no additional resonance or increase in acceleration magnitude due to the proposed modification of electro-pneumatic hammer.

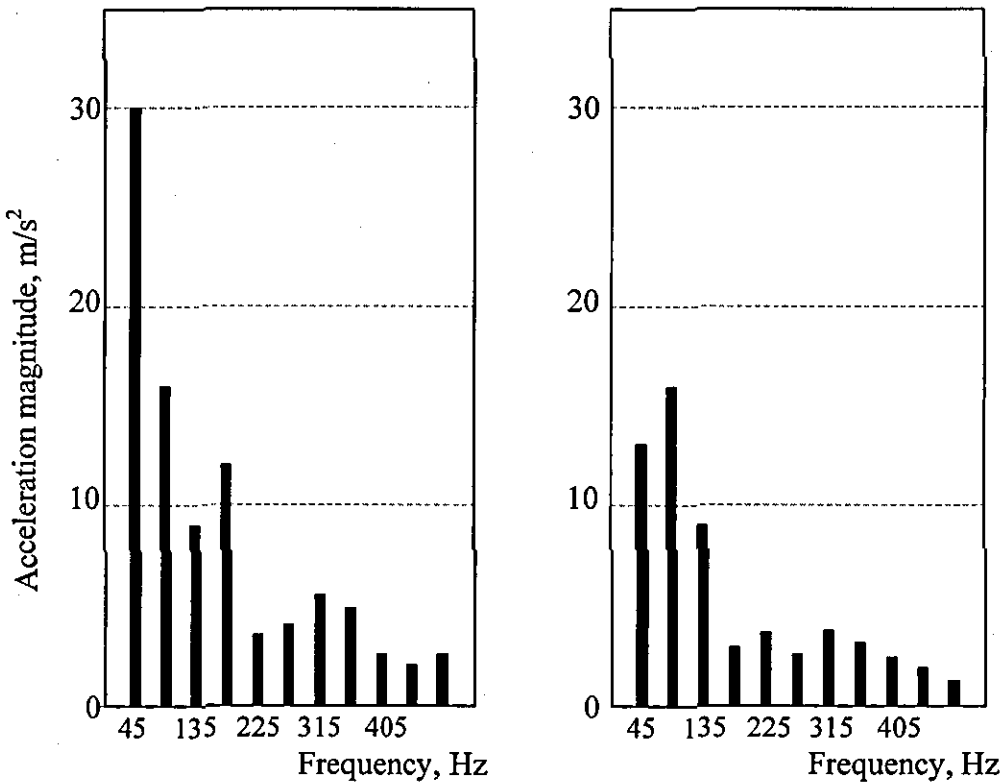


Figure 6.8. The spectrum of the hand acceleration for the original model of electro-pneumatic hammer (left) and the model with modified source of excitation (right).

Figure 6.9 compares the acceleration force applied to the striker for the original model and the model with the modified source of excitation.

The shaded area is the closest quasi-optimal excitation for each model obtained using formula (4.6)-(4.5). A comparison of the quasi-optimal excitation for the original model and the modified one shows that the duration of the positive acceleration impulse is doubled while the value of the impulse is decreased by a factor of 2.3. From Figure 6.3, it can be seen that the effect of extending impulses correlates well with the quasi-optimal excitation with condensed acceleration impulse obtained in [48]. Increasing the duration of impulse, results in a reduction in its magnitude without affecting the performance of the tool. Comparison between the

striker motion for the system with a stiff piston and the system with a piston with an additional flexible element shows that modification of the source of excitation enables a striker motion that is closer to the optimal one.

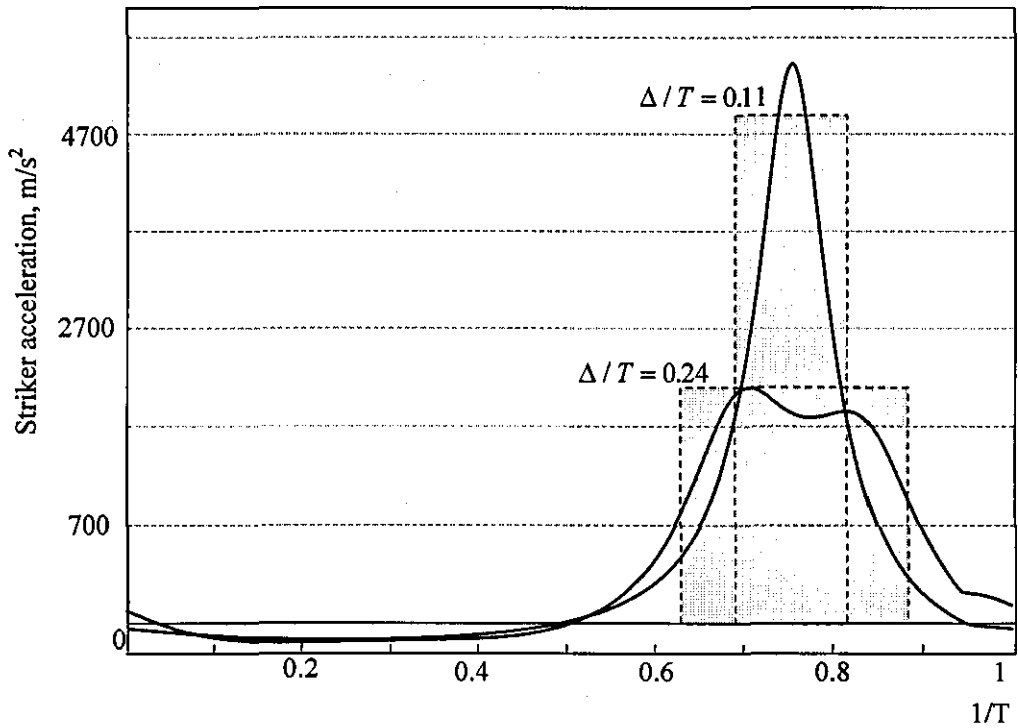


Figure 6.9. Comparison of different excitations; solid lines– striker acceleration obtained by numerical simulations, dashed lines– corresponding quasi-optimal excitations with condensed acceleration impulses.

Figure 6.10 compares the striker motion obtained by numerical simulations for the original electro-pneumatic hammer, hammer with modified source of excitation and the theoretical optimal striker motion obtained in reference [48].

Even though changes in the velocity and displacement due to modification are not very noticeable, the acceleration curve shows a significant extension of the duration of positive impulse and reduction of its magnitude.

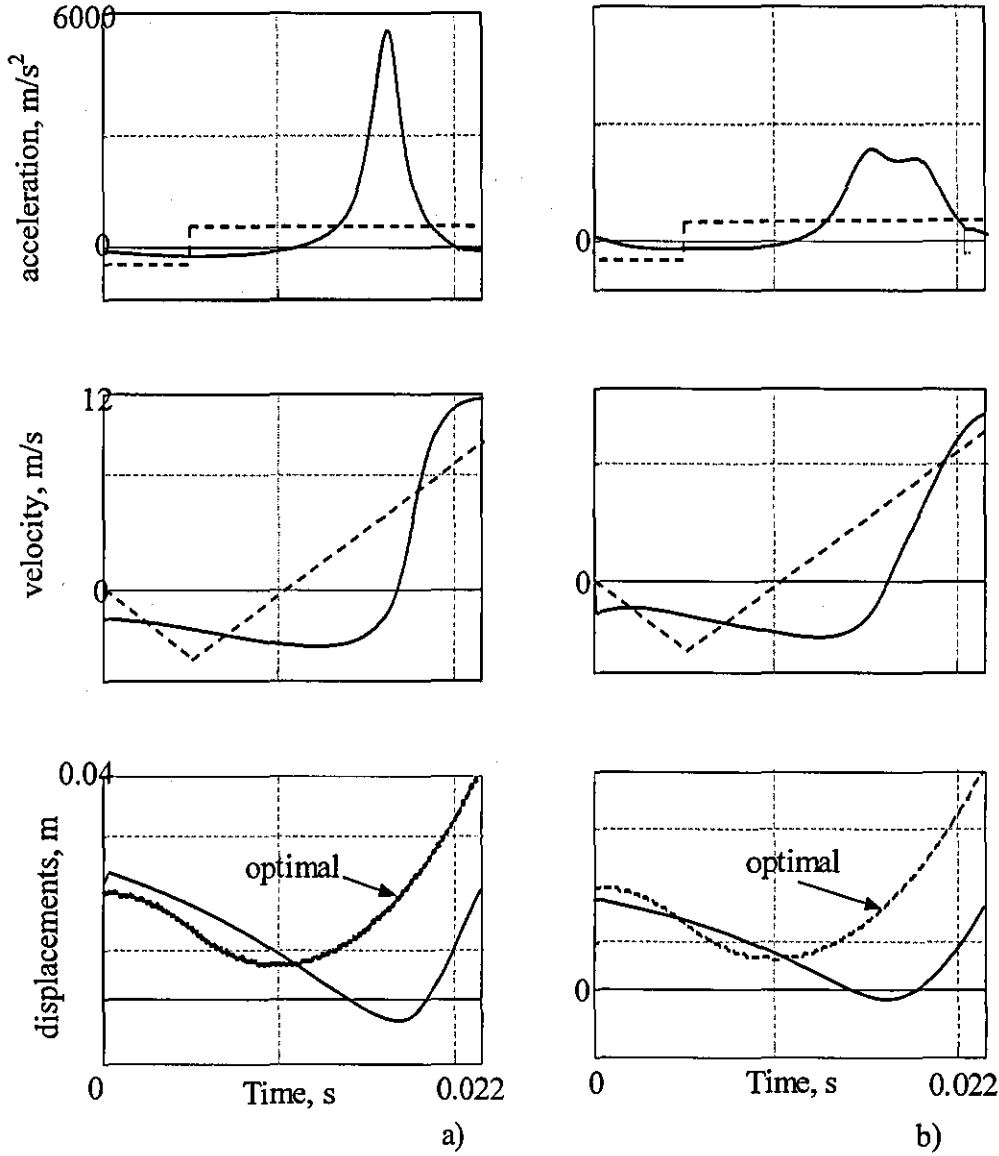


Figure 6.10. a) Striker motion for stiff piston, dash line-optimal striker motion [48],
b) Striker motion for piston with flexible element, dash line-optimal
striker motion.

The extension of the accelerating impulses not only reduces the peak force of the pneumatic impact, but also improves the control of the striker motion. Additional flexibility that is added to the driving piston enables an increase in the time of the actual control of the striker motion by the driving piston. Figure 6.11 estimates the angle of the crank rotation when the striker accelerates towards the pick by the force developed within the pneumatic chamber.

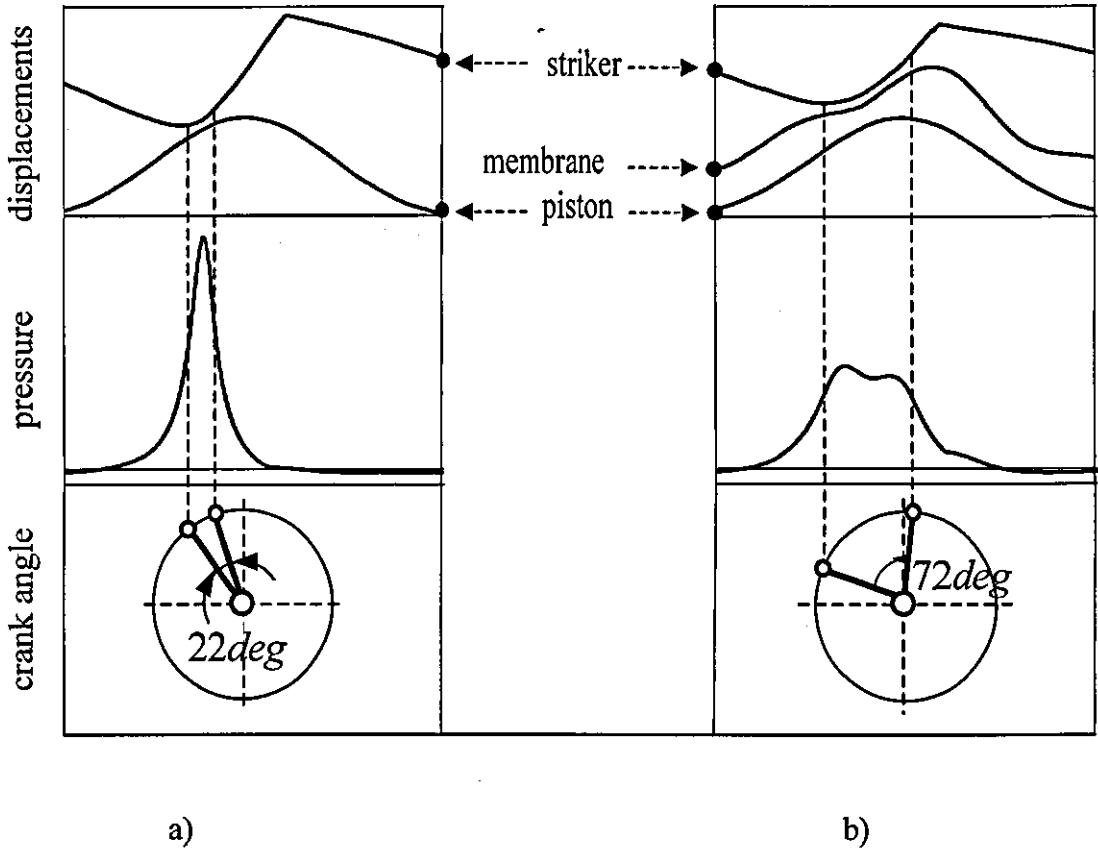


Figure 6.11. Schematics of crank rotation for the stage of positive acceleration impulse;
a) original model of percussion machine, b) model with additional compliant element.

As can be seen from Figure 6.11, during the compression, an additional flexible element attached to the piston provides fixed distance between the striker and the driving piston, which is equal to 3mm (see Figure 6.11 (b)). In case of “rigid” driving piston the striker and the piston come close only for a very short time, thus producing unnecessary high pneumatic impulse. In the present study, this distance and associated time interval are called the “effective distance” and the “time of effective striker control”. Hence, the time of effective striker control was estimated as $22deg$ of crank revolution for the original model (see Figure 6.11 (a)), while introduction of the additional flexible element improves this value to $72deg$ (Figure 6.11 (b)).

6.4 Conclusions and discussions

Confirmation of results of the general optimal theory for hand-held percussion machines [48], obtained in the framework of realistic models, gives way to the new design concepts of these machines with reduced vibration loading on operators.

Modification of the excitation source of the electro-pneumatic hammer by implanting an additional linear spring-mass-damper element to the driving piston enables significant improvement in the excitation performance of the hand-held percussion machine. The flexible element extends the duration of the pneumatic impulses between the driving piston and the striker, thereby reducing their values and relieving the load on the operator.

R.m.s. of weighted casing acceleration was calculated similarly to the reference model of the electro-pneumatic hammer (see Section 4.4). The numerical value of casing acceleration in one axis parallel to the percussion direction was found to be 4.6m/s^2 (or 7.7m/s^2 after it was multiplied by a factor of 1.7 before being compared with guidance on vibration exposure based on the vibration total value). Referring to Figure 4.21, the vibration hazard produced by electro-pneumatic hammer with modified source of excitation can be estimated. Figure 6.12 shows the r.m.s. of the modified hammer with reduced vibration.

The acceptable duration of daily exposure for such a machine is more than 3 hours (such acceptable duration of vibration exposure was about 15 min for the original hammer). This result can be further improved by a combination of this method with traditional methods of vibration protection.

The modified source of excitation also provides better control of the striker motion. The possibility of further improvement by introducing nonlinearity into this element may be investigated in the future.

The universal *AC* motor that is currently in use in electro-pneumatic hammer possesses “stiff” characteristic, which allows employment of uniform crank rotation in numerical simulations. However, possible fluctuations in operating frequency will disrupt the extension of pneumatic impulses and might even worsen the vibration effect. Appropriate controller maintaining operating frequency of the machine or semi-active self-tuning element attached to the driving piston can help to overcome this problem.

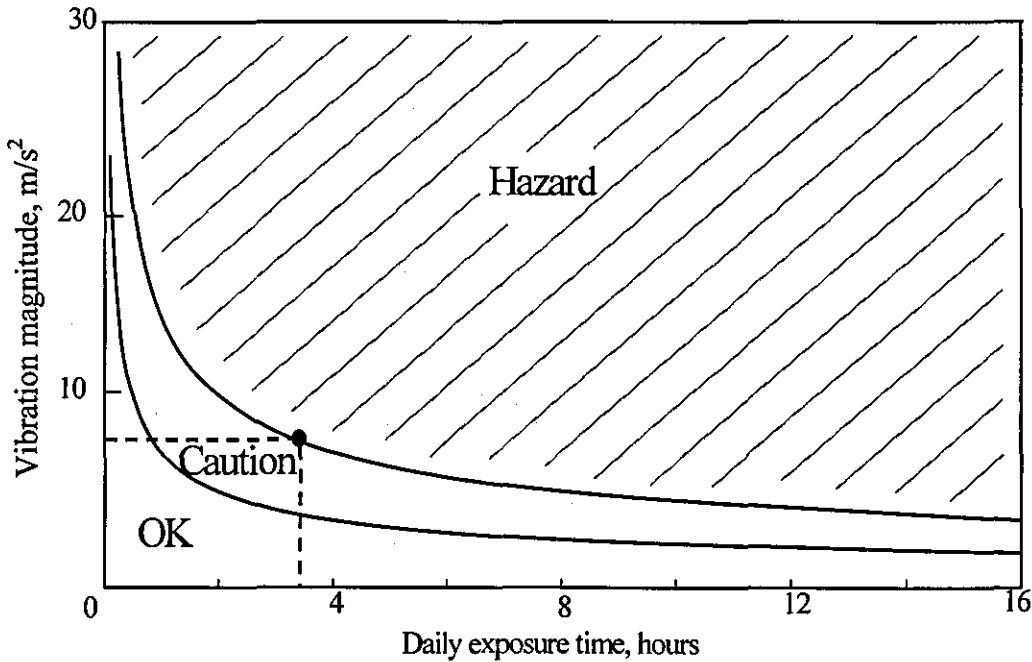


Figure 6.12. The relationship between vibration magnitude and duration for energy-equivalent exposures.

Practical implementation of such an element is a challenging task. Small mass, high stiffness and large displacement of this additional element that are necessary to provide extension of pneumatic impulses together with a high level of stress applied to the piston of electro-pneumatic hammer require careful design.

Chapter 7

Design of a vibration attenuation system for the hand-held percussion machine

Vibration isolation is a simple and the most widespread method of vibration protection. However, in case of hand-held percussion machine, effective frequency range of passive vibration isolation is limited as the lowest possible stiffness of an isolator between the machine and the operator restricted from safety and controllability reasons. At the same time, combination of this method with some other methods of vibration protection might provide better vibration attenuation.

7.1 Principle of vibration attenuation system

In [92, 93] it was shown that a tuned dynamic absorber in combination with a stiff and heavily damped vibration isolator could be successfully used for the simultaneous dynamic suppression of vibration at the driving frequency and also in a high-frequency span. This principle can be used in the design of a vibration attenuation system for a hand-held percussion machine. There is no need to prevent whole casing of the machine from vibrating, because, in order to protect the operator, attenuation of handle vibration would be sufficient

So, a high frequency range of handle acceleration can be reduced by a vibration isolator placed between the handle and the casing, while the fundamental harmonics of acceleration unaffected by vibration isolation, might be reduced by a dynamic absorber attached to the handle. Application of such a vibration attenuation system in a hand-held percussion machine was first mentioned in [60]. Unfortunately, this idea was not developed further and no models, experiments or practical designs employing this principle have been reported.

In a vibration attenuation system for a hand-held power tool, the handle is isolated from the casing of the tool in order to achieve dynamic de-coupling between the handle and the casing. Thereafter, the dynamic absorber, attached to the handle, suppresses the fundamental frequency of the handle acceleration, while the casing motion remains the same. The fundamental frequency component of handle oscillation need not be reduced by the vibration isolator, consequently, the natural frequency of the isolator may be even higher than the driving frequency and is chosen primarily from stability and safety reasons.

The handle is significantly lighter than the whole casing. So, once the handle is isolated from the casing, the fundamental frequency component of handle acceleration can be suppressed by the dynamic absorber with very small effective mass. Several dynamic absorbers may be optionally used depending on the parameters of the isolator placed between the handle and the casing, i.e. if the second or the third harmonics of handle acceleration were not sufficiently reduced by vibration isolation, these may be successfully suppressed by additional relatively small dynamic absorbers.

7.2 Dynamic modeling and numerical simulations of the electro-pneumatic hammer with vibration attenuation system

In order to evaluate the effect of vibration attenuation, a previously developed dynamic model of the electro-pneumatic hammer (see Figure 4.4) is used. Figure 7.1 shows time history and spectrum of acceleration perceived by the operator of original

electro-pneumatic hammer without vibration isolation (referring to Figure 4.4, acceleration of the body “ m_1 ” that represents operator hand will be called hand acceleration).

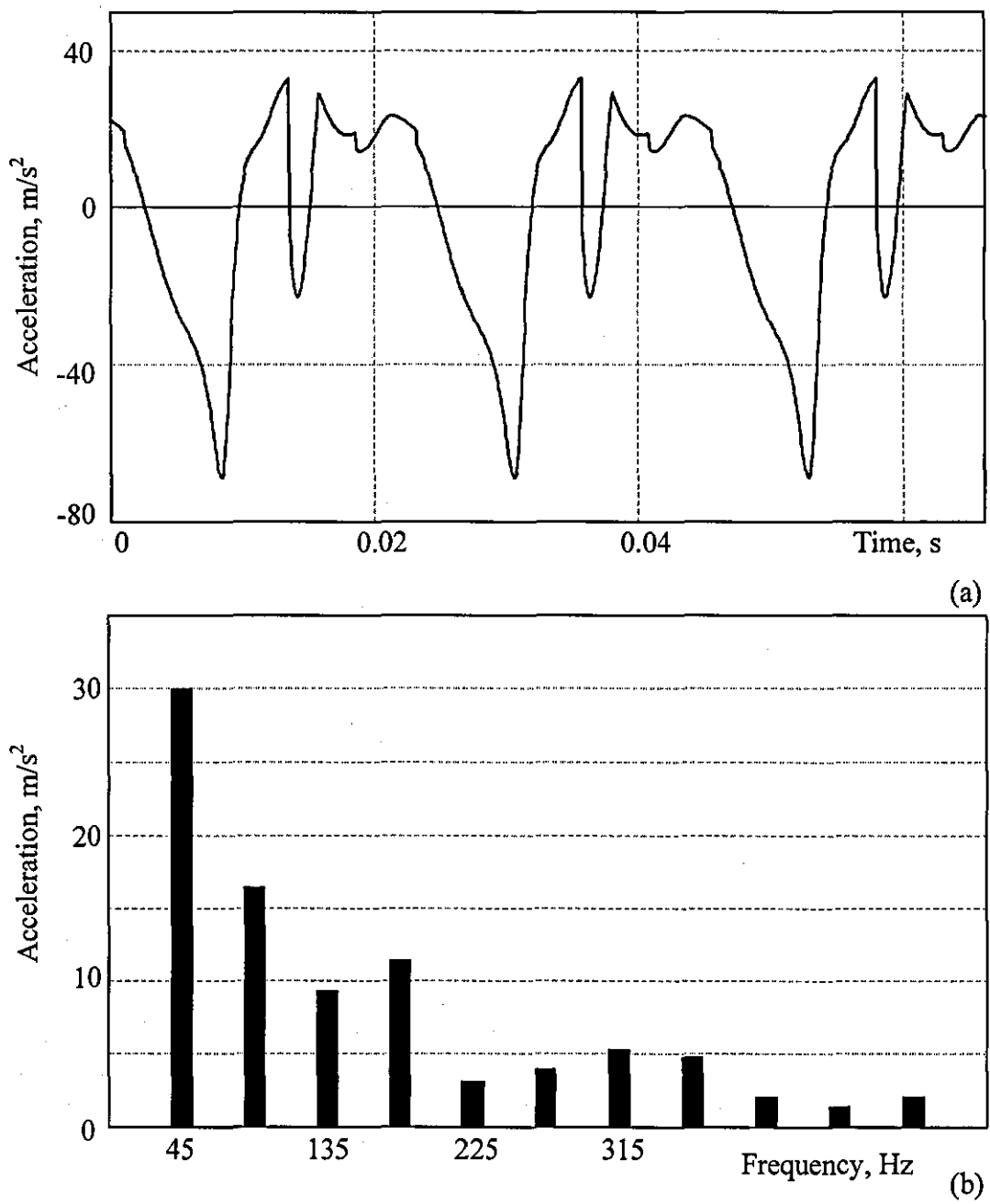


Figure 7.1. Time history and spectrum of the hand acceleration.

As was already mentioned, acceleration produced by electro-pneumatic hammer is of impulsive nature with the r.m.s. magnitude 29.5 m/s^2 and the peak to peak

amplitude 101 m/s^2 . The spectrum contains harmonics that are multiple to the driving frequency 45Hz , with the first four harmonics being of the most significant magnitude.

7.2.1 Vibration isolation

The handle of a percussion machine is usually covered by rubber-like material in order to isolate harmonics of a higher order perceived by an operator. This isolator is represented in the model as a spring-damper combination, k_2, c_2 (see Figure 4.4). In order to obtain a reference model of the electro-pneumatic hammer without vibration isolation, the following parameters of spring dashpot combination between the handle and hand-arm system were set:

$$\Omega_2 = \sqrt{\frac{k_2}{m_1}} = 2.5 \times 10^4 \text{ rad/s} \text{ and } \zeta_2 = \frac{c_2}{2\Omega_2 m_1} = 0.1.$$

Now, in order to attenuate vibration, this isolator is placed between the operator hand and the handle of the tool must satisfy the following criteria:

- frequency of impacts – 45Hz ;
- energy of impact between the pick and treated material – 1.5J ;
- tool performance has to be independent of fluctuations of feed force or hand-arm system parameters;
- static deflection of an isolator under applied feed force shall not exceed 15mm .

In order to obtain optimal parameters of vibration isolator, that will provide maximum vibration attenuation and satisfy all the above criteria, simulations were run for different values of k_2 and c_2 . Figure 7.2 shows the results of the numerical simulations. Here, r.m.s. of hand acceleration is shown as a function of natural frequency and loss factor of an isolator placed between the operator's hand and the handle of the hammer. For the sake of convenience, contour lines are also shown on a horizontal plain and labelled with correspondent magnitudes of r.m.s.

As can be seen from Figure 7.2, r.m.s. of hand acceleration as a function of parameters of the vibration isolators is a monotone function, which decreases with

natural frequency and loss factor of vibration isolator. All combinations of k_2 and c_2 that are shown in Figure 7.2, provide an operating regime with prescribed energy and frequency of impacts. As was stated previously, feed force and parameters of a hand-arm system are likely to vary during tool operation. Fill area on a “natural frequency-loss factor” plain shows all possible combinations of k_2, c_2 that secure stability of the tool performance during these variations.

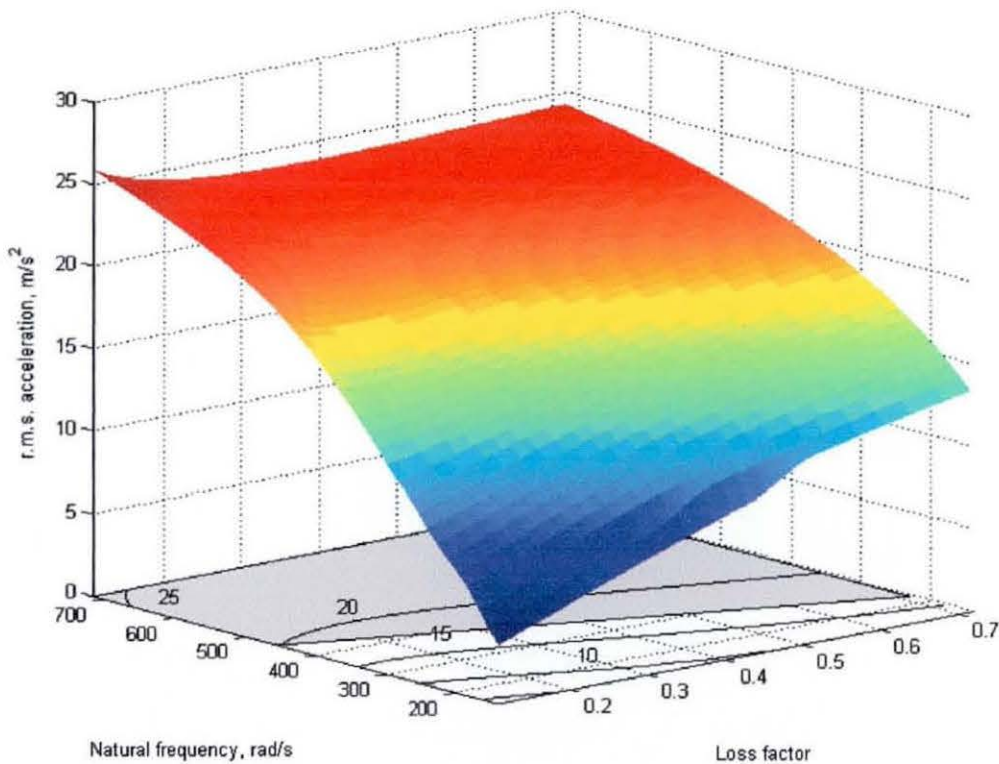


Figure 7.2. R.m.s. of hand acceleration as a function of parameters of isolator between the handle and the hand-arm system.

Any combination of the isolator parameters that lie within the marked area could be used for vibration isolation and would provide a similar effect. In practice, the choice of an optimal vibration isolator depends on different factors (practical implementation, materials available, manufacturing requirements etc.). However, the purpose of the current investigation is to demonstrate qualitative characteristics of such vibration isolation. Thus, the chosen parameters of the vibration isolator are not defined by only one optimal value. They lie within a range of possible values that

provide similar vibration isolation. Finally, the chosen parameters of the vibration isolator placed between the hand and the handle are:

$$\Omega_2 = \sqrt{\frac{k_2}{m_1}} = 410 \text{ rad / s}, \quad \zeta_2 = c_2 / 2m_1\Omega_2 = 0.22.$$

Figure 7.3 shows the time history and spectrum of hand acceleration for an electro-pneumatic hammer with a vibration isolator placed between the handle of the machine and a hand-arm system. The dashed line shows hand acceleration without the vibration isolation.

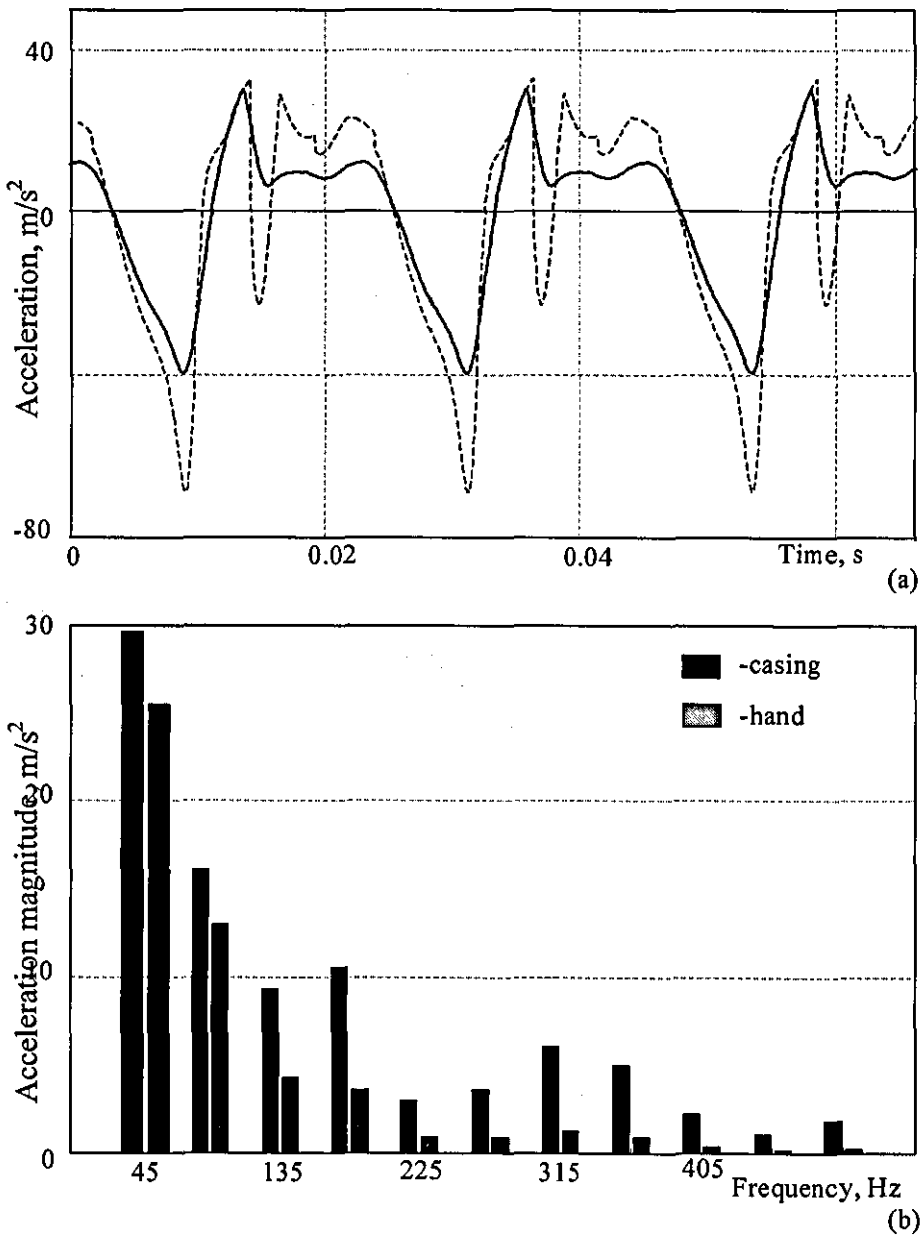


Figure 7.3. Time history and spectrum of hand acceleration.

The r.m.s. and peak to peak amplitude of hand acceleration were reduced by a factor of 1.4 and 2 correspondingly. The effect of the vibration isolation in the frequency domain can be seen in Figure 7.3(b) that shows spectra of the casing acceleration and the acceleration perceived by the operator. As expected, vibration isolator reduced high-frequency harmonics, while most significant low-frequency harmonics remained unchanged. Further variation of parameters of vibration isolator cannot noticeably improve this result, because employing an isolator with lower stiffness will worsen operating safety and lead to instability and possible disruption of the machine operation.

In order to achieve dynamic de-coupling between the casing and the handle, the two-stage vibration isolation was introduced, as the handle was additionally isolated from the casing of the machine. Figure 7.4 shows dynamic model with both-side isolated handle. Here, the second vibration isolator is represented as spring-damper combinations (k_h, c_h) between the casing and the handle. Handle mass (m_h) is 0.35kg, hence casing mass (m_2) becomes 7.65kg, while the rest of the parameters remain the same as in the reference model.

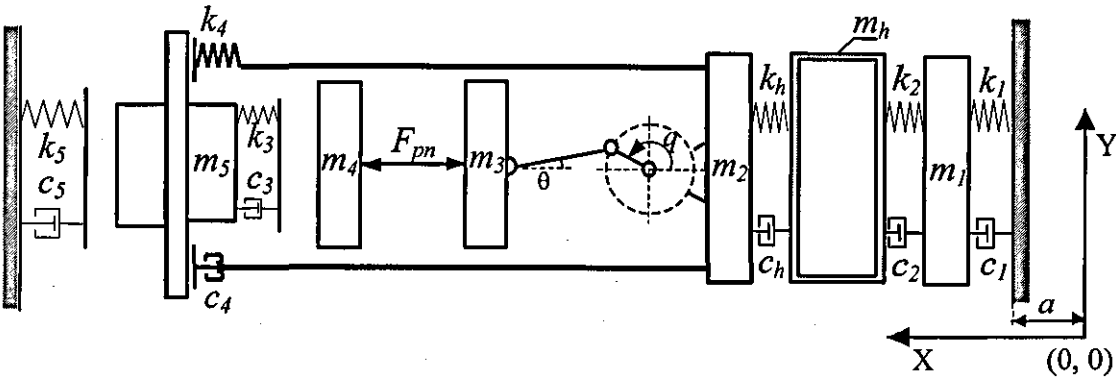


Figure 7.4. Dynamic model of an electro-pneumatic hammer with both-side isolated handle.

Figure 7.5 shows the Simulink block diagram representing the dynamic model of an electro-pneumatic hammer. Each block in this diagram is a subsystem that has been developed according to Eqs. (4.5)-(4.23) and represents motions of each mass

or forces applied. The diagram is very similar to one built earlier apart from one new block that represents the handle of the machine.

Apart from dynamic de-coupling between the casing and the handle, the second vibration isolator, which is placed between the casing of the machine and the handle, provides additional vibration attenuation. The criteria for optimal parameters of such an isolator remain the same as for the first isolator: impact frequency 45 Hz, energy of pick impact against material being treated 1.5 J, restriction on maximum static displacement under applied feed force and necessity to retain a controllability of the machine by an operator.

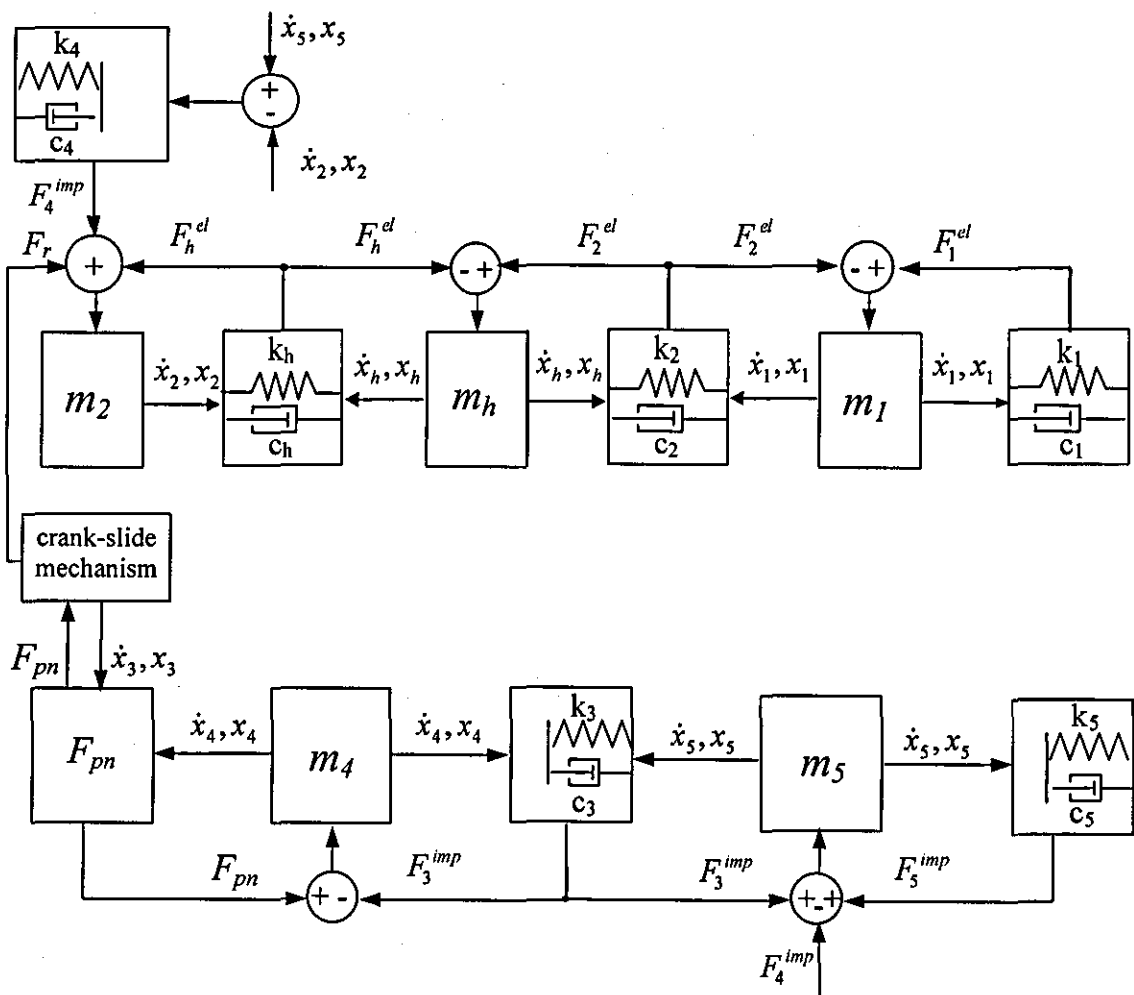


Figure 7.5. Simulink block diagram of the pneumatic hammer.

Simulations were run for every combination of the parameters $\Omega_2, \zeta_2, \Omega_h$ and ζ_h . As an example, Figure 7.6 shows the r.m.s. of hand acceleration as a function of Ω_h

and ζ_h while $\Omega_2 = 802.3 \text{ rad/s}$ and $\zeta_h = 0.22$. Similar functions were obtained for every other pair Ω_2 and ζ_2 , so this set of parameters was chosen as one that provides maximum vibration attenuation.

R.m.s. of hand acceleration as a function of vibration isolators parameters is uniform monotone function. The lower magnitude of r.m.s. of hand acceleration corresponds to the lower values of natural frequency and loss factor of the isolators, however, the greatest achievable effect of reducing the hand acceleration still does not exceed a factor of 2.

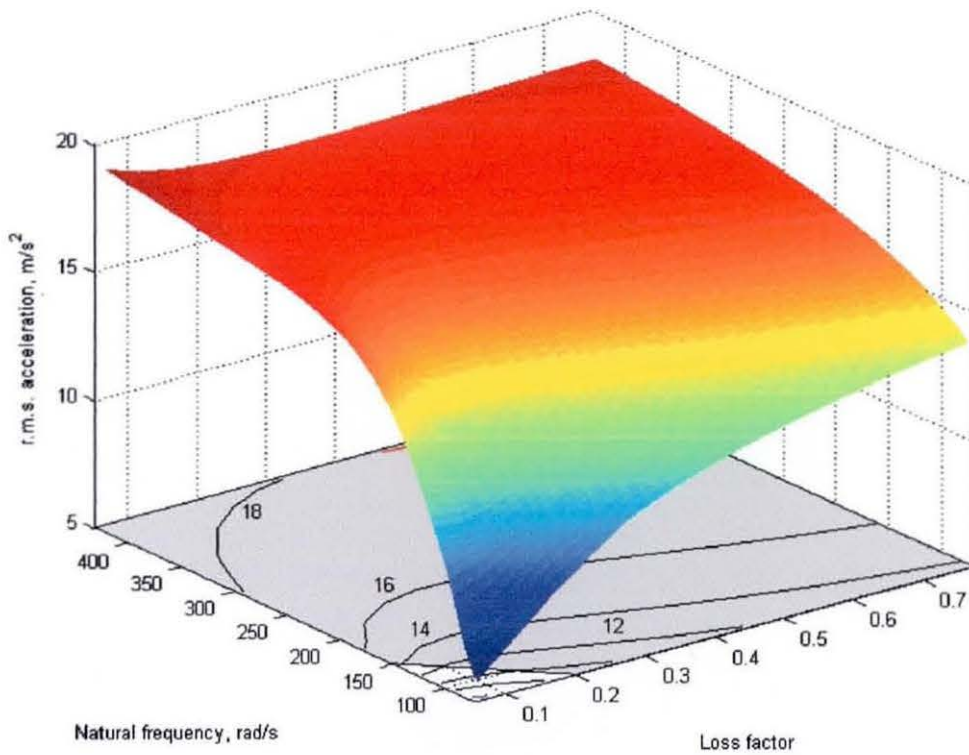


Figure 7.6. R.m.s. of hand acceleration as a function of Ω_h, ζ_h , where

$$\Omega_2 = 802.3 \text{ rad/s} \text{ and } \zeta_2 = 0.22.$$

As in the previous case, the fill area on the “natural frequency-loss factor” plane corresponds to regimes which satisfy the prescribed conditions and are not sensitive to changes in feed force or hand-arm system parameters.

There is a number of possible combinations of vibration isolators parameters satisfying all conditions. Once again, the following parameters within the marked

area that have been chosen as an example for further investigation are not the only optimal, but representative combination:

$$\Omega_h = \sqrt{\frac{k_h}{m_h}} = 389.8 \text{ rad/s}, \quad \zeta_h = c_h / 2m_h\Omega_h = 0.26,$$

$$\Omega_2 = \sqrt{\frac{k_2}{m_1}} = 802.3 \text{ rad/s}, \quad \zeta_2 = c_2 / 2m_1\Omega_2 = 0.22.$$

Figure 7.7 shows spectra of acceleration of the casing, the handle and the hand-arm system, after vibration isolators have been installed. Vibration isolators in the electro-pneumatic hammer reduce the second and higher harmonics of the hand acceleration by a factor of 1.2 and 8.5, respectively.

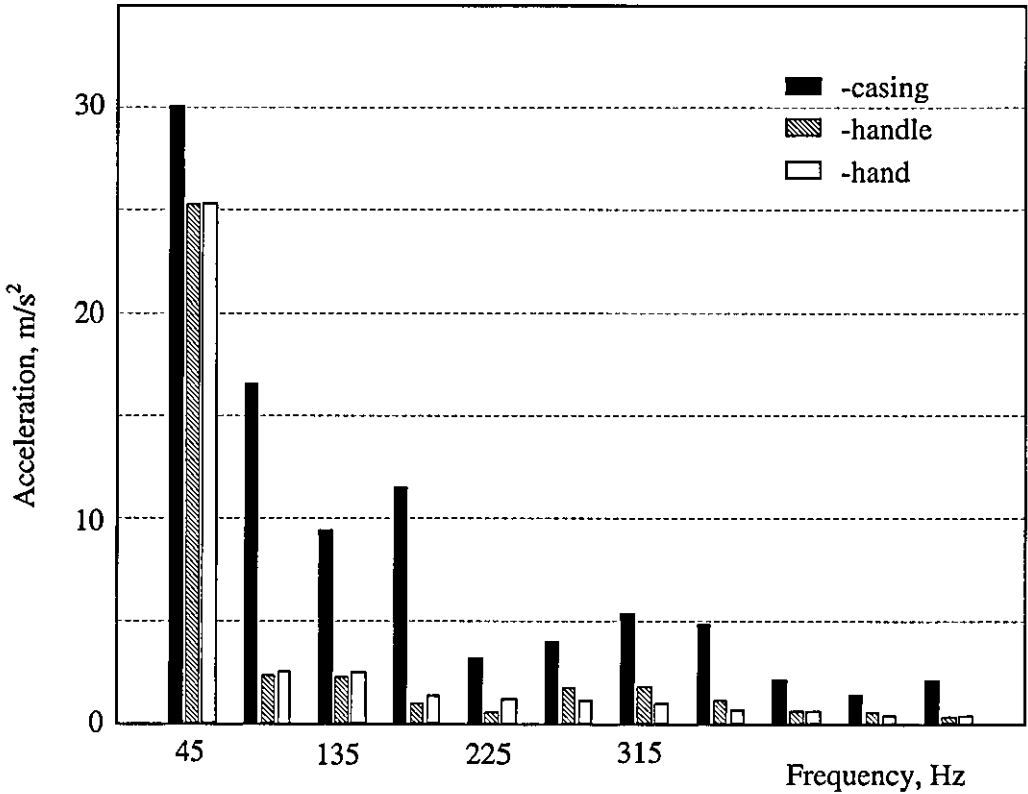


Figure 7.7. Spectra of accelerations of the casing, the handle and operator hand.

Figure 7.8 portrays the time history of the accelerations of the casing, the handle and the operator hand.

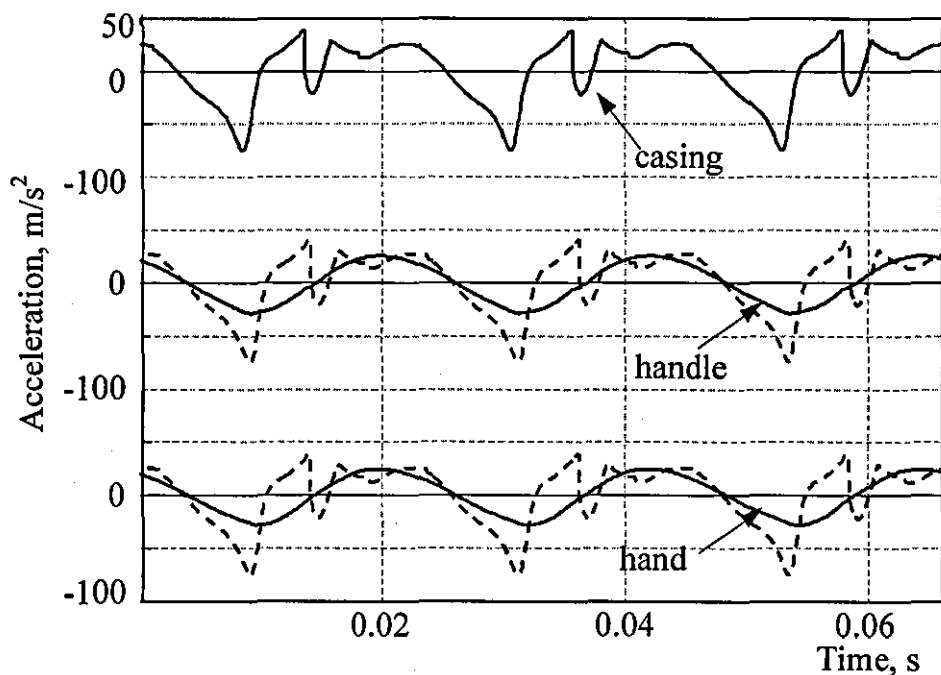


Figure 7.8. Time history of accelerations of the casing, handle and operator hand; dashed line-original electro-pneumatic hammer without vibration isolation; solid line-electro-pneumatic hammer with both-side isolated handle.

From Figure 7.8, the peaks of time history of hand acceleration curve have been flattened by vibration isolation. R.m.s. and peak to peak amplitude of the hand acceleration were reduced by a factor of 1.6 and 2.1 respectively.

Figure 7.9 shows time histories of the displacements of the casing, the handle and the hand.

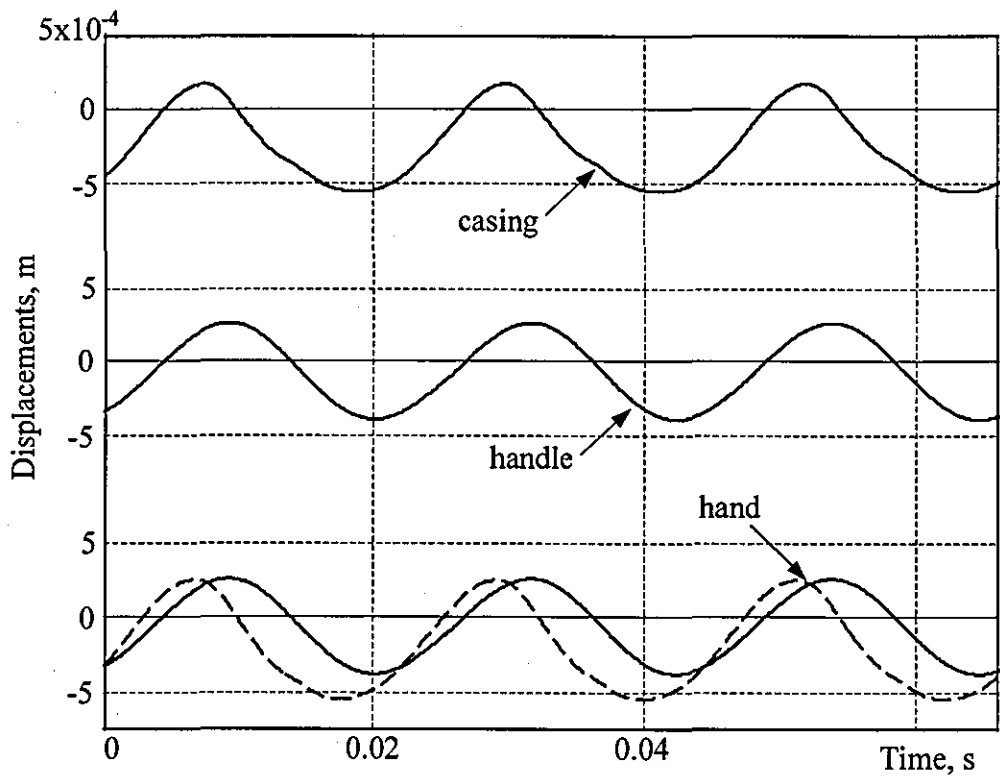


Figure 7.9. Time histories of the casing, the handle and the hand absolute displacements; dashed line-hand displacement for electro-pneumatic hammer without vibration isolation.

As can be seen, vibration isolators did not significantly reduce the handle and the hand displacements (the peak to peak amplitude of the hand displacement was reduced by a factor of 1.4).

As in the previous case, further significant improvement of vibration attenuation by simple optimisation of parameters of vibration isolators is not possible.

Results of numerical simulations confirm that vibration isolation is very effective for attenuating high-frequency content of vibration produced by hand-held power tools. However, for the studied electro-pneumatic hammer, vibration isolators are ineffective at attenuating the fundamental harmonic of vibration, which is of highest magnitude. Consequently, passive vibration isolation is not sufficient to reduce hazardous vibration produced by electro-pneumatic hammer till a permissible level.

The invariance of the operating frequency of the electro-pneumatic hammer suggests employing a tuned dynamic absorber in order to suppress the fundamental

harmonic of vibration. Once the handle has been isolated from the casing of the machine, there is no need to suppress the casing motion. The dynamic absorber with a small effective mass can be attached to the handle. The mass of the handle is small in comparison with the mass of whole machine, so effective mass of the absorber will not cause undesirable increase in load upon the operator due to increased mass of the machine.

7.2.2 Vibration isolation in combination with dynamic absorber

Figure 7.10 shows the dynamic model of electro-pneumatic hammer with the dynamic absorber attached to the handle that is isolated from the casing of the machine.

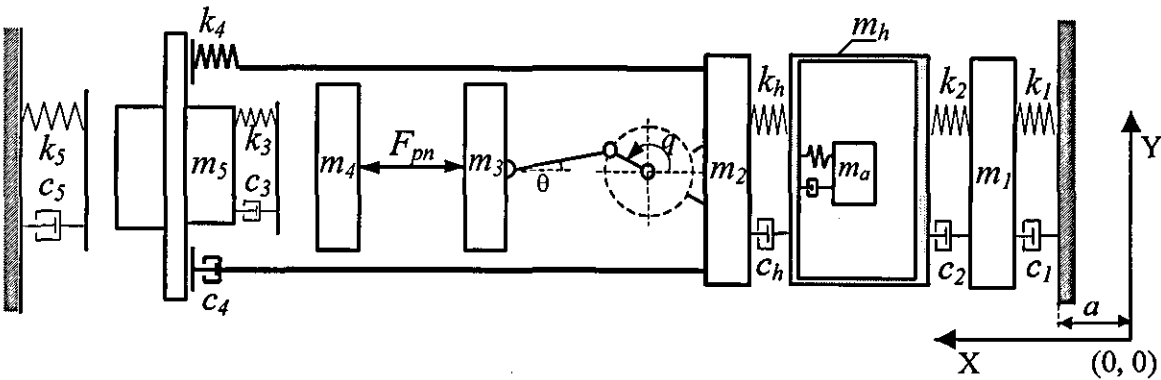


Figure 7.10. Dynamic model of the electro-pneumatic hammer with vibration protection system.

Simulink block diagram built for this dynamic model is shown in Figure 7.11. Subsystem “ m_a ” represents motion of dynamic absorber attached to the isolated handle by spring dashpot combination “ k_a, c_a ”. The rest of the blocks are the same as in the original model of unprotected electro-pneumatic hammer.

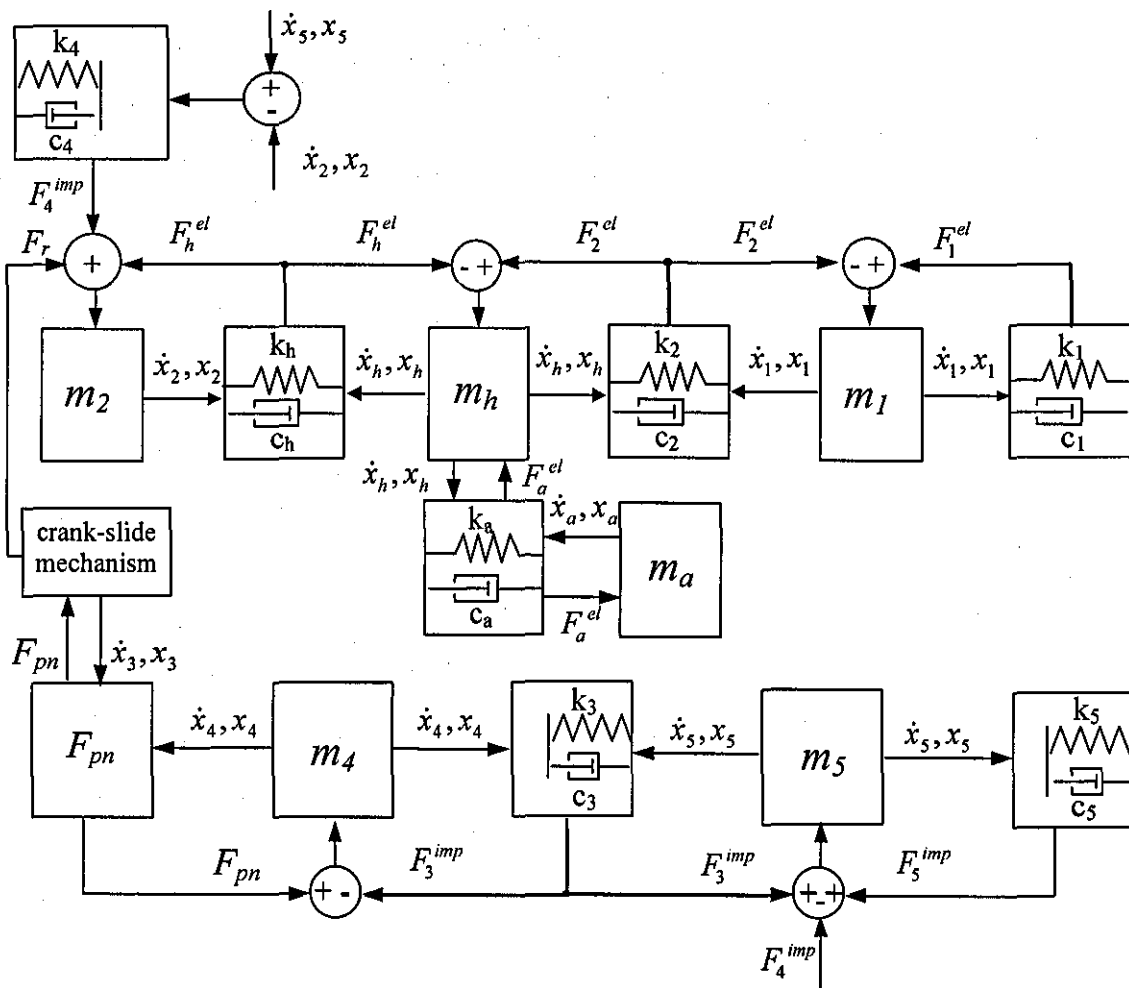


Figure 7.11. Simulink block diagram of the pneumatic hammer with vibration protection system.

Figure 7.12 shows the Simulink block diagram of the isolated handle and the dynamic absorber attached to it.

The dynamic absorber attached to the system reduces vibration by producing counter-force applied to the system. This counter force is proportional to the amplitude of motion at the point of attachment of the dynamic absorber. Hence, in order to avoid large absorber displacement, the effective mass of the dynamic absorber is usually 5-25% of effective dynamic mass of the system in correspondent mode shape. Low damping of the dynamic absorber improves its performance in terms of vibration suppression. These are the general recommendations for choosing parameters of a dynamic absorber, whereas optimal values of these parameters have to be chosen for every particular case.

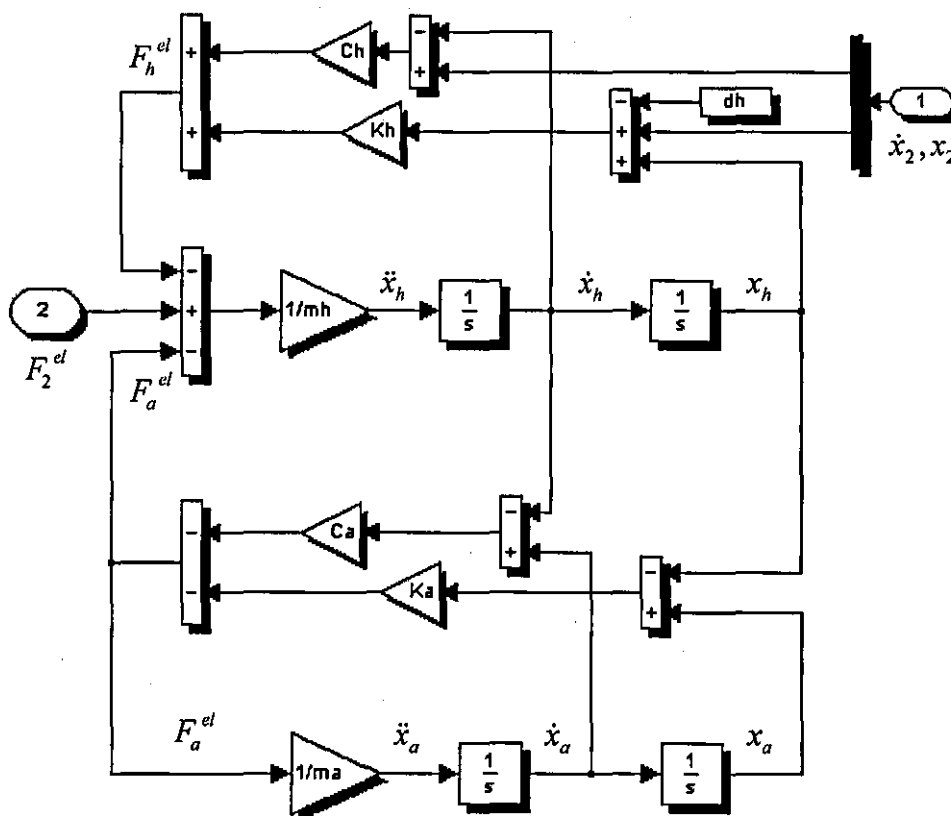


Figure 7.12. Simulink block diagram of isolated handle with attached dynamic absorber

In order to find the optimum parameters of dynamic absorber for the developed vibration attenuation system, numerical simulations have been run for different values of tuning frequency of the absorber. It was found to be equal to the driving frequency 45 Hz. Then simulations have been run for different values of mass and loss factor of the dynamic absorber attached to the handle and tuned to the fundamental frequency 45 Hz.

The performance of the dynamic absorber has been characterised using the following ratios between the characteristics of the hand acceleration for the original electro-pneumatic hammer without vibration protection and the same machine with vibration protection system:

K_{rms} – suppression ratio of r.m.s. of hand acceleration;

K_{fh} – suppression ratio of amplitude of the fundamental harmonic of the hand acceleration;

K_{pktoPk} – suppression ratio of peak to peak amplitude of the hand acceleration;

K_{sh} – suppression ratio of amplitude of the second harmonic of the hand acceleration.

In Figure 7.13, K_{rms} , K_{pktoPk} , K_{fh} and K_{sh} are shown as functions of mass and loss factor of dynamic absorber.

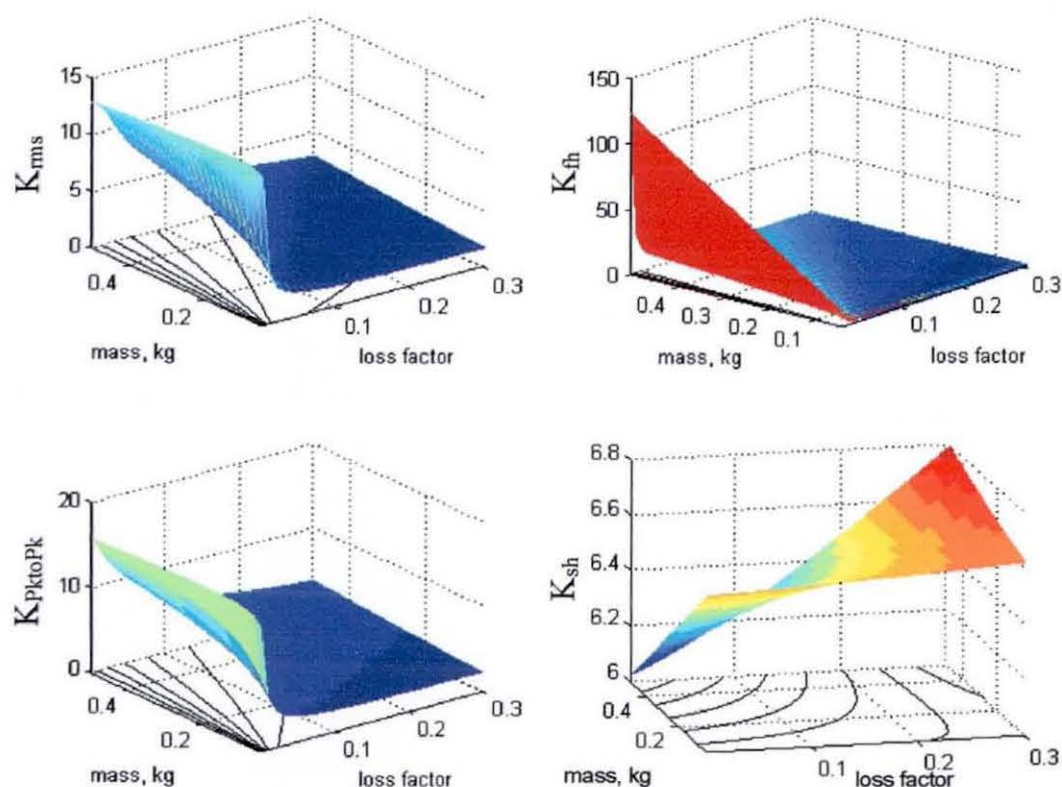


Figure 7.13. Vibration attenuation system with dynamic absorber attached to isolated handle.

The contour lines on the horizontal plane are drawn at regular intervals of functions magnitudes and give a good idea about the slope of characteristics. As can be seen, coefficients of r.m.s., amplitude of fundamental harmonic and peak to peak amplitude suppression increase sharply when the loss factor decreases from 0.05 to 0 (for small values of loss factor, mass of the absorber practically does not affect its performance). According to these results, for the dynamic absorber with reasonably

low damping (loss factor is about 0.01) tuned to the driving frequency, the essential reduction of the hand acceleration can be achieved even for the small value of absorber effective mass. Amplitude of the second harmonic of hand acceleration slightly increases due to changes in amplitude-frequency characteristic of the whole system, which are caused by attachment of dynamic absorber. At the same time, the dynamic absorber attached to the handle does not affect the frequency and energy of impacts, casing acceleration and the stability of the performance of the electro-pneumatic hammer.

The dynamic absorber with mass $m_a = 0.18\text{kg}$, natural frequency $\Omega_a / 2\pi = 45\text{Hz}$, and loss factor $\zeta_a = c_a / 2m_a\Omega_a = 0.01$ has been chosen for further investigations.

Figure 7.14 shows the spectra and the time histories of the casing and the hand acceleration for the electro-pneumatic hammer with vibration attenuation system. In order to illustrate the effect of vibration isolation system, the scale is the same for all graphs.

The dynamic absorber does not affect high frequency range, while it significantly suppresses fundamental harmonic of hand acceleration. As a result, the r.m.s. of the acceleration of an operator hand was reduced by a factor of 9. The magnitude of the fundamental harmonic of acceleration was reduced by a factor of 35 and the peak to peak amplitude of acceleration by a factor of 13 as compared with electro-pneumatic hammer without vibration attenuation.

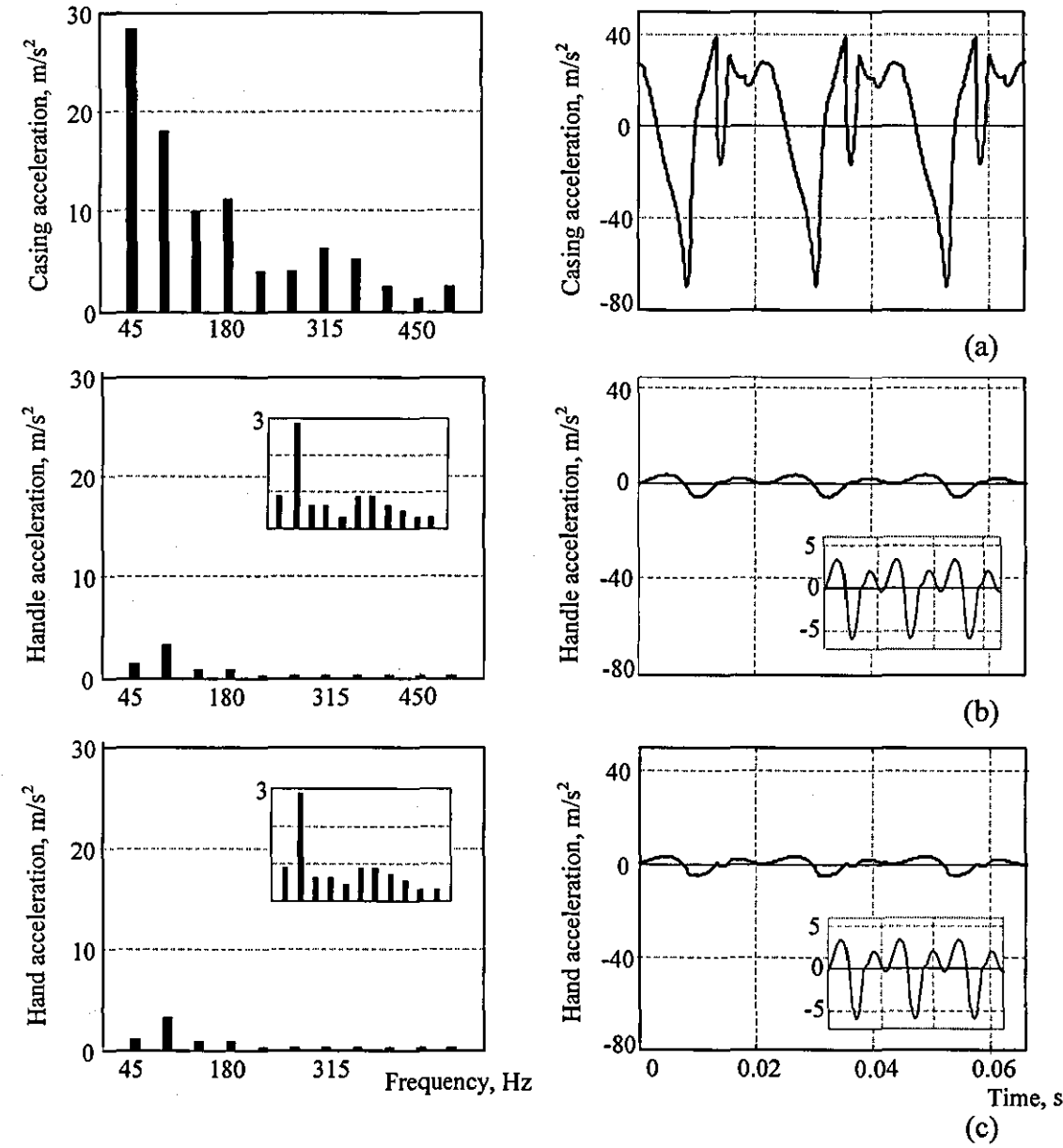


Figure 7.14. Spectrum and time history of acceleration of the casing (a), the handle (b) and operator hand (c). Small windows are zoomed time history of accelerations.

Figure 7.15 shows time histories of displacements of the casing, the handle and the hand-arm system. Compared to the system without dynamic absorber, displacements of the handle and hand are noticeably reduced (peak to peak amplitude of the handle and the hand absolute displacements are reduced by a factor of 15).

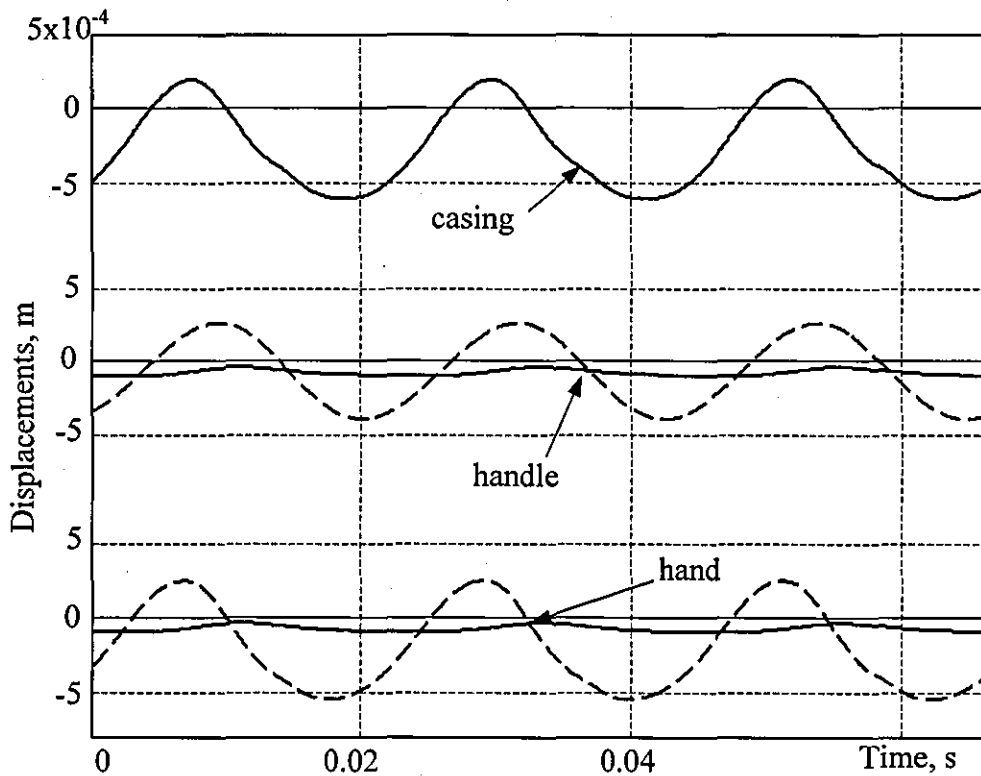


Figure 7.15. Time histories of the casing, the handle and the hand absolute displacements.; dashed line-displacements of the handle and the hand without vibration isolation.

The mass of the handle is small in comparison with the mass of the whole machine, so an advantage of the dynamic absorber being attached to the isolated handle instead of the casing is the small effective mass of the dynamic absorber. In the studied vibration attenuation system mass ratio is:

$$\mu = m_a / m_m = 0.02,$$

where m_m is the mass of the whole hammer. The absorber absolute displacement is 2.85 mm.

In the case of a similar system with a dynamic absorber attached to the casing, the same effect in vibration suppression can be achieved for a mass ratio μ of 0.1, which means that an additional weight of 0.8 kg needs to be used for a machine with a mass of 8 kg. As was repeatedly stated above, an increase of weight of hand-held power tool results in an increase of load on the operator and therefore is undesirable.

The small mass of the dynamic absorber that is sufficient for effective vibration suppression, permits the use of several dynamic absorbers attached to the handle and tuned to the second, the third and etc. harmonics of hand acceleration. This means that in such systems of vibration attenuation there is no need to employ vibration isolator with the lowest possible stiffness taking the risk of possible disruptions and compromising safety of operation of electro-pneumatic hammer.

However, maximum allowable stiffness of a vibration isolator is also limited. When the stiffness of the vibration isolator between the handle and the casing is higher than a certain critical value, dynamic de-coupling between the casing and the handle is disrupted. In this case dynamic absorber becomes involved in the casing motion. The effective mass of the dynamic absorber is very small compared to the mass of the casing. Hence the effect of the dynamic absorber attached to the handle worsens.

In the current model, such effect occurs when the natural frequency of the isolator (placed between the handle and the casing) is higher than 990 rad/s and depends weakly on the loss factor of the isolator. This upper limit of isolator stiffness depends on operating frequency, ratio between the mass of the whole machine and the handle, mass of the dynamic absorber and can be easily found for every particular case.

Effect of vibration attenuation can be further improved by employing a secondary dynamic absorber tuned to the second harmonic of acceleration. Dynamic model and Simulink block diagram of electro-pneumatic hammer with two dynamic absorbers attached to the isolated handle are very similar to the previous one and are therefore not shown separately.

The optimal tuning frequency for this secondary absorber was found to be 90.15 Hz . Coefficients K_{rms} , K_{pkopk} , K_{fh} and K_{sh} as functions of mass and loss factor of the absorber were found after a number of numerical simulations. Figure 7.16 shows results of numerical simulations. Here, parameters of the primary dynamic absorber: $\Omega_a / 2\pi = 45 \text{ Hz}$, $m_a = 0.18 \text{ kg}$ and $\zeta_a = 0.01$ while parameters of the second absorber are varied.

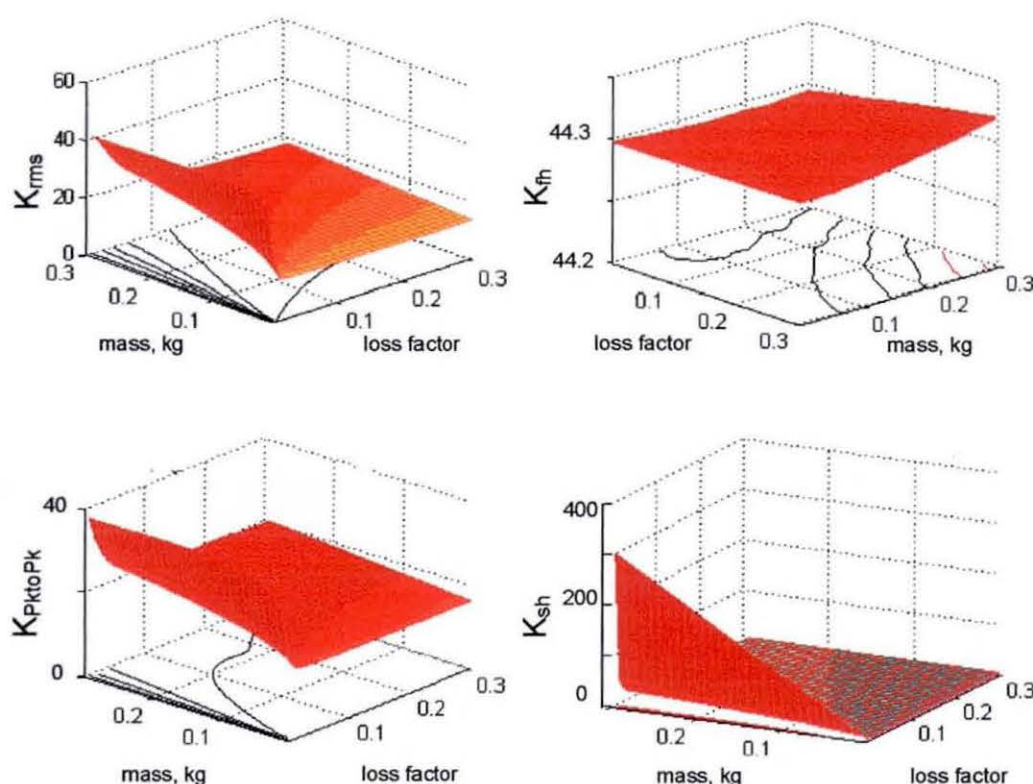


Figure 7.16. Vibration attenuation system with two dynamic absorbers attached to the isolated handle of electro-pneumatic hammer.

Results of numerical simulations (see Figure 7.16) show that the second absorber with a low damping and small mass attached to the handle significantly improves performance of the vibration attenuation system. In comparison with the system with one dynamic absorber attached to the both-side isolated handle coefficients K_{rms} and K_{pktoPk} increased approximately by a factor of 2. As before, the contour lines on the horizontal plane are drawn at regular intervals of functions magnitudes. There is a sharp increase in K_{rms} , K_{pktoPk} and K_{sh} for the small values of loss factor of dynamic absorber. Secondary dynamic absorber attached to the handle does not have any visible effect on the amplitude of the fundamental harmonic of hand acceleration as well as overall performance of electro-pneumatic hammer.

Based on these results, the following parameters of the secondary dynamic absorber were chosen:

$$m_{a1} = 0.035 \text{ kg}, \quad \Omega_{a1} / 2\pi = 90.15 \text{ Hz} \quad \text{and} \quad \zeta_{a1} = 0.01.$$

Figure 7.17 shows the spectra and the time history of the casing and the hand acceleration for the electro-pneumatic hammer with two dynamic absorbers attached to the isolated handle ($m_a = 0.18kg$, $\Omega_a / 2\pi = 45Hz$ and $\zeta_a = 0.01$).

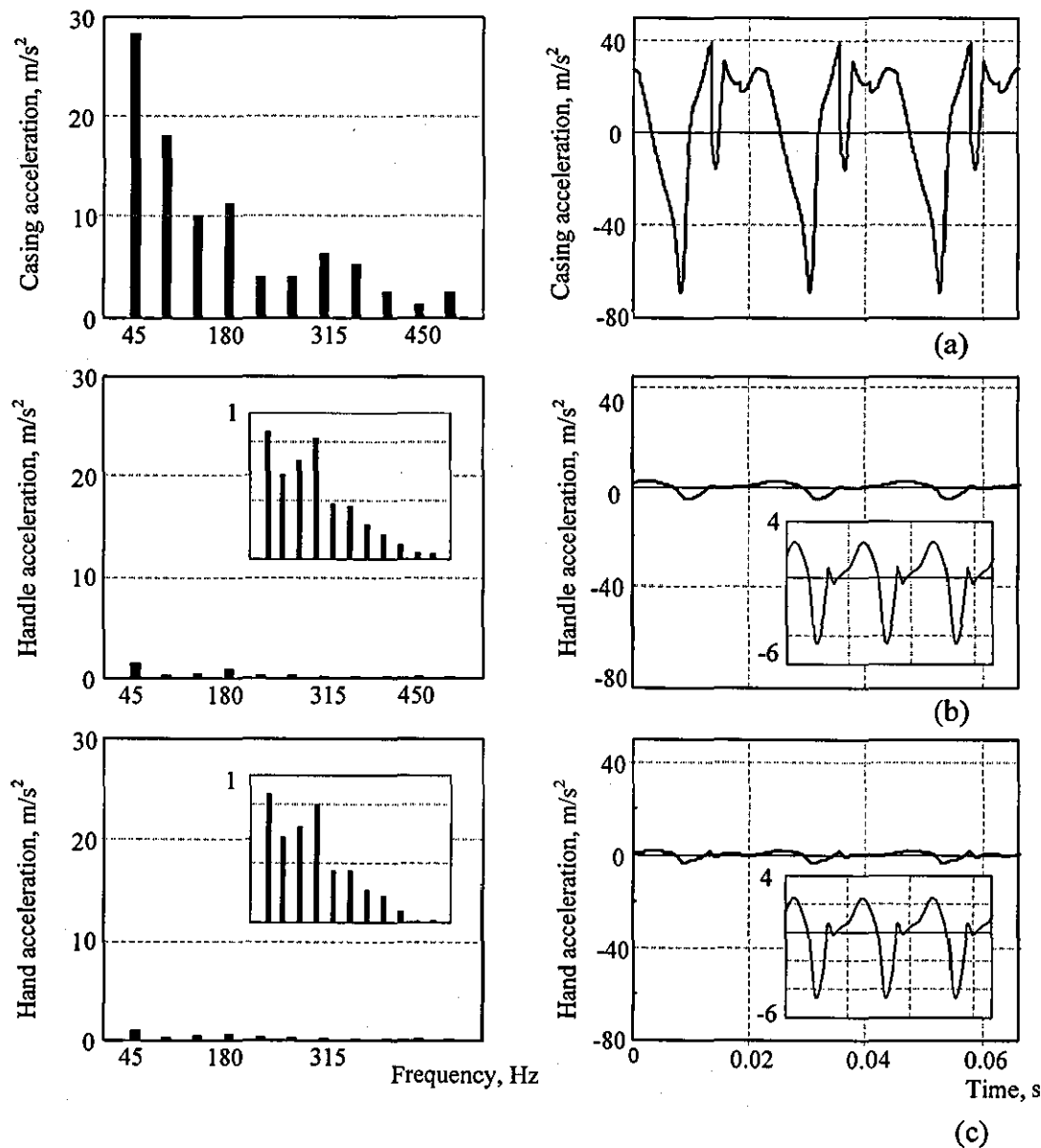


Figure 7.17. Spectrum and time history of acceleration of the casing (a), the handle (b) and the operator hand (c) for the system with two dynamic absorbers attached to the handle. Small windows are zoomed time histories of acceleration.

In order to illustrate effect of vibration isolation system, the scale is the same for all graphs. However, accelerations of the hand and the handle are so small, that additional windows on the main graphs show the same graphs on an enlarged scale.

The r.m.s. of the hand acceleration is now 2.3 m/s^2 and has been reduced by a factor of 13 in comparison with the reference model of the electro-pneumatic hammer without vibration isolation. The magnitudes of the fundamental and the second harmonic of hand acceleration are reduced by a factor of 35 (the second absorber does not affect the fundamental harmonic of the oscillation) and 50 respectively. Peak to peak amplitude of hand acceleration was reduced by a factor of 14.

Figure 7.18 shows time histories of absolute displacements of the casing, the handle and the hand-arm system. The vibration attenuation system reduced the absolute displacements of the hand by a factor of 20 in comparison with reference model without vibration isolation.

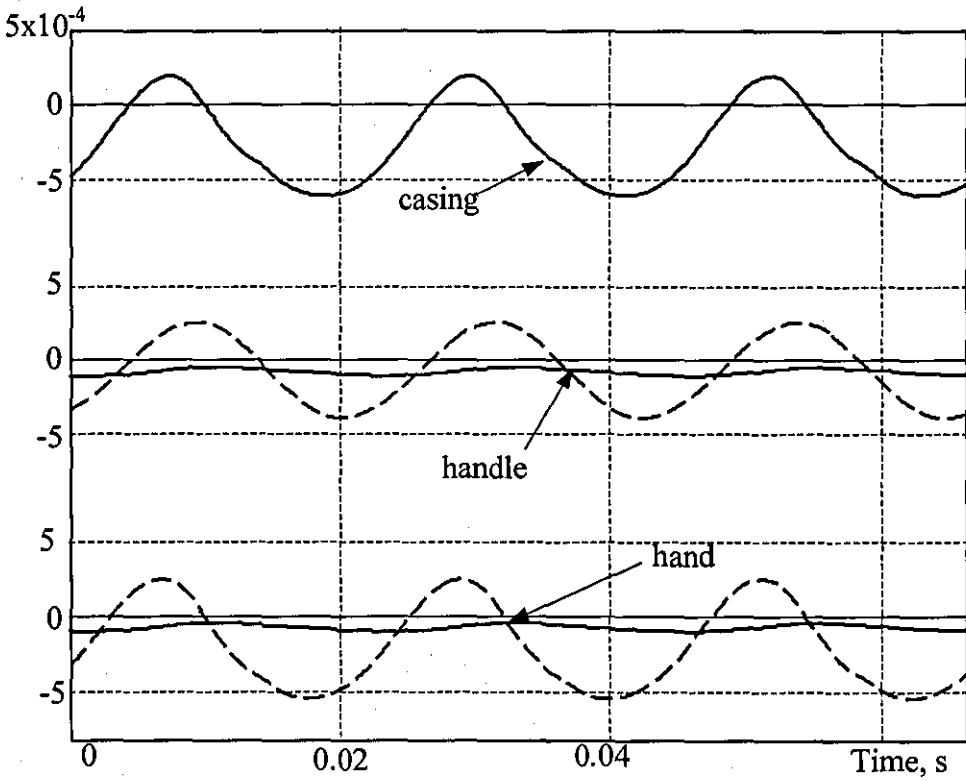


Figure 7.18. Time histories of the casing, the handle and the hand absolute displacements; dashed line-displacements of the handle and the hand for electro-pneumatic hammer without vibration attenuation system.

The mass ratio for the second absorber is:

$$\mu_1 = m_{a1} / m_m = 0.004$$

The absolute displacement of the secondary absorber is 0.6 mm. The ratio between the mass of the two absorbers and the mass of the whole machine is about 3%. Displacements of the primary and secondary absorbers were 2.85mm and 0.6 mm correspondingly.

An experiment was carried out to verify the results obtained by numerical simulations.

7.3 Experimental verification

Laboratory facilities did not allow building a working prototype of electro-pneumatic hammer with vibration attenuation system. To overcome this, the mechanical system that represents handle-hand-arm system was built, while the electro-dynamic shaker attached to the handle reproduced the casing acceleration.

7.3.1 Mechanical set-up

Figure 7.19 shows a schematic diagram of the experimental rig. The experimental rig layout is shown in Figure 7.20.

The system under test includes the handle attached to the electro-dynamic shaker (Ling Dynamic System, model V409) through a metal elastic mounting and connected through a similar mounting to the mass-spring combination which represents the hand-arm system.

In order to verify results of numerical simulations, acceleration reproduced by the shaker was similar to the casing acceleration obtained by numerical simulations. The shaker was attached to the handle by Shock Tech¹ wire isolator that represented vibration isolator between the casing and the handle of the electro-pneumatic hammer. This wire isolator consisted of a stainless steel cable wound between light alloy bars and possessed weak non-linearity, due to the friction between wires. However, the damping provided by this isolator was higher in comparison with normal coil spring and it ideal for present experimental studies.

¹ See <http://www.shocktech.com>

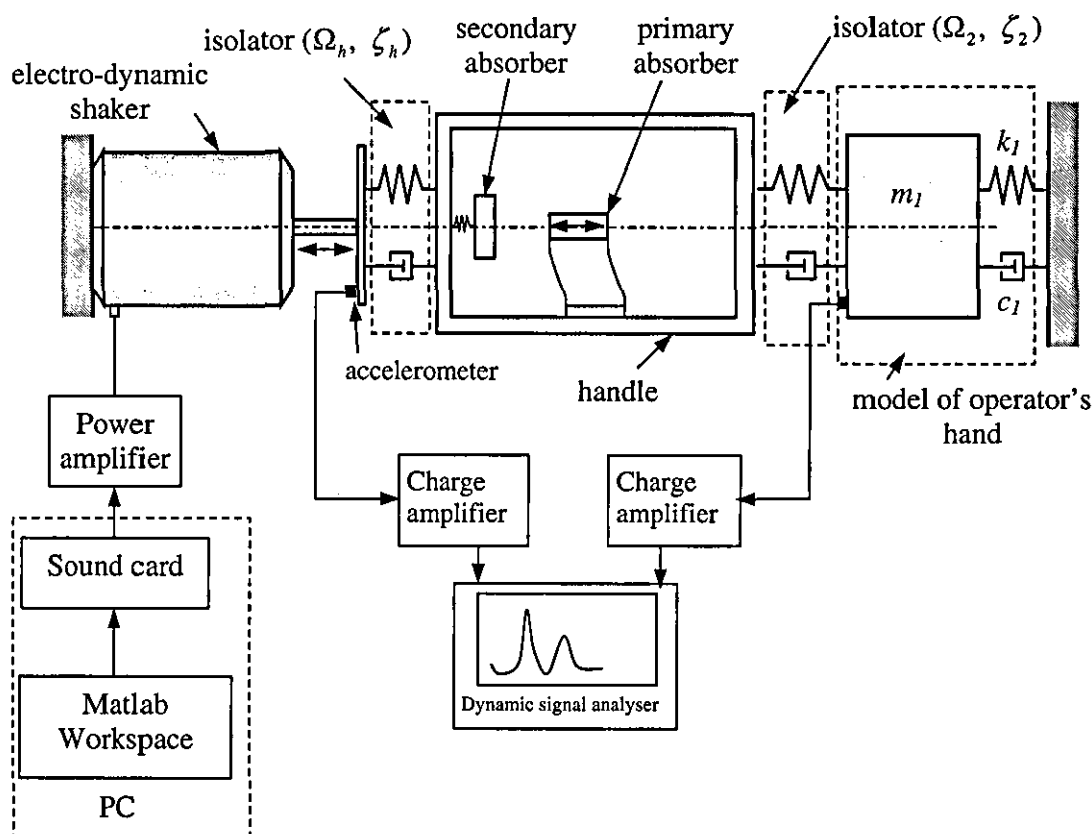


Figure 7.19. Schematic diagram of the experimental rig.

The wire isolator had motion freedom in vertical and torsion directions. In the case of possible misalignment between the moving platform of the shaker and the handle, this fact could have caused vibration of the handle in directions other than horizontal. In order to avoid vertical and torsion vibrations of the handle, which were neglected in the current investigation, four flat springs (width-30mm, thickness-0.041mm, length-200mm) were placed between the handle and the mounting table (see Figure 7.20 (a)). Such springs prevented the handle from vibration in vertical or torsion directions without affecting the behaviour of the experimental mechanical system in horizontal direction.

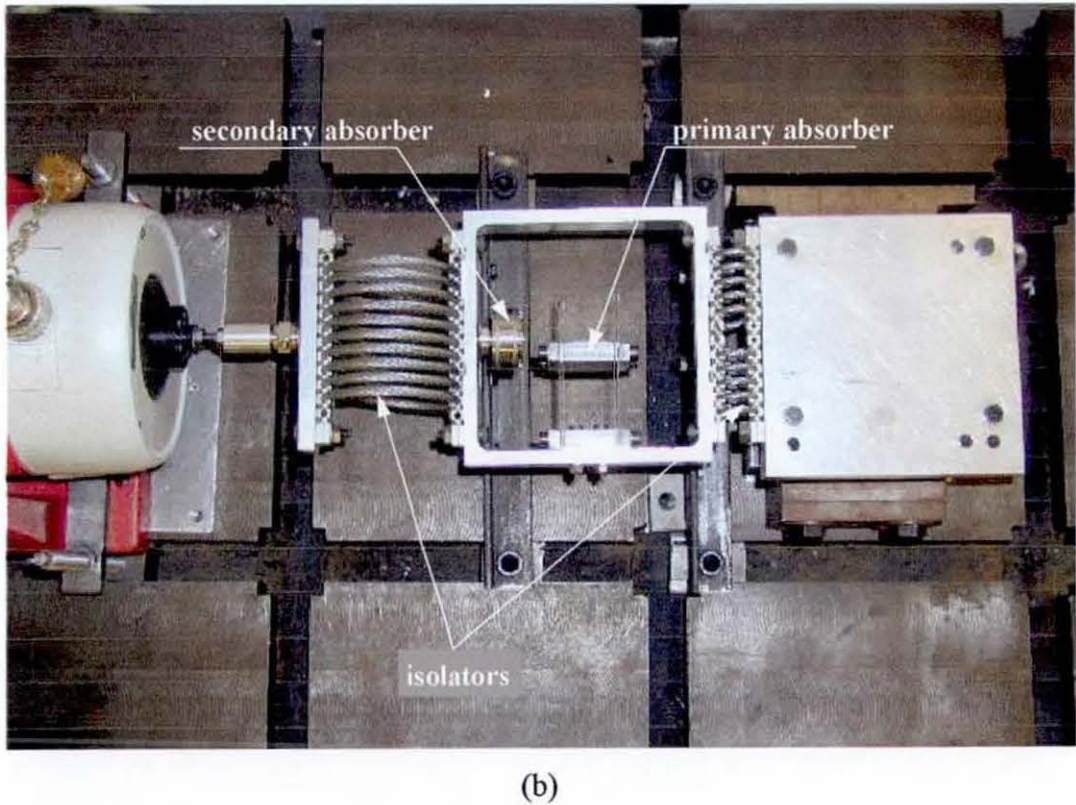
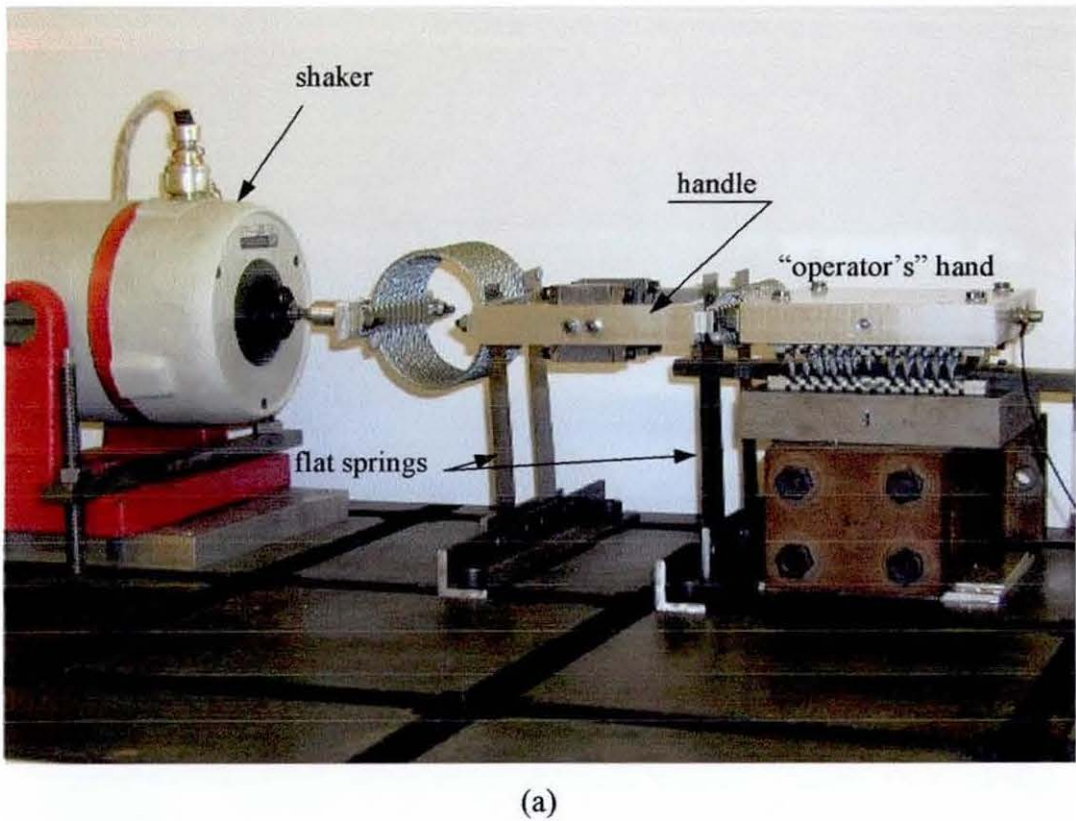


Figure 7.20. Experimental rig.

The second vibration isolator between the handle and the hand-arm system was represented in experimental rig by smaller Shock Tech wire isolator.

A mechanical model of hand-arm system was built as the mass attached to the mounting table by means of two isolators (see Figure 7.20 (b)). The stiffness and the damping ratio of this mechanical system corresponded to the hand-arm system parameters used in numerical simulations. Figure 7.21 shows accelerance transfer function of mechanical equivalent of the hand and arm. Accounting for non-linearity of isolators, sweep sine was carried out for the same level of excitation that would be applied to the system during further experimental studies.

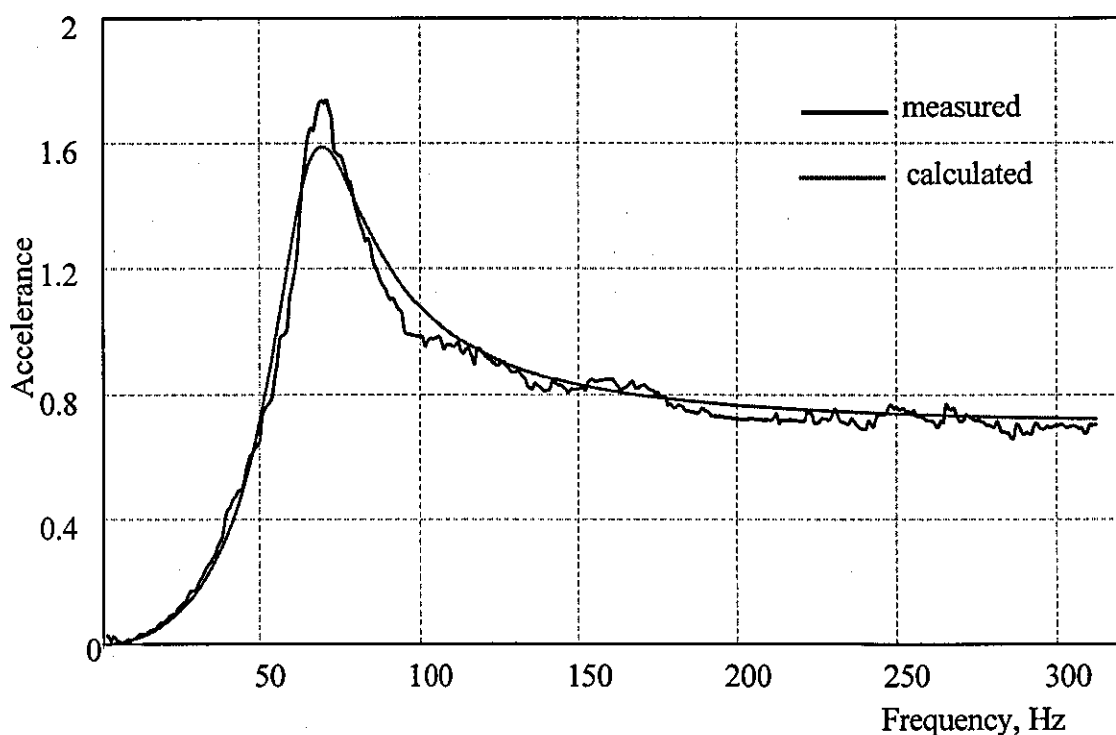


Figure 7.21. Accelerance transfer function of mechanical model of hand-arm system.

Figure 7.21 also shows results of curve fitting procedure, where the method of least squares was used. The numerical values obtained by curve fitting:

$$m = 1.44 \text{ kg}, \Omega = 41 \text{ rad/s and } \zeta = 0.224.$$

As can be seen, these values are very close to the parameters of the hand-arm system obtained by the experiment in Chapter 3, so the current system can be successfully

used in further experimental studies as a simplified mechanical model of the hand and arm.

The electro-dynamic shaker was driven by a standard PC sound card through a power amplifier (B.K. Electronics MXF 400). The accelerations of the different parts of the system have been measured using an accelerometer (Brüel & Kjær Type 4393) and amplified by a charge amplifier (Brüel & Kjær Type 2635) before it was sent to a dynamic signal analyser (Data Physics Corporation DP 104) as is shown in Figure 7.19.

All structures and most electrical devices have inherent resonant frequencies. Present electro-mechanical experimental rig includes power amplifier, shaker and mechanical system, and consists of both electrical (e.g. amplifier, magnetic coil, flexures, etc) and structural components (e.g. shaker flexure and head, fixture and test mechanical system). Therefore it has several resonant frequencies in the range of testing. These resonant frequencies can cause a signal to be amplified or attenuated as it passes through the vibration test system. What is more, the degree of amplification or attenuation varies depending on the frequency of the signal. Without proper compensation of the system's dynamics the signal that passed through the system will be distorted and will not achieve the desired output.

The analog signal applied to the shaker was converted from a digital data generated in Matlab by means of a Data Acquisition Toolbox built within the Matlab computing environment. In order to obtain acceleration on the output of the shaker that is similar to the casing acceleration, obtained by numerical simulations, it is necessary to compensate for the influence of the entire electro-mechanical system that includes the power amplifier, the shaker and the tested mechanical system.

7.3.2 Synthesis of the excitation signal

Assuming that distortion of the signal by sound card can be neglected, distortion of the signal that passes from the sound card through the entire electro-mechanical system can be overcome by measuring the complex frequency response function (FRF) between the output of the sound card and the acceleration of the mounting

table of the shaker. Then the original digital data need to be multiplied by an inverse function before being sent to the sound card.

The procedure is relatively simple for SDOF systems. Some electro-magnetic shakers equipped with controllers that use transfer function equalisation to compensate for the dynamics of the shaker test system. However, difficulties arise due to the degree of complexity of the tested mechanical system.

Figure 7.22 shows a typical module of the FRF, $|H(j\omega)|$, measured between the output of the sound card and the acceleration measured on the output of the shaker. The tested mechanical system consisted of the both-side isolated handle and the mechanical equivalent of the hand-arm system.

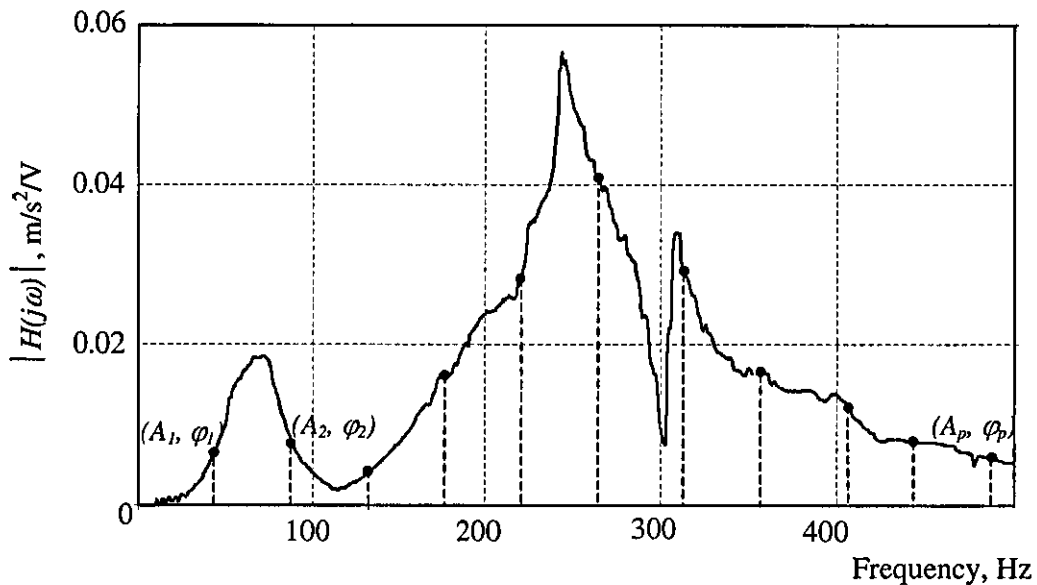


Figure 7.22. The module of the FRF between the output of the sound card and the acceleration reproduced by the shaker.

As can be seen from Figure 7.22, FRF of experimental rig has three distinctive peaks in 600 Hz frequency range. Retrieving acceptable analytical expression of an inverse function that can be used for signal compensation is difficult, because available electronic devices cannot provide required amplification for high frequency range. At the same time, finding an analytical expression that would be satisfactory for both module and phase of FRF is difficult.

In the case of periodic excitation, compensation for the dynamics of electro-mechanical system can be achieved by measuring the system response only at specific discrete frequencies that are a multiple to the driving frequency (see Figure 7.22) instead of the complete transfer function. System response may be expressed in terms of amplitudes (A) and phases (φ) in the following manner:

$$\begin{aligned} A_p &= |H(jp\omega_0)|, \\ \varphi_p &= \arg(H(jp\omega_0)), \end{aligned} \quad (7.1)$$

where $H(j\omega)$ is the FRF obtained in the above experiment as a ratio between acceleration measured on the moving platform of the shaker and the analog output of the sound card; ω_0 is the fundamental frequency; $p=1, 2, \dots, 11$. The FRF was measured over a 600Hz frequency range because amplitudes of higher harmonics of acceleration perceived by the operator were found to be insignificant.

Figure 7.23 schematically shows synthesis of the digital signal with compensated influence of the tested electro-mechanical system. Casing acceleration obtained by numerical simulations, \ddot{x}_2 (see Figure 7.4) was represented by a Fourier series, namely, a series of sine and cosine waves of frequencies $p\omega_0$ and amplitudes b_p and a_p correspondingly:

$$\ddot{x}_2(t) = a_0 + \sum_{p=1}^{11} (a_p \cos p\omega_0 t + b_p \sin p\omega_0 t), \quad (7.2)$$

where $a_0 = 0$ and whole procedure was carried out by using Simulink block for frequency analysis described earlier (see Section 4.3.3).

The final compensated excitation signal was synthesised as a sum of sine and cosine waves with phases φ_p and amplitudes calculated as a ratio a_p / A_p and b_p / A_p as shown in Figure 7.23:

$$\text{signal}(t) = \sum_{p=1}^{11} \left(\frac{1}{A_p} (a_p \cos(p\omega_0 t - \varphi_p) + b_p \sin(p\omega_0 t - \varphi_p)) \right), \quad (7.3)$$

here $\text{signal}(t)$ is the compensated excitation signal.

Due to system non-linearities, the values of A_p and φ_p were slightly adjusted manually in order to obtain the closest match between the time history of the shaker acceleration and the theoretical casing acceleration.

After the numerical compensated excitation signal was obtained, it was stored in Matlab workspace. Analog output subsystems convert digital data stored on computer to real analog signals that can be sent to the sound card. The Data Acquisition Toolbox provides access to the analog output subsystems through an analog output object (see Figure 7.19). M-file with procedure of converting digital signal to analog signal is in Appendix C.

As a result of the entire procedure, the electrical signal applied to the shaker was synthesised in such a way that the acceleration reproduced by the shaker was similar to the casing acceleration obtained in numerical simulations. It should be noted that any further changes in mechanical part being tested would lead to changes in FRF of experimental rig and therefore compensated excitation signal shall be adjusted accordingly.

The system of vibration attenuation with one vibration isolator placed between the handle and the hand-arm is simple and there is no real necessity in experimental verification of numerical results as they are quite straightforward. So, the system with both-side isolated handle was considered first (shaker, handle and system representing hand-arm system were arranged as shown in Figure 7.20, dynamic absorbers were not attached).

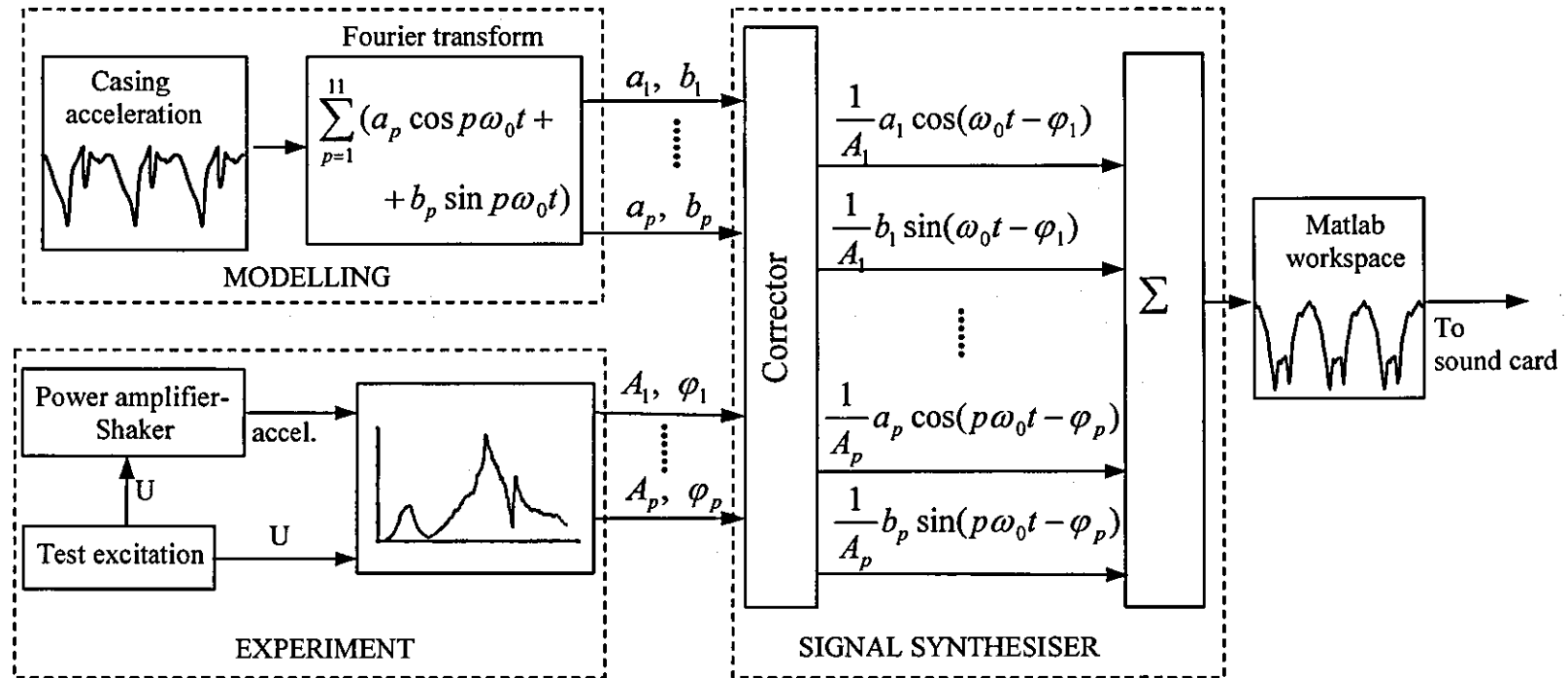


Figure 7.23. Diagram showing synthesis of the excitation signal.

Figure 7.24 shows a screen snap shot from the signal analyser, where the final electrical signal measured on the output of the sound card and the acceleration measured on the output of the shaker are shown.

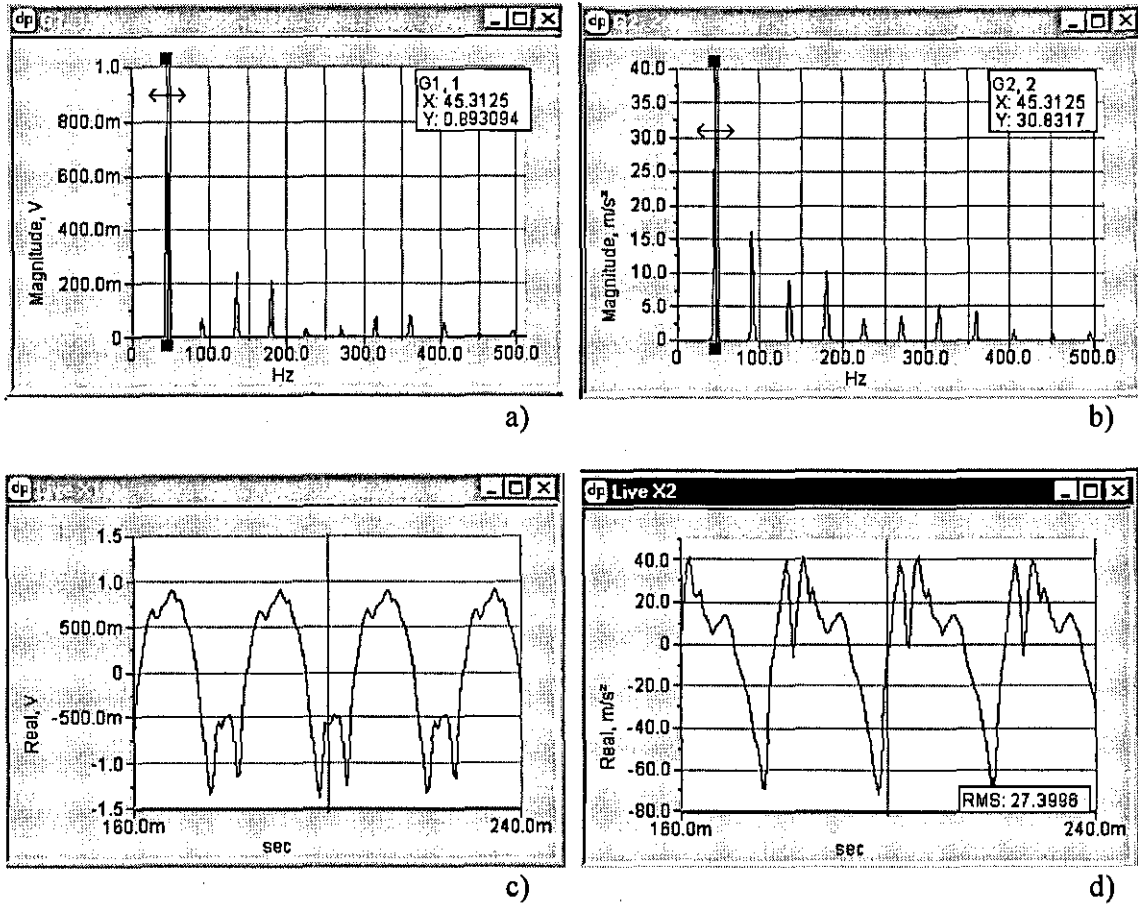


Figure 7.24. Screen shot from the signal analyser. (a), (c) – spectrum and time history of electrical signal, (b), (d)– spectrum and time history acceleration reproduced by the shaker.

The spectrum of the shaker acceleration is almost identical to the spectrum of casing acceleration obtained by numerical simulations (see Figure 7.1). As can be seen from Figure 7.24 original digital data were significantly modified before being sent to the sound card. In some cases, reproduced spectrum of excitation would be sufficient for investigating dynamic behaviour of a system in frequency domain. However, for accurate reproduction of casing-handle interaction in hand-held percussion machine, peak amplitudes of casing acceleration must be accounted for, hence time history of excitation is equally important. The time history of the casing acceleration obtained by numerical simulations and acceleration measured on the

moving platform of the shaker, for the system with both-side isolated handle, are shown in Figure 7.25.

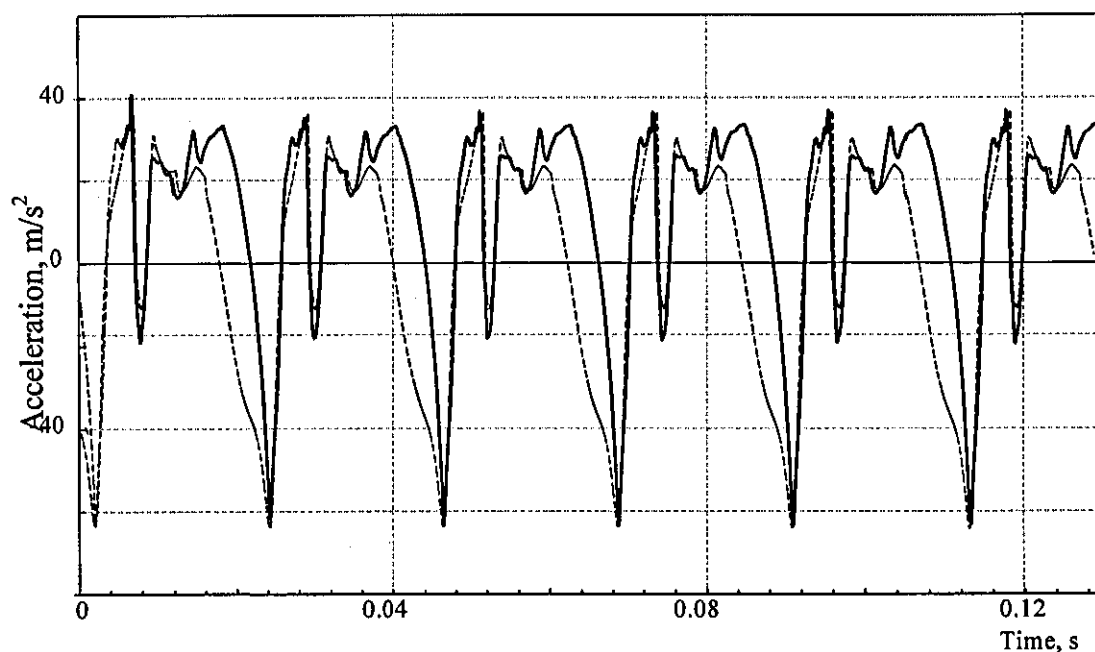


Figure 7.25. Time histories of the casing acceleration obtained by numerical simulations (dashed line) and the acceleration reproduced by the shaker (solid line).

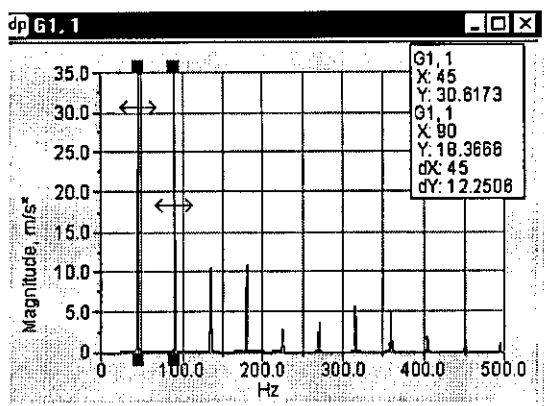
It can be seen that the time histories of numerical and experimental (obtained at the output of the shaker and applied to the handle) accelerations are very similar. The r.m.s. of numerical casing acceleration is 29.5 m/s^2 , peak to peak amplitude is 103 m/s^2 and for acceleration reproduced by the shaker these values are 27.4 m/s^2 and 110 m/s^2 , correspondingly.

7.3.3 Experimental results

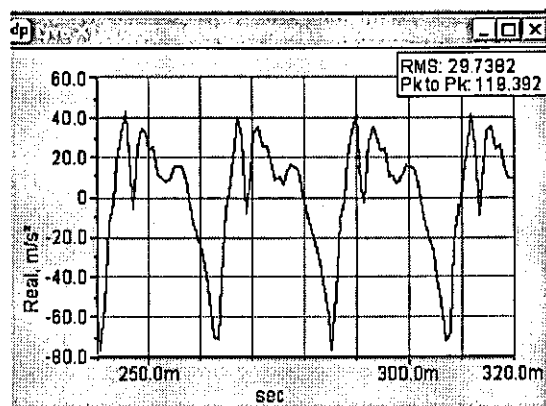
Once the shaker can reproduce the casing acceleration, the effect of a vibration attenuation system can be observed and compared with results of numerical simulations by measuring acceleration of the mass that represents hand-arm system (see Figure 7.20).

Vibration attenuation system with both-side isolated handle and no dynamic absorbers attached was tested first.

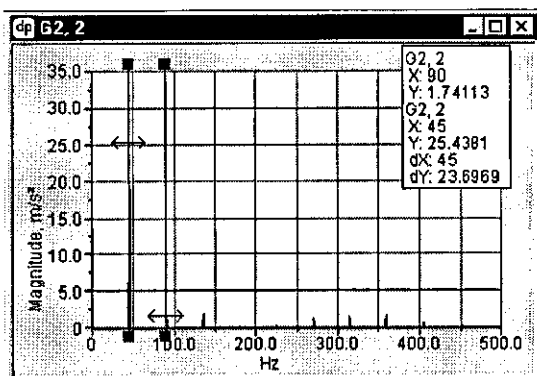
Figure 7.26 shows spectrum and time histories of shaker acceleration applied to the handle, acceleration measured on the handle and acceleration measured on the mechanical equivalent of the hand-arm system



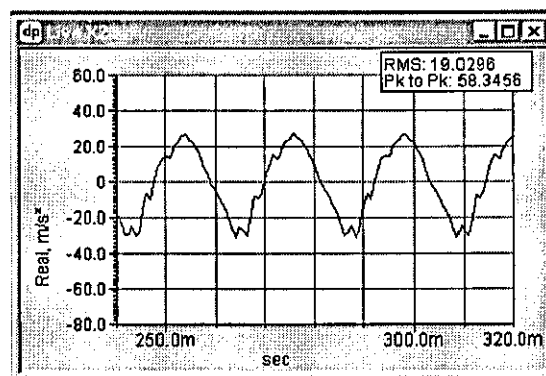
(a)



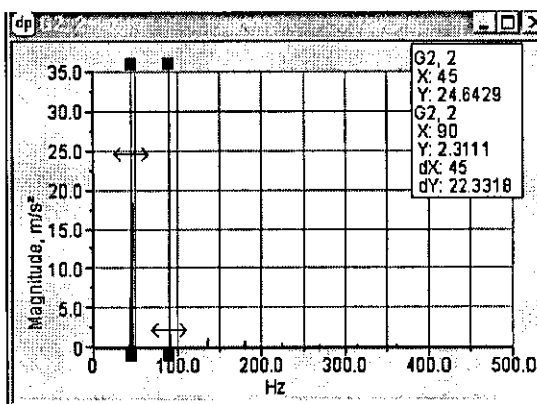
(b)



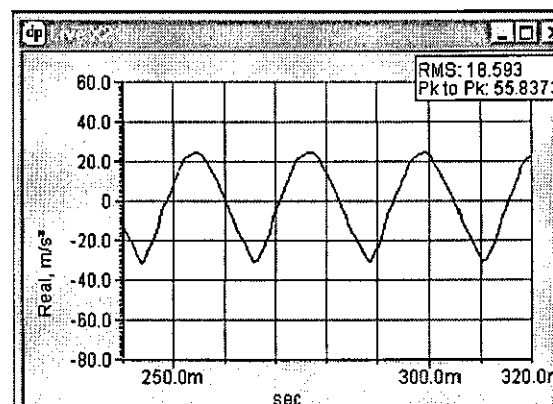
(c)



(d)



(e)



(f)

Figure 7.26. System with both-side isolated handle.

- (a), (b) - spectrum and time history of the “casing” acceleration;
- (c), (d) - spectrum and time history of the “handle” acceleration;
- (e), (f) - spectrum and time history of the “hand” acceleration.

As can be seen, experimental results are in good agreement with results obtained by numerical simulations. The vibration isolators practically do not reduce the amplitude of the fundamental harmonic of acceleration, but the second and higher harmonics have been attenuated very successfully. Time history of the “hand” acceleration was also smoothed by vibration isolation. The r.m.s. of hand acceleration was reduced by a factor of 1.6, peak to peak amplitude of acceleration by a factor of 2.2, amplitude of the fundamental harmonic by a factor of 1.25 and amplitude of the second harmonic by a factor of 11.

Figure 7.27 shows time histories of “casing”, “handle” and “hand” displacements.

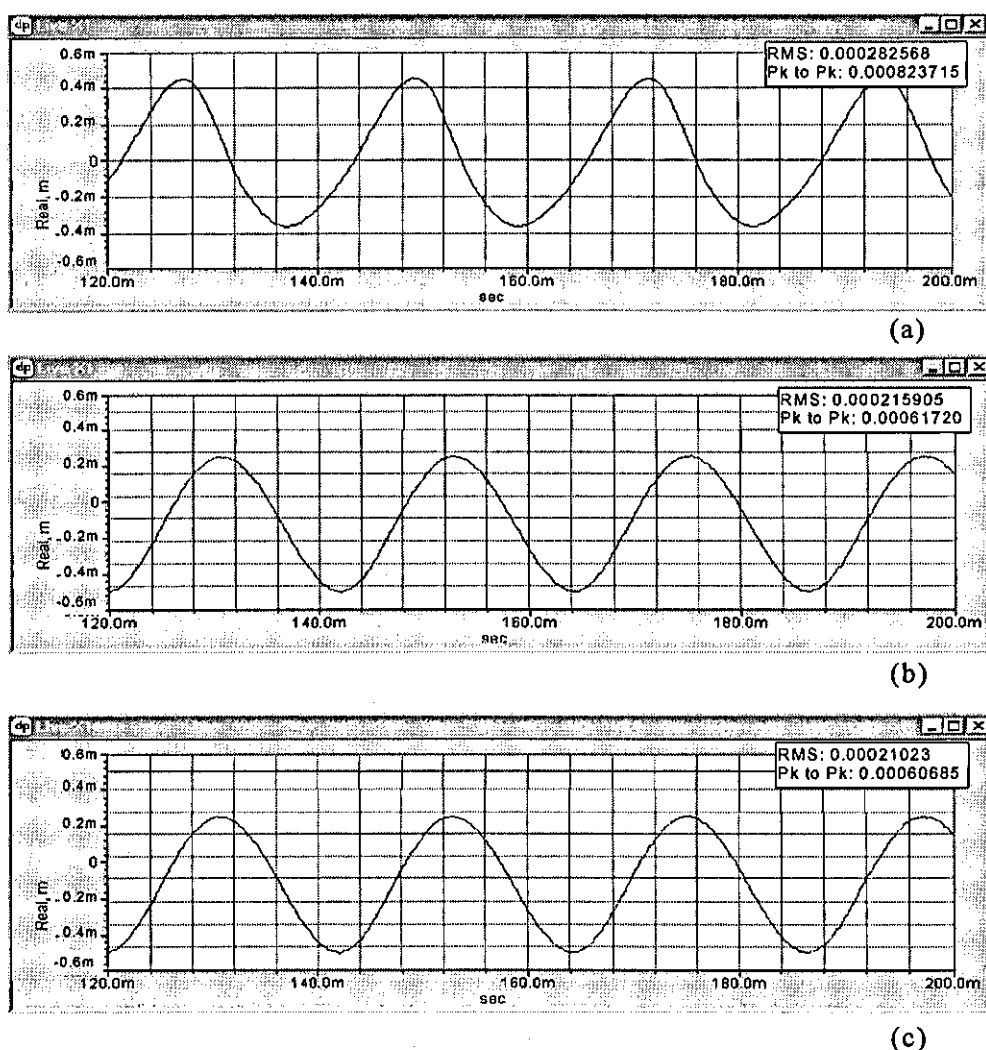


Figure 7.27. System with both-side isolated handle.

- (a) time history of “casing” displacement;
- (b) time history of “handle” displacement;
- (c) time history of “hand” displacement.

Vibration isolators reduced peak amplitude of “handle” and “hand” displacement by a factor of 1.3 in comparison with “casing” displacement.

At the second stage of the experiment, one dynamic absorber tuned to the fundamental frequency was attached to the handle (see Figure 7.20 (b)). This absorber will be referred to as “primary absorber”. The flexural of the above dynamic absorber was designed as four flat cantilever springs (length-40mm, width-30mm, thickness-0.041mm) separated by steel liners, in order to eliminate friction between the springs and maintain low loss factor. The absorber had a mass 0.18 kg, while its natural frequency was tuned to 45 Hz by displacing the mass along the flat springs. The length-width ratio of the flat springs secure linear motion of dynamic absorber in direction parallel to the direction of excitation. In order to ensure that the dynamic absorber produced only axial counter-force, symmetrical attachment of the dynamic absorber to the handle would be preferable. However, the main advantage of present design is an easy tuning of dynamic absorber. Providing that centres of gravity of the absorber and the handle coincide, cantilever design (as shown in Figure 7.20) works well. The possible difference in the position between the mass of the absorber and the centre of gravity of the handle might cause the torque of the handle about its vertical axis. In this case, the torque was compensated by flat springs between the handle and the mounting table (see Figure 7.20 (a)).

Figure 7.28 shows a screen shot from the dynamic signal analyser with the spectra and the time histories of the shaker, the “handle” and the “hand” acceleration for the system with one dynamic absorber attached to the both-side isolated handle.

Vibration attenuation system with single dynamic absorber, tuned to the fundamental harmonic of the signal applied to the handle, reduces the r.m.s. of the “handle” and the “hand” acceleration by a factor of 8, amplitude of the fundamental harmonic by a factor of 62 and the peak to peak amplitude of acceleration by a factor of 7 in comparison to the system without vibration attenuation. Attachment of the dynamic absorber leads to the additional high-frequency component in time history of “handle” acceleration in comparison with the system without dynamic absorber (see Figure 7.26). It could be due to the fact that after suppression of the fundamental harmonic of acceleration, the second harmonic becomes dominant. The second vibration isolator between the “handle” and the “hand” slightly reduces the second harmonic of acceleration and smoothes time history of the “hand” acceleration.

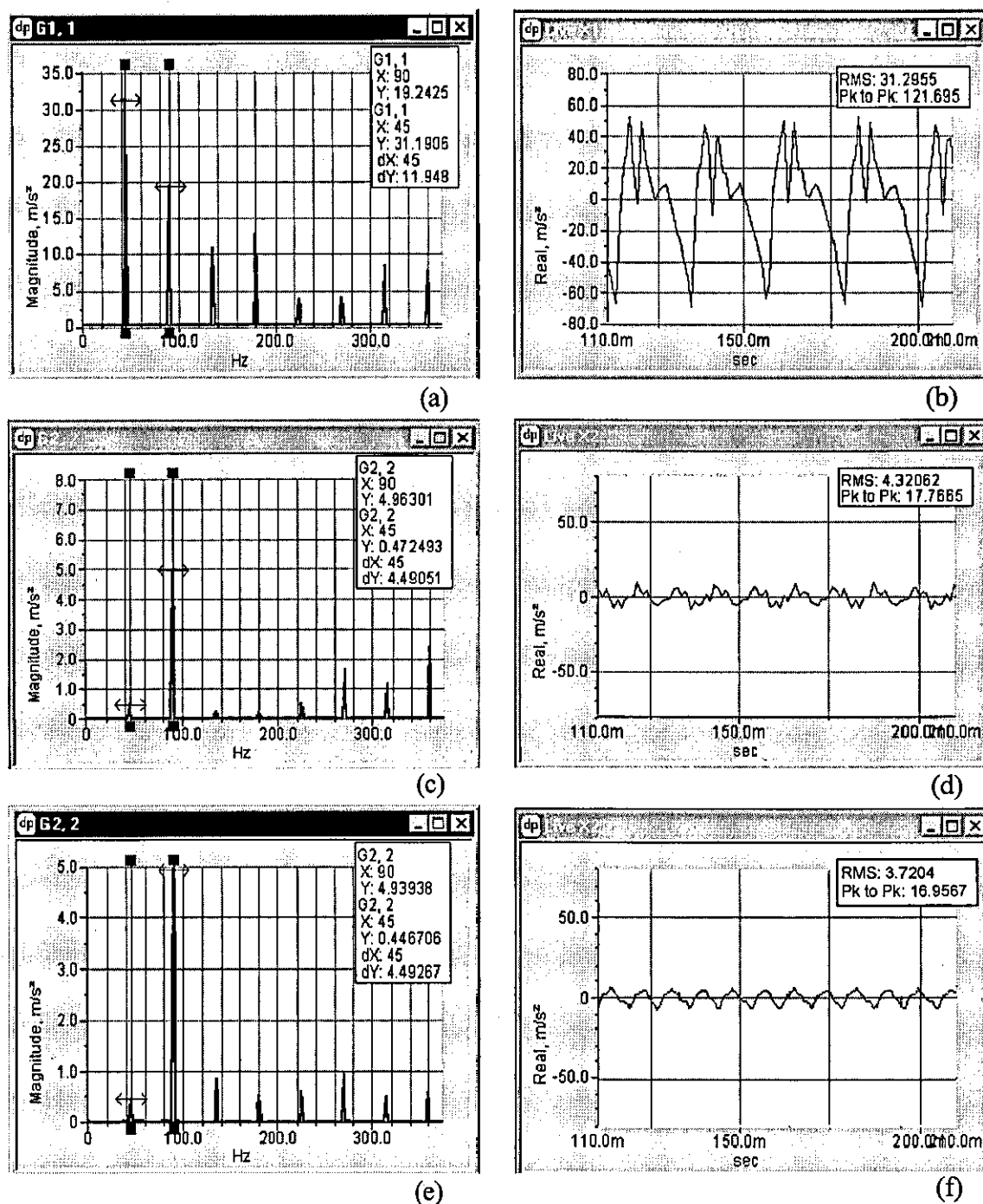
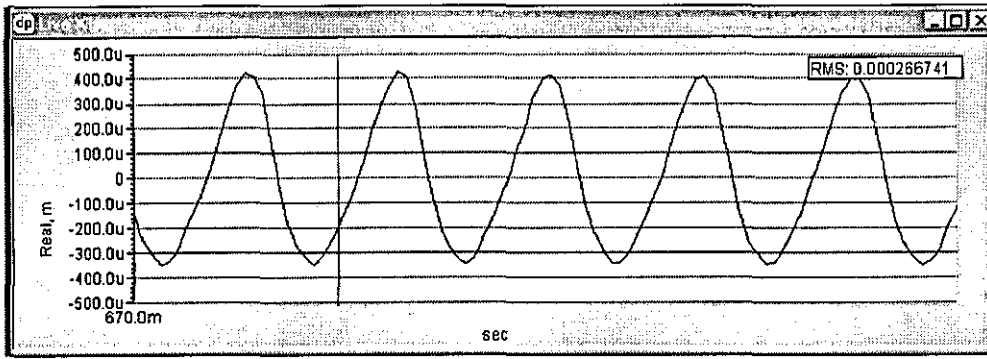


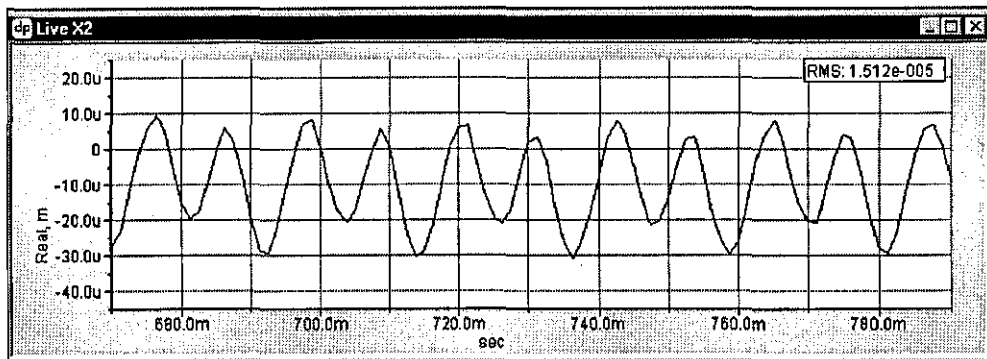
Figure 7.28. System with primary dynamic absorber.

- (a), (b) - spectrum and time history of the “casing” acceleration;
 (c), (d) - spectrum and time history of the “handle” acceleration;
 (e), (f) - spectrum and time history of the “hand” acceleration.

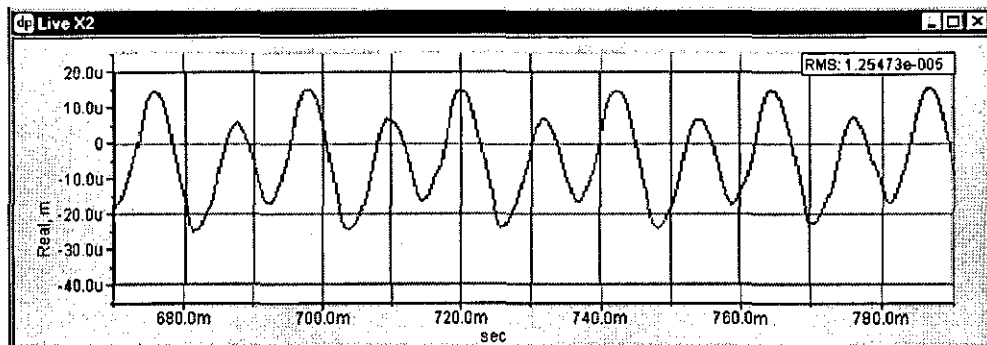
Figure 7.29 shows time histories of the “casing”, the “handle” and the “hand” absolute displacements.



(a)



(b)



(c)

Figure 7.29. System with primary dynamic absorber.

- (a) - time history of "casing" displacement;
- (b) - time history of "handle" displacement;
- (c) - time history of "hand" displacement.

According to these measurements, the vibration attenuation system with one dynamic absorber attached to the both-side isolated handle, reduces absolute displacement of the "handle" and the "hand" by a factor of 20.

This resulting vibration attenuation effect can be improved by employing a second dynamic absorber. In further study it will be referred to as the secondary absorber.

The measured time histories and spectra for the “casing”, the “handle” and the “hand” acceleration are shown in Figure 7.30; the time histories of absolute displacements of the casing, the handle and the hand are shown in Figure 7.31.

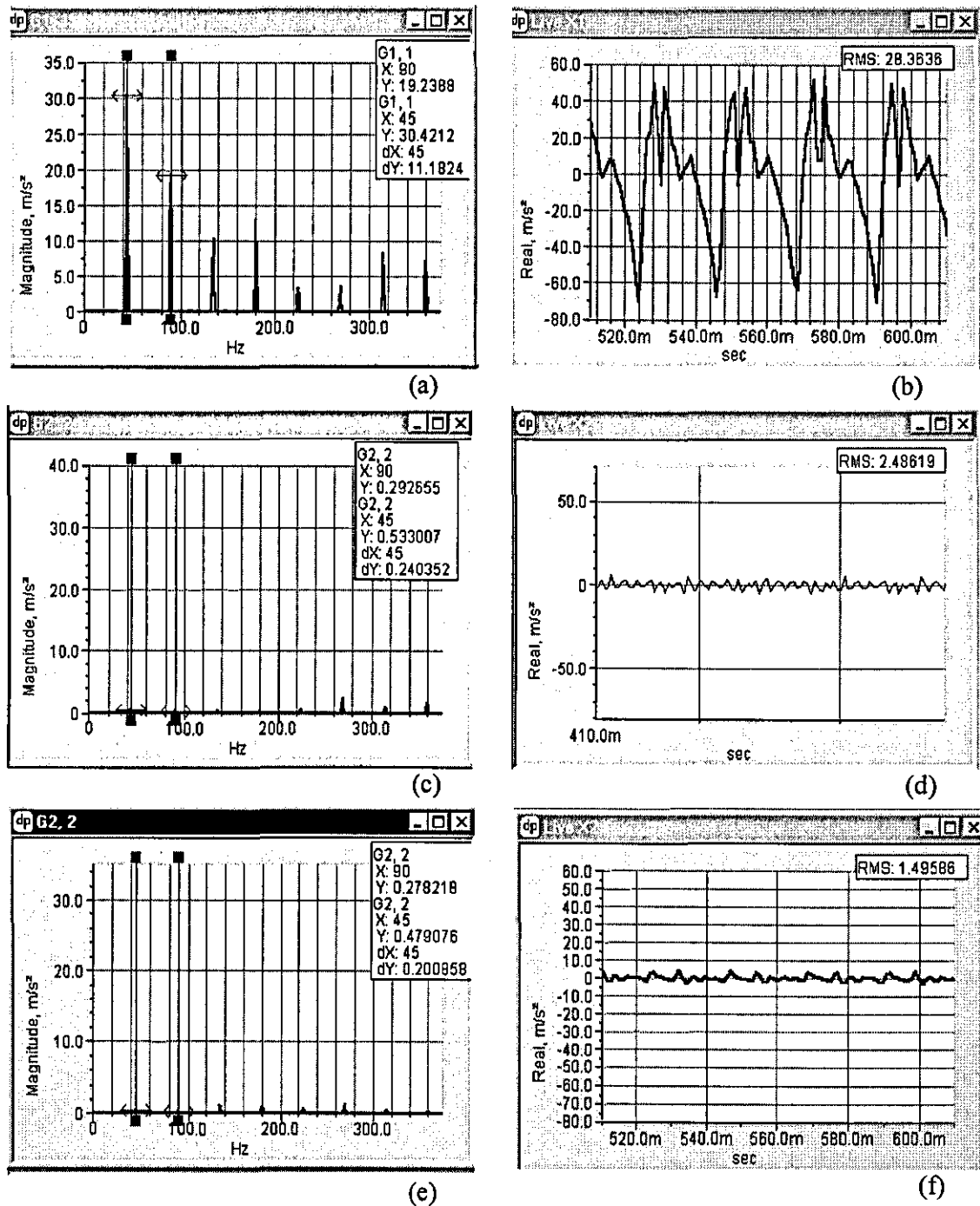


Figure 7.30. System with two dynamic absorbers.

- (a), (b) - spectrum and time history of the “casing” acceleration;
- (c), (d) - spectrum and time history of the “handle” acceleration;
- (e), (f) - spectrum and time history of the “hand” acceleration.

The secondary absorber was attached to the handle as shown in Figure 7.20 (b) by flexural elements that are designed as all-metal “Oxford” type flat springs providing a low loss factor. The absorber was tuned to the second harmonic of excitation. Its mass was 0.035kg, providing a mass ratio of the machine mass to the absorber mass, $\mu_1 = 0.4\%$.

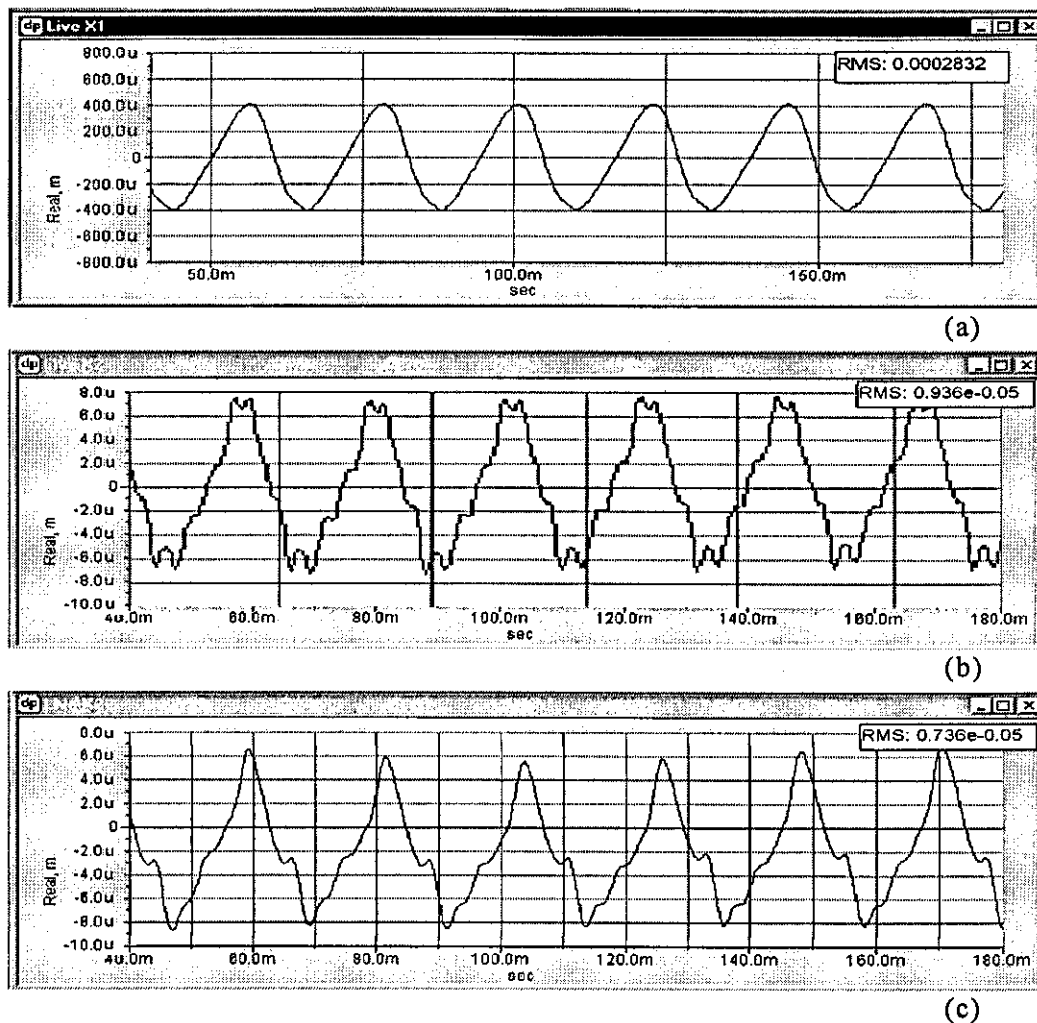


Figure 7.31. System with two dynamic absorbers.

- (a) - time history of “casing” displacement;
- (b) - time history of “handle” displacement;
- (c)- time history of “hand” displacement.

The amplitudes of the fundamental and the second harmonics of acceleration were reduced significantly, such that they cannot be seen on the same scale as the shaker acceleration. The cursors show the exact harmonics amplitudes (small windows on

the right-hand side of the main graphs). In comparison with the system without vibration isolation, the r.m.s. of the “hand” acceleration was reduced by a factor of 19, the fundamental harmonic by a factor of 62, the second harmonic by a factor of 70 and peak to peak amplitude of acceleration by a factor of 16.

The vibration attenuation system with two dynamic absorbers attached to the both-side isolated handle, reduces absolute displacement of the “handle” and the “hand” by a factor of 30.

7.4 Frequency response of vibration attenuation system

Effectiveness of a conventional tuned dynamic absorber deteriorates as the excitation frequency differs from the tuning frequency. Furthermore, the dynamic absorber introduces an additional degree-of-freedom into the composite system, so if tuning is incorrect, the attachment of the dynamic absorber may even bring the composite system into resonance with the excitation force.

In order to gain some idea about frequency response of the developed vibration attenuation system, a series of additional experiments were carried out. Excitation frequency was modulated around the centre frequency of 45Hz, while acceleration applied by the shaker and the “hand” acceleration were measured in the same manner as in previous experiments. For every point of measurement, the excitation signal was synthesised in such a way, that amplitudes of harmonics and time history of excitation signal were the same as in all preceding experiments. Experimental results were compared with the results obtained by numerical simulations.

The performance of the vibration attenuation system was characterised using introduced earlier ratios between the characteristics of the hand acceleration for the original electro-pneumatic hammer without vibration protection and the same machine with vibration attenuation system (see Section 7.2.2.). Figure 7.32 shows K_{rms} (suppression ratio of r.m.s. of hand acceleration) and K_{fh} (suppression ratio of amplitude of the fundamental harmonic of hand acceleration) as a measured functions of driving frequency of the electro-pneumatic hammer (for vibration

attenuation system with one dynamic absorber). The same functions obtained by numerical simulations are shown as thick lines in Figure 7.32.

There is a certain disagreement between experimental and numerical curves. Differences between experimental rig and dynamic model and non-linearity of experimental rig might be a cause of it. However, the general view of the experimental and the numerical curves is quite similar, especially for the frequency range below 45 Hz.

Results of this test showed that even at detuning of driving frequency of 5%, reduction of the r.m.s. and amplitude of the first harmonic of the “hand” acceleration was still better for the system with the dynamic absorber compared to the simple two-stage vibration isolation system.

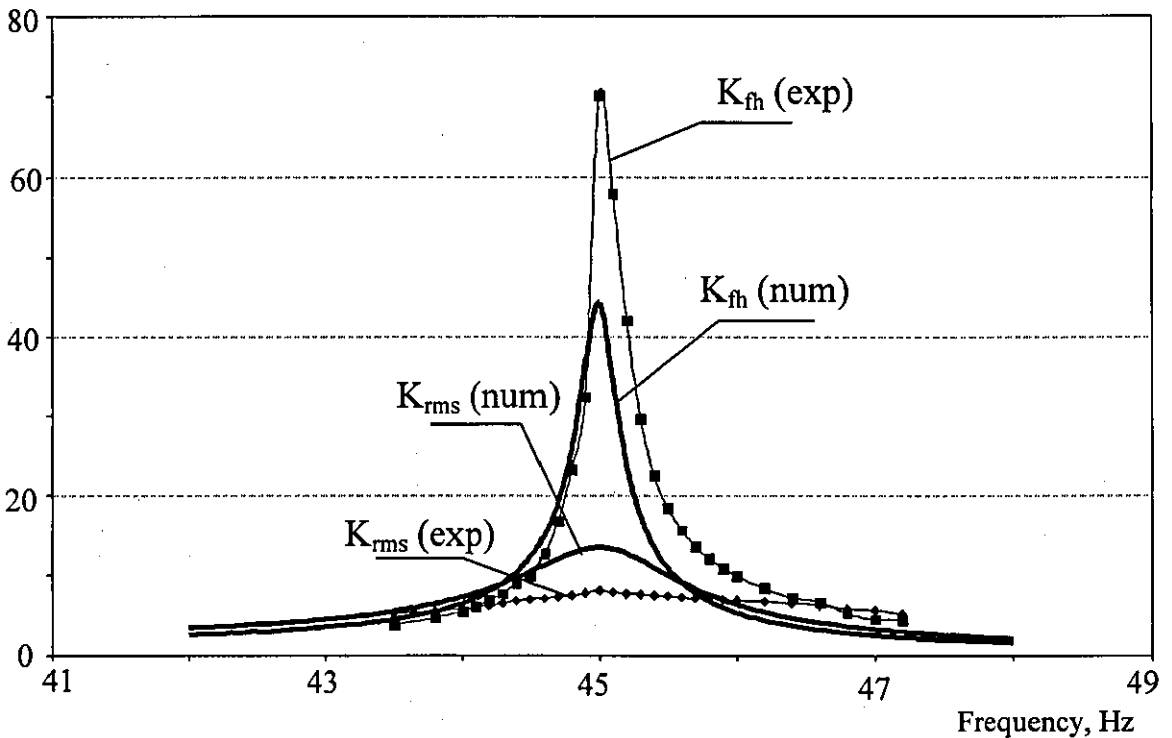


Figure 7.32. Sensitivity of the vibration attenuation system to the changes in operating frequency.

The sensitivity to the changes in the driving frequency for the system with two dynamic absorbers has been obtained in a similar manner, by measuring coefficients K_{rms} and K_{sh} (suppression ratios of the r.m.s. of hand acceleration and amplitude of

the second harmonic of hand acceleration). Experimental and numerical results are shown in Figure 7.33.

The sensitivity curve of vibration attenuation system with two absorbers is very similar to the system with one absorber (sensitivity of the K_{fh} is not shown because with second absorber attached to the handle the curve remains the same as for the system with one dynamic absorber).

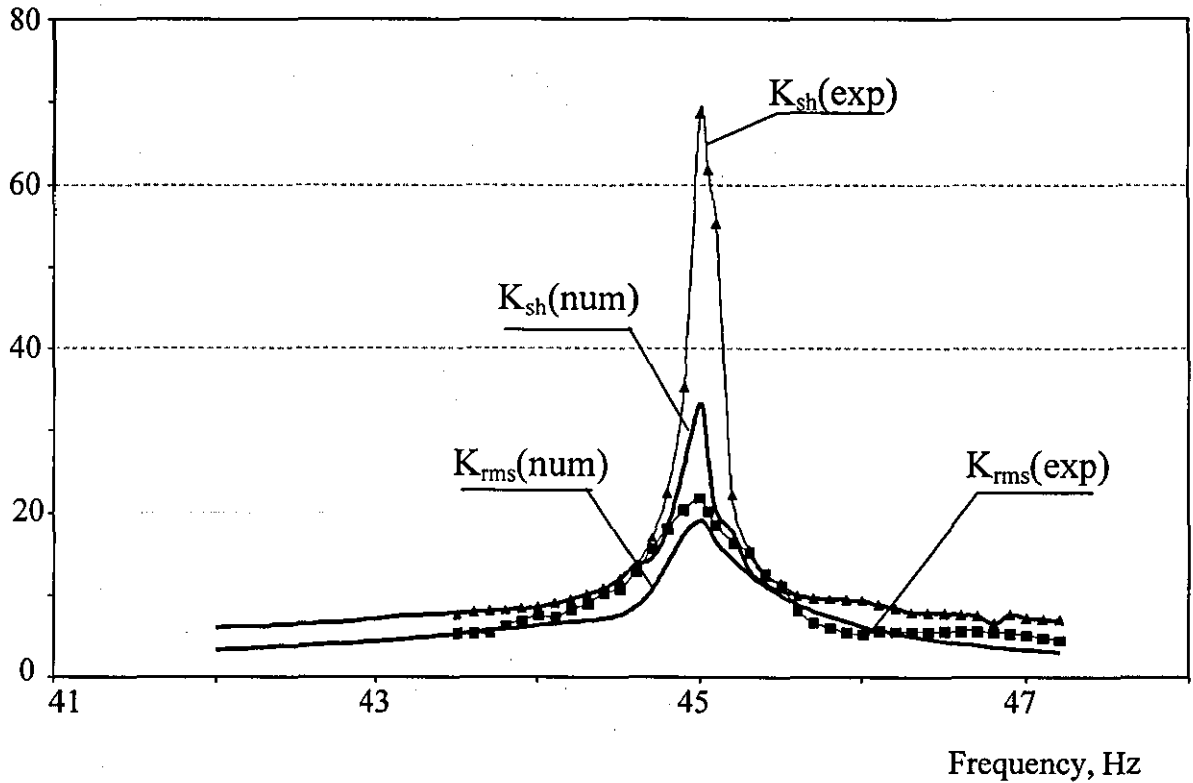


Figure 7.33. Sensitivity of vibration attenuation system with two absorbers attached to the isolated handle to changes in operating frequency.

It appears that there is no resonance that could arise in the system in case of fluctuations of driving frequency. As expected, developed vibration attenuation system is most effective in a relatively narrow frequency range; hence, an appropriate controller or some other means should maintain operating frequency of the electro-pneumatic hammer.

7.5 Conclusions and discussions

A passive system of vibration attenuation for the hand-held percussion machine was developed. This system combines the properties of vibration isolation for reduction of vibration in the high frequency range and dynamic absorbers for suppression of the dominant harmonics of acceleration that are not affected by vibration isolation. Such a combination has several advantages, especially important for vibration protection of an operator of hand-held percussion machine.

Firstly, low-frequency harmonics of acceleration perceived by an operator reduced by dynamic absorbers, therefore, there is no need to use vibration isolators with low natural frequency compromising the controllability and safety of tool operation. Secondly, dynamic absorber, attached to the handle isolated from the casing, suppresses acceleration of a light handle only, so effective mass of the absorber is small. This fact allows the use of several small dynamic absorbers and achieves even greater vibration attenuation without serious increase in the mass of the machine. Finally, the developed vibration attenuation system can be easily implemented into the existing design of a hand-held percussion machine without significant additional costs.

According to numerical simulations, vibration attenuation system with two dynamic absorbers reduced r.m.s. of the hand acceleration by a factor of 13, peak to peak amplitude by a factor of 14 and, finally, absolute displacement of the hand-arm system by a factor of 20. Mass ratio between mass of absorbers and mass of the whole hammer was 3%, while absolute displacements of the absorbers tuned to the fundamental and the second harmonic of the hand acceleration were 2.85 and 0.6 mm respectively.

Referring to the Figure 4.21 we can further estimate effect of the vibration attenuation system in comparison with the original model of electro-pneumatic hammer. The r.m.s. of the weighted acceleration perceived by the operator for a new hammer with vibration attenuation system corrected for vibration total value is 0.5 m/s^2 . According to Figure 7.34 such an electro-pneumatic hammer can be safely used for more than 16 hours of daily exposure.

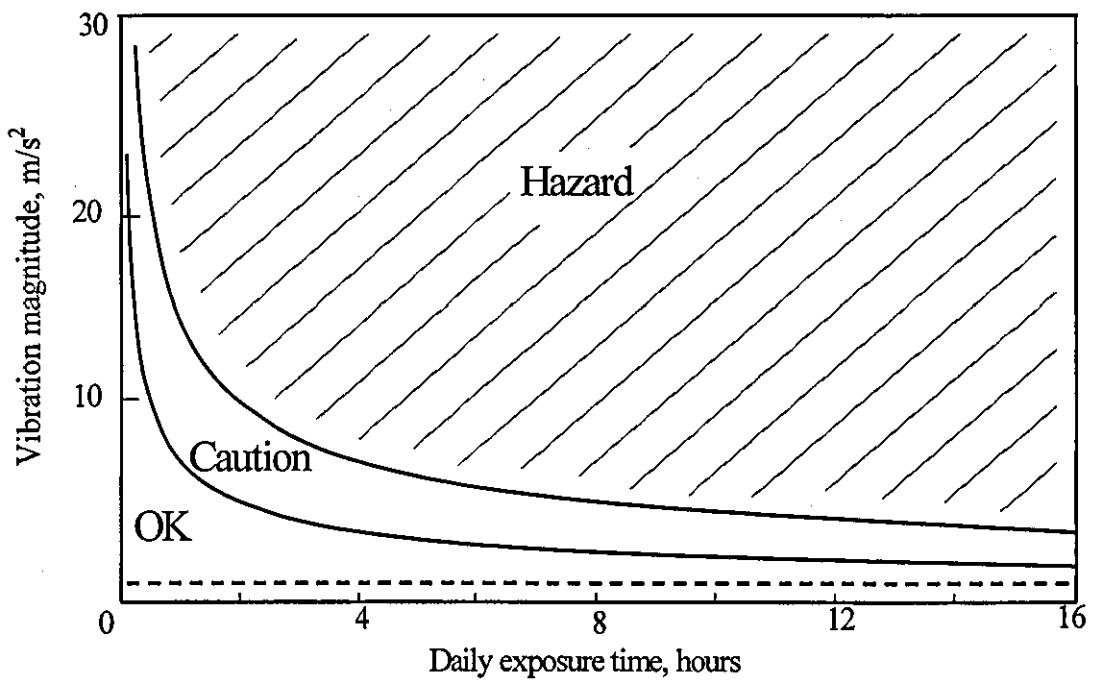


Figure 7.34. The relationship between vibration magnitude and duration for energy-equivalent exposures.

However, as was repeatedly mentioned above, this conclusion based on frequency-weighted magnitude of acceleration obtained from dynamic model describing hammer in one axis (parallel to the percussion direction) only, so the real acceleration produced by the electro-pneumatic hammer might be even higher.

Results of numerical simulations have been confirmed by experiment where mechanical system represented handle-hand interaction, while electro-magnetic shaker attached to the handle reproduced casing acceleration.

According to the results of numerical simulations, the developed vibration attenuation system is independent from the changes in feed force or parameters of an operator. At the same time, frequency analysis of the vibration attenuation system showed that such system is effective in a relatively narrow frequency range. Consequently, in order to improve performance of such a system, the appropriate controller or some other means of maintaining the driving frequency constant should be used.

The spectrum of acceleration perceived by the operator contains linked frequencies. This fact suggests that the system could be further improved by

employing a dynamic absorber that would suppress several linked frequencies simultaneously. There are several studies on multi-degree-of-freedom torsional dynamic absorbers [94], so theoretically this concept could be extended for longitudinal vibration. Alternatively, an impact dynamic absorber could be used. This absorber consists of a small rigid mass in a container that is firmly attached to the main mass. The mass may collide with the walls of its container during the motion of the system, which accounts for the non-linearity. Such absorber may have an advantage of suppressing several harmonics simultaneously, however, possible instabilities and complex procedure of optimisation and tuning of such absorber is a point of concern.

Chapter 8

Concluding remarks

In the previous chapters, various aspects of hand-transmitted vibration and dynamics of hand-held percussion power tools have been investigated and discussed. This last chapter is devoted to the discussion of the main conclusions arising from the present study.

A literature review of modern hand-transmitted vibration standards and medical aspects of HAVS has indicated complex interactions between many relevant to HAVS variables. It has also shown that the available exposure and epidemiological data are insufficient to establish a clear exposure-response relationship for disorders caused by hand-transmitted vibration. There is extensive clinical literature on this subject, but little is known of the mechanism of the injury or the actual forces responsible. However, as far as the development of low-vibration percussion machine is concerned, the following parameters have been selected in the present study as the main factors responsible for HAVS: magnitude and impulsiveness of acceleration perceived by an operator and muscle tension of an operator (i.e. feed force, grip force etc.). In order to investigate the interaction between the operator and the tool, a dynamic model of a hand-arm system has been included in the dynamic analysis of a hand-held percussion machine.

There are a number of existing dynamic models of hand and arm. These vary from SDOF lumped parameter linear models to four-degree-of-freedom non-linear models with distributed parameters. Most of these models were obtained by measuring the driving point mechanical impedance and are in good agreement with experimental data. However, there is a significant difference between these models and thus there is no single universal model. Therefore, an experiment was carried out in order to develop a dynamic model depicting operator-machine interactions for the present study. The experimental results have shown that with certain simplifications, a hand-arm system may be represented as a SDOF lumped parameter system. The resulting model is rather simplistic and does not allow for changes in feed and grip force of the operator. Neither is the non-linearity of the hand and arm reflected in the model. However, as the study has shown, the model can be successfully used as a part of the complex dynamic model of a hand-held percussion machine.

As a basis for further study, an electro-pneumatic hammer was chosen as a representative hand-held percussion machine. After a preliminary analysis of the main sources of vibration in an electro-pneumatic hammer and parameters affecting the dynamics of the tool, a dynamic model of an electro-pneumatic hammer was developed. The one-axis lumped parameter five-degree-of-freedom model includes the hand-arm system, the feed force, the casing of the machine, the crank-slide mechanism, the striker, the pick and the work-piece. Due to the complexity and non-linearity of this model, analytical investigations are difficult, hence, numerical simulations were performed using Simulink (part of Matlab environment).

Optimum parameters of an electro-pneumatic hammer were found by using Monte-Carlo optimisation in such a manner that the electro-pneumatic hammer operates with a pre-designed frequency and energy of impact, while the acceleration perceived by the operator is minimal. Results of numerical simulations were in good agreement with available experimental data and enabled a detailed analysis of the dynamics of the electro-pneumatic hammer. The results have confirmed that the force of the striker acceleration and the force of impact between the pick and the buffer mounted on the casing are the main sources of harmful vibration produced by an electro-pneumatic hammer.

Based on the analysis of current methods available for reducing vibration of hand-held percussion machines, the main design criteria for a vibration attenuation system were specified as follows:

- Restricted size and weight of additional elements
- High static stiffness as compared with a dynamic one

Analysis of excitation in an electro-pneumatic hammer has been performed by Babitsky [48], who showed that modification of the excitation could reduce unfavourable vibration and also relieve the load on the drive. Introduction of an additional linear spring-mass-damper element to the driving piston proposed in the present study, as the development of the above concept, reduced pneumatic impulses between the driving piston and the striker, which is one of the main sources of hand-transmitted vibration in piston-operated hand-held tools. Numerical simulations confirmed that such a flexible element extends the duration of pneumatic impulses thereby reducing their magnitude and relieving the load on the operator. The modified source of excitation allows realisation of the striker motion that is closer to the optimal excitation.

As a second part of the present study, a passive vibration attenuation system that combined the principles of vibration isolation and dynamic absorption was developed. Such a system consisted of a vibration isolator placed between the casing and the handle of the machine and a tuned dynamic absorber attached to the handle. Operating frequency of an electro-pneumatic hammer is relatively constant, so the dynamic absorber suppresses the fundamental frequency of acceleration perceived by the operator, while the vibration isolator reduces the high frequency components. The mass of the handle is small in comparison with the casing mass, thus a dynamic absorber with a small effective mass is sufficient in suppressing the fundamental harmonic of handle vibration. This fact allows the use of several dynamic absorbers tuned to different frequencies for even greater vibration attenuation. Since low-frequency harmonics are reduced by dynamic absorbers, a vibration isolator with a relatively high stiffness can be employed between the casing and the handle. Such an isolator provides dynamic de-coupling between the casing and the handle and attenuates only the higher frequencies, so its stiffness can be chosen such that it provides optimal stability and controllability of the machine by the operator. The proposed vibration attenuation system is simple. It can be easily implemented into the existing design of a percussion machine and provides significant reduction of vibration perceived by the operator. Results of numerical simulations have been verified by experiment.

8.1 Present contribution

Relative to the objectives set out at the beginning of the present study (as formulated in Section 1.2), the main contributions of the thesis are:

1. A detailed dynamic model of an electro-pneumatic hammer was developed. The model included operator-machine coupling, all major parts of the machine and their interactions responsible for hand-transmitted vibration. The dynamic model of an electro-pneumatic hammer was built in Simulink and enabled numerical simulations of the machine. These were found to be in good agreement with experimental data. Such a model can be applied for the detailed dynamic analysis of a piston-operated hand-held percussion machine and optimal design of a vibration attenuation system or such a machine.
2. Excitation mechanism of an electro-pneumatic hammer was modified by attaching an additional spring-mass-damper element to the driving piston. Such a modification allows extension of pneumatic impulses between the driving piston and the striker, thereby reducing their magnitudes and consequently attenuation of the vibration perceived by the operator.
3. A passive vibration attenuation system that combines vibration isolation and dynamic absorption principles was developed. Results of numerical simulations were confirmed by experiment showed that such a passive system is very effective in reducing hand-transmitted vibration over a wide frequency range. The main advantages of such a system with respect to vibration attenuation of a hand-held percussion machine are the possibility of employing a relatively stiff vibration isolator between the operator and the casing, a small effective mass of dynamic absorbers attached to the handle and easy implementation of the system into an existing design.

8.2 Recommendations for future work

The present study has proposed two different and complementary methods for vibration attenuation of a hand-held percussion machine based on a detailed dynamic

analysis of this type of machinery. There is a potential for further work to improve on the present results and these ideas are discussed below.

1. The dynamic model of the electro-pneumatic hammer that was developed in the present study incorporated certain simplifications. Vibration was considered only in the direction parallel to the stroke direction under the assumption that vibration in this direction is dominant. However, in order to get a comprehensive idea about hand-transmitted vibration produced by this type of machinery, other directions should be considered. The model could also be modified to include the dynamic model of the AC commutator motor, grip force of an operator and torsion vibration due to torque of the resistance force applied to the crank-slide mechanism and transferred to the rotor of the motor.

2. Modification of crank-slide mechanism by means of an additional flexible element attached to the driving piston was analytically investigated. Such a modification has considerable potential for further development as it can be used not only in an electro-pneumatic hammer, but also in other piston-operated machines where high magnitudes of pneumatic or combustion impulses cause undesirable effects. Practical implementation of such elements is an interesting and challenging task and could be the subject of further research. There is potential for further work to investigate the possibility of creating a semi-active flexible element that can tune itself to the operating frequency.

3. Possible experimental investigations could lie in the development and implementation of the proposed vibration attenuation system for a real electro-pneumatic hammer that incorporates the design of a control system that will support the operating frequency.

REFERENCES

1. Griffin, M. J. 1990 *Handbook of Human Vibration*. Academic Press, London.
2. *Health and Safety Commission*. Health & Safety Executive. *Health and safety Statistics* 2000/2001. HSE Books, ISBN 0 7176 2110 3
3. *Health and safety Executive*. Regulatory impact assessment of the physical agents (vibration) directive 2002/44/EC (2002, August 20). [Online]. Available: <http://www.hse.gov.uk/ria/vibrate/vibrate.pdf>
4. Pelmear P. L., Wasseman D. E. 1998 *Hand-Arm Vibration. A comprehensive guide for occupational health professionals*. Second edition. OEM Press, Beverly Farms.
5. Lundborg G., Dahlin L. B. 1995 *Vibration-induced hand problem Current Trends in Hand Surgery*. Elsevier Science, Oxford.
6. *Health and Safety Executive* 1994 Hand-arm vibration HS(G)88 ISBN 0 7176 0743 7
7. Kyriakides K. 1988 *Survey of exposure to hand-arm vibration in Great Britain* Research Paper 26 HSE (Out of print).
8. Wasserman D. E. 1987 *Advances in Human Factors/Ergonomics*. Vol.8. Human aspects of occupational Vibration. Elsevier Science, Amsterdam. Oxford.
9. Brammer A. J., Taylor W. 1982 *Vibration effects on the hand and arm in industry*. John Wiley & Sons, Inc, New York
10. Taylor W., Pelmear P. L. 1975 *Vibration White Finger in Industry*. Academic Press, London.
11. Taylor W. 1974 *The vibration syndrome*. Academic Press, London, New York.
12. Bovenzi M. 1998 *International Archive Occupational and Environmental Health* 71, pp 509-519. Exposure-response relationship in the hand-arm vibration syndrome: an overview of current epidemiology research.
13. Reynolds D. D., Jokel C. 1974 *American Industrial Hygiene Association Journal* October, pp 613-622. Hand-arm vibration-an engineering approach.
14. Griffin M. J. 1997 *Occupational and Environmental Medicine* 54 (2), pp 73-89. Measurement, evaluation and assessment of occupational exposures to hand-transmitted vibration.

15. Pelmeur P. L., Leong D., Taylor W., Nagalingam M., Fung D. 1989 *Journal of Occupational Medicine* **31**(11), pp 902-908. Measurement of vibration of hand-held tools: Weighted or Unweighted?
16. *British Standards Institution* 2001 Mechanical vibration-Measurement and evaluation of human exposure to hand-transmitted vibration. Part 1. General requirements. BS EN ISO 5349-1:2001. London: British Standards Institution.
17. *British Standards Institution* 2002 Mechanical vibration-Measurement and evaluation of human exposure to hand-transmitted vibration. Part 1. Practical guidance for measurement at the workplace. BS EN ISO 5349-2:2002. London: British Standards Institution.
18. *International Organisation for Standardisation*. 1986 Mechanical vibration-Guidelines for the measurement and the assessment of human exposure to hand-transmitted vibration, International Standard 5349. (Withdrawn, superseded).
19. Griffin M. J. 1998 *8-th International Conference on Hand-Arm Vibration*, 9-12 June, Umeå, Sweden, pp 243-259. Standards for the evaluation of hand-transmitted vibration and the prevention of adverse effects.
20. Ikeda K., Ishizuka H., Sawada A., Urushiyama K. 1998 *Industrial Health* **36**, pp 197-208. Vibration acceleration magnitudes of hand-held tools and workpieces.
21. Burström L., Lundström R., Hagberg M., Nilsson T. 1998 *Safety Science* **28** (1), pp 3-14. Comparison of different measures for hand-arm vibration exposure.
22. Donati P. 2001 *Vibration Injury Network* Evaluation of occupational exposures to hand-transmitted vibration: frequency weighting and exposure duration (a preliminary survey). Appendix H4A to Final Report. [Online]. Available: http://www.human-vibration.com/VINET_final_report_m/pdf_files/Appendix_H4A.pdf
23. *National Institute for Occupational Safety and Health* 1989 Criteria for a recommended standard. Occupational exposure to hand-arm vibration. NIOSH, pp 89-106. [Online]. Available: <http://www.cdc.gov/niosh/89-109.html>
24. Starck J. 1984 *Scandinavian Journal of Work and Environmental Health* **10**, pp 171-178. High impulse acceleration levels in hand-held vibratory tools.
25. Starck J., Farkkila M., Aatola S., Pyykko I. and Korhonen O. 1983 *British Journal of Industrial medicine* **40**, pp 426-433. Vibration syndrome and vibration in pedestal grinding.

26. Pelmear P. L., Kusiak R., Leong D. 1995 *Journal of Low Frequency Noise and Vibration* **14**, 2, pp 73-79. Hand-arm vibration syndrome associated with impact vibration.
27. Pelmear P.L., Wills M. 1997 *Journal of Occupational and Environmental Medicine* **39** (11), pp 1092-1096. Impact Vibration and hand-Arm Vibration Syndrome.
28. Burström L., Sörensson A. 1999 *International Journal of Industrial Ergonomics* **23**, pp 585-594. The influence of shock-type vibrations on the absorption of mechanical energy in the hand and arm.
29. Sörensson A., Burström L. 1999 *International Journal of Acoustics and Vibration* **4** (2), pp 59-64. Energy absorption in the hand and arm system exposed to impact vibration with high frequency contents.
30. Kihlberg S. 1995 *International Journal of Industrial Ergonomics* **16**, pp 1-8. Biodynamic response of the hand-arm system to vibration from an impact hammer and a grinder.
31. Burström L., Lundström R. 1994 *Ergonomics* **37** (5), pp 879-890. Absorption of vibration energy in the human hand and arm.
32. *British Standards Institution* 1987 Guide to Measurement and evaluation of human exposure to vibration transmitted to the hand. British Standard, British Standard 6842:1987.
33. Kinne J., Melzig-Thiel R. 1996 *Central European Journal of Public Health* **40**, pp 53-56. Derivation of mean impedance curves as a basis for mechanical models of the human hand-arm system.
34. Jahn R., Hesse M. 1986 *Scandinavian Journal of Work Environment Health* **12**, pp 343-346. Applications of hand-arm models in the investigation of the interaction between man and machine.
35. Mishoe J. W., Suggs C. W. 1977 *Journal of Sound and Vibration* **53**, pp545-558. Hand-arm vibration. Part II. Vibration responses of human hand.
36. Reynolds D. D., Falkenberg R. J. 1984 *Journal of Sound and Vibration* **95**, pp 499-514. A study of hand vibration on chipping and grinding operators. Part II. Vibration responses of human hand.
37. Suggs C. W., 1972 *The Vibration Syndrome. Proceeding on the Medical Engineering and Legal Aspects of Hand-Arm vibration, University of Dundee* 12-

- 14 July 1972 (Taylor W, ed), pp 169-186. Modelling of the dynamic characteristic of the hand-arm system. London: Academic press.
38. Reynolds D. D., Soedel W. 1972 *Journal of Sound and Vibration* **21**, pp 339-353. Dynamic response of the hand-arm system to a sinusoidal input.
39. Miwa T., Yonekawa Y., Nara A., Kanada K., Baba K. 1979 *Industrial Health* **17**, pp 85-122. Vibration isolators for portable vibrating tool. Part1. A grinder.
40. Gurram R., Rakheja S., Gouw G. J. 1995 *International Journal of Industrial Ergonomics* **16**, pp 135-145. Mechanical impedance of the human hand-arm system subject to sinusoidal and stochastic excitation.
41. Reynolds D. D. and Keith R. H. 1977 *Journal of Sound and Vibration* **51** (2) pp 237-253. Hand-arm vibration. Part I: Analytical model of the vibration response characteristics of the hand.
42. Cherian T., Rakheja S., Bhat R. B. 1996 *International Journal of Industrial Ergonomics* **17**, pp 455-467. An analytical investigation of an energy flow divider to attenuate hand-transmitted vibration.
43. Fritz M. 1991 *Journal of Biomechanics* **24** (12), pp 1165-1171. An improved biomechanical model for simulating the strain of the hand-arm system under vibration stress.
44. Wood L. A., Suggs C. W. and Abrams C. F., Jr 1978 *Journal of Sound and Vibration* **57** (2), pp 157-169. Hand-arm vibration. Part III: A distributed parameter dynamic model of the human hand-arm system.
45. Rakheja S., Wu J. Z., Dong R. G., Schopper A. W. and Boileau P. E. 2002 *Journal of Sound and Vibration* **249** (1), pp 55-82. A comparison of biodynamic models of the human hand-arm system for applications to hand-held power tools.
46. *International Standard Organisation*. Mechanical vibration and shock-free mechanical impedance of the human hand-arm system at the driving point. ISO 10068: 1998
47. Astashev V. K., Babitsky V. I., Kolovsky M. Z. 2000 *Dynamics and control of machines*. Springer, Berlin.
48. Babitsky V. I. 1998 *Journal Sound and Vibration* **214**, 165-182. Hand-held percussion machine as discrete non-linear converter. Erratum 1999, **222**.
49. Babitsky V. I. 1998 *Theory of vibro-impact systems and applications*. Springer, Berlin. (Revised translation from Russian 1978 Moscow: Nauka).

50. Lavendel E.E ed. 1981 *Vibration operations and equipment*. Vol. 4. In: *Vibration in engineering 1978–1981*, Volumes 1-6. Ed. Chelomey V. L. Mashinostroenie, Moscow; (in Russian).
51. Crede C. E. 1965 *Shock and vibration concepts in engineering design*. Prentice-Hall, Inc., Englewood Cliffs, N J.
52. Babitsky V. I., Veprik A. M. 1998 *Journal of Sound and Vibration* **218**, pp 269-292. Universal bumpered isolator for severe environment.
53. Fu C. C. and Paul B. 1968 *International Journal of Solid Structures* **4**, pp 897-905. Stability of motion of impact tools.
54. Gottfried B. S., Weisman J. 1973 *Introduction to optimization theory*. PrenticeHall, Inc. Englewoods Cliffs, N J.
55. Gall D. A. 1965 *A practical Multifactor optimization criterion*. In *Recent Advances in optimization techniques*, eds. Lavi A. and Vogl T. P., Wiley, New York.
56. Sobol I. M. 1968 *Monte-Carlo Method*. Nauka, Moscow, (in Russian).
57. Kreyzig E. 1993 *Advanced engineering mathematics-7th* ed. John Wiley & Sons, Inc.
58. Soundranayagam S. A. 2000 Investigation of nonlinear transformation of impulses in impact units for improvement of hammer drill performance. PhD Thesis, Loughborough University.
59. Health Directorate. Health and Safety Executive. Hand-arm and whole body vibration. [Online]. Available: <http://www.hse.gov.uk/hthdir/noframes/vibrate/criteria.htm>.
60. Byhovskiy I. I., Goldshtein B. G. 1977 *Principles of design of vibration-safe portable tools*. Mashinostroenie, Moscow, (in Russian).
61. *Atlas Copco manual*. 1982 4th ed. Atlas Copco.
62. Linguist B., ed. *Ergonomic tools in our time*. Atlas Copco, 1990
63. Anderson S. 1976 *RDR-36-a new chipping hammer with unique design*. Atlas Copco, Stockholm
64. Auerbach E I 1981 in *Vibration effects on the hand and arm in industry* eds Brammer A.J. and Taylor W. pp 11-315. An investigation of chipping hammer vibration.
65. Health and Safety Executive. 1997 *Vibration Solutions. Practical Ways to reduce the Risk of Hand-arm Vibration Injury*. HS(G)170 ISBN 0 7176 09545.

66. Ohtsu S., Kawakami Y., Kaneda K. 1985 *Transactions of Japan Society of Mechanical Engineers* **476**, pp 1218-1223. Study on vibration reduction of concrete breakers. (2nd report, Vibration reduction due to the dynamic balancer driven by positive cam, and vibration isolation due to the elastic coupling between crank shaft and motor).
67. Nikitin J. F. et al. 1983 *Pneumatic tool*. United States Patent number 4,402, 369
68. Cherng J. G., and Peng S.-L. 1993 *Proceedings-SPIE The international Society of Optical Engineers* **1923** (2), pp 1527-1534. Modal characteristics and passive damping for pneumatic percussive rivet tools.
69. Pyykko I. et al., 1976 *Scandinavian Journal of Work Environment Health* **2**, pp 87-95. Transmission of vibration in the hand-arm system with special reference to changes in compression force and acceleration.
70. Rivin E. I. 2003 *Passive vibration isolation*. The American Society of Mechanical Engineers, New York.
71. Harris C. M., Crede C. E. ed., 1961 *Shock and Vibration Handbook*. McGraw-Hill Book Co. Inc, New York. Toronto, London.
72. Rao S. S. 1995 *Mechanical vibrations* 3rd ed. Addison-Wesley Publishing Company, Inc.
73. Meirovitch L. 2001 *Fundamentals of vibrations*. McGraw-Hill Book Co. Inc, New York.
74. Ksiazek M. 1997 *Shock and Vibration* **4** (4), pp 281-291. Synthesis of optimal isolation systems of hand-transmitted vibration.
75. Kolovsky M. Z. 1999 *Nonlinear dynamics of active and passive systems of vibration protection*. Springer, Berlin.
76. Balandin D. V., Bolotnik N. N. and Pilkey W. D. 1998 *Shock and Vibration* **5**, pp 73-87. Review: optimal shock and vibration isolation.
77. Barber A. ed., 1989 *Pneumatic Handbook* 7th edition,. Trade & Technical Press Limited, England
78. Hundal M. S. 1980 *Shock and Vibration Digest* **12** (9), pp 17-21. Literature review-pneumatic shock absorbers and isolators.
79. Palej R., Piotrowski S., Stojek M. 1993 *Journal and Sound and Vibration* **168** (2), pp 299-306. Mechanical properties of an active pneumatic spring.
80. Ormondroyd J, Den Hartog J. P. 1928 *Transactions of the American Society of Mechanical Engineers* **50**, pp 9-22. The theory of the dynamic vibration absorber.

81. Den Hartog J.P. 1956 *Mechanical Vibrations*. McGraw-Hill, New York.
82. Snowdon J.C. 1968 *Vibration and shock in damped mechanical systems*. John Wiley & Sons, New York.
83. Sun J. Q., Jolly M. R., Norris M. A. 1995 *Special 50th anniversary design issue, Transactions of the ASME* **117**, pp 234-242. Passive, adaptive and active tuned vibration absorbers-a survey.
84. Babitsky V.I. 1995 Dynamic absorption of oscillations in *Shock and Vibration Protection* Vol. 6. In: *Vibration in engineering*. Second edition. Ed. Frolov K. V. Mashinostroenie, Moscow; (in Russian).
85. Roberson R. E. 1952 *Journal of the Franklin Institute* **254**, pp 205-220. Synthesis of a non-linear dynamic vibration absorber.
86. Hunt J. B. and Nissen J. C. 1982 *Journal of Sound and Vibration* **83**, pp 573-578. The broadband dynamic vibration absorber.
87. Jordanov I. N. Cheshankov B. I. 1988 *Journal of Sound and Vibration* **123**, pp 157-170. Optimal design of linear and non-linear dynamic vibration absorbers.
88. Rice H. J. 1986 *Journal of Sound and Vibration* **108**, pp 526-532. Combinational instability of the non-linear vibration absorber.
89. Semercigil S. E., Lammers D. and Ying Z. 1992 *Journal of Sound and Vibration* **156**, pp 445-459. A new tuned vibration absorber for wide band excitation.
90. Masri S. F. and Caughey T. K. 1966 *Journal of Applied Mechanics* **33**, pp 586-592. On the stability of the impact damper.
91. Inman D. J. *Engineering vibration*. 1996 Prentice Hall, Inc., London
92. Veprik A. M., Babitsky V. I., Pundak N. and Riabzev S. V. 2000 *Shock and Vibration* **7**, pp 1-17. Vibration control of linear split stirling cryogenic cooler for airborne infrared application.
93. Veprik A. M., Babitsky V. I., Pundak N., Riabzev S. V. 2002 *Proceedings of Nineteenth International Cryogenic Engineering Conference*, 22 - 26 July 2002, Grenoble, France. Vibration and thermal control of a linear cryogenic cooler.
94. Chao C. P. and Shaw S. W. 2000 *Journal of Sound and Vibration* **231** (2), pp 411-431. The dynamic response of multiple pairs of subharmonic torsional vibration absorbers.

Appendix A

Search routine for optimal parameters of dynamic model of an electro-pneumatic hammer

A.1. M-file *parameters.m*.

```
%set high and low boundary of search for every parameter of
optimisation
clear variables

par1low =0.05;% driving piston mass,  $m_3$ , kg
par1high =0.25;
par2low =0.02;% length of the pressure camera,  $S$ , m
par2high =0.05;
par3low =0.01;% striker mass,  $m_4$ , kg
par3high =0.03;
par4low =0.02; % stroke length,  $d$ , m
par4high =0.05;
par5low =100*6.28;% buffer natural frequency,  $\Omega_2$ , rad/s
par5high =500*6.28;
par6low =0.05;% buffer loss factor,  $\zeta_2$ 
par6high =0.5;

f=1;% number of optimisation step
save('C:\Optimis\numiter','f')
fname=strcat('C:\Optimis\bounds',num2str(f));
save(fname,'par1high','par1low','par2low','par2high','par3low',
'par3high','par4low','par4high','par5low','par5high','par6low',
'par6high');

%set initial conditions
f=0;

eval(['max_pick_vel' num2str(f) '=0'])
```

```

fname=strcat('C:\Optimis\opt_pick_',num2str(f));
save(fname,strcat('max_pick_vel', num2str(f)));
eval(['RMS_hand_acc' num2str(f) '=120'])
fname=strcat('C:\Optimis\opt_RMS_',num2str(f));
save(fname,strcat('RMS_hand_acc', num2str(f)));

```

search

A.2. M-file *search.m*.

%generate random numbers, perform N simulations for each
optimisation %step, record result of each simulation

```
clear all
```

```
load('C:\Optimis\numiter');% load number of optimisation step
```

```
%set number of simulations for each optimisation step
```

```
if f==1
```

```
    N=5000
```

```
else f>=2
```

```
    N=(0.98^f)*5000
```

```
end
```

```
save('C:\Optimis\iter','N')
```

```
istart=1;
```

```
for i=istart:istart+N
```

```
    save('C:\Optimis\step','i')
```

```
        clear all
```

```
        load('C:\Optimis\step')
```

```
        load('C:\Optimis\numiter');
```

```
        H=strcat('C:\Optimis\bounds',num2str(f));
```

```
        load(H)
```

```
%generate random set of parameters within search area
```

```
    for k=1:6
```

```
        eval(['par'num2str(k) '=par'num2str(k)'low+  
              (par'num2str(k)'high-par'num2str(k)'low)*rand'])
```

```
    end
```

```
% set parameters
```

```
    m3=par1;
```

```
    S=par2;
```

```
    m4=par3;
```

```
    d=par4;
```

```
    omega2=par5;
```

```
    e2=par6;
```

```
%load all parameters of dynamic model
```

```

    hammer
%run Simulink model
    sim('hammer_opt')

%calculate frequency of pick impacts against treated material
    Funct=pick_vel;
    A=0.8*max(Funct(length(Funct)-40000:length(Funct)));
    Fun=Funct(length(Funct)-40000:length(Funct));
    Res=Fun-A;
    z=length(Fun);
    k=0;
    for l=2:z;
        if Res(l)*Res(l-1)<=0;
            if Res(l-1)<=0&Res(l)>0;
                k=k+1;
            end
        end
    end
    Freq=k/2;
%calculate maximum of pick velocity just before impact against
%treated material
    Max_pick_vel=max(Fun);
%calculate r.m.s. of hand acceleration
    RMS_hand_acc=(sum(hand_acc.^2)/length(hand_acc)).^0.5;

%save results of simulation
    fname=strcat('C:\Optimis\simul_',num2str(f),'_',num2str(i));
    save(fname,'S','m3','d','m4','omega2','e2','Max_pick_vel',
        'RMS_hand_acc','Freq');
    load('C:\Optimis\iter')

end

analysis

```

A.3. M-file *hammer.m*

%contains all pre-designed parameters of dynamic model of an electro-pneumatic hammer

```

A=0.0015*pi/4;%cross section area of the driving piston, m2
p=101300;%athmospheric pressure, Pa
r=0.02;%crank radius, m
l=0.06;%length of the connecting rod, m

m1=1.44;%mass representing hand-arm system, kg
m2=8;%casing mass, kg
m5=0.35;%pick mass, kg
omega2=2800*6.28;%rad/sec

```



```

e2=0.1;
omega3=2.08e+004;%rad/s
e3=0.5;
omega5=1500*6.28;%rad/s
e5=0.7;

k1=243000;%N/m
c1=265;%Ns/m
k2=(omega2^2)*m1;%
c2=2*e2*omega2*m1;
k3=(omega3^2)*m4*m5/(m4+m5);
c3=2*e3*omega3*m4*m5/(m4+m5);
k4=(omega4^2)*m2*m5/(m2+m5);
c4=2*e4*omega4*m2*m5/(m2+m5);
k5=(omega5^2)*m5;
c5=2*e5*omega5*m5;

Keq=1/(1/k1+1/k2+1/k4+1/k5);
P=150;%feed force, N
a=P/Keq;
d1=P/k1;
d2=P/k2;
d4=P/k4;
d5=a-(P/k1+P/k2+P/k4);

```

A.4. M-file *analysis.m*

```

%contains algorithms of analysis of the results of previous step
%of optimisation, selection of the best set of optimisation
%parameters and new search area for the next step of optimisation.

clear all;

k=0;kr=0;optr_vel4=0;optr_RMS=0;indr=0;t=0;
%load number of optimisation step and consequent number of
simulations
load('C:\Optim\numiter');
load('C:\Optim\iter');

%open each file with simulation results and create arrays containing
%r.m.s. of hand acceleration, impact frequency and parameters of
%optimisation
for i=1:N
G=strcat('C:\Optimis\simul_',num2str(f),'_',num2str(i));
load(G);
res_pick_vel(i)=Max_pick_vel;
res_freq(i)=Freq;
res_RMS(i)=RMS_hand_acc;
par1(i)=m3;
par2(i)=S;
par3(i)=m4;

```

```

par4(i)=d;
par5(i)=omega2;
par6(i)=e2;

%select regimes with pre-designed frequency of impact 45Hz
if res_freq(i)==45;
    k=k+1;
    ind(k)=i;
    opt_pick(k)=res_pick_vel(i);
    opt_RMS(k)=res_RMS(i);
%select regimes with pre-designed impact frequency and velocity of
pick %impact against treated material
    if res_pick_vel(i)>=2.8;
        kr=kr+1;
        indr(kr)=i;
        optr_pick(kr)=res_pick_vel(i);
        optr_RMS(kr)=res_RMS(i);
    end
end
end

%save arrays containing r.m.s. of hand acceleration, velocity of
pick %impact and number of simulations that satisfy pre-designed
conditions
fname=strcat('C:\Optimis\min',num2str(f));
save(fname,'f','optr_pick','optr_RMS','indr');
fname=strcat('C:\Optimis\max',num2str(f));
save(fname,'f','opt_vel4','opt_RMS','ind');

%in case of several sets of optimisation parameters that satisfy
both
%of pre-designed conditions as optimum set select regime with
minimum %r.m.s. of hand acceleration
if kr>=2
    y=find(optr_RMS==min(optr_RMS))
    z=indr(y);
    save('C:\Optim\best','z')
    min_z=min(optr_RMS);
    G=strcat('C:\Optimis\opt_RMS_',num2str(f-1));
    load(G);
    n=z;
    eval(['RMS_hand_acc' num2str(f) '=min_z'])
%compare with best previously obtained r.m.s. of hand acceleration
    if eval(['RMS_hand_acc' num2str(f-1) '-
        RMS_hand_acc' num2str(f) '>=0.01*RMS_hand_acc' num2str(f-1)])
        fname=strcat('C:\Optimis\opt_RMS_',num2str(f));
        save(fname, strcat('RMS_hand_acc', num2str(f)), 'n');
        eval(['max_pick' num2str(f) '=optr_pick(y)']);
        fname=strcat('C:\Optimis\opt_pick_',num2str(f));
        save(fname, strcat('max_pick', num2str(f)));
    else

```

```

G=strcat('C:\Optimis\opt_pick_',num2str(f-1))
load(G);
eval(['opt_RMS=RMS_hand_acc' num2str(f-1)]);
eval(['opt_vel4=max_pick' num2str(f-1)]);
fname=strcat('C:\Optimis\opt_RMS_',num2str(f));
save(fname, strcat('RMS_hand_acc', num2str(f)));
f=f-1;
fname=('C:\Optimis\result_parameters');
save(fname, 'f', 'opt_pick', 'opt_RMS', 'par1', 'par2', 'par3',
'par4', 'par5', 'par6');
disp('stop simulation')
%stop optimisation
break
end
else
%select regime with highest pick impact velocity, when maximum pick
%velocity obtained during current optimisation step is lower than
%pre-designed value
y=find(opt_pick==max(opt_pick));
z=ind(y);
save('C:\Optimis\best', 'z')
max_z=max(opt_pick);
G=strcat('C:\Optimis\opt_pick_',num2str(f-1))
load(G);
n=z;
eval(['max_pick' num2str(f) '=max_z'])
%compare current best value of r.m.s. of hand acceleration with best
%previously obtained value of r.m.s.
if eval(['max_pick' num2str(f) '-max_pick'
num2str(f-1) '>=0.005*max_pick' num2str(f-1)])
eval(['RMS_hand_acc' num2str(f) '=opt_RMS(y)']);
fname=strcat('C:\Optimis\opt_RMS_',num2str(f));
save(fname, strcat('RMS_hand_acc', num2str(f)));
fname=strcat('C:\Optimis\opt_vel4_',num2str(f));
save(fname, strcat('max_pick', num2str(f)), 'n');
else
G=strcat('C:\Optimis\opt_RMS_',num2str(f-1))
load(G);
eval(['opt_RMS=RMS_hand_acc' num2str(f-1)]);
eval(['opt_pick=max_pick' num2str(f-1)]);
fname=strcat('C:\Optimis\opt_pick_',num2str(f));
save(fname, 'opt_pick');
fname=strcat('C:\Optimis\opt_RMS_',num2str(f));
save(fname, 'opt_RMS');
f=f-1;
fname=('C:\Optimis\result_parameters');
save(fname, 'f', 'opt_pick', 'opt_RMS', 'par1', 'par2', 'par3',
'par4', 'par5', 'par6');
disp('stop simulation')
%stop optimisation
break

```

```

        end
    end

    %set new search area with the "best" set of parameters of
    optimisation %as a new centre
    H=strcat('C:\Optimis\bounds',num2str(f));
    load(H);
    load('C:\Optimis\best')
    for i=1:6
        G=strcat('par', num2str(i), '(z)');
        Q=strcat('par', num2str(i), 'high');

        bound=eval(['(par' num2str(i) 'high-par' num2str(i) 'low)*0.95']);
        if bound<=0.001*eval(Q);
            eval(['par' num2str(i) 'low = par' num2str(i) 'low;']);
            eval(['par' num2str(i) 'high =par' num2str(i) 'high;']);
        else eval(['par' num2str(i) 'low = eval(G)-bound;']);
            if eval(['par' num2str(i) 'low<0']);
                eval(['par' num2str(i) 'low = 0']);
            end
        eval(['par' num2str(i) 'high = eval(G)+bound;']);
    end
end

%save new search area and start next optimisation step
f=f+1
save('C:\Optimis\numiter','f')
fname=strcat('C:\Optimis\bounds',num2str(f));
save(fname,'par1high','par1low','par2low','par2high','par3low',
      'par3high','par4high','par4low','par5low','par5high','par6low',
      'par6high');

search

```

Appendix B

Frequency calculation

```
%specify function for frequency calculation
    Funct=pick_vel;
%specify level of acceptable deviation of function magnitude
    A=0.8*max(Funct(length(Funct)-40000:length(Funct)));
    Fun=Funct(length(Funct)-40000:length(Funct));
    Res=Fun-A;
    z=length(Fun);
    k=0;
%calculate number of level crossings
    for l=2:z;
        if Res(l)*Res(l-1)<=0;
            if Res(l-1)<=0&Res(l)>0;
                k=k+1;
            end
        end
    end
%calculate frequency
    Freq=k/2;
```

Appendix C

Parameters of dynamic model of electro-pneumatic hammer with modified source of excitation.

```
clear all;

A=0.0015*pi/4;
p=101300;
r=0.02;
l=0.06;

m1=1.44;%mass representing hand-arm system, kg
m2=8;%casing mass, kg
m3=0.13;%driving piston mass, kg
m4=0.2;%striker mass, kg
m5=0.35;%pick mass, kg
S=0.0314;%length of pressure camera, m
d=0.0304;%stroke length, m
omega2=2800*6.28;%rad/sec
e2=0.1;
omega3=2.08+004;%rad/s
e3=0.5;
omega4=1.22+003;%rad/s
e4=0.26;
omega5=1500*6.28;%rad/s
e5=0.7;

me=0.0746;%mass of additional element, kg
omega=901.8962;%rad/s
e=0.0516;
de=0.02;%distance between piston and undistorted flexible element

ke=me*(omega^2);
ce=2*e*omega*me;
k1=243000;%N/m
```

```
c1=265;%Ns/m
k2=(omega2^2)*m1;%
c2=2*e2*omega2*m1;
k3=(omega3^2)*m4*m5/(m4+m5);
c3=2*e3*omega3*m4*m5/(m4+m5);
k4=(omega4^2)*m2*m5/(m2+m5);
c4=2*e4*omega4*m2*m5/(m2+m5);
k5=(omega5^2)*m5;
c5=2*e5*omega5*m5;

Keq=1/(1/k1+1/k2+1/k4+1/k5);
P=150;%feed force, N
a=P/Keq;
d1=P/k1;
d2=P/k2;
d4=P/k4;
d5=a-(P/k1+P/k2+P/k4);
```

Appendix D

Analog output

```
%converts digital data stored in Matlab Workspace to analog signal
AO = analogoutput('winsound');
%adds hardware channels to the sound card
chans = addchannel(AO, 1);
%defines an output time of ten seconds
duration = 10;
%sets the rate at which an analog output subsystem converts digital
data %to analog data
set(AO, 'SampleRate', 8000);
%finds out actual rate set by the engine
ActualRate = get(AO, 'SampleRate');
%calculates the length of the output data
len = ActualRate*duration;
%the trigger occurs just after trigger function manually issued
set(AO, 'TriggerType', 'Manual');
%specifies a linear scaling of the data as it is queued in the
engine
set(chans, 'UnitsRange', [-1200 1200]);
%specifies the range of the analog output hardware subsystem
set(chans, 'OutputRange', [-1 1]);
%specifies the number of additional times queued data is output
set(AO, 'RepeatOutput', 6);
%creates m-by-n array where m is the number of samples to output and
n is %the number of output channels; "signal" is the Matlab variable
saved in %the Workspace
data = [signal];
%data is queued in the engine
putdata(AO, data);
%starting the device object
start(AO);
%issuing a manual trigger
trigger(AO);
%indicates if the device object and hardware device are running
runstate = AO.Running;
while strcmp(AO.Running, 'On')
```



```
end  
% removes engine form memory and other physical resources  
delete(AO);
```